Shear Testing of Prestressed High Performance Concrete Bridge Girders

A Thesis
Presented to
The Academic Faculty

By

Robert A. Haines

In Partial Fulfillment
Of the Requirements for the Degree
Master of Science in Civil Engineering

Georgia Institute of Technology
August 2005

Shear Testing of Prestressed High Performance Concrete Bridge Girders

Approved by:

Dr. Lawrence F. Kahn, Chair
School of Civil and Environmental Engineering
Georgia Institute of Technology

Dr. Kimberly Kurtis
School of Civil and Environmental Engineering
Georgia Institute of Technology

Dr. Reid W. Castrodale
Director of Engineering
Carolina Stalite Company

Date Approved: May 17, 2005

ACKNOWLEDGEMENTS

The completion of this Master's Thesis would not have been possible without the support and encouragement of many people.

First, I would like to thank God for giving me guidance, patience, and the strength to persevere, even when it seemed hopeless. Through him, anything is possible.

Secondly, I would like to thank my loving family, Mark, Nina, and Jon. Mom, thank you for always knowing when to call and give encouragement; Dad, thanks for always being there to give me advice about anything and everything; and Jon, thank you for being such a great brother. I am so proud of all of you, and I am so happy to be a part of your lives. Without your support, this project would not have been possible.

Next, I would like to thank my beautiful fiancé, Erin, for loving me more and more each day. Seeing your smiling face kept me encouraged and positive, even through the most difficult times. Thanks for all of the lunches, and most of all, thanks for always being there to listen. I love you with all of my heart and I cannot wait to start our new life together.

Special thanks to Dr. Larry Kahn for being an excellent mentor and advisor through every step of my Master's degree program. His wisdom and guidance were fundamental in the completion of this project. I feel that I gained a world of knowledge from him in only a small amount of time; and I will cherish that knowledge throughout my career.

Student researchers Scott Canfield, Richard Jennings, Alen Horta, Mauricio Lopez, and Javier Silva provided assistance during all phases of this project and without their help, the completion of this project would not have been possible. Mamoud Azari

also provided assistance for the many tasks performed at the Georgia Tech Structures and Materials Laboratory. His cooperation and help is also deeply appreciated.

Special thanks to Dr. Kimberly Kurtis of Georgia Tech and Dr. Reid Castrodale of Carolina Stalite Company, who donated their time and patience to make the completion of this research possible. Their expert advice was invaluable.

Special thanks to the businesses and organizations that made this research possible:

The Federal Highway Administration and the Georgia Department of Transportation sponsored the research reported herein through a pool-funded project under Georgia DOT Research Project No. 9-9510-0-97-50550, Task Order No. 64. Standard Concrete Products of Atlanta, Georgia provided Georgia Tech researchers with equipment, manpower, and materials for construction of the two precast, prestressed HPC girders. Lafarge Concrete of Atlanta, Georgia provided all Grade 1 HPC concrete and manpower for the placement of the composite decks for both girders. INSTEEL provided all 0.6-in. diameter prestressing strand. SMI Steel, Gerdau Ameristeel, and Macuch Steel Products, Inc. provided all mild steel reinforcement. These sponsors and their advice and cooperation are gratefully acknowledged.

The conclusions and opinions expressed herein are those of the authors and do not necessarily represent the opinions, conclusions, or specifications of the Federal Highway Administration the Georgia Department of Transportation, or any other sponsoring or cooperating organization.

TABLE OF CONTENTS

LIST OF TABLES

LIST OF FIGURES

LIST OF SYMBOLS

Report	AASHTO Standard	AASHTO LRFD	Description
a	--	--	Compression stress block
a_s	--	--	Shear span, distance from support to point load on girder
A_c	--	--	Cross sectional area of composite girder (combined area of girder and deck)
A_c`	--	A_c	Area of girder on flexural tension side of member
A_g	--	--	Cross sectional area of girder
AASHTO	--	--	American Association of State Highway and Transportation Officials
A_{ps}	A_s*	A_{ps}	Area of prestressing steel
A_{pse}	--	--	Effective area of prestressed reinforcement adjusted inside the transfer or development length regions
A_v	A_v	A_v	Area of shear (stirrup) reinforcement
BCL	--	--	Distance from bottom of girder to center line of bottom row of prestressing strands
b`	b_w	b_v	Web width
CM	--	--	Cementitious Materials
CR		CR_c	Prestress loss due to creep of concrete
CSS	--	--	Concrete Surface Strain
DAQ	--	--	Data Acquisition
D	d_b	d_b	Diameter of prestressing strand
DEMEC	--	--	Detachable Mechanical Strain Gage
d_e	--	d_e	Effective depth from extreme compression fiber to the centroid of the tensile force in the tensile reinforcement
d_p	d_p	d_p	Distance from compression fiber to centroid of prestressed reinforcement
d_v	--	d_v	Effective shear depth
E_c	E_c	E_c	Modulus of elasticity of concrete based on 6 x 12 cylinder
E_{ci}	--	--	Modulus of elasticity of concrete based on 6 x 12 cylinder at strand release
E_{ps}	--	--	Elastic modulus of prestressing steel (ksi)
ES	ES	ES	Prestress loss due to elastic shortening
f_c’	f_c’	f_c’	Concrete compressive strength at specified time
f_{ci}'	f_{ci}'	f_{ci}'	Concrete compressive strength at strand release
f_d	f_d	--	Tensile stress at the extreme tensile fiber due to

Report	AASHTO Standard	AASHTO LRFD	Description
			the dead load of the girder and slab
f_{pc}	f_{pc}	--	Stress in concrete due to effective prestress force (after all losses) at centroid of composite section resisting externally applied loads
f_{ps}	f_{su}*	f_{ps}	Stress in prestressed reinforcement at nominal strength of member
f_{psred}	--	--	Reduced fps based on development length
f_{pt}	--	--	Stress in prestressing strand just prior to strand release
f_{pu}	f_s'	f_{pu}	Specified tensile strength of prestressed reinforcement
f_r	f_r	f_r	modulus of rupture of concrete
f_{se}	f_{se}	f_{pe}	Effective prestressing stress after losses
f_{si}	--	--	Stress in prestressing strand just after strand release
f_y	f_y	f_{sy}	Specified yield strength of non-prestressed reinforcement
h	h	h	Overall depth of the composite girder; Also used as relative humidity for shrinkage calculations
I_c	--	--	Moment of inertia of composite girder (girder and deck)
I_g	--	--	Moment of inertia of girder
l_d	l_d	--	Development length of prestressing strand (In AASHTO Standard, l_d refers to non-prestressed reinforcement development length)
l_{fb}	--	--	Flexural bond length. Additional length over which the strand should be bonded so the stress f_{ps} may develop in the strand at the nominal strength of the member.
l_t	--	--	Transfer length of prestressing strand
LOLAX	--	--	Low relaxation loss prestressing strand
$M_{d/nc}$	--	$M_{d/nc}$	Non-composite total Dead Load Moment
M_{cr}	--	M_{cr}^*	Cracking moment
M_D	--	--	Non-composite Moment due to girder self-weight
M_{max}	--	--	Maximum observed experimental moment
M_n	--	--	Nominal moment strength
M_{SD}	--	--	Non-composite Moment due to deck self-weight
n	n	--	Modular Ratio
RE	CR_s	--	Prestress loss due to relaxation of prestressing steel

Report	AASHTO Standard	AASHTO LRFD	Description
s	s	s	Spacing of shear reinforcement
SH	SH	SH	Prestress loss due to concrete shrinkage
t	--	--	age of concrete (days) for creep and shrinkage calculations
t'	--	--	age of concrete at loading (days) for creep and shrinkage calculations
TCL	--	--	Distance from top of girder to center line of top row of prestressing strands
W/CM	--	--	Water to Cementitious Materials Ratio
w_c	w_c	w_c	Unit weight of concrete
V_c	V_c	V_c	Nominal shear strength provided by concrete
V_{ci}	V_{ci}	--	Nominal shear strength provided by concrete when diagonal cracking results from combined shear and moment
V_{cw}	V_{cw}	--	Nominal shear strength provided by concrete when diagonal cracking results from excessive principal tensile stress in the web
V_d	V_d	V_d	Shear force from dead load of girder plus deck slab
V_s	V_s	V_s	Nominal strength provided by shear reinforcing steel
V_p	V_p	V_p	Vertical component of the effective prestressing force
VWSG	--	--	Vibrating Wire Strain Gage
α	--	--	Shrinkage constant depending on member shape and size
α	--	α	Angle of inclination of transverse reinforcement to longitudinal axis
b	--	b	Factor indicating ability of diagonally cracked concrete to transmit tension
β_1	β_1	β_1	Concrete strength factor
ε_b	--	--	Calculated strain at bottom of girder
ε_{sh}	--	--	Shrinkage strain
ε_{cu}	--	--	Ultimate concrete compressive strain
ε_{ps}	--	--	Strain in prestressing strands at nominal strength
ε_{psmax}	--	--	Maximum observed strain in prestressing strands
ε_{su}	--	--	Breaking tensile strain of prestressing strand
ε_x	--	ε_x	Longitudinal strain in the web reinforcement on the flexural tension side of the member
$\varepsilon_{xadj.}$	--	ε_x	Longitudinal strain in the web reinforcement on the flexural tension side of the member if initial strain is negative

Report	AASHTO Standard	AASHTO LRFD	Description
γ	--	--	Creep coefficient parameters (ACI-209)
γ_p	--	--	Factor for prestressing steel type
Γ	--	--	Stress-to-strength ratio at loading for creep calculations
ω_p	ω_p	ω_p	Ratio of prestressing
$ø_t$	--	--	Creep coefficient at age "t" loaded at t′
$ø_u$	--	--	Ultimate creep coefficient
ρ_p	ρ_p	ρ^*	Ratio of prestressing steel
ρ_v	ρ_w	--	$A_s/b_w d$
ψ	--	--	Creep constant depending on member shape and size

SUMMARY

An 89 ft.-2in. long PCI Modified Bulb Tee 56 was constructed for shear testing at the Georgia Institute of Technology, Structural Engineering and Materials Research Laboratory. This girder used the same HPC that was used in the Jonesboro Rd. demonstration bridge located in Henry County, GA.

The girder concrete had a 56-day compressive strength of 13,820 psi (95.3 MPa). A composite deck 8-in. thick and 60-in wide was placed on top of the girder using unshored construction. The deck's Grade 1 high performance concrete (HPC) mixture had a 56-day compressive strength of 6,700 psi (46.2 MPa). The girder was prestressed using 44 0.6-in. diameter LOLAX strands tensioned to 75 percent of strand ultimate stress. Grade 60 transverse shear reinforcement was spaced at different dimensions along the length of the girder.

Shear tests were conducted at the west and east end and near the west quarterspan location of the BT-56 girder. The concentrated load was located approximately 143 in. from the center of bearing for each test; the approximate shear span to total depth ratio was 2.2. Test E1 had a stirrup spacing of 7 in. and contained 2 pick-up loops; Test W1 had an average stirrup spacing of 16.75 in. and contained two pick-up loops; Test W2 had a stirrup spacing of 24 in. and did not contain any pick-up loops.

Tests E1 and W1 were not tested to failure due to equipment limitations. They were loaded until the capacity of the testing equipment was reached. Despite the inability to rupture the girder during the two tests, information was obtained about the concrete

shear strength and the serviceability of the BT-56 girder. Test W2 was tested to failure with an ultimate shear force of 653 kips (2,904 kN).

The AASHTO Standard Specifications (2002), ACI-Alternate method, AASHTO LRFD Specifications (2004), and the Variable Angle Truss Model (VATM) were used to examine the shear capacity of the BT-56 girder. The AASHTO Standard Specifications (2002) provided a conservative prediction of cracking (V_{cw}) and ultimate shear capacity (V_n); the ratio of experimental to predicted ultimate strength was 1.48. The ACI-Alternate method listed in ACI 318 Section 11.4.2.2 for predicting concrete shear strength gave V_{cw} with experimental-to-predicted ratios as low as 0.8 for the 24-in. stirrup spacing. The AASHTO LRFD Specifications (2004) provided a conservative prediction of ultimate shear capacity, Vn for Test W2, with an experimental-to-predicted ratio of 1.36. The VATM gave an overly conservative prediction of the ultimate shear capacity and was the least accurate of the three methods.

The AASHTO Standard, 1998 AASHTO LRFD, and 2004 AASHTO LRFD results were compared to results obtained from previous research. The data from the BT-56 girder matched the results found from many other research programs. There was a clear improvement between the 1998 and 2004 AASHTO LRFD Specifications. For cracking, the AASHTO Standard Specification (2002) was the most consistent and most accurate. For ultimate shear capacity, both the AASHTO Standard (2002) and AASHTO LRFD (2004) methods were conservative and accurate. When minimal amounts of shear reinforcement were used, the AASHTO Standard method best predicted the shear capacity. The AASHTO LRFD (2004) method became unconservative when the transverse reinforcement ratios exceeded the maximum limit of $8\sqrt{f_c'}b_w d$. Use of both

the AASHTO Standard (2002) and LRFD (2004) is recommended for use with HPC with compressive strengths up to 14,000 psi (96 MPa).

CHAPTER 1

INTRODUCTION

This project is the final task of an experimental investigation into the feasibility of using high performance concrete (HPC) prestressed bridge girders in Georgia. The previous tasks of this investigation have studied issues such as the following:

- An analytical investigation of using HPC to increase span lengths of Georgia bridge girders.
- Selection and design of an actual bridge using HPC prestressed girders, in order to study and monitor the behavior.
- Development of HPC mix designs and evaluate HPC properties.
- Evaluation of HPC production capability and round robin evaluation.
- Prestressing strand transfer and development length study.
- Construction and testing of AASHTO Type II, HPC bridge girders.
- Demonstration bridge construction and evaluation using Type II and Type IV girders.

The final task detailed in this report includes the design, construction, and ultimate strength testing of two large prestressed concrete girders. The two girders constructed were an AASHTO Type IV and a PCI Modified Bulb Tee 56. These girders contained

the same HPC that was used in the demonstration bridge construction project and were designed to contain the maximum number of prestressing strands possible.

The final task was divided into two separate reports, one detailing the ultimate flexure strength of the two girders, and one reviewing the ultimate shear strength of the BT-56. The first report (Canfield, 2005) included the following aspects:

- Construction of two composite girders, an AASHTO Type IV and PCI modified Bulb Tee 56 with the same mix designs as those used in the Jonesboro Road, demonstration bridge.
- Static load tests on the girders to determine the actual flexure strengths to compare to the strengths predicted by the AASHTO Standard (1996 and 2002) and AASHTO LRFD (2004) Specifications for Highway Bridges.
- Transfer lengths of each girder to compare with those of Type II girders tested by Reutlinger and Kahn (2000).
- Prestress losses for each girder to compare with values predicted by AASHTO Standard (2002) and AASHTO LRFD (2004) Specifications.
- Effect a composite deck thermal and shrinkage strain has on girder deflections.

This report, which is the second part of the final task, provides a detailed investigation of the ultimate shear strength of the BT-56 girder. The shear strength of the Type IV girder was not tested due to laboratory constraints. After the BT-56 girder was tested in shear, it was determined that the testing equipment did not have the capacity to test the ultimate strength of the Type IV girder. This report will include the following aspects:

- Construction of the two composite girders, an AASHTO Type IV and PCI modified Bulb Tee 56 with the same mix designs as those used in the Jonesboro Road, demonstration bridge.
- Static load tests of the BT-56 girder and discussion of the actual shear strength as compared to the strengths predicted by the ACI 318-02 code, the AASHTO Standard (2002) and AASHTO LRFD (2004) Specifications for bridge design.

1.1 Research Objective

The objective of the research described herein was to determine the shear performance of a full-scale PCI Modified Bulb Tee 56 with grade 270, low-relaxation, 0.6-in. (15mm) diameter prestressing strands. The cracking shear and ultimate shear strengths were tested and determined at three different sections of the girder. Cracking and ultimate shear calculations were performed using current American Concrete Institute (ACI, 2002) and American Association of State Highway Transportation Officials (AASHTO) code provisions (AASHTO Standard, 2002 and AASHTO LRFD, 2004). Comparisons were to determine whether or not the codes were conservative. Also, the behavior of the BT-56 girder was to be compared to previous shear test results of the smaller AASHTO Type II girders to determine if there is a size effect regarding shear strength of HPC prestressed girders.

1.2 Need for Research

The need for this research is the lack of data on actual shear strengths oflarge, HPC prestressed bridge girders. Although a few full scale tests have been conducted on similar girder sections in other states, the behavior of HPC is dependent on locally available aggregates. As such, GDOT was interested in testing girders produced locally to verify results found by other states. The previous shear tests conducted earlier in this research program were performed on minimally prestressed Type II girders (Dill and Kahn 2000). Therefore, there was a need to test fully prestressed, large HPC girders and to determine the accuracy of the current design specifications. Previous tests for both small and large girders have shown that the AASHTO specifications are conservative for the shear design of HPC bridge girders.

1.3 Scope

Both the Type IV and the BT-56 girders were designed and constructed in the same manner. However, the testing in this report was limited to investigating the cracking and ultimate shear strengths of the BT-56 only. The girders were designed with concrete compressive strength of 10,000 psi (69 MPa) design strength. Composite decks were constructed using a Grade 1 HPC, nominal 7,000 psi (48.3 MPa).

Shear tests were performed at three locations on the BT-56 girder. Both ends were tested and a support was then moved to test the west quarterspan of the girder. The shear spans for all three tests were approximately 143 in. from the supports. The three sections were tested until ultimate failure or ultimate capacity of the testing equipment.

1.4 Organization

Chapter 2 gives a background on shear testing performed on prestressed HPC bridge girders. It details testing on small and large girders along with results and comparisons to the AASHTO Standard and LRFD Specifications. Chapter 3 discusses the design and construction process for both girders, including their composite decks. Chapter 3 also covers the instrumentation used inside of each girder and deck. Chapter 4 discusses all of the concrete material specimen testing and results. Chapter 5 discusses the shear test set-up, followed by a presentation and discussion of the shear results in Chapter 6. Finally, Chapter 7 presents conclusions and recommendations drawn from this study.

CHAPTER 2

BACKGROUND

2.1 Introduction

This chapter discusses past experimental research pertaining to the shear performance of prestressed HPC bridge girders. One important characteristic that often affected the shear capacity of prestressed HPC bridge girders was the shear span that was used. Shear/bond failures occurred when shear spans were less than the experimental development length. Many of the projects discussed in this literature review studied the transfer and development length of prestressing strands in HPC girders. While their main purpose was to examine the bond behavior of prestressing strands in HPC, the tests did induce shear cracking and shear behavior was observed in many of the specimens. Therefore, this chapter provides a brief discussion of the previous research that has been performed on the transfer and development length of prestressing strand in HPC girders. Prestress losses were another important factor affecting the shear capacity of prestressed HPC girders. The definition of prestress losses, along with a brief discussion of previous research concerning losses is provided in this chapter. Finally, the shear performance of various prestressed HPC girders is discussed. It is important to note that only specimens that experienced pure shear failures or minimal shear/bond failures were used for comparison in this research.

2.2 Transfer and Development Length

Transfer length is defined as the distance required from the end of the girder to transfer the effective force, f_{se}, of the prestressing strands into the concrete member. The development length is the distance required to fully develop the bond strength of the strands to provide the ultimate flexural moment strength of the girder. Two components make up the development length; one is the transfer length and the other is the flexural bond length. The flexural bond length is defined as the length beyond the transfer length needed to fully develop the maximum strand stress, f_{ps}, in the girders. The total development length is shown in Figure 2.1.

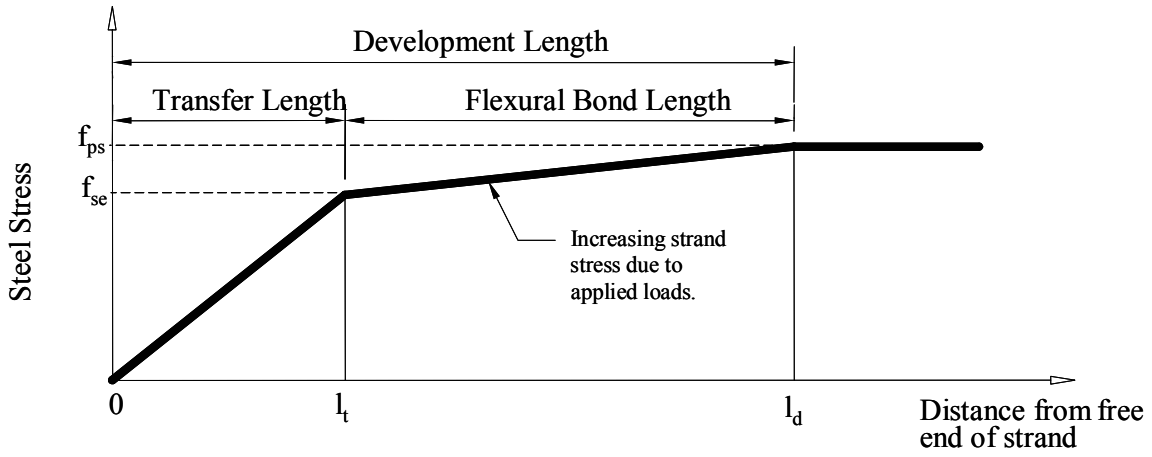

Figure 2.1 Idealized development length for prestressing strands

A detailed transfer length study was performed in a study by Reutlinger and Kahn (1999) in Task 5 of this project called "Direct Pull-Out Capacity and Transfer Length of 0.6-inch Diameter Prestressing Strand in High-Performance Concrete". The factors that affect the transfer length have been found to be the strand surface condition, concrete compressive strength, size of prestressing strand, age of concrete, amount of prestress,

release method, amount of confining steel in the transfer zone, strand spacing, depth of concrete below the strand, degree of concrete consolidation, amount of confining concrete (cover), and stiffness of the concrete (Reutlinger and Kahn, 1999). Table 2.1 provides a summary of the factors affecting transfer length and Table 2.2 lists the different equations that Reutlinger and Kahn (1999) used to study transfer length. An analysis of the experimental transfer length for both full-scale girders along with comparisons to multiple prediction equations can be found in "Testing of High Performance Concrete Pretensioned Bridge Girders", (Canfield and Kahn, 2005).

Table 2.1 Summary of factors that affect transfer length (Dill and Kahn, 2000)

Factor	Effect
Surface Condition	
Cleaned	Decrease
Weathered	Decrease
Release Method	
Gradual	Decrease
Sudden	Increase
Increase in:	
Concrete compressive strength	Decrease
Concrete elastic modulus	Decrease
Size of strand	Increase
Amount of prestress	Increase
Amount of concrete below strand	Increase
Amount of confining reinforcement	None
Strand spacing	None

Table 2.2 Summary of transfer length prediction equations (Dill and Kahn, 2000)

Source	Transfer Length Expression	Equation	Year introduced
AASHTO Standard Specification(1996)	$l_t = 50D$	(2.1)	1973
ACI 318-99	$l_t = 50D$	(2.2)	1963
AASHTO LRFD(1998)	$l_t = 60D$	(2.3)	1994
ACI Commentary	$l_t = \frac{f_{se}D}{3}$	(2.4)	1963
Martin and Scott(1976)	$l_t = 80D$	(2.5)	1976
Zia & Mostafa(1977)	$l_t = 1.5\frac{f_{si}}{f_{ci}'}d_b - 4.6$	(2.6)	1977
Deatherage, Burdette & Chew (1994)	$l_t = \frac{f_{si}D}{3}$	(2.7)	1989
Russell (1992)	$l_t = \frac{f_{se}d_b}{2}$	(2.8)	1992
Mitchell, Cook, Khan & Tham (1993)	$l_t = 0.33\, f_{si}d_b\sqrt{\frac{3}{f_{ci}'}}$	(2.9)	1993
Buckner (1994)	$l_t = \frac{1250 f_{si}d_b}{E_{ci}}$	(2.10)	1994

where:

d_b = Prestressing strand diameter
D = Prestressing strand diameter
E_{ci} = Modulus of elasticity at transfer
f_{ci}' = Concrete compressive strength at release
f_{se} = Effective stress in the prestressing strand after all prestress losses
f_{si} = Stress in the prestressing strand immediately after transfer (f_{pt}-ES)
l_t = Transfer length

Dill and Kahn (2000) performed research on development lengths of four different HPC prestressed girders. The researchers tested Type II HPC girders with one full layer of 0.6 in. diameter prestressing strands at the bottom of each girder. Both ends of each girder were loaded until failure. Two of the beams were cast with Grade 2 HPC

and two were cast with Grade 4 HPC. The Grade 2 HPC had a design compressive strength of 10,000 psi (69.0 MPa) and an experimental average of 13,430 psi (92 MPa) at 56 days. The Grade 4 HPC had a design compressive strength of 14,000 psi (96.5 MPa) and obtained a 56 day mean strength of 16,106 psi (111 MPa). The research found that when the embedment length (distance from the end of the girder to the point load) was less than 80 in., all girders experienced extensive shear cracking and bond failures with strand slip greater than 0.10 in. When embedment lengths were greater than 80 in., ductile, flexure failures resulted with good bond performance and end slip less than 0.05 in. Despite the difference in the two grades of concrete, it was found that the bond characteristics were similar. The development length of the strands for the Type II girders, independent of compressive strength, was 80 in. Dill and Kahn (2000) compared the experimental results with many prediction equations and found four that were considered to be most appropriate. The four equations were the AASTHO Standard (1996), ACI 318-99, Zia and Mostafa (1977), and Lane (1998); these equations are listed in Table 2.3. The Zia and Mostafa equation gave the best prediction of the actual development length, even when the actual concrete strength was used (Zia and Mostafa had proposed that f_c' be limited to 8,000 psi). The AASHTO and ACI equation for development length was independent of concrete compressive strength. However, it still provided a good, fairly conservative prediction of development length. Both Lane equations also gave good, slightly conservative predictions when the concrete strengths were limited to 10,000 psi, as recommended by Lane.

Table 2.3 Summary of development length equations (Dill and Kahn 2000)

Source	Development Length Expression	Grade 2 Pred./Exp.	Grade 4 Pred./Exp.	Equation
AASHTO and ACI	$l_d = \left(f_{ps} - \frac{2}{3} f_{se} \right) D$	1.2	1.2	(1.11)
Zia and Mostafa	$l_d = \left(1.5 \frac{f_{si}}{f'_{ci}} D - 4.6 \right) + 1.25 \, (f_{su} - f_{se}) \, D$	1.12	1.1	(1.12)
Lane (95% confidence) with f'c limited to 10,000 psi	$l_d = \left(\frac{4 f_{pt} \, D}{f'_c} D - 5 \right) + \left(\frac{6.4 (f_{su} - f_{se}) D}{f'_c} + 15 \right)$	1.21	1.21	(1.13)
Lane (Mean) with f'c limited to 10,000 psi	$l_d = \left(\frac{4 f_{pt} \, D}{f'_c} D - 21 \right) + \left(\frac{6.4 (f_{su} - f_{se}) D}{f'_c} + 26 \right)$	1.15	1.15	(1.14)

where:

D: Prestressing strand diameter
ES: Prestress loss due to elastic shortening
f_c': Concrete compressive strength at 56 days
f_{ci}': Concrete compressive strength at release
f_{ps}: Stress in the prestressing strand at nominal strength
f_{pt}: Stress in prestressing strand prior to transfer
f_{se}: Effective stress in the prestressing strand after allowance for all prestress losses
f_{si}: Stress in the prestressing strand immediately after transfer (f_{pt} − ES)
f_{su}: Stress in the prestressing strand at ultimate strength
l_d: Development length

These development length findings and equations were used to predict the embedment lengths for the BT-56 girder shear tests.

2.3 Prestress Losses

2.3.1 Definition of Prestress Losses

The loss of prestress was defined in the Precast/Prestressed Concrete Institute (PCI) Design Handbook (1999) as the reduction of tensile stress in prestressing strands due to shortening of the concrete around the strands, relaxation of the strand stress, and external factors which reduce the total initial force before it is applied to the concrete. The sources of loss of prestress that must be considered for the design of pretensioned concrete member are identified by the AASHTO specification as follows:

1. Elastic shortening of concrete
2. Creep of concrete
3. Shrinkage of concrete
4. Relaxation of tendons

Losses could be estimated in a number of different ways. The calculated losses depended on the strength and stiffness of the concrete, the temperature of the member during and after curing, the force in the prestressing strands, the type of strands, and the type of prestressing jacks used for tensioning. Because of the many variables, it was difficult to say which prediction equations better predicted prestress losses.

Some design specifications provided conservative design predictions of prestress losses in all types of concrete members. Canfield (2005) concluded that the AASHTO Standard (2002) and AASHTO LRFD (2004) Specifications were two methods that were conservative and good for design. However, extensive research on different types of

concrete in different applications was necessary in order to obtain job-specific prestress loss equations (Shams and Kahn, 2000).

2.3.2 Prestress Loss Research

Research on prestress losses was performed by Shams and Kahn (2000) on four AASHTO Type II girders and six 9 in. x 18 in. x 14 in. beams over a period of one year. Half of the specimens were Grade 2 HPC and the other half were Grade 4 HPC. The Type II girders in this study were the same girders used in the transfer and development length studies previously mentioned (Reutlinger and Kahn, 1999). The research found that the AASHTO-LRFD (1998) specifications and the PCI Design Handbook (1999) were very conservative when predicting the losses. The research also found that the step-function method and the time-step analysis predicted the time-dependant responses of HPC pretensioned beams within ± 10 percent. As the concrete compressive strength increased, the initial and time dependant prestress losses and cambers decreased. It was also determined that precast HPC beams with $f_c' > 10{,}000$ psi (69.0 MPa) exhibited approximately 50 percent less time-dependant prestress losses than those of precast beams made of conventional concrete. The report proposed new prediction equations based on the data used in the study. The details of the prestress-loss research can be found in "Time-Dependant Behavior of High Performance Concrete" by Shams and Kahn, (2000).

2.4 Literature Review

A brief literature review follows. A review of shear tests performed on HPC girders in Georgia is provided, detailing the shear performance of Grade 2, Grade 4, and lightweight HPC in AASHTO Type II girders. It is important to note that the research performed in Georgia was primarily used to determine transfer and development lengths of 0.6-in. diameter prestressing strands in HPC and light-weight HPC. The shear results were secondary, and no pure shear failures occurred. Therefore, the results from the Georgia Research were not used to compare with the results from this report. Shear strength research of HPC girders ranging in size from small laboratory beams to AASHTO PCI Bulb-Tee 72 girders is presented. For comparisons, only specimens that experienced pure shear failures and minimal shear/bond failures were examined. Limited research has been conducted on the pure shear behavior of large HPC girders.

2.4.1 Shear Tests on HPC girders in Georgia

2.4.1.1 Dill and Kahn (2000)

Dill and Kahn (2000) performed a study on the development length of 0.6-in. diameter prestressing strand in high-performance concrete. This was part of Task 5 of the current FHWA-GDOT pooled fund study. Four AASHTO Type II girders were pretensioned with ten 0.6-in. (15mm) diameter, Grade 270, low relaxation, prestressing strands. The main purpose of the study was to examine development lengths of the 0.6-in. (15 mm) diameter prestressing strands in two grades of HPC. The two grades of HPC were Grade 2 and Grade 4 with minimum 56-day design compressive strengths of 10,000

psi (69.0 MPa) and 14,000 psi (96.5 MPa), respectively. The average accelerated cured, 56-day strengths obtained for the Grade 2 and Grade 4 concretes were 13,430 psi (92.6 MPa) and 16,100 psi (111 MPa), respectively. The four 33 ft. long AASHTO Type II girders, two of each HPC grade, were fabricated at Standard Concrete Products (SCP) in Atlanta, GA. Each end of each girder was tested, totaling eight tests.

A full layer of 8 prestressing strands spaced at 2 in. (51 mm) on-center was located in the bottom flange and 2 strands were located at the top. All of the strands were straight, fully tensioned, and fully bonded. They were subjected to a measured jacking stress of 207 ksi (1427 MPa).

A composite deck was placed on each specimen using Grade 1 HPC with an average 56 day strength of 7,740 psi (53.3 MPa). Each deck was 8 in. deep and 30 in. wide, and the deck was placed using shored construction. Figure 2.2 shows the typical cross section and transformed sectional properties of the specimens used.

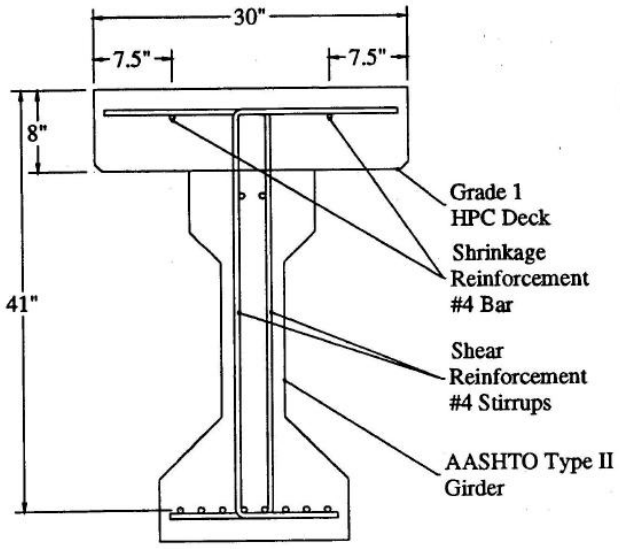

Transformed Sectional Properties		
HPC	Grade 2	Grade 4
$A\ (in^2)$	555	536
$I\ (in^4)$	124,180	119,688
y_t (in)	20.1	21.1
y_b (in)	23.9	22.9
$S_t\ (in^3)$	6186	5666
$S_b\ (in^3)$	5191	5232

1 inch = 25.4 mm

Figure 2.2 Typical Cross section and transformed sectional properties for Type II girders (Dill and Kahn, 2000)

In the research, different shear spans and embedment lengths were used to properly bound and understand the development lengths of the specimens. Figure 2.3 shows the different embedment lengths and shear spans used. These lengths were determined by using embedment lengths predicted by various equations studied in the research.

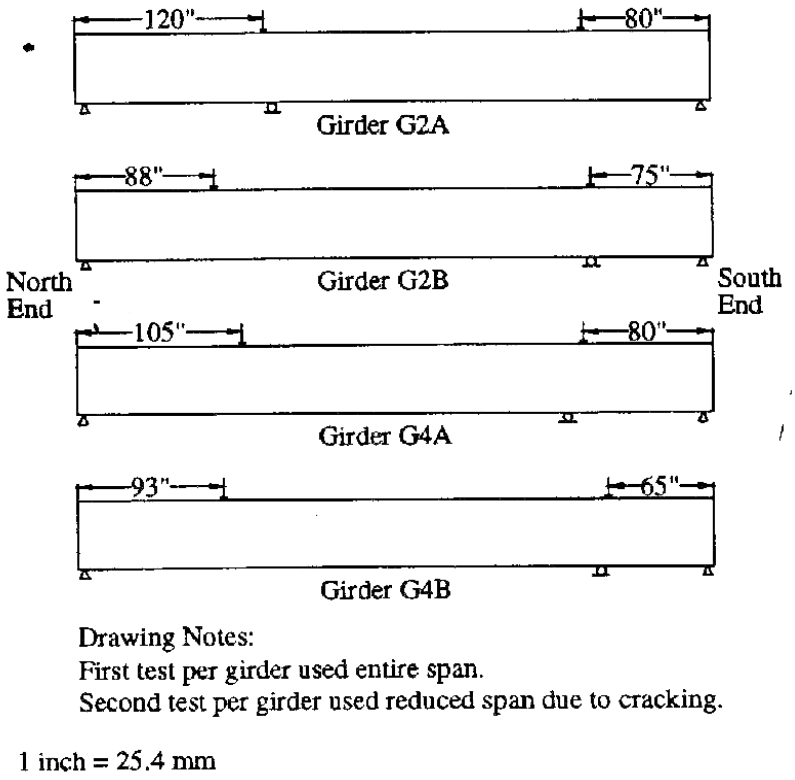

Figure 2.3 Embedment lengths for Type II girders (Dill and Kahn, 2000)

For each grade of HPC, the shear reinforcement at one girder end was based upon the standard details of the Georgia Department of Transportation. The spacing of the remaining shear reinforcement was based on the predicted nominal strength required to cause bond failure. The stirrups used were two mirrored C-shaped # 4 bars. The shear

reinforcement was designed to prevent a shear failure at the beam end regions and promote a flexural or bond failure. Figure 2.4 shows the shear reinforcement spacing used in the four different specimens.

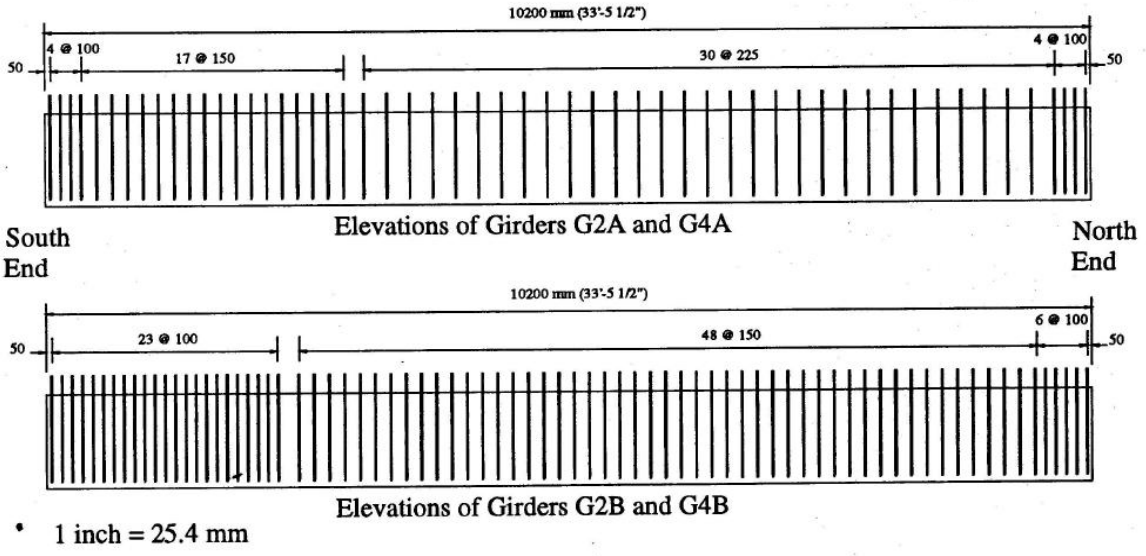

Figure 2.4 Typical shear stirrup spacing in Type II girders (Dill and Kahn, 2000), dimensions in millimeters

All of the specimens experienced different levels of shear cracking, which allowed the AASHTO and ACI equation predicting web shear, $V_{cw,}$ to be compared to the experimental cracking values found. The experimental values were determined by the first visible sign of cracking in each specimen. Table 2.4 provides a summary of the predicted and experimental web shear cracking found by Dill and Kahn (2000). The AASHTO Standard equations for concrete shear strength are given in Equations 2.1 and 2.2.

$$V_{cw} = (3.5\sqrt{f'_c} + 0.3 f_{pc}) b_w d + V_p \quad (2.1)$$

$$V_{ci} = 0.6\sqrt{f'_c} b_w d + V_d + \frac{V_i M_{cr}}{M_{\max}} \quad (2.2)$$

Where,

b_w = Web width

d = Distance from extreme compression fiber to centroid of longituindal tension reinforcement, but need not be less than 0.80h for prestressed members

f'_c = Specified compressive strength of concrete, psi

f_{pc} = Compressive stress in concrete at centroid of cross section resisting externally applied loads at the centroid of the composite section.

M_{cr} = Moment causing flexural cracking at section due to externally applied loads

$M_{\max}$ = Maximum factored moment at section due to externally applied loads

V_{ci} = Nominal shear strength provided by concrete when diagonal cracking results from combined shear and moment.

V_d = Shear force at section due to unfactored dead load

V_p = Vertical component of effective prestress force at section

Table 2.4 Summary of web shear cracking (Dill and Kahn, 2000)

		Predicted	Experimental
Test	Shear Span	V_{cw}*	V_{cw}
(units)	(inches)	(kips)	(kips)
G2A North	114	150	177.1
G2A South	74	158	209.8
G2B North	82	150	191.3
G2B South	69	150	211.0
G4A North	101	158	178.8
G4A South	74	158	177.1
G4B North	89	158	178.5
G4B South	61	158	251.3

* Values taken at one half the shear span, AASHTO Standard and ACI Method.

1 inch = 25.4 mm

1 kip = 4.448 kN

All eight tests experienced some level of shear cracking, and the cracking shears were all conservatively predicted by the AASHTO Standard specifications. On average, the predicted cracking shear, $V_{cw,}$ was 30% lower than the actual cracking shear for the Grade 2 HPC, and 25% lower for the Grade 4 HPC.

Of the eight tests performed, only three demonstrated an ultimate shear failure. The three specimens that experienced shear failures were G2B South, G4A South, and G4B South. The shear spans for these three specimens were 69 in., 74 in., and 61 in., respectively. The embedment lengths for the pretensioned strands in these specimens were 75 in., 80 in., and 65 in., respectively. These shear spans were conducive to shear failures, and the embedment lengths were all well short of the required development length of 96.2 in. based on the AASHTO and ACI codes. All three of the shear controlled specimens experienced a significant amount of strand slip and bond failure. G2B South, G4A South, and G4B South experienced 0.40 in., 0.31 in., and 0.27 in. slip, respectively. The rest of the tests on the Type II girders failed in flexure; embedment lengths were adequate to reach the ultimate strength, f_{ps}, of the strands. Because of the bond failure, the predicted ultimate shear strengths based on the ACI 318-99 and AASHTO LRFD (1998) Specifications for the three specimens that failed in shear were higher than the actual values, causing unconservative predictions. The ACI method gave shear strengths that over-predicted the actual shear capacity for the Grade 2 HPC by 15 percent and the Grade 4 HPC by 18 percent. The AASHTO LRFD method predicted values that were, on average, 16.5 percent higher than the actual shear capacity for the Grade 2 HPC, and 5.6 percent higher for the Grade 4 HPC. The actual strengths were controlled by bond failure, and the full shear capacities of the girders were not developed.

Table 2.5 shows a summary of all eight tests detailing mode of failure and code equation accuracy.

Table 2.5 Summary of applied shear and shear resistance (Dill and Kahn, 2000)

			ACI Method		AASHTO Method	
Test ID (Units)	Shear Span (in)	V_{exp} (kips)	V_n (kips)	$\frac{Vexp}{V_n}$	V_n (kips)	$\frac{Vexp}{V_n}$
G2A North	114	182	267	0.68	224	0.81
G2A South	74	286	334	0.86	294	0.97
G2B North	82	262	326	0.80	317	0.83
G2B South	69	293	346	0.85*	351	0.83*
G4A North	101	215	275	0.78	211	1.02**
G4A South	74	254	334	0.76*	299	0.85*
G4B North	89	242	334	0.72	331	0.73
G4B South	61	329	372	0.88*	317	1.04***

* Shear failure occurred at less load than calculated capacity. (unconservative)
** AASHTO incorrectly predicts shear failure.
*** AASHTO correctly predicts shear failure.
1 inch = 25.4 mm
1 kip = 4.448 kN

A final point of research for the shear behavior of the AASHTO Type II girders was the crack inclination and number of stirrups crossed by the diagonal shear cracks. All predicted values of crack inclination assumed a shear failure which occurred at the maximum observed experimental load. The crack angles were predicted by using the variable angle truss model and assuming that the entire shear force was carried by the stirrups and that all stirrups were yielding. On average, the predicted crack angles were within ±10 percent of the actual, observed crack angles. The data for the crack angles are presented in Table 2.6.

Table 2.6 Crack inclination and number of stirrups crossed (Dill and Kahn, 2000)

	s (in)	Experimental θ (deg.) (Crack angle)	Experimental # of stirrups crossed	Predicted* θ (deg.) (Crack angle)	Predicted* # of stirrups crossed	$\theta_{exp}/\theta_{pred}$
G2A-N	9	31.1	4.2	31.0	6.2	1.00
G2A-S	6	33.1	8.0	30.2	9.6	1.10
G2B-N	6	30.6	7.2	32.3	8.8	0.95
G2B-S**	4	38.2	9.8	40.3	9.8	0.95
G4A-N	9	33.5	4.8	27.2	7.2	1.23
G4A-S**	6	32.9	8.0	33.2	8.5	0.99
G4B-N	6	30.0	8.0	34.3	8.2	0.87
G4B-S**	4	41.8	8.7	37.2	11.0	1.12

* Based on maximum experimental shear, and assumes all shear carried by stirrups.
** Shear/Bond failure
1 in. = 25.4 mm

2.4.1.2 Meyer, et al. (2002)

Meyer, et al. (2002) performed a study on the behavior of lightweight high performance concrete in prestressed bridge girders. The research provided an analytical investigation of High Strength Lightweight Concrete (HSLC) for pretensioned bridge girders. After the analytical study was completed, trial concrete mixtures were designed and tested to obtain optimal lightweight concrete that could be used in girder test specimens. Six AASHTO Type II girders made with HSLC were used in this research. They were designed to be tested at both ends and at the center. The center tests were designed to provide an additional test for each girder, and to determine the shear characteristics of the girders with full development of the prestressing strands. The transfer length, development length, flexural capacity, and shear capacity were examined.

The prestressing strands used were 0.6-in. diameter, 270 ksi, 7-wire low relaxation strands provided by Insteel. As with the research performed by Dill and Kahn (2000), 8 strands were placed in a single bottom row, with two more being placed in the top of the girders. All strands were initially stressed to 0.75*fpu, or 202.5 ksi.

The HSLC that was used in the laboratory girders had 56 day design concrete compressive strengths of 8,500 psi (58.6 MPa) and 10,000 psi (68.9 Mpa). The actual beam concrete had average 56 day accelerated cured strengths of 9,245 psi (63.7 MPa) and 10,750 (74.1 MPa). The girders were labeled G1 and G2 for the 8,500 and 10,000 psi mixtures, respectively.

Composite decks were placed on the six girder specimens to increase the moment arm in the girders. Increasing the moment arm, "jd", not only caused a higher strain in the prestressing steel, but also emulated the actual conditions found in existing bridge structures. Each composite deck was 11.5 in. thick and 19 in. wide.

The shear reinforcement spacing used in this research varied based on different conditions of the research. The stirrups used were two mirrored C-shaped # 4 bars at various spacings throughout each girder. Three different shear stirrup configurations were used for the three G1 girders, and the same three configurations were used for the three G2 girders.

There were a total of 18 tests performed on the Type II girders; 9 on each grade of concrete. The shear spans and embedment lengths were placed at approximately 70 percent, 85 percent, 95 percent, and 100 percent of l_d where l_d was determined by the 1996 AASHTO Standard Specifications. The point at which the failure transitioned from a shear/bond failure to a flexural failure was the point at which the strand was considered

fully developed. The girder test configurations for all 9 tests are presented in Table 2.7. L_1 was the total span length, L_2 was the cantilevered section that occurred after the first two tests were performed, and L was the total girder length.

Table 2.7 Girder test configurations (Meyer et al., 2002)

Test Configuration	Stirrup Density	Point Load Placement Criteria	Shear Span "a" (inches)	Distance "L_1" (inches)	Distance "L_2" (inches)	Distance "L" (inches)
1	Single	l_d	90	456	0	456
2	Double	$0.70*l_d$	61	316	0	456
3	Double	$0.85*l_d$	75	456	0	456
4	Single	$0.95*l_d$	85	504	0	504
5	Single	$0.70*l_d$	61	321	0	456
6	Single	$0.85*l_d$	75	369	0	504
7	Minimum	a/d=2.28	82	185	140	456
8	Minimum	a/d=2.67	96	210	135	456
9	Minimum	a/d=3.33	120	244	135	504

d = 47.5 inches

The shear results were compared to the prediction equations given by the AASHTO Standard Specifications (1996), the ACI Alternate approach, which is detailed in Chapter 6.2.2, and the AASHTO LRFD Specifications (1998). Another tool used in this research was the Variable Angle Truss Model (VATM), which was used to determine the force in the bottom strands near the girder ends to determine the bond stress. It is important to note that all the prediction equations were calculated using the lightweight concrete factor, λ, equal to 0.85, to account for the natural sand-lightweight aggregate.

The initial cracking shears were obtained from close examination of the girders at the time of the test and confirmed by the principle strain plots. Table 2.8 gives an overview of all cracking tests performed on the girders. The cracking shears predicted by

each method were conservative by varying amounts, depending on the shear span and stirrup spacing. The ACI alternate method seemed to most closely predict the concrete cracking shear, V_{cw}. The AASHTO Standard specification conservatively predicted V_{cw} to be 26.2 percent less than the experimental value. The LRFD method grossly underestimated the concrete cracking strength by an average of 435 percent. However, the concrete shear contribution determined by the LRFD method was not meant to predict the cracking shear of the girders. It was created to more accurately estimate the total shear capacity, V_n of concrete girders.

Table 2.8 Overview of initial cracking shears (Meyer et al., 2002)

Test #	$V_{c\text{-}EXP}$ Exp. (kips)	V_{cw} AASHTO Standard (kips)	V_{cw} ACI Alternate (kips)	V_c AASHTO LRFD (kips)	Percent Diff. Exp. vs. Standard	Percent Diff. Exp. vs. ACI Alt	Percent Diff. Exp. vs. LRFD
G1A-E *	145.0	104.1	124.0	24.7	39.4%	16.9%	488%
G1A-W	120.0	107.1	127.5	26.3	12.1%	-5.9%	356%
G1A-C *	134.0	98.5	118.0	23.5	36.1%	13.6%	470%
G1B-E *	140.0	105.5	125.5	24.7	32.7%	11.6%	466%
G1B-W	141.2	103.9	123.6	24.3	35.9%	14.2%	482%
G1B-C *	136.1	98.9	118.4	25.0	37.6%	14.9%	445%
G1C-E *	123.5	101.5	120.7	23.6	21.7%	2.3%	423%
G1C-W	134.2	104.0	123.3	23.6	29.0%	8.8%	468%
G1C-C	94.0	96.7	115.8	24.6	-2.8%	-18.8%	282%
G2A-E	178.6	114.4	135.7	26.0	56.1%	31.6%	588%
G2A-W	157.3	118.1	139.5	28.8	33.2%	12.8%	447%
G2A-C *	140.0	109.4	130.6	25.0	27.9%	7.2%	460%
G2B-E	163.1	114.6	136.1	25.2	42.3%	19.8%	549%
G2B-W	148.0	117.4	138.7	25.8	26.1%	6.7%	473%
G2B-C *	120.4	110.5	131.9	25.2	9.0%	-8.7%	377%
G2C-E	143.4	112.0	133.0	25.6	28.1%	7.8%	461%
G2C-W	122.4	113.4	134.2	27.1	8.0%	-8.8%	352%
G2C-C	107.0	107.3	128.1	31.3	-0.2%	-16.5%	241%
G1 Avg	129.8	102.2	121.9	24.5	26.8%	6.4%	431%
G2 Avg	142.2	113.0	134.2	26.7	25.6%	5.8%	439%
G1 Std Dev					14.1%	11.9%	68.9%
G2 Std Dev					17.8%	15.2%	104.1%

* Girder failed in shear at ultimate as primary or secondary failure mode

Where : $$\text{Percent difference} = \frac{\text{Exp.} - \text{Pred.}}{\text{Pred.}}$$

Figure 2.5 shows the concrete cracking shear strength, $V_{c\text{-}Exp,}$ versus the stirrup spacing to determine concrete cracking strength with different amounts of shear reinforcement. The results show that the $V_{c\text{-}Exp}$ is higher when there is more shear reinforcement in the girders. It was determined that there was an apparent ceiling existing for the tensile strength of the HSLC because both grades converged. Meyer, et al. (2002) determined that the V_c values at the maximum stirrup spacing truly reflected the concrete shear capacity of the girders.

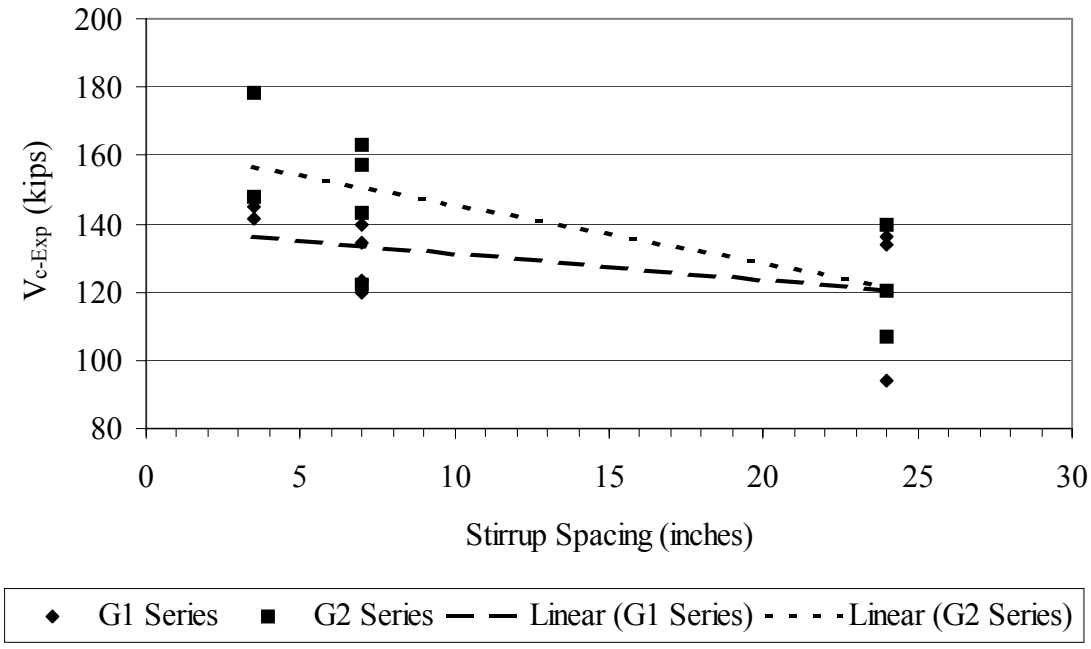

Figure 2.5 Concrete shear strength, V_c versus stirrup spacing (Meyer et al., 2002)

The cracking shear was further investigated by obtaining a normalized tension strength factor, $\xi_{t,}$ for the different girders. The value was obtained from the ACI alternate method, which specifies a diagonal principle tensile strength of $4\lambda\sqrt{f'_c}$ and a specified diagonal tension factor, $\xi_{t,}$ of 4. The experimental diagonal tension stress was back calculated using the experimental shear capacity, V_c. Then, a normalized diagonal tension strength factor was obtained to compare to the ACI alternate method. Table 2.9 shows the diagonal tension strength factors and Figure 2.6 plots the tension factors vs. stirrup spacing. The horizontal line in the graph represents the ACI recommended strength factor.

Table 2.9 Normalized diagonal tension strength factors, ξ_t (Meyer et al., 2002)

Test #	Stirrup Spacing (inches)	ACI Alternate Predicted Diagonal Tension Strength $f_{t\text{-}Pred}$" (psi)	Experimental Diagonal Tension Strength $f_{t\text{-}Exp}$" (psi)	Normalized Diagonal Tension Strength Factor ξ_t
G1A-East	3.5	333	415	4.99
G1A-West	7	333	304	3.66
G1A-Center	24	333	396	4.76
G1B-East	7	333	389	4.67
G1B-West	3.5	333	402	4.83
G1B-Center	24	333	404	4.85
G1C-East	7	321	332	4.14
G1C-West	7	321	363	4.52
G1C-Center	24	321	238	2.96
G2A-East	3.5	356	525	5.89
G2A-West	7	356	424	4.77
G2A-Center	24	356	393	4.41
G2B-East	7	356	461	5.18
G2B-West	3.5	356	392	4.40
G2B-Center	24	356	312	3.51
G2C-East	7	349	389	4.46
G2C-West	7	349	304	3.49
G2C-Center	24	349	268	3.17

G1 Average	3.5	409	4.91
G2 Average	3.5	459	5.15
G1 Average	7	347	4.25
G2 Average	7	395	4.48
G1 Average	24	346	4.19
G2 Average	24	324	3.70

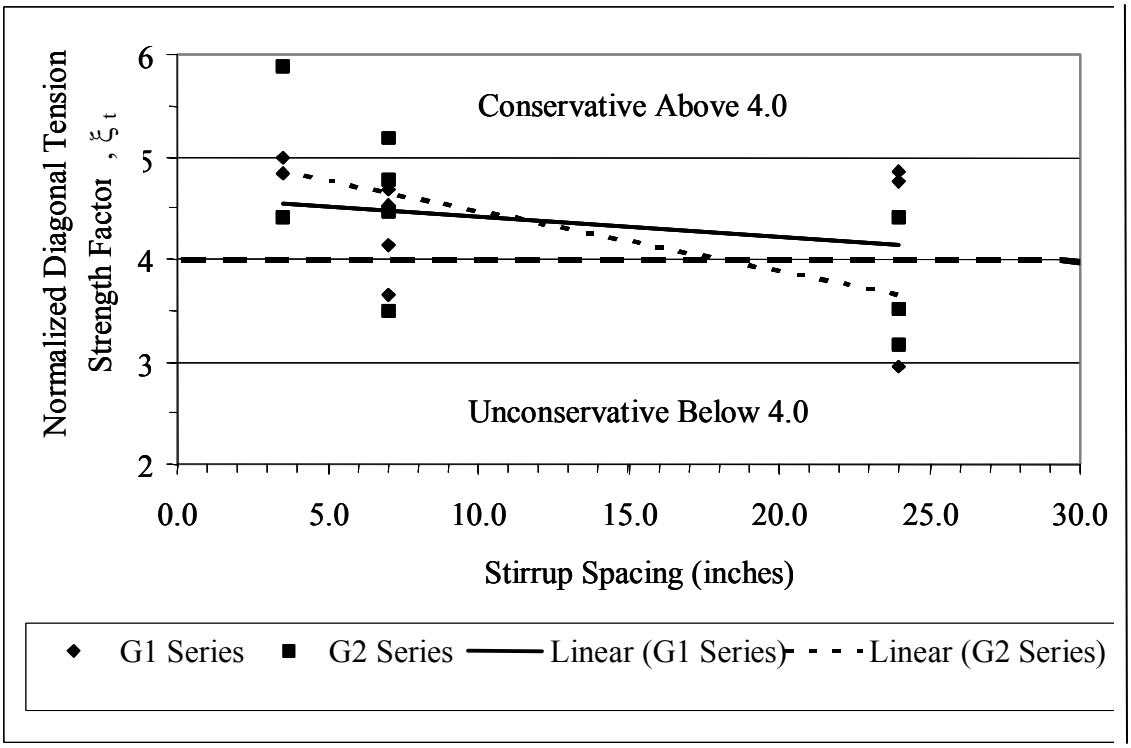

Figure 2.6 Diagonal tension strength factor, ξ_t vs. stirrup spacing (Meyer et al., 2002)

Table 2.10 provides the ultimate shear capacity obtained by the girder tests that experienced shear, shear slip, or shear-flexure as their primary mode of failure. It is important to note that the terms V_n and V_u were used interchangeably in this research. The table shows that the AASHTO Standard technique produced conservative results overall. It predicted values 52 percent lower than experimental values for the Grade 1 concrete and values 68 percent lower for the Grade 2 concrete. Limiting the yield strength to 60 ksi caused the prediction to be even more conservative. Because of the large stirrup spacing for the center tests, the AASHTO LRFD Specification predicted an ultimate shear strength capacity that was much less than the experimental shear strength. It penalized the girders with large stirrup spacing by providing very low concrete shear contributions, which caused the overall predictions to be up to 211 percent lower than the

experimental shear values. The LRFD Specification seemed to predict shear capacities very similar to the Standard Specification when the stirrup spacing was closer. Figure 2.7 shows the normalized ultimate shear capacity versus stirrup spacing to better show how the Standard and LRFD Specifications differ.

Table 2.10 Predicted vs. experimental ultimate shear values (Meyer et al. 2002)

Test #	AASHTO Standard f_y = 62 ksi V_u (kips)	AASHTO Standard f_y = 60 ksi V_u (kips)	AASHTO LRFD f_y = 62 ksi V_u (kips)	Exp. V_u (kips)	Percent Diff. Exp vs Std 62	Percent Diff. Exp vs Std 60	Percent Diff. Exp vs LRFD
G1A-Center	138.7	137.4	103.8	258.0	86.0%	87.8%	148.5%
G1B-East	243.3	238.9	241.1	312.2	28.3%	30.7%	29.5%
G1B-Center	138.6	137.3	104.3	234.1	68.9%	70.5%	124.5%
G1C-East	238.4	234.0	255.5	289.2	21.3%	23.6%	13.2%
G2A-Center	149.5	148.2	82.3	255.9	71.2%	72.7%	211.0%
G2B-Center	150.9	149.6	102.7	246.3	63.2%	64.6%	139.9%
G1 Average					51.1%	53.2%	78.9%
G2 Average					67.2%	68.7%	175.5%
G1 Std Dev					31.3%	31.0%	67.5%
G2 Std Dev					5.7%	5.7%	50.3%

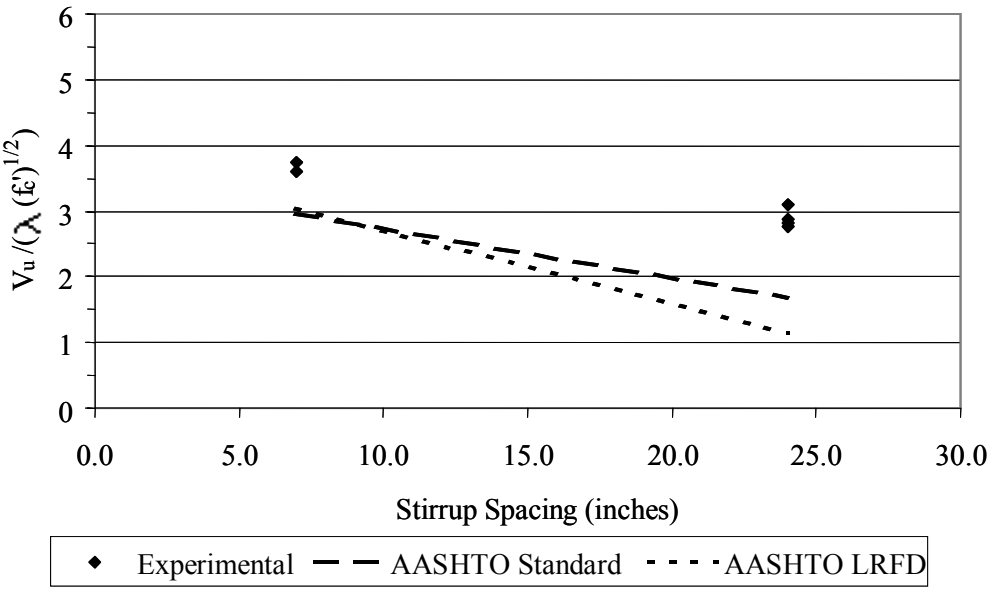

Figure 2.7 Normalized ultimate shear capacity, V_u, vs. stirrup spacing (Meyer et al., 2002)

The variable angle truss model was another method used by Meyer, et al. (2002) to estimate the shear capacity of the HSLC girders. The VATM predicted values 35 percent lower than experimental values for the tests that did not have the 24 in. spacing. The tests that did have the larger spacing were extremely conservative because the VATM did not take into account the concrete contribution to shear strength. Table 2.11 shows the results for the VATM.

Table 2.11 Variable angle truss model results (Meyer et al., 2002)

Test #	VATM V_n (kips)	Experimental V_n (kips)	Percent Difference Experimental vs. VATM
G1A-Center	49.6	258.0	420.1%
G1B-East	223.2	312.2	39.9%
G1B-Center	49.6	234.1	372.0%
G1C-East	223.2	289.2	29.6%
G2A-Center	49.6	255.9	416.0%
G2B-Center	49.6	246.3	396.6%

G1 Average	215.4%
G2 Average	406.3%

In all, Meyer, et al. (2002) found that the AASHTO Standard Specifications provided a conservative prediction of the lightweight concrete and ultimate shear capacity when the shear steel capacity was capped at a yield stress of 60 ksi. The ACI-Alternate design procedure listed in ACI 318 Section 11.4.2.2 for predicting shear strength produced some unconservative predictions for concrete compressive strengths over 10,000 psi. It was also found that the AASHTO LRFD Specifications provided a conservative prediction of ultimate strength. The VATM provided an overconservative prediction of the shear capacity in HSLC.

2.4.2 Shear Tests on HPC Girders

2.4.2.1 Elzanaty, et al. (1986)

Elzanaty, et al. (1986) performed tests on 34 pretensioned beams. Eighteen were constructed without stirrups, and 16 were constructed with stirrups. The concrete

strength in these girders ranged from 6,000 psi (41.4 MPa) to 11,400 psi.(78.6 MPa). The girders tested in the research were small scale specimens shaped like PCI Bulb-Tees and AASHTO Type I girders. The bulb-tee shaped specimens were 14 in. tall, with a 20 in. wide top flange. The Type I shaped girders were 18 in. tall with 8 in. wide top and bottom flanges. They were prestressed with 4 0.6-in. or 0.5-in. diameter low relaxation seven wire Grade 270 strands. The primary goal of the research was to investigate the effect of concrete strength on the shear strength of prestressed concrete beams and to compare the test results with the 1983 ACI code provisions for shear.

For the tests performed on beams without stirrups, it was found that the ACI equations for both web shear, V_{cw}, and flexure-shear, V_{ci}, were adequately conservative. The research found that as the concrete compressive strength, f_c', increased, the ratio of test-to-predicted values increased (became more conservative) for the web-shear cracking, and decreased (less conservative) for the flexure-shear cracking. The research also found that as the shear span to depth ratio, a/d, increased, the ratio of test-to-predicted values decreased for both web and flexure shear. The ratios for the amount of prestressing and non-prestressed reinforcement were found to have no effect on web shear, V_{cw}. However, as both ratios decreased, so did the flexure-shear, V_{ci}.

For the tests performed on beams with stirrups, it was found that the ACI equations, although slightly inconsistent, predicted conservative values for both web and flexure shear. It was found that stirrups had no effect on the diagonal cracking loads; meaning that a beam with or without stirrups will begin to crack at the same load. The amount of horizontal reinforcement, both prestressed and non-prestressed, increased the shear strength of the beams. The shear strength increased as the shear reinforcement

increased. The ACI code shear design provisions underestimated the effect of increasing the shear reinforcement for diagonal tension failures and overestimated the effect of increasing shear reinforcement for shear compression failures. Table 2.12 shows a summary of the results obtained for the beams with shear reinforcement. The results for the beams with no stirrups are not presented because it was determined by Elzanaty, et al. (1986) that stirrups made no difference in the initial diagonal cracking of prestressed HPC beams. The CW beams experienced web shear failure, and the CI beams experienced shear flexure. The data from this test were referenced by Shahawy and Cai (1999) and compared to both AASHTO Standard (1996) and ACI 318-99 and to AASHTO LRFD (1998). Data from this comparison are presented in Table 2.15 in the Shahawy and Cai (1999) literature section.

Table 2.12 Test results of prestressed test beams with stirrups (Elzanaty, et al., 1986)

Beam	f_c', psi	P_e, kips	a/d	Shear Reinforcement	$V_{c,\,test}$, kips†	$V_{c,\,ACI}$, kips	$\frac{V_{c\,test}}{V_{c\,ACI}}$	V_u, test	$\frac{V_{utest}}{V_{nACI}}$	Stirrup effectiveness	Concrete effectiveness
(a) CW series											
CW10	10600	98.8	3.8	# 3 at 10 in.	24.4	20.3	1.2	39	1.32	1.56	1.46
CW11	8100	96.4	3.8	# 3 at 10 in.	21.5	18.8	1.15	35.2	1.25	1.46	1.38
CW12	5800	96.8	3.8	# 3 at 10 in.	19.2	17.4	1.1	31.6	1.18	1.32	1.28
CW13	10500	135.8	3.8	# 3 at 10 in.	27.6	24	1.15	41	1.23	1.46	1.32
CW14	10700	137.2	3.8	# 3 at 7 in.	27.8	24.2	1.15	42.2	1.12	1.08	1.19
CW15	10200	97.3	3.8	# 3 at 10 in.	22.6	19.9	1.13	33.8	1.15	1.19	1.22
CW16	10600	136.4	3.8	# 3 at 10 in.	27.5	24.1	1.14	42	1.25	1.54	1.35
CW17	10100	136.7	3.8	# 2 at 10 in.	27.7	23.9	1.16	32	1.14	1.23	1.19
(b) CI series											
CI10	10600	98.9	5.8	# 3 at 8 in.	18.8	16.3	1.16	31.8	1.32	1.65	1.47
CI11	8100	96.8	5.8	# 3 at 8 in.	18	15.5	1.17	28.6	1.23	1.34	1.34
CI12	5800	97.2	5.8	# 3 at 8 in.	18.6	14.9	1.25	27.5	1.21	1.13	1.31
CI13‡	10500	135.4	5.8	# 3 at 8 in.	18	20.7	0.87	34.8	1.22	1.18	1.3
CI14	10700	137.8	5.8	# 3 at 5 in.	24.2	21	1.15	37	1.1	1.02	1.16
CI15	10200	97.4	5.8	# 3 at 8 in.	17.6	16	1.1	27.2	1.14	1.22	1.21
CI16	10600	136.8	5.8	# 3 at 8 in.	26.3	20.9	1.26	36.7	1.28	1.32	1.38
CI17	10100	136.5	5.8	# 2 at 8 in.	25.5	20.7	1.23	29.1	1.2	1.34	1.27

Note: All beams with stirrups had three # 3 reinforcing bars except CI16 and CW 16 which had three # 7. All beams of CW series had a/d = 3.8, while all beams of CI series had a/d = 5.80

* 1000 psi = 6.895 Mpa

† 1 kip = 4.448 kN

‡ This beam had an accidental deficiency in diagonal cracking load. An average value of Vci = 25.5 kips based on test results of beams of CI series was assigned to the beam.

2.4.2.2 Hartmann, Breen and Kreger (1988)

Hartmann, et al. (1988) provided a comprehensive study of the shear strength of high performance concrete (HPC) girders. The ten specimens tested were Texas 18 in. girders shaped similarly to AASHTO Type I girders. The girders were designed to have 1.3 times the amount of flexural capacity to guarantee an ultimate shear failure. The concrete used for all girders had a design compressive strength of 12,000 psi (82.7 MPa). Actual f_c' values are given in Table 2.13. The beams were constructed with different numbers of 3/8 in. diameter Grade 270, seven wire, low relaxation prestressing strands.

Series 1 girders had 6 straight strands, Series 2 girders had 17 straight strands, and Series 3 had 13 straight strands with four of them draped.

Six of the specimens had high strength monolithically cast decks while the other four had normal strength composite decks with an average strength of 4,325 psi. The primary variable was the amount of shear reinforcement provided. Series 1 girders were designed with the minimum amount of shear steel reinforcement to better understand the actual concrete shear behavior. They also contained only one layer of prestressing strands placed at the bottom of each specimen. Series 2 was designed with extremely heavy shear reinforcement. These specimens were designed to exceed the amount of shear reinforcement allowed by the code to determine if the levels could be raised for use with high strength concrete. Series 3 girders were designed to check intermediate behavior. Two of the specimens had the current AASHTO/ACI maximum reinforcement of $V_s = 8\sqrt{f_c'}b_w d$. The other two specimens contained an intermediate level of shear reinforcement.

The research found that the ACI code equation for V_{cw} was fairly accurate in three tests, and conservative in the other three tests. The cracking equation for V_{cw} was only compared to Series 1 and Series 2 specimens. Series 3 specimens had already been cracked due to previous flexural testing. The average test-to-predicted value was 1.06 for the six specimens. Table 2.13 shows the cracking and ultimate values for all ten of the tests performed.

In ultimate strength predictions, the research found that the ACI provisions were generally conservative. The lowest prediction value for the 10 specimens was only 2 percent below the actual strength. The data showed that as the ratio of shear

reinforcement increased, the conservative nature of the code provisions decreased. The Series 2 specimens, which were reinforced above the code maximum at $V_s = 12\sqrt{f_c'}b_w d$ and $V_s = 15\sqrt{f_c'}b_w d$, showed that the ACI prediction equations became unconservative. When the code maximum of $V_s = 8\sqrt{f_c'}b_w d$ was used in the Series 3 specimens, the predicted values were conservative. The Series 3 specimen predictions were calculated at ultimate in two different fashions, which can be seen in Table 2.13. The first prediction, labeled ACI 1, followed all code allowances, including the d = 0.8h recommended for the effective depth. The V_c calculations used are shown in Equations 2.1 and 2.2. The total shear capacity, V_n, was determined using Equation 2.3.

$$V_n = V_c + \frac{A_v f_y d}{s} \qquad \text{(kips)} \qquad (2.3)$$

Where,

A_v = Area of shear reinforcement
d = 0.8h
f_y = Actual yield strength of shear reinforcement, not limited to 60 ksi
s = Stirrup spacing at section in question
V_c = Concrete shear strength based on the minimum of V_{ci} and V_{cw}
V_n = Nominal shear strength, according to ACI 318-83

The second method, labeled as ACI 2, used a more detailed approach, which calculated the depth of shear reinforcement based on the centroid of the straight strands in the specimens. The detailed method also added a concrete shear strength term to account for the composite deck. The detailed method is shown in Equation 2.4. Actual steel stirrup yield stresses were used in all V_s calculations, even when they exceeded 60 ksi. Actual concrete strengths were also used and not limited to 10,000 psi. It was found

that the detailed method was more accurate, but that the ACI recommended method was adequate and conservative.

$$V_n = (3.5\sqrt{f_c'} + 0.3f_{pc})b_w d + V_p + 2\sqrt{f'_{cd}}\, b_w d + \frac{A_v f_y d}{s} \quad \text{(kips)} \qquad (2.4)$$

Where,

A_v = Area of shear reinforcement
b_w = Web width
d = Distance from the extreme compression fiber to the centroid of straight strands
f_c' = Specified compressive strength of concrete, psi
f'_{cd} = Concrete compressive strength of the composite deck
f_{pc} = Compressive stress in concrete at centroid of cross section resisting externally applied loads at the centroid of the composite section
f_y = Actual yield strength of shear reinforcement, not limited to 60 ksi
s = Stirrup spacing at section in question
V_p = Vertical component of effective prestress force at section

The ACI 318-83 code provisions were found to be generally conservative for the cracking and ultimate shear capacity of high strength concrete prestressed sections. The equations gave the most accurate results with the least amount of scatter than any of the other methods reviewed. It was also found that as the shear reinforcement approached $V_s = 19.3\sqrt{f'_c}\, b_w d$, the code provisions became slightly unconservative, even for high strength concrete.

Table 2.13 Test results and AASHTO/ACI predictions for current test program

(Hartmann, Breen and Kreger, 1988)

Specimen	f_c' (psi)	Load Stage	Test (kips) (1)	ACI 1* (kips) (2)	(1) / (2)	ACI 2* (kips) (3)	(1) / (3)
1-1	11300	V_c	26.9	23.4	1.15		
		V_u	35.4	23.4	1.51		
1-2	11300	V_c	22.9	23.4	0.98		
		V_u	34.4	25.9	1.33		
1-3	11300	V_c	26.7	23.4	1.14		
		V_u	36.7	27.8	1.32		
2-1	10800	V_c	32.9	33.1	0.99		
		V_u	97.9	93	1.05		
2-2	10800	V_c	32.9	33.1	0.99		
		V_u	106.9	107.9	0.99		
2-3	10800	V_c	35.9	33.1	1.08		
		V_u	104.9	107.9	0.97		
3-1	13000	V_u	64.2	61.2	1.05	64.9	0.99
3-2	13160	V_u	66.2	61.6	1.07	65	1.02
3-3	11500	V_u	42	36.6	1.15	39.5	1.06
3-4	11500	V_u	49.8	36.7	1.36	39.4	1.26
				V_c Avg.	1.06	V_u Avg.	1.08
				V_c std.	0.09	V_u std.	0.11
				V_u Avg.	1.18		
				V_u std.	0.18		

*ACI 1, d = .8h

*ACI 2, d = d_p of straight strands

std. = standard deviation

2.4.2.3 Deatherage, et al. (1994)

An in-depth study of the development length of ½ in., ½ in. special, $^9/_{16}$ in., and 0.6 in. 270 ksi low relaxation strands was conducted in 1989 at the University of Tennessee, Knoxville. The different strands were used in 31 ft. AASHTO Type I

prestressed concrete bridge girders. The initial prestress in all the strands was designed to be 202.5 ksi, or 75 percent of the specified ultimate strength of the strands. The concrete design strength for all of the AASHTO girders at 28 days was 5,000 psi (34.5 MPa); actual strengths varied from 3,780 psi to 5,500 psi. Most of the 40 tests performed exhibited extensive shear and flexure cracking, and 38 of the tests experienced a flexural ultimate failure. Only three of the tests experienced an ultimate shear failure. Data on the shear failures and their comparisons to the 1996 AASHTO Standard and the 1998 AASHTO LRFD codes are presented in the Shahawy and Cai (1999) section in Table 2.16.

2.4.2.4 Tawfiq (1995)

A study performed at Florida State University in 1995 researched the cracking and shear capacities of six 41-ft. long AASHTO Type II high strength concrete girders. The concrete strengths used were 8,000 psi (55.2 MPa), 10,000 psi (68.9 MPa), and 12,000 psi (82.7 Mpa). Composite decks 8 in. deep, and 42 in. wide were placed on all Type II girder specimens. Two girders of each concrete strength were constructed; one with the AASHTO recommended shear reinforcement (R), and one with double that amount (2R). The standard design shear spacing (R) contained two # 4 bars at 6 in. and 12 in. on center. The prestressing strands were all placed in the same configuration, with 18 straight strands. The girders contained four different sizes of 270 ksi low relaxation prestressing strands including $^{3}/_{8}$ in., $^{7}/_{16}$ in., ½ in., and 0.6 in. Two different shear spans were used for the testing. The north end had a shear span of 108 in., and the south end had a shear span of 91 in. The research predicted that the 108 in. length would be

extremely close to the actual development length, and that the 91 in. shear span would be well within the development length.

Most specimens failed due to general bond slip. The north end of the girders with the regular amount of reinforcement experienced the least amount of bond slip of any of the test specimens. Only one of the north end tests experienced a pure shear failure with no strand slip. The south end tests demonstrated extensive strand slipping that caused the codes to over-predict the shear capacity of the girder specimens. It was found that doubling the shear reinforcement was not effective in increasing the shear capacity of the test specimens when the tests were at or inside the development length. If the tests had been performed outside of the development length, the extra shear reinforcement might have been more effective.

The concrete strength was found to have different effects on the shear strength depending on the amount of reinforcing and the actual concrete strength. The six tests with the double reinforcement demonstrated an increase in shear strength with an increase in compressive strength. The six tests with the standard amount of reinforcement showed constant shear strength for the 8,000 psi (55.2 MPa) and 10,000 psi (68.9 MPa) mixes and slightly decreasing shear strength for the 12,000 psi (82.7 MPa) mix. For all tests, there was a total increase in shear strength of 4.7 percent between the 12,000 and 8,000 psi mixtures. When tested inside the development length, the compressive strength was found to have little effect on the shear strength because the compressive strength had little effect on the bond strength.

The amount of steel resisting the shear forces was not critical to the strength of the specimens in this study. The controlling factor became the bond strength of the

prestressed strands in each girder. The specimens were failing because of bond failure rather than web-shear failure. If the mode of failure was bond/shear in the R specimens, then the 2R specimens were guaranteed to experience failure in a bond/shear mode, because of the increased steel shear capacity, V_s.

Table 2.14 shows the experimental shear of each specimen and the resulting code predictions. The ACI 318-89 detailed method and the AASHTO Standard method (1989) were identical at the time of this research. However, ACI had a simplified version for determining the shear strength of the concrete which was used for the ACI values in Table 2.14. The ACI simplified equation for concrete shear strength was given as Equations 2.5 and 2.6.

$$V_c = \left(0.6\sqrt{f'_c} + 700\frac{V_u d}{M} \right) b_w d \qquad \text{(kips)} \qquad (2.5)$$

Where,

$$2\sqrt{f'_c}\, b_w d < V_c < 5\sqrt{f'_c}\, b_w d$$

The ACI code also used the 45° truss model with an upper limit to compute the steel contribution to resisting shear forces.

$$V_s = \frac{A_v f_y d}{s}, \quad \text{where} \quad V_s < 8 b_w d \sqrt{f'_c} \qquad \text{(kips)} \qquad (2.6)$$

All three methods predicted increasing shear strength when the web reinforcement was doubled. The AASHTO and ACI codes both limited the amount of shear carried by the steel stirrups, while the LRFD code limited the total shear capacity. All the codes over-predicted the shear strength of the 2R specimens because of the bond failure. For the regularly reinforced specimens, the AASHTO LRFD and ACI codes had, on average, test-to-predicted values of 1.12 and 1.04, respectively. The AASHTO Standard code overestimated the shear strength of the R specimens by an average of 11 percent. The ACI simplified method was the most accurate of the three, despite the fact that only one specimen experienced a pure shear failure.

Table 2.14 Test shear and predicted shear values (Tawfiq, 1995)

					Predicted Values			Test Shear/Predicted shear		
Girder	f_c' (psi)	Shear Span (in.)	*Test shear (kips)	Failure	AASHTO 1989 (kips)	ACI (kips)	AASHTO LRFD 1994 (kips)	AASHTO 1989	ACI	AASHTO LRFD 1994
R-8-N	8,150	102	275	BFS	311	263	252	0.88	1.05	1.09
R-10-N	10,130	102	281	FS	320	276	256	0.88	1.02	1.10
R-12-N	11,040	102	277	BFS	327	281	257	0.85	0.99	1.08
R-8-S	8,120	85	300	BWS	310	263	252	0.97	1.14	1.19
R-10-S	9,910	85	297	BWS	320	276	254	0.93	1.08	1.17
R-12-S	11,040	85	274	BWS	326	281	256	0.84	0.98	1.07
2R-8-N	8,150	102	233	BFS	323	276	381	0.72	0.84	0.61
2R-10-N	10,130	102	238	BFS	354	305	410	0.67	0.78	0.58
2R-12-N	11,040	102	277	BFS	367	322	413	0.75	0.86	0.67
2R-8-S	8,120	85	254	BWS	322	276	383	0.79	0.92	0.66
2R-10-S	9,910	85	243	BWS	353	305	414	0.69	0.80	0.59
2R-12-S	11,040	85	285	BWS	367	322	415	0.78	0.89	0.69
							Avg. R	0.89	1.04	1.12
							Avg. 2R	0.73	0.85	0.63

* The test shear was taken at $^h/_2$, per AASHTO 1989
BFS = bond / flexure-shear
BWS = bond / web shear
FS = flexure-shear

Table 2.15 shows the experimental shear of each specimen at the load point so that values obtained from a strut and tie analysis could be obtained. The strut and tie predictions were, on average, 16 percent conservative for the R specimens and 5 percent conservative for the 2R specimens. It is important to note that the test shear was taken at the point load for each test in Table 2.15. In Table 2.14, the test shear was taken at the specified critical section, which was $^{h}/_{2}$.

Table 2.15 Test shear and strut and tie predicted shear (Tawfiq, 1995)

Girder	f'_c (psi)	Shear Span (in.)	Span length (ft.)	Test shear at load (kips)	Predicted Shear (kips)	Test / predicted
R-8-N	8,150	102	40	270	181.3	1.49
R-10-N	10,130	102	40	277	225.4	1.23
R-12-N	11,040	102	40	272	245.6	1.11
R-8-S	8,120	85	28	228	180.6	1.26
R-10-S	9,910	85	28	233	220.5	1.06
R-12-S	11,040	85	28	273	245.6	1.11
2R-8-N	8,150	102	40	296	214	1.38
2R-10-N	10,130	102	40	293	265.9	1.10
2R-12-N	11,040	102	40	270	289.8	0.93
2R-8-S	8,120	85	28	250	213.2	1.17
2R-10-S	9,910	85	28	239	260.2	0.92
2R-12-S	11,040	85	28	281	289.8	0.97
					Average	1.14

2.4.2.5 Shahawy and Batchelor (1996)

Shahawy and Batchelor (1996) tested 20 AASHTO Type II prestressed concrete girders. The girders varied in length from 21 ft. to 41 ft. and contained three different sizes of prestressing. The types of strands used were ½ in., ½ in. special, and 0.6-in. diameter 270 ksi low relaxation strands. The shear reinforcement was two # 4 grade 60 reinforcing bars spaced at 6, 8, and 12 in. from the ends of the girders to the middle, respectively. The amount of shear reinforcement was designed based on the 1989 AASHTO Standard Specifications, and the amounts were varied from that required, to up to 3 times that which was required. All girders had 8-in. thick and 42 in. wide composite decks, and the girders were prestressed in different configurations, depending on the strand diameters. There were no draped strands in these girders, and the number of strands ranged from 13 for the 0.6 in. diameter strands to 18 for the ½ in. diameter strands. The girder concrete had a 28-day compressive strength of 6,000 psi (41.4 MPa).

The research compared the experimental results to the AASHTO Standard Specifications (1989) and found them to be accurate and conservative. When specimens with no reinforcement were tested, the concrete shear strengths were 50 percent higher than AASHTO Standard predictions. As the shear reinforcement ratio increased and the maximum code limits were imposed, the AASHTO Standard Specification requirements became more accurate, closing in on a test-to-predicted value of 1.0. Only when the shear reinforcement was 3 times the amount required did the AASHTO Standard code have a test-to-predicted ratio less than 1.

The test results were also compared to the AASHTO LRFD Specifications (1994). They were found to be inconsistent and not as accurate as the AASHTO Standard

Specifications. When there was no reinforcement in the beams, the tested shear strengths were 2 times higher than the predicted strength given by the LRFD Specifications. When the required amount of reinforcement was used according to the AASHTO Standard Specifications, the LRFD Specifications varied from test-to-predicted values of 2.08 to values of 0.86. For shear reinforcement amounts that were 2 and 3 times the required amount, the LRFD Specification provided test-to-predicted values as low as 0.5 (unconservative).

The research examined the shear span to depth ratio and its effect on the experimental and predicted shear strengths. It was found that the LRFD Specifications overestimated the shear strength for a/d ratios of 1.5 and below, and underestimated the shear strength for a/d ratios of 2.0 and above. As the a/d ratio increased, the LRFD Specifications became increasingly conservative and grossly underestimated the actual shear capacity. The underestimation caused a considerable increase in the shear reinforcement requirements. The AASHTO Standard Specification was slightly conservative and more accurate than the LRFD Specifications at all of the tested a/d ratios. At an a/d ratio of 2.5, the AASHTO Standard Specification equation was accurate and slightly conservative for any amount of reinforcing steel. As the a/d ratio increased, the AASHTO Standard Specifications became increasingly conservative.

The research also studied the concrete cracking shear strength, and its prediction based upon the two specifications. It was determined that the LRFD code grossly underestimated the concrete shear strength, V_c, at a/d ratios of 1.5 and greater. The AASHTO Standard code, however, gave very good predictions of the cracking shear at a/d ratios greater than 2.0.

The data obtained in this study was better represented and compared to the more recent specifications in the report done by Shahawy and Cai, (1999), which is summarized in Section 2.4.2.7. The data based on the more recent specifications are presented in Table 2.17.

2.4.2.6 Cumming, Shield and French (1997)

Cumming et al. (1997) tested two 43 ft. long Mn/DOT 45M sections that were 45 in. deep at the University of Minnesota. A total of four shear tests were performed; one at each end of each girder. These girders were similar in shape to AASHTO Type IV girders. The concrete used had a 28 day design compressive strength of 10,500 psi (72.4 MPa). Girder I was constructed with regular limestone aggregate with a compressive strength of 11,330 psi (78 MPa) and Girder II was constructed with glacial gravel aggregate with microsilica with a compressive strength of 9,315 psi (64 MPa). A 4 ft. wide, 9 in. thick composite concrete deck with a compressive strength of 5,660 psi (39 MPa) was added to each girder. Each girder contained 46 0.6-in. diameter 270 ksi low relaxation prestressing strands on 2-in. centers. Girder ends IA, IB, and IIC had 4 draped and 8 debonded strands while Girder end IID contained 12 draped strands and no debonded strands.

The research compared five different empirical shear capacity methods to the test results. The five models were the ACI 318-95 Simplified Method, the ACI 318-95 Detailed Method (AASHTO 1989), the Modified Compression Field Model (AASHTO LRFD 1994), the Truss Model, and the Modified Truss Model. The Truss Model only accounted for the shear stirrup strength at yield and neglected the concrete shear

contribution with a minimum compression angle of 25°. The Modified Truss Model included an estimation for concrete strength shown in Equation 2.7.

$$V_{cr} = Kf_t b_w d \qquad \text{(kips)} \qquad (2.7)$$

Where,

$$f_t = 2\sqrt{f_c'} \qquad \text{and} \qquad K = \sqrt{1 + \frac{f_{pc}}{f_t}}$$

Shear capacities were calculated for measured and nominal properties. The measured properties did not limit the mild steel reinforcement to 60 ksi, and did not limit the strength of the prestressing strands or concrete strength. The use of measured properties caused slightly more accurate, but less conservative, shear predictions for all four tests.

All five methods proved to be conservative and acceptable for the shear design of prestressed girders. Tables 2.16 and 2.17 show the ratio of tested values to predicted values for the different prediction methods based on nominal and measured properties. The predicted capacities for each method were calculated at the code specified critical section. The critical section was approximately 3 ft. from the center of bearing as determined by the ACI 318-95 code. The 3 ft. critical section was used for all methods except for the AASHTO LRFD Specifications (1994) which specified the length as approximately 4.45 ft.

The difference between IA and IB were simply the different types of stirrups used. End IA used # 4 inverted U stirrups without leg extensions and End IB used # 4 inverted U stirrups with 90° leg extensions running parallel to the axis of the girder. The stirrup leg extensions gave additional strength to the girders that was only accounted for

by the Truss Model. The other codes did not specify the direction of a stirrup hook as long as the bars had sufficient development length. The results indicate, however, that by adding a 90° hook to the bottom of stirrups will create additional shear strength.

Girders IB and IIC were constructed with different types of aggregate to examine aggregate interlock effects on prestressed concrete girders. It was found that the concrete shear strength increased with the more angular aggregate. Therefore, the concrete shear strength, V_c, was greatly increased for girder IIC. As can be seen from Tables 2.16 and 2.17, all five methods underestimated the ultimate shear strength of girder IIC by much more than they underestimated the ultimate shear strength of girder IB.

The difference between end IIC and IID was the configuration of prestressing strands in the section. End IID contained the 12 draped strands and was not tested to failure due to testing equipment limitations. The research concluded that the increased number of angled strands in the web caused additional local web compression, increased dowel action, and web confinement.

Table 2.16 Test-to-predicted ratios based on nominal properties (Cumming, Shield and French 1997)

Models	**End IA** (Test/Pre.)	**End IB** (Test/Pre.)	**End IIC** (Test/Pre.)	**End IID** (Test/Pre.)	Mean (Test/Pred.)	Coef. Var.
ACI 318-95 Simplified Method	1.65	1.71	2.00	2.34	1.92	16.5
ACI 318-95 Detailed Method	1.43	1.48	1.73	1.73	1.59	10.0
AASHTO LRFD (1998)	1.39	1.43	1.68	1.85	1.59	13.6
Truss Model ($25° < \theta < 70°$)	3.57	3.69	4.34	4.77	3.20	13.8
Modified Truss Model ($25° < \theta < 70°$)	1.38	1.42	1.66	1.75	1.55	11.7

Table 2.17 Test-to-predicted ratios based on measured properties (Cumming, Shield and French 1997)

Models	**End IA** (Test/Pre.)	**End IB** (Test/Pre.)	**End IIC** (Test/Pre.)	**End IID** (Test/Pre.)	Mean (Test/Pred.)	Coef. Var.
ACI 318-95 Simplified Method	1.49	1.56	1.93	2.27	1.81	20.0
ACI 318-95 Detailed Method	1.36	1.43	1.74	1.72	1.56	12.30
AASHTO LRFD (1998)	1.22	1.30	1.64	1.84	1.50	19.50
Truss Model ($25° < \theta < 70°$)	2.84	2.43	3.59	3.94	3.20	21.50
Modified Truss Model ($25° < \theta < 70°$)	1.22	1.30	1.55	1.71	1.45	15.50

2.4.2.7 Shahawy and Cai, (1999)

Based on the research performed in this study, a new approach to the shear design of concrete members was proposed. In this research, the results and design method were compared with various research findings from the past. The researchers in this report performed extensive analysis on previous research and compared the shear design methods of the AASHTO Standard (1996) and AASHTO LRFD (1998) Specifications to the experimental data. The article summarized the results of Elzanaty, Nilson, and Slate, (1986), Burdette and Chew, (1994), and Shahawy and Batchelor, (1996). Tables 2.18, 2.19, and 2.20 show the results of all tests, and their comparisons with the two design methods.

All experimental data in this article were compared to the most recent versions of the two design specifications. Therefore, the findings of the original research on the accuracy of the AASHTO Standard or AASHTO LRFD Specifications changed with use of the newer specifications. The data presented here is based on the 1998 LRFD code and the 1996 AASHTO Standard code whereas the predictions from Elzanaty, et al.

(1986) were based on the 1983 ACI code, the predictions from Deatherage, et al. (1994) and Shahawy and Batchelor (1996) were based on the 1989 AASHTO Standard and the 1994 LRFD Specifications. This caused the prediction values to change slightly, resulting in different levels of accuracy for the predicted values in the separate reports.

Table 2.18 shows the results obtained from the research performed by Elzanaty, Nislon, and Slate (1986). Both codes remained conservative for every specimen tested in this research. Specimens CW1 through CW9 and CI1 through CI9 had no shear reinforcement, and the cracking shear strength was the ultimate strength. The rest of the specimens had varying amounts of shear reinforcement. All of the CW specimens experienced web shear failures and the all of the CI specimens experienced shear-flexure failures.

Shahawy and Cai (1999) were able to examine the accuracy of the AASHTO Standard (1996) and the AASHTO LRFD Specifications (1998) codes for web-shear, shear flexure, and ultimate shear. On average, the Standard and LRFD Specifications had test-to-predicted values of 1.18 and 2.65 for the concrete web shear strength, $V_{cw,}$ respectively. For the specimens that failed due to shear-flexure, they had test-to-predicted values of 1.16 and 2.28, respectively. For ultimate shear capacity, V_n, the Standard and LRFD codes had test-to-predicted values of 1.22 and 1.74, respectively.

Table 2.19 shows the results obtained from the research performed by Deatherage, et al. (1994). Most of the results obtained from this research were controlled by flexural behavior. However, there were three specimens that experienced a diagonal, shear failure that were summarized and compared to the two prediction methods. The predicted shear capacity predicted using the AASHTO Standard Specifications method

was unconservative for the three shear failures with an average test-to-predicted ratio of 0.68. This was due to the fact that there was significant strand slip in each of the three specimens. The reason for the significant strand slip was that the shear spans were all less than 70 in., which was less than the calculated development length. The predicted shear capacity using the AASTHO LRFD method was conservative, despite the amount of strand slip, with a test-to-predicted ratio of 1.13. The LRFD Specification remained conservative because the maximum capacity was limited by the amount of longitudinal reinforcement requirement.

Table 2.20 and Figure 2.8 give the results obtained from Shahawy and Batchelor, (1996) in their study of prestressed concrete Type II girders. Shahawy and Cai, (1999) compared the results from the previous research to the AASHTO Standard and LRFD Specifications. The specimen nomenclature represents the type of strand, the amount of reinforcement, and the end of the beam that was tested. The first letter indicates the type of strand that was used, 0.5 in. or 0.5 in. special (A or B, respectively). The different strands were placed in different configurations to obtain the same total amount of prestressing force in all of the specimens. The number located next to the R indicates how much more or less shear reinforcement was provided based on the AASHTO Standard design criteria.

The findings of these results show that, overall, the AASHTO Standard and LRFD Specifications had test-to-predicted values of 1.21 and 1.19, respectively. These percentages are based on all testing data, not factoring in the type of failure that occurred before the ultimate shear capacities were obtained. Comparing the predictions when a

shear failure with no bond slip occurred, the AASHTO Standard code test-to-predicted value was 1.24, and the LRFD code test-to-predicted value was 1.15.

Table 2.18 Comparisons between predicted and experimental values from Elzanaty, Nilson and Slate (1986). (Shahawy and Cai, 1999)

Test Specimen	Shear span ratio (a/d)	Test V_c (kips)	Test V_u (kips)	AASHTO (kips)			LRFD (kips)			V_c Test / Standard	V_c Test / LRFD	V_u Test / Standard	V_u Test / LRFD
				V_c	V_s	V_n	V_c	V_s	V_n				
CW1	2.9	31.1	31.1	23.96	0	23.96	17.78	0	17.78	1.30	1.75	1.30	1.75
CW2	3.75	28	28	23.88	0	23.88	17.03	0	17.03	1.17	1.64	1.17	1.64
CW3	5	26.4	26.4	23.08	0	23.08	16.17	0	16.17	1.14	1.63	1.14	1.63
CW4	3.75	28.6	28.6	24.26	0	24.26	17.35	0	17.35	1.18	1.65	1.18	1.65
CW5	3.75	27.9	27.9	24.04	0	24.04	17.14	0	17.14	1.16	1.63	1.16	1.63
CW6	3.75	23.8	25.2	20.65	0	20.65	13.83	0	13.83	1.15	1.72	1.22	1.82
CW7	3.75	25.2	23.8	20.37	0	20.37	15.01	0	15.01	1.24	1.68	1.17	1.59
CW8	3.75	20.2	20.2	17.74	0	17.74	12.09	0	12.09	1.14	1.67	1.14	1.67
CW9	3.75	22.7	22.7	19.27	0	19.27	12.91	0	12.91	1.18	1.76	1.18	1.76
CI1	7.8	17.5	17.5	16.02	0	16.02	15.53	0	15.53	1.09	1.13	1.09	1.13
CI2	5.8	25	25	20.99	0	20.99	16.51	0	16.51	1.19	1.51	1.19	1.51
CI3	4	27.2	27.2	24.34	0	24.34	17.65	0	17.65	1.12	1.54	1.12	1.54
CI4	5.8	24.4	24.4	21.28	0	21.28	16.78	0	16.78	1.15	1.45	1.15	1.45
CI5	5.8	26.9	26.9	21.1	0	21.1	16.62	0	16.62	1.27	1.62	1.27	1.62
CI6	5.8	18.3	20.5	16.95	0	16.95	12.41	0	12.41	1.08	1.47	1.21	1.65
CI7	5.8	20.5	18.3	16.61	0	16.61	14.9	0	14.9	1.23	1.38	1.10	1.23
CI8	5.8	19.5	19.5	15.63	0	15.63	11.55	0	11.55	1.25	1.69	1.25	1.69
CI9	5.8	19.9	19.9	16.19	0	16.19	12.05	0	12.05	1.23	1.65	1.23	1.65
CW10	3.8	24.4	39	19.97	8.55	28.52	6.06	12.5	18.56	1.22	4.03	1.37	2.10
CW11	3.8	21.5	35.2	18.46	8.55	27.01	5.39	12.82	18.21	1.16	3.99	1.30	1.93
CW12	3.8	19.2	31.6	17.14	8.55	25.69	4.57	13.58	18.15	1.12	4.20	1.23	1.74
CW13	3.8	27.6	41	23.62	8.55	32.17	7.4	17.65	25.05	1.17	3.73	1.27	1.64
CW14	3.8	27.8	42.2	23.86	12.2	36.08	6.52	21.04	27.56	1.17	4.26	1.17	1.53
CW15	3.8	22.6	33.8	19.63	8.55	28.18	5.92	12.42	18.34	1.15	3.82	1.20	1.84
CW16	3.8	27.5	42	23.73	8.55	32.28	7.41	17.74	25.15	1.16	3.71	1.30	1.67
CW17	3.8	27.7	32	23.52	3.89	27.41	13.11	8.28	21.39	1.18	2.11	1.17	1.50
CI10	5.8	18.8	31.8	16.39	8.32	24.71	6.11	9.77	15.88	1.15	3.08	1.29	2.00
CI11	5.8	18	28.6	15.58	8.32	23.9	5.42	10.11	15.53	1.16	3.32	1.20	1.84
CI12	5.8	18.6	27.5	15.03	8.32	23.35	4.62	10.81	15.43	1.24	4.03	1.18	1.78
*CI13	5.8	18	34.8	20.87	8.32	29.19	7.41	13.36	20.77	0.86	2.43	1.19	1.68
CI14	5.8	24.2	37	21.21	13.3	34.52	6.5	17.21	23.71	1.14	3.72	1.07	1.56
CI15	5.8	17.6	27.2	16.12	8.32	24.44	5.97	9.7	15.67	1.09	2.95	1.11	1.74
CI16	5.8	26.3	36.7	21.06	8.32	29.38	7.48	13.51	20.99	1.25	3.52	1.25	1.75
CI17	5.8	25.5	29.1	20.92	3.78	24.7	11.51	7.41	18.92	1.22	2.22	1.18	1.54
									Mean $V_{c/pred.}$	1.17	2.46		
									Mean $V_{n/pred.}$			1.22	1.74
									Maximum	1.30	4.26	1.37	2.10
									Minimum	0.86	1.13	1.07	1.13

* This beam experienced an accidental failed due to web shear instead of shear flexure

.

Table 2.19 Comparisons between predicted and experimental values from Deatherage, et al. (1994). (Shahawy and Cai, 1999)

Specimen	Shear span ratio (a/d)	Test V_u (kips)	AASHTO (kips)			LRFD (kips)			Test / Standard	Test / LRFD
			V_c	V_s	V_n	V_c	V_s	V_n		
5S-1-EXT	2.88	109	81.64	93.76	175.4	14.57	163.99	105.58	0.62	1.03
5S-4-EXT	2.8	112	76.02	91.51	167.54	14.19	165.87	98.96	0.67	1.13
6-2-INT	2.98	116	69.62	87.24	156.86	12.88	174.91	93.87	0.74	1.24
							Mean V_c		0.68	1.13
							Maximum		0.74	1.24
							Minimum		0.62	1.03

Table 2.20 Comparisons between predicted and experimental values from Shahawy and Batchelor (1996). (Shahawy and Cai, 1999)

Specimen	Shear Span	Failure Mode	Shear span ratio (a/d)	Test V_u (kips)	AASHTO 1996 (kips)			LRFD 1998 (kips)			Test / Standard	Test / LRFD
					V_c	V_s	V_n	V_c	V_s	V_n		
A0-00-R,N	85	Shear / bond	2.1	313	91.17	114.85	206.01	28.03	159.69	187.72	1.52	1.67
A0-00-R,S	85	Shear	2.1	276	84.70	114.85	199.55	28.14	159.80	187.94	1.38	1.47
A1-00-M,N	102	Shear / bond	2.5	141	93.60	11.39	104.98	91.58	22.35	113.93	1.34	1.24
A1-00-M,S	124	Shear / bond	3.1	168	90.15	11.39	101.54	76.46	22.35	98.81	1.65	1.70
A1-00-R/2,N	102	Shear / bond	2.5	166	93.60	52.44	146.04	44.90	88.10	132.99	1.14	1.25
A1-00-R/2,S	124	Shear / bond	3.1	173	90.15	35.94	126.09	45.14	68.07	113.21	1.37	1.53
A1-00-R,N	102	Shear / bond	2.5	210	93.60	104.89	198.48	29.29	134.02	163.32	1.06	1.29
A1-00-3R/2,N	102	Shear / bond	2.5	207	93.60	157.33	250.93	26.17	203.27	**193.71**	0.82	1.07
A4-00-0R,N	102	Shear	2.3	93.9	83.48	0.00	83.48	99.84	0.00	99.84	1.12	0.94
A4-00-0R,S	85	Shear	2.3	97.6	83.48	0.00	83.48	99.85	0.00	99.85	1.17	0.98
A4-00-0R,N	90	Shear	1.8	101	82.37	0.00	82.37	104.51	0.00	104.51	1.22	0.96
A4-00-0R,S	90	Shear	1.8	106	82.37	0.00	82.37	104.51	0.00	104.51	1.28	1.01
B0-00-R,N	102	Shear / bond	2.5	220	92.57	105.65	198.22	30.62	135.76	166.38	1.11	1.32
B0-00-R,S	124	Shear	3.1	206	89.10	72.65	161.75	65.67	100.41	136.07	1.27	1.51
B1-00-0R,N	60	Shear / bond	1.5	166	78.93	0.00	78.93	106.90	0.00	106.90	2.10	1.55
B1-00-0R,S	54	Shear / bond	1.3	155	78.09	0.00	78.09	107.25	0.00	107.25	1.98	1.45
B1-00-R,N	60	Shear / bond	1.52	245	78.93	140.86	219.80	29.21	192.03	221.25	1.11	1.11
B1-00-R,S	54	Shear / bond	1.3	232	78.09	146.86	224.95	27.67	199.42	227.10	1.03	1.02
B1-00-2R,N*	60	Shear / bond	1.5	262	78.93	**158.76**	237.70	20.73	396.80	**294.46**	1.10	0.89
B1-00-2R,S*	54	Shear / bond	1.3	247	78.09	**158.76**	236.85	20.32	408.80	**302.74**	1.04	0.82
B1-00-3R,N*	60	Shear / bond	1.5	264	78.93	**158.76**	237.70	19.74	580.72	**339.49**	1.11	0.78
B1-00-3R,S*	54	Shear / bond	1.3	263	78.09	**158.76**	236.85	20.25	586.02	**350.43**	1.11	0.75
B1-00-2R2,N*	60	Shear / bond	1.5	268	78.93	**158.76**	237.70	20.75	396.80	**293.94**	1.13	0.91
B1-00-2R2,S*	54	Shear / bond	1.3	255	78.09	**158.76**	236.85	20.30	408.80	**303.09**	1.08	0.84

* Maximum reinforcement limit exceeded

Bold: Limited by V_s maximum in AASHTO or longitudinal requirement in LRFD

Mean Test / Predicted			
	0R	1.48	1.15
	1R	1.22	1.31
	2R	1.09	0.86
	3R	1.11	0.76

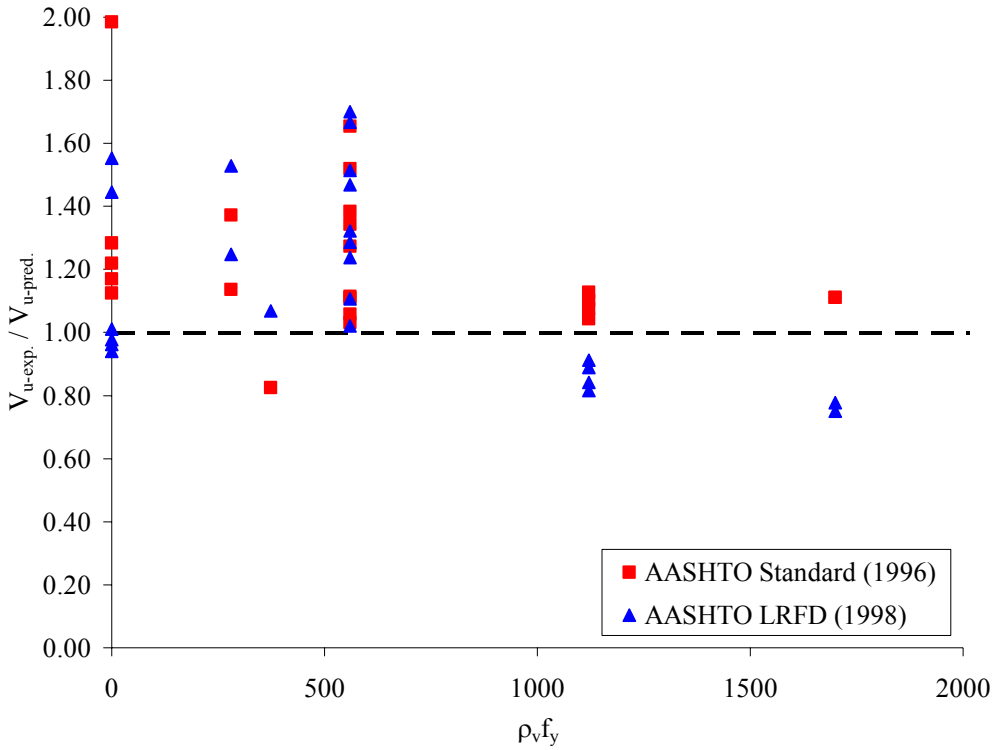

Figure 2.8 AASHTO Standard and LRFD test-to-predicted values vs. stirrup spacing (Shahawy and Cai, 1999)

2.4.2.8 Ma, Tadros and Baishya (2000)

Ma et al. (2000) tested two NU 100 I-girders which were fabricated with concrete design strengths of 8,000 psi (55.2 MPa). The actual test day strengths were 8,100 psi (55.8 MPa) for Specimen A and 10,780 psi (74.3 MPa) for Specimen B. The girders were shaped similarly to a PCI bulb-tee with a much wider bottom flange. The girders had heights of 43.3 in. and web widths of 6.9 in. Composite decks 7.5 in. thick and 49 in. wide were cast on each beam with design concrete strengths of 5,000 psi (34.5 MPa). The actual deck concrete strengths on testing day for Specimens A and B were 7,200 psi (49.6 MPa) and 5,100 psi (35.2 MPa). The variables in the research were draped strands vs. debonded strands, different types of shear reinforcement with different steel grades,

including conventional double-legged stirrups, vertical welded wire fabric, and orthogonal welded wire fabric.

Specimen A was 78 ft. long with 30 - 270 ksi low relaxation 7 wire strands. At one end of Specimen A, four strands were draped over a distance of 28 ft. At the other end, 2 strands were debonded for 20 ft. and 2 strands were debonded for 10 ft. The shear reinforcement was conventional reinforcement with a specified yield strength of 60 ksi. At one end, two # 5 bars were used spaced at 9 in. on center. At the other, two layers of vertical welded wire fabric (D14) was used with a spacing of 4 in. on center between wires.

Specimen B was 71 ft. long with 38 prestressing strands. Specimen B had 12 strands debonded at different lengths along the girder. The shear reinforcement was deformed welded wire with specified yield strength of 80 ksi. At one end, two layers of vertical D20 WWF was used with wires spaced at 4 in. on center. At the other end, two layers of orthogonal D20 WWF was used with wires spaced at 4 in. on center. The size and spacing of the WWF varied throughout the section with half of the specimen having orthogonal WWF and the other half having just vertical WWF.

The shear spans for all tests were 54 in. which was well within the development length. However, one feature of this shear research was that the ends of the strands were hooked into end diaphragms to ensure no bond slip when the girders were tested. All of the strands at both ends of both specimens were bent upward at approximately 60° and extended 60 to 70 in. Blocks of concrete were then cast around the extended strands. Therefore, full tension tie capabilities were developed for the strands. One final test was

performed with the same shear span with no end block to restrain the prestressing strands. In that test, the capacity of the member was limited by bond failure, as expected.

Table 2.21 shows the results obtained from this study. It found that both the AASHTO Standard (1996) and AASHTO LRFD (1998) Specifications produced conservative predictions of shear capacity of precast prestressed concrete I-girders. It also found that, although not all specimens had the maximum reinforcement of $0.25f_c'b_wd_v + V_p$ given by the LRFD code, all tests produced shear capacities in excess of the maximum allowed by the code. Also, it was determined that the AASHTO Standard maximum shear value was too restrictive and unnecessarily required the widening of concrete webs. Even when the yield strengths of the shear reinforcement were increased to 80 ksi, both codes still had conservative predictions.

The values in Table 2.21 show that, on average, the AASHTO Standard and AASHTO LRFD Specifications had conservative test-to-predicted values of 1.63 percent and 1.41, respectively. All four tests experienced shear failures with web crushing as the primary mode of failure. The specimen nomenclature in Table 2.21 indicates the girder, type of reinforcement, spacing, design concrete strength, and embedment. For example, ARO5908X indicates that the test was performed on specimen A, with two # 5 reinforcing bars spaced at 9 in. on center with an 8,000 psi design concrete strength (testing day f_c' = 8,100 psi (55.8 MPa) for Specimen A and 10,780 (74.3 MPa) psi for Specimen B) and anchored prestressing strands.

Table 2.21 Summary of test results (Ma, Tadros, and Baishya, 2000)

Test Specimen	d (in.)	d_v (in.)	f_y, ksi	$V_{cr\text{-}test}$, kips	$V_{u\text{-}test}$, kips	Mode of failure	V_n Standard	V_n LRFD	AASHTO Standard (1996) Maximum $*12\sqrt{f'_c}\,b_w d$	AASHTO LRFD (1998) Maximum $*0.25 f'_c b_w d_v$	Test / Standard	Test / LRFD
ARO5908X	43.8	42.0	60	243.02	629.47	Web crushing	323	348	277	506	1.95	1.81
AVW14408X	48	46.2	60	134.2	593.01	Web crushing	330	370	304	545	1.80	1.60
BVW20408X	47.6	45.4	80	195.33	589.8	Web crushing	510	533	301	536	1.16	1.11
BOW20408X	47.6	45.4	80	250	>820.3	Did not fail	510	726	301	536	>1.61	>1.13
AVW14608Y	48	46.2	60	246.86	459.86	Shear / bond	N/A	N/A	N/A	N/A	N/A	N/A

* b_w = 5.9 in.

A fifth test was performed with no prestressing strand anchorage. After all four of the main tests were performed, the anchorage block and damaged section were cut off of one end of Specimen A. This caused the strands to have no anchorage beyond the development length allowed by the shear span, which was 54 in. The shear cracking occurred at close to the same load as for all the other tests. However, significant slippage and shear/bond failure occurred when the specimen was tested to failure because of the shear span length being well inside the development length. Predicted values were not calculated for the final test.

2.4.2.9 Russell, Bruce, and Roller (2003)

Russell et al. (2003) tested three 96 ft. long, 72 in. deep pretensioned bulb-tee girders to evaluate behavior under static shear loadings. The three girders had a design compressive strength of 10,000 psi (69.0 MPa) and incorporated 0.6 in. diameter, Grade 270, low relaxation prestressing strands. The three girders were called BT6, BT7, and

BT8. The actual testing day concrete strengths for the three girders were 11,685 psi (80.6 MPa), 12,565 psi (86.6 MPa), and 11,580 psi (79.8 MPa), respectively. Each girder contained 24 strands with six strands debonded at the each end of each girder. Two of the girders (BT7 and BT8), designed using the AASHTO LRFD Specifications (1998), had all six strands debonded for a length of 9 ft. The other girder (BT6), designed using the AASHTO Standard Specifications (1996), had debonded lengths of 21, 24, and 30 ft. Each girder was fitted with a 10 ft wide, 8 in. thick composite deck with a concrete design strength of 4,200 psi (29 Mpa). The actual testing day concrete deck strengths were 5,320 psi (36.7 MPa), 7,640 psi (52.7 MPa), and 7,095 psi (48.9 MPa).

The shear reinforcement for each girder was divided into three regions. The end regions consisted of 2 # 5 bars or two D31 wires at 4 in. on center for a length extending 32 in. The second region consisted of shear reinforcement between the end of the first region and the point loads for each test. This region was considered the critical section, and had shear reinforcement consisting of 2 # 4 bars at 10 in. on center, 6.5 in. on center, and 15 in. on center for three of the tests. The other three tests had two layers of D20 welded wire fabric at 8 in. on center, 12 in. on center, and 18 in. on center. The third region, or middle of each girder, consisted of 2 # 4 bars at 16 in. on center or two layers of D20 welded wire fabric at 16 in. centers.

The shear span for all of the tests was 120 in. which was outside of the calculated development length. However, most of the tests experienced varying amounts of strand slip that indicated that there was not sufficient bond strength.

Table 2.22 shows the results produced by this research for the AASHTO Standard and LRFD specifications. The specified properties were the properties based on nominal

design dimensions and material strengths. The measured properties were the properties based on laboratory material testing and physical measurements. The measured strengths included the self weight shear, loading equipment shear, and applied shear. Some variation in the measured strengths occurred because the calculated critical section for shear was not the same for all analyses, and this affected the contribution of the self weight to the measured shear strength.

It was found in this study that the AASHTO Standard Specifications (2002) had test-to-predicted values of 1.75 and 1.64 percent for the specified and measured concrete cracking strengths, V_c, respectively. It also showed that the test-to-predicted values at ultimate were, on average, 1.69 and 1.55 for the specified and measured ultimate shear values. It is important to note that these averages would have been more conservative if either end of the BT-7 girder could have been tested to failure and not limited by testing equipment.

It was found that the AASHTO LRFD Specifications (1998) greatly underestimated the concrete shear strength contribution for all of the tests and had test-to-predicted values of 2.7 and 2.44 for the specified and measured concrete cracking strengths, V_c, respectively. The gross underestimation of the concrete shear strength exhibited by the LRFD Specification was caused because the calculated concrete shear contribution was not meant to predict cracking shear, but to predict the amount of shear force that could be carried across a crack. The results also showed that the AASHTO LRFD Specification had test-to-predicted values of 1.80 and 1.50 for the specified and measured ultimate shear values. The LRFD Specification limited the member capacity based on the longitudinal reinforcement requirement. Girder BT-6 suffered greatly from

this provision because it did not contain a sufficient amount of longitudinal reinforcement. If the reinforcement, which was meant to inhibit strand slip and bond failure, was not provided, the LRFD Specification grossly underestimated the ultimate shear strength. The LRFD specification provided a test-to-predicted value of 2.25 for the ultimate strength of the BT6 girder.

The report concluded that all measured shear strengths were greater than the strengths calculated using the AASHTO Standard (1996) and the AASHTO LRFD (1998) Specifications. Using nominal dimensions and properties yielded a less accurate, more conservative shear strength than found using the measured f_c', f_{ps}, and f_y values. Russell et al. (2003) also concluded that the shear design approach given by both specifications is acceptable and conservative for high performance concrete with f_c' up to 13,000 psi (90 MPa). It was shown that reinforcement yield strengths greater than 60 ksi could be utilized in the design of prestressed concrete girders.

Table 2.22 Comparison of tested shear capacities to AASHTO Standard and AASHTO LRFD predictions using nominal and measured girder properties (Russell, Bruce and Roller 2003)

AASHTO Standard (1996)													
Girder	Shear Reinforcement	Specified Properties				Measured Properties				Specified		Measured	
		$V_{c\text{-}test}$	$V_{c\text{-}predicted}$	$V_{u\text{-}test}$	$V_{u\text{-}predicted}$	$V_{c\text{-}test}$	$V_{c\text{-}predicted}$	$V_{u\text{-}test}$	$V_{u\text{-}predicted}$	$V_{c\text{-}test}/V_{c\text{-}predicted}$	$V_{u\text{-}test}/V_{u\text{-}predicted}$	$V_{c\text{-}test}/V_{c\text{-}predicted}$	$V_{u\text{-}test}/V_{u\text{-}predicted}$
BT-6 Live	No. 4 @ 10 in.	309	187	630	371	308	203	630	395	1.65	1.70	1.52	1.59
BT-6 Dead	D20 @ 12 in.	314	187	596	366	313	204	595	422	1.68	1.63	1.53	1.41
BT-7 Live	No. 4 @ 6.5 in.	339	187	654[a]	471	339	203	653[a]	499	1.81	1.39	1.67	1.31
BT-7 Dead	D20 @ 8 in.	342	187	639[a]	456	341	196	638[a]	523	1.83	1.40	1.74	1.22
BT-8 Live	No. 4 @ 15 in.	335	187	645	310	334	198	644	327	1.79	2.08	1.69	1.97
BT-8 Dead	D20 @ 18 in.	327	186	600	306	327	192	600	338	1.76	1.96	1.70	1.78
AASHTO LRFD (1998)													
Girder	Shear Reinforcement	Specified Properties				Measured Properties				Specified		Measured	
		$V_{c\text{-}test}$	$V_{c\text{-}predicted}$	$V_{u\text{-}test}$	$V_{u\text{-}predicted}$	$V_{c\text{-}test}$	$V_{c\text{-}predicted}$	$V_{u\text{-}test}$	$V_{u\text{-}predicted}$	$V_{c\text{-}test}/V_{c\text{-}predicted}$	$V_{u\text{-}test}/V_{u\text{-}predicted}$	$V_{c\text{-}test}/V_{c\text{-}predicted}$	$V_{u\text{-}test}/V_{u\text{-}predicted}$
BT-6 Live	No. 4 @ 10 in.	303	118	625	440 278[b]	303	132	625	454 326[b]	2.57	2.25	2.30	1.92
BT-6 Dead	D20 @ 12 in.	308	119	590	435 275[b]	308	127	590	474 344[b]	2.59	2.15	2.43	1.72
BT-7 Live	No. 4 @ 6.5 in.	334	106	648[a]	534 478[b]	334	123	648	556 549[b]	3.15	1.36	2.72	1.18
BT-7 Dead	D20 @ 8 in.	336	108	634[a]	522 467[b]	336	117	634	578 573[b]	3.11	1.36	2.87	1.11
BT-8 Live	No. 4 @ 15 in.	329	135	639	385 336[b]	329	156	639	406 390[b]	2.44	1.90	2.11	1.64
BT-8 Dead	D20 @ 18 in.	321	136	594	381 333[b]	322	143	595	419 408[b]	2.36	1.78	2.25	1.46

[a] Test stopped at the load capacity of the test equipment

[b] Strength limited by longitudinal reinforcement

2.4.2.10 Summary

A number of shear tests have been performed on high performance concrete precast prestressed girders. One of the goals of the testing at Georgia Tech was to investigate the shear behavior of large, HPC prestressed girders. All of the tests included in this literature review contained high performance concrete. Only two projects conducted tests on composite girders larger than AASHTO Type II.

The majority of the tests discussed in this literature review experienced shear/bond failures. This type of failure was caused because the tests were performed with the load point inside the development length of the strands. When a shear/bond failure occurred, different research found varying amounts of accuracy for both the AASHTO Standard and AASHTO LRFD Specifications. Generally, when a shear/bond failure occurred, the ultimate load was lower than if the failure was pure shear. Despite the lower value, both codes remained conservative for most past research. Dill and Kahn (2000) and Tawfiq (1995) found that neither code was conservative when the shear/bond failures occurred. The longitudinal reinforcement requirement in the 1998 and 2004 AASHTO LRFD Specifications may have made the predicted shear capacities more conservative. It was found that the more the bond failure and strand slip occurred, the less conservative both codes became. For later comparison, the results from specimens with large amounts of strand slip were not used.

For most shear failures, the ACI Code and AASHTO Standard Specifications were accurate and conservative in predicting either web-shear or flexure shear capacity. The AASHTO LRFD Specifications varied with different tests, but remained mostly conservative when predicting ultimate shear capacity. Shahawy and Batchelor (1996)

and Tawfiq (1995) reported that as the amount of shear reinforcement increased, even above the code maximums, the predictions became less and less conservative. Shahawy and Batchelor found that the AASHTO LRFD Specifications became unconservative when the reinforcement was above two times the recommended design amount. The trend from underestimation to overestimation was found to be much greater for the AASHTO LRFD Specification than for the AASHTO Standard Specification.

Finally, both codes seemed to remain fairly consistent when different testing parameters were used. Both codes were conservative, by close to the same amount, for all sizes and shapes of girders. This showed that both methods for predicting shear capacity should remain conservative for all tests performed on the BT-56 girder in this research. The predicted shear capacities also remained conservative when various shear reinforcements, concrete strengths, and prestressing configurations were used. Table 2.20 shows a summary of all research examined in this literature review. It is important to note that much of the data presented in Table 2.20 was not used in later comparisons because of the shear/bond failures that occurred in many of the test specimens.

Table 2.23 Experimental comparison of the shear capacity of prestressed girders

						AASHTO Standard (2002)		AASHTO LRFD (1998)		Truss Model
Authors	Year	Reference Type	Tests	f_c' max (psi)	Strands	V_c (Test/Pred.)	V_n (Test/Pred.)	V_c (Test/Pred.)	V_n (Test/Pred.)	V_n (Test/Pred.)
Elzanaty, et al.	1986	CI Series	17	11,400	4 - 0.6 in.	1.17	1.21	n.a.	n.a.	n.a.
		CW Series	17	11,400	4 - 0.6 in.	1.15	1.21	n.a.	n.a.	n.a.
Hartmann, Breen, & Kreger	1988	Series 1	3	11,300	6 - $^3/_8$ in.	1.09	1.39	n.a.	n.a.	n.a.
		Series 2	3	10,800	17 - $^3/_8$ in.	1.02	1	n.a.	n.a.	n.a.
		Series 3	4	13,160	13 - $^3/_8$ in.	n.a.	1.16	n.a.	n.a.	n.a.
Deatherage, et al.	1994	AASHTO I	3	5,000	11 - 0.5 in.	n.a.	0.68	n.a.	1.13	n.a.
Tawfig	1995	AASHTO II,R	6	11,040	18 - $^3/_8$ - 0.6 in.	n.a.	0.89	n.a.	n.a.	1.16
		AASHTO II, 2R	6	11,040	18 - $^3/_8$ - 0.6 in.	n.a.	0.73	n.a.	n.a.	1.05
Shahawy and Batchelor	1996	AASHTO II, 0R	6	7,600	18 - 0.5 in.	n.a.	1.28	n.a.	1.67	n.a.
		AASHTO II, M	2	7,300	18 - 0.5 in.	n.a.	1.25	n.a.	2.67	n.a.
		AASHTO II, R/2	2	7,100	18 - 0.5 in.	n.a.	1.25	n.a.	2.32	n.a.
		AASHTO II, R	12	8,480	18 - 0.6 in.	n.a.	1.19	n.a.	1.63	n.a.
		AASHTO II, 3R/2	4	7,600	18 - 0.6 in.	n.a.	1.05	n.a.	1.41	n.a.
		AASHTO II, 2R	8	7,820	18 - 0.5s in.	n.a.	0.99	n.a.	0.82	n.a.
		AASHTO II, 3R	6	7,680	18 - 0.5s in.	n.a.	0.96	n.a.	0.71	n.a.
Cumming, Shield, and French	1997	Mn/DOT 45M	3	11,330	46 - 0.6 in.	n.a.	1.4	n.a.	1.26	2.64
		Mn/DOT 45M	3	9,315	46 - 0.6 in.	n.a.	1.73	n.a.	1.74	3.77
Ma, Tadros, and Baishya	2000	NU 1100 I	3	8,000	30 - 0.6 in.	n.a.	1.88	n.a.	1.71	n.a.
		NU 1100 I	3	8,000	38 - 0.6 in.	n.a.	>1.39	n.a.	>1.12	n.a.
Dill and Kahn	2000	AASHTO II, G2	4	13,430	10 - 0.6 in.	1.3	0.78	n.a.	0.87	n.a.
		AASHTO II, G4	4	16,100	10 - 0.6 in.	1.24	0.75	n.a.	0.73	n.a.
Meyer and Kahn	2002	AASHTO II, G1	9	9,245	10 - 0.6 in.	1.31	1.53	5.31	1.45	3.15
		AASHTO II, G2	9	10,750	10 - 0.6 in.	1.29	1.69	5.38	2.75	5.06
Russell, Bruce, and Roller	2003	*PCI BT-72	2	10,000	24 - 0.6 in.	1.52	1.5	2.37	1.82	n.a.
		**PCI BT-72	4	10,000	24 - 0.6 in.	1.7	1.57	2.49	1.35	n.a.

* Girder designed with AASHTO Standard

** Girder designed with AASHTO LRFD

CHAPTER 3

GIRDER DESIGN AND CONSTRUCTION

3.1 Girder Design

3.1.1 Design Parameters

As discussed in Chapter 1, one objective of this task was to estimate the ultimate strength of the composite girders used in the Jonesboro Road Bridge, which were AASHTO Type II and Type IV, HPC girders with an 8 inch thick composite deck. Construction and testing of the Type II girders was completed in an earlier task of this project, "Direct Pull-out Capacity, Transfer and Development Length of 0.6-in. Diameter Prestressing strand in High-Performance Concrete" (Kahn, Dill, Reutlinger 2000). An AASHTO Type IV girder was one of the sections chosen for testing in this research to match the girders in the Jonesboro Road Bridge. In addition, a PCI modified BT-56 was also chosen for testing in order to evaluate the shear capacity of large sections.

The prestressing strand (0.6-in. diameter, 270 ksi, low relaxation strand) and mix design for each girder were the same as that used in the Jonesboro Road Bridge (Slapkus and Kahn, 2002).

Duplicating the length and strand arrangement of the 127 ft.-2 in. girders spaced at 91 in. o.c. of the Jonesboro Road Bridge was not possible due to constraints of the structures laboratory at the Georgia Institute of Technology. The total weight of the composite girder had to be below the combined capacity of the two overhead cranes, which was 60 tons total (54431 kg) and the width of the deck had to be less than the maximum spacing between columns in the load frame which was 77-in. (1956 mm).

From these parameters, it was decided to use a girder length of 89 ft-2 in. (27.2 m), and a deck 8-in. (203.2 mm) thick and 5-ft (1524 mm) wide for both girders. The concrete mixture design from the Jonesboro Road Bridge was used for the two large girders and is discussed later in this section. The Jonesboro Road Bridge decks were constructed with 7,000

3.1.2 Girder Design Process

The exact strand arrangement of the Jonesboro Rd Bridge girders could not be duplicated because of reduced girder length, therefore, the objective of the test was to have a flexural capacity of the laboratory Type IV girder as close to that of the bridge girders as possible. In addition, the laboratory BT-56 girder was to have a design which maximized the number of prestressing strands, and ideally matched the flexural capacity of the Type IV girder. The girders were designed based on flexural capacity because the flexural capacity of each was to be determined.

The GDOT in-house beam design program "BRPSBM1" was used to obtain an initial design of each girder. The program is based on the AASHTO Standard Specifications for Highway Bridges, Sixteenth Edition (1996). The program allowed the user to either design or analyze simple span prestressed girders. A partial list of the input data required for the GDOT design program is given below.

- Girder type, span length, bearing distance, girder spacing and deck thickness
- Loads such as; HS20 live load, barrier loads, future paving loads and self weights
- Deck and girder concrete strengths and concrete unit weight
- Prestressing strand diameter and type, in addition to limit of initial prestressing

- Spacing between strands, number of strands per row as well as straight or draped configuration

Multiple iterations were performed, in which the deck thickness and girder spacing were varied to obtain the maximum number of strands in each girder and the closest flexural capacity to that of the Jonesboro Bridge girders. The flexural test results and example design output from the GDOT program can be found in "Testing of High Performance Concrete Pretensioned Bridge Girders", (Canfield and Kahn, 2005).

An extensive Excel spreadsheet was created to analyze a given girder design, using the requirements of the AASHTO Standard Specifications, 17th Edition (2002). The purpose of the spreadsheet was to verify the results of the GDOT program and to allow further variation of strand arrangements and eccentricities. Iterations were performed using the Excel program to try to further increase the number of strands in each girder, and in addition, to match the strand contribution to the girder's shear capacity to that of the bridge girders. The Excel program, like the GDOT program, checked stresses in each girder against the allowable stresses presented in the AASHTO Standard Specifications (2002), given below in Table 3.1. The final strand arrangements are shown in cross sections at midspan and ends of each girder in Figure 3.1. All strands were spaced 2-in. on-center in each direction. Figures 3.2 and 3.3 present the side elevations of each girder, which show the hold-down distances of 4.5 ft from each girder centerline.

Table 3.1 AASHTO (2002) allowable stresses

Initial tension with no long term losses	$3\sqrt{f_{ci}'}$
Initial compression with no long term losses	$0.6 f_{ci}'$
Tension at service with long term losses	$6\sqrt{f_c'}$
Compression at service with long term losses (prestress force plus permanent dead load)	$0.6 f_c$`
Modulus of rupture	$7.5\sqrt{f_c'}$

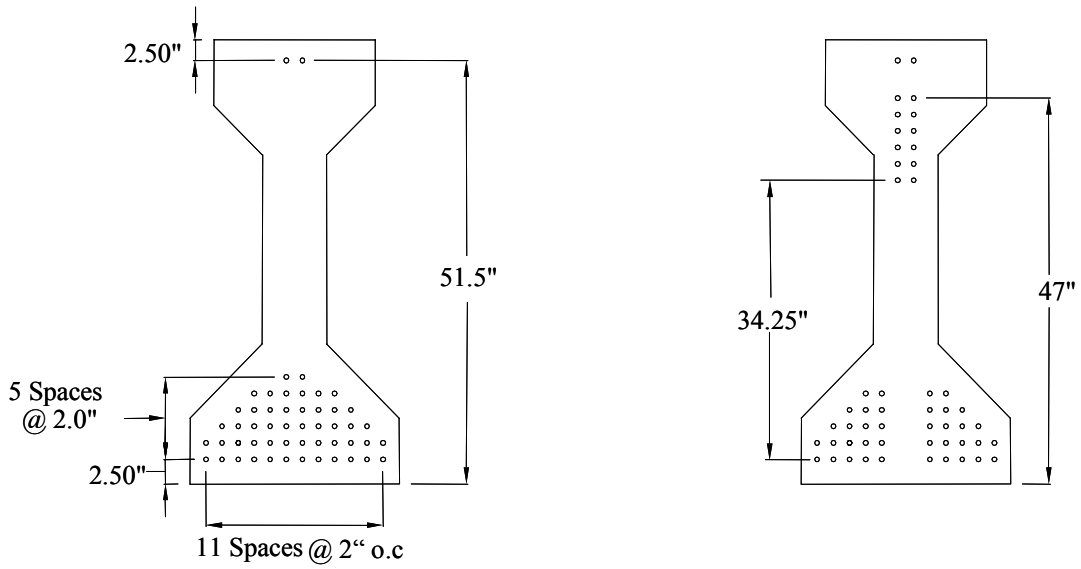

SECTION AT MIDSPAN SECTION AT END

Type IV Strand Arrangement

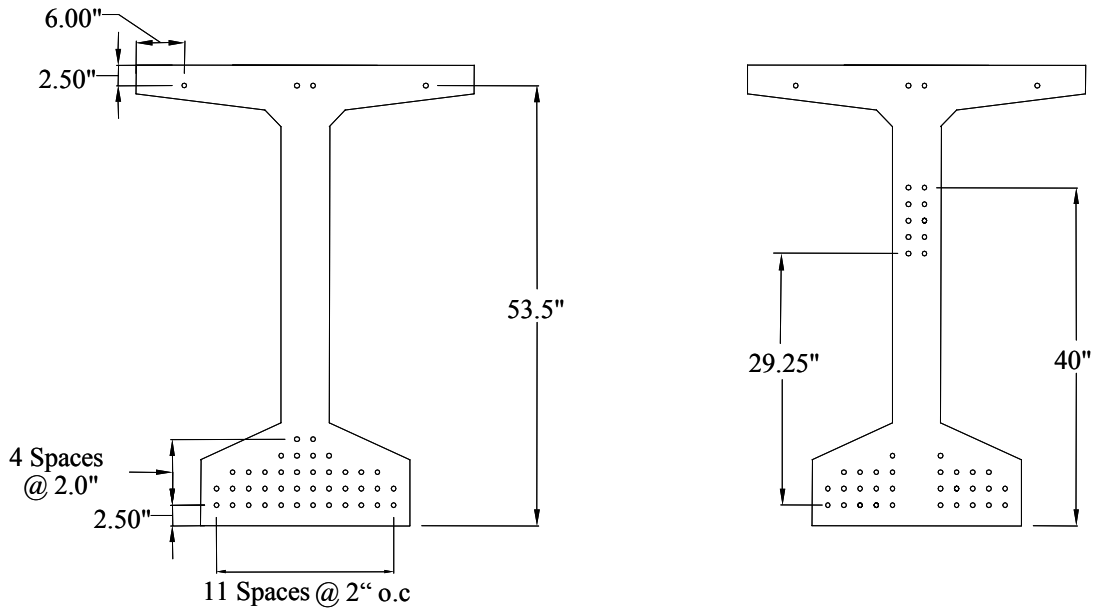

SECTION AT MIDSPAN SECTION AT END

BT-56 Strand Arrangement

Figure 3.1 Cross section showing strand arrangements at midspan and end of girders

The design of the shear reinforcement came from two sources, the GDOT program and a more conservative design, which was based on the Jonesboro Road bridge girders. The actual stirrup spacing used in the Jonesboro Road bridge girders was half of the GDOT program specified stirrup spacing. This was a common practice of the GDOT bridge engineer. The stirrup spacing in the Type IV Jonesboro Road bridge girder was 8.5-in on each end and 20-in. in the middle. To mimic the Jonesboro Bridge stirrup spacing, the final strand arrangement for both laboratory girders was analyzed by the GDOT program. This GDOT program stirrup spacing was used in one half of each girder. The remaining half of each girder used half of the GDOT program specified spacing. Figures 3.2, 3.3 and 3.4 present the final design of the Type IV and BT-56 girders, respectively. The figures show the strand eccentricities and stirrup spacing, including the different sizes of shear reinforcement.

Initial shear calculations were performed for both girders using their nominal design properties. Their capacities were determined at each end assuming the girder supports would not be changed and that the shear span would be 143 in. The actual shear test set up is discussed in Chapter 5 and the nominal shear capacities for both girders are presented in Chapter 6.

Figure 3.2 Type IV girder strand arrangement and shear reinforcement details

Figure 3.3 Modified BT-56 girder strand arrangement and shear reinforcement details

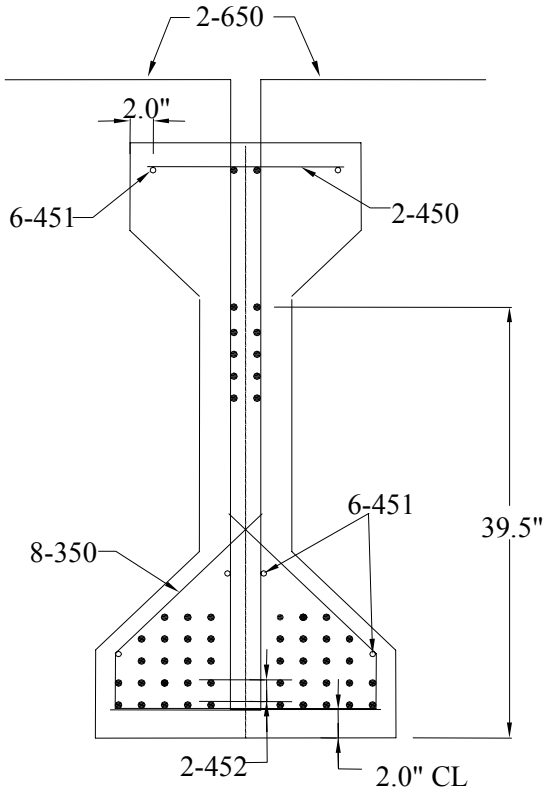

Type IV End Reinforcement

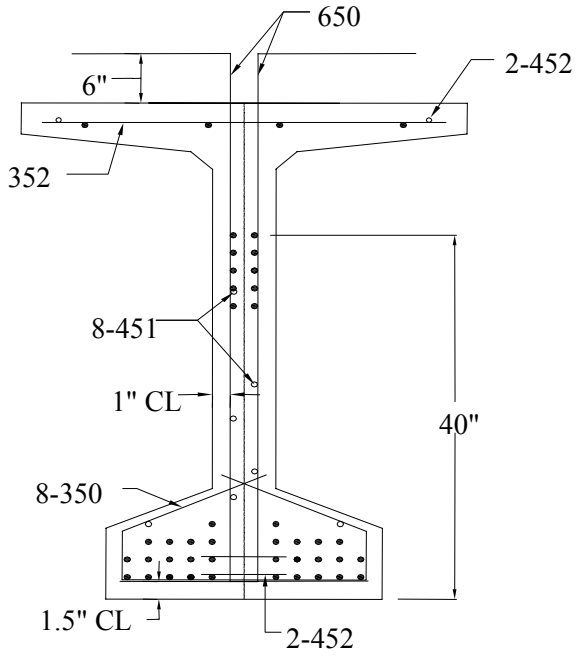

BT-56 Girder End Reinforcement

Figure 3.4 End view of Type IV and BT-56 girders

3.2 Girder Construction and Instrumentation

The Type IV and BT-56 girders were constructed at Standard Concrete Products (SCP) in Atlanta, Georgia. They were both constructed on the same prestressing bed. The construction began on April 21st, 2004 with the preparation of the girder forms and ended with the final cut down process on April 24th.

The Type IV girder had eight more prestressing strands than the BT-56, and as such was cast first, on April 22nd at 6:30 PM. The following day, after the concrete achieved the required compressive strength at release, the 10 strands not required in the BT-56 were cut. The BT-56 was then cast at 5:00 PM that same day, April 23rd. The following day, April 24th, at approximately 10:00 AM, all of the remaining strands were cut. A more detailed discussion of the strand arrangements and girder construction is presented later in this chapter.

3.2.1 Girder Instrumentation

Throughout construction, different types of instrumentation were installed both on the formwork and within each girder. The following section details the type and number of instruments used, and the locations of each type of instrumentation.

3.2.1.1 Load Cells

Prior to tensioning the prestressing strands, load cells were placed on 14 strands at the dead end of the prestressing bed. Each load cell was made at the Georgia Tech Structures Laboratory. The material chosen was a structural aluminum, alloy 6020, which has a yield stress of 42 ksi. The load cells were 4 in. tall, with a 1.75-in. outer diameter and a 0.75-in center hole. Each load cell had two longitudinal strain gages and two

transverse strain gages epoxy bonded to them. Figure 3.5 shows the load cell dimensions and strain gauge locations. The gages were wired in a full bridge configuration, to take into account the transverse strain, and also to mitigate temperature effects. The attached strain gages were manufactured by Micro Measurements, and were designated "CEA-13-250UW-350." The CTE of each gauge approximately matched the coefficient of thermal expansion (CTE) of the aluminum alloy of 13 με/°F, and had a gauge length of 0.25 in. (6.35 mm). They were all calibrated at the structures laboratory on a Satek MKIII 800RD 800 kip capacity compression machine which is calibration certified annually. The configuration of the load cells on each girder is shown in Figure 3.6, where a circle indicates a load cell. Also shown in the figure are the ten strands not common to both girders, marked by an "x".

National Instruments equipment was used to monitor and record the data from the load cells. The software used was Labview by National Instruments, and Figure 3.7 shows the data acquisition system in use at SCP.

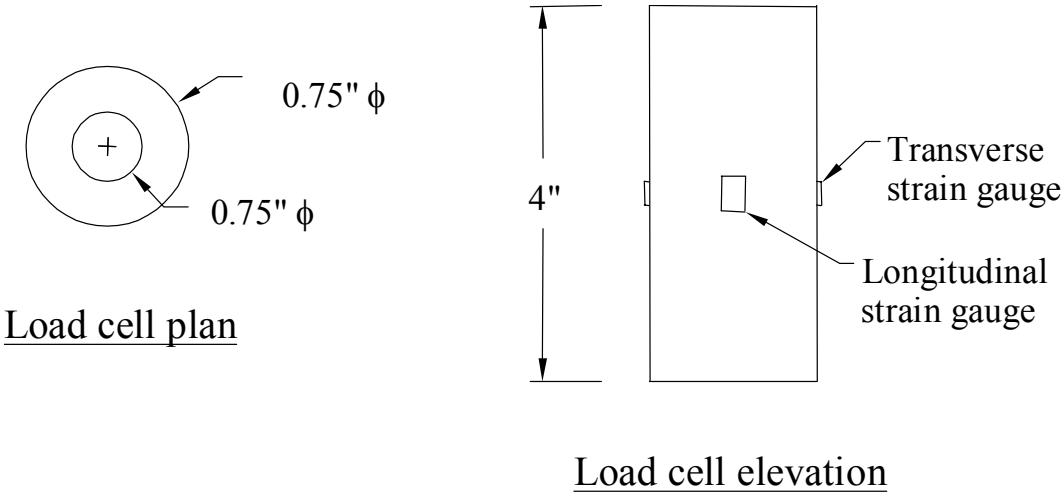

Figure 3.5 Load cell diagram

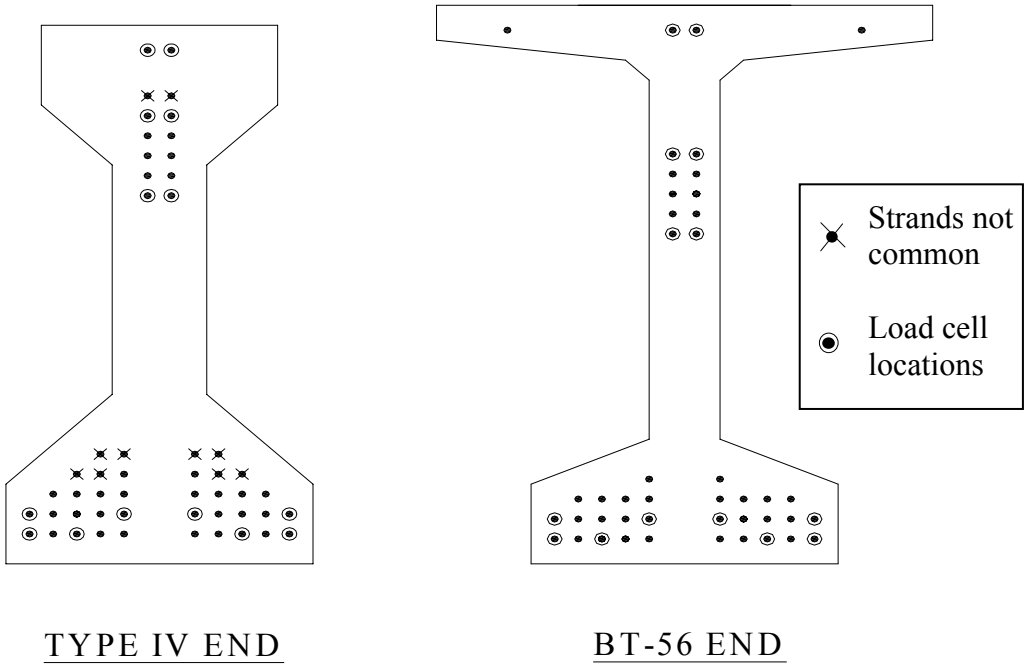

Figure 3.6 Girder cross sections showing load cell locations

Figure 3.7 Measuring the prestressing load immediately after tensioning

3.2.1.2 DEMEC Strips

In order to measure concrete surface strain (CSS), DEMEC insert strips were installed on the formwork for each girder. The CSSs were used to determine transfer length at each girder end and obtain strain profiles at each midspan. The strips were placed at the approximate level of both top and bottom layers of prestressing strands at the ends and middle of each girder. Figure 3.8 shows the location of each insert strip on each girder. Each DEMEC strip contained concrete inserts spaced at two inches on center. The strip was later removed after the concrete hardened. Figure 3.9 shows a detailed drawing of the DEMEC insert strip and how they were attached to the formwork. The embedment strips were constructed from a steel bar 1 ½-in. wide x ¼-in. thick. The

DEMEC strips had mounting screws every 10 to 12 in. for easy attachment to the metal forms at SCP. A close-up of a DEMEC strip is shown in Figure 3.10.

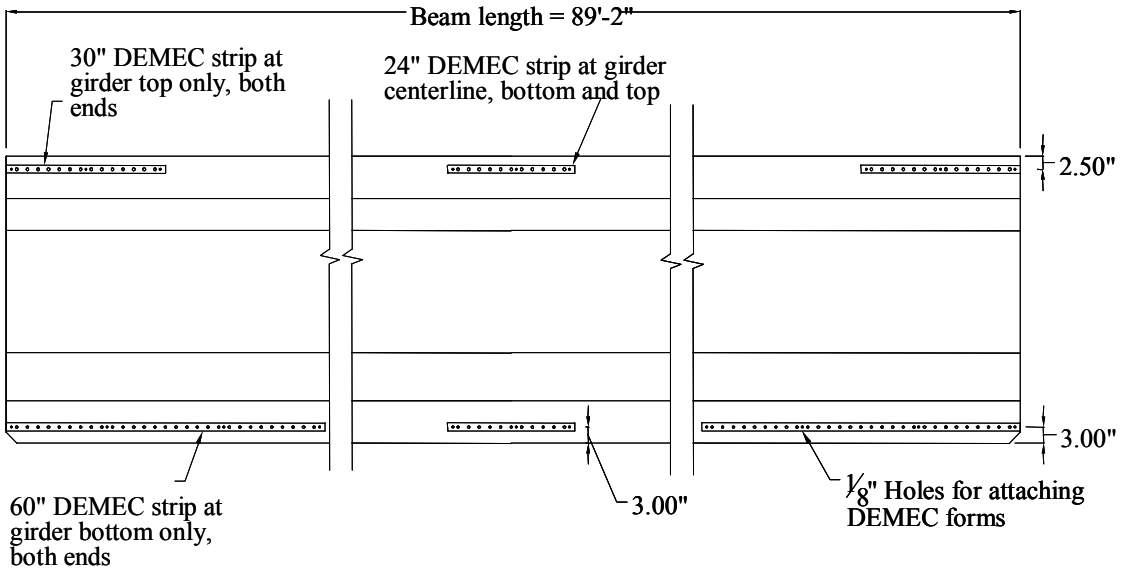

Figure 3.8 DEMEC strip locations for both girders

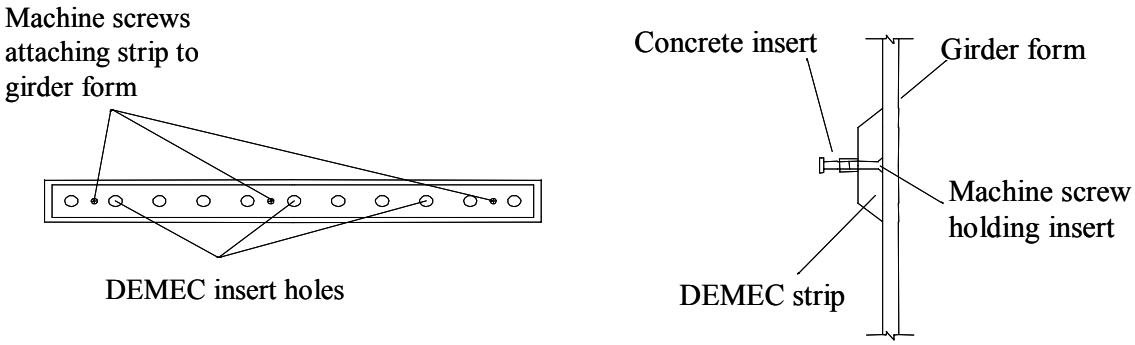

Figure 3.9 DEMEC strip construction and installation

Figure 3.10 Installation of a DEMEC embedment on girder formwork

3.2.1.3 Taut Piano Wire

A small diameter piano wire was installed on one side of each girder in order to determine girder camber and deflection at midspan. The wire was anchored at one girder end, directly over the bearing, and strung over a pulley at the other girder end, again, directly over the bearing. A ten-pound weight was attached to the end of the wire to ensure constant tension. At midspan, a metal ruler and a mirror were attached to the girder directly behind the taut wire. Figure 3.11 shows the locations of the attachments needed for the taut wire apparatus, and Figure 3.12 shows the attached ruler and mirror at midspan. To read this device, researchers lined up their eyesight so that the wire's reflection could not be seen in the mirror. This ensured that there was no parallax when measurements were taken.

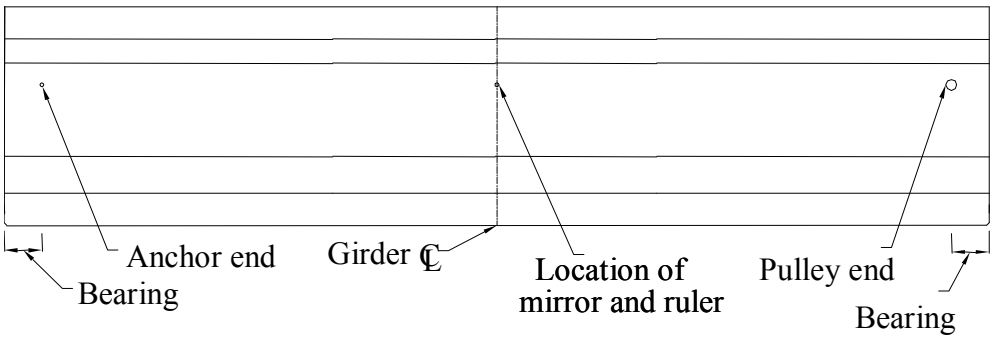

Figure 3.11 Locations of taut wire attachments

Figure 3.12 Attached ruler and mirror at midspan

3.2.1.4 Vibrating Wire Strain Gages and Thermocouples

Geokon low modulus vibrating wire strain gages (VWSG) with a 6-in. gauge length, and attached thermistors were installed at quarterspan and midspan of each girder,

as shown in Figures 3.13 and 3.14. Accurate temperature information was essential for thermal corrections of strain measurements, as well as measuring the thermal changes due to hydration. As such, thermocouples were used as a backup for the VWSG thermistors. The gages were placed at varying heights to obtain comprehensive strain profiles. A total of 6 VWSG were installed into each girder, 3 at midspan and 3 at quarterspan, and three thermocouples were installed at the midspan of each girder.

The labeling system for the VWSGs consisted of either an "M" or "Q" for midspan or quarterspan, followed by the gauge number, 5 through 7. The naming of the thermocouples consisted simply of "TC" and the instrument number, 3 through 5. Figure 3.12 shows the location of instruments at midspan of each girder, and Figure 3.13 shows the instrument locations at quarterspan of each girder. The congestion of strands in the bottom flange of each girder made placing the M7 gages on the girder centerline impossible. Therefore, the M7 gages were installed in the outer portion of each bottom flange. Pictured in Figure 3.15 are the three VWSGs at midspan, and Figure 3.15 shows a close-up view of the VWSG. Because of limitations of the data acquisition system, thermocouples were installed, but not measured in the BT-56; temperature data were obtained by using the VWSG thermistors.

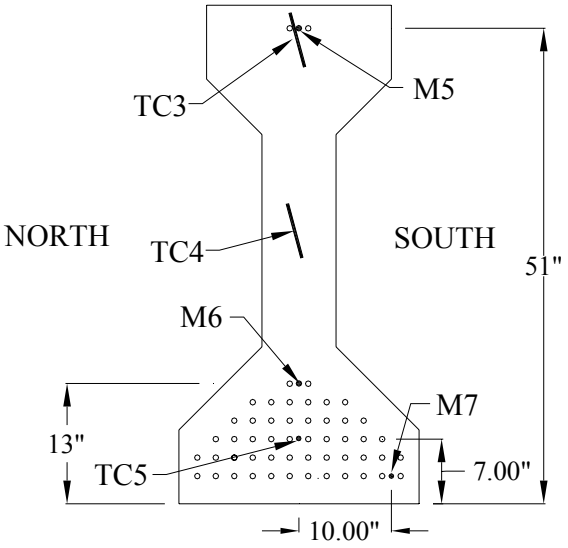

TYPE IV SECTION AT MIDSPAN

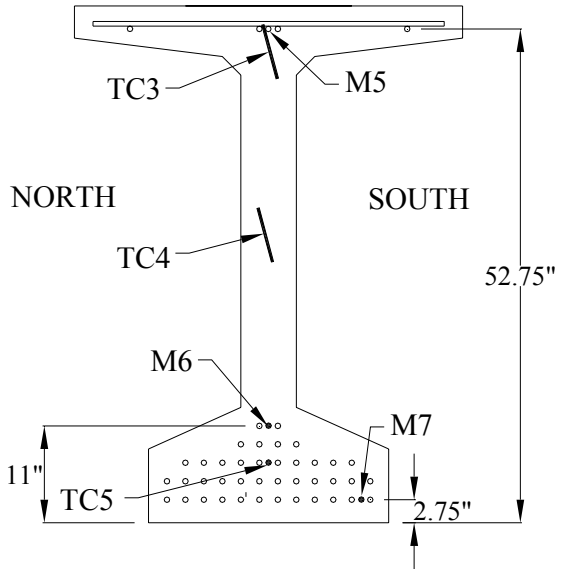

BT-56 SECTION AT MIDSPAN

Figure 3.13 Cross sections showing instrument locations for both girders at midspan

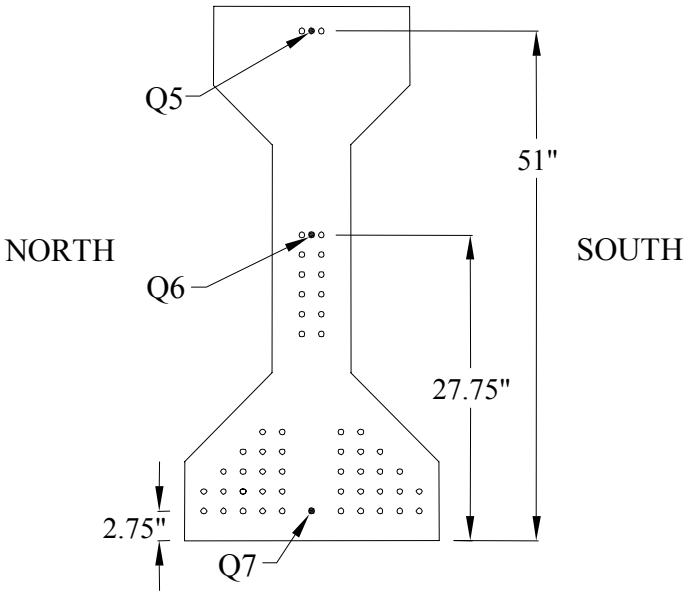

TYPE IV SECTION AT QUARTERSPAN

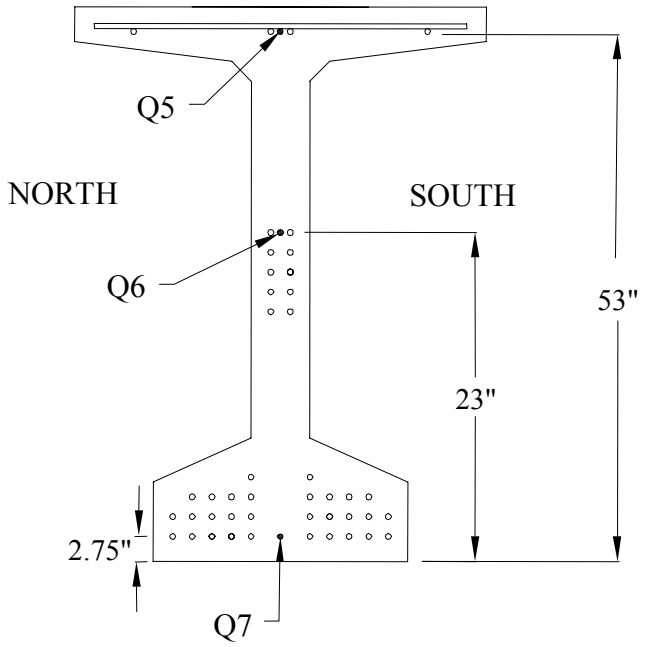

BT-56 SECTION AT QUARTERSPAN

Figure 3.14 Cross sections showing instrument locations for both girders

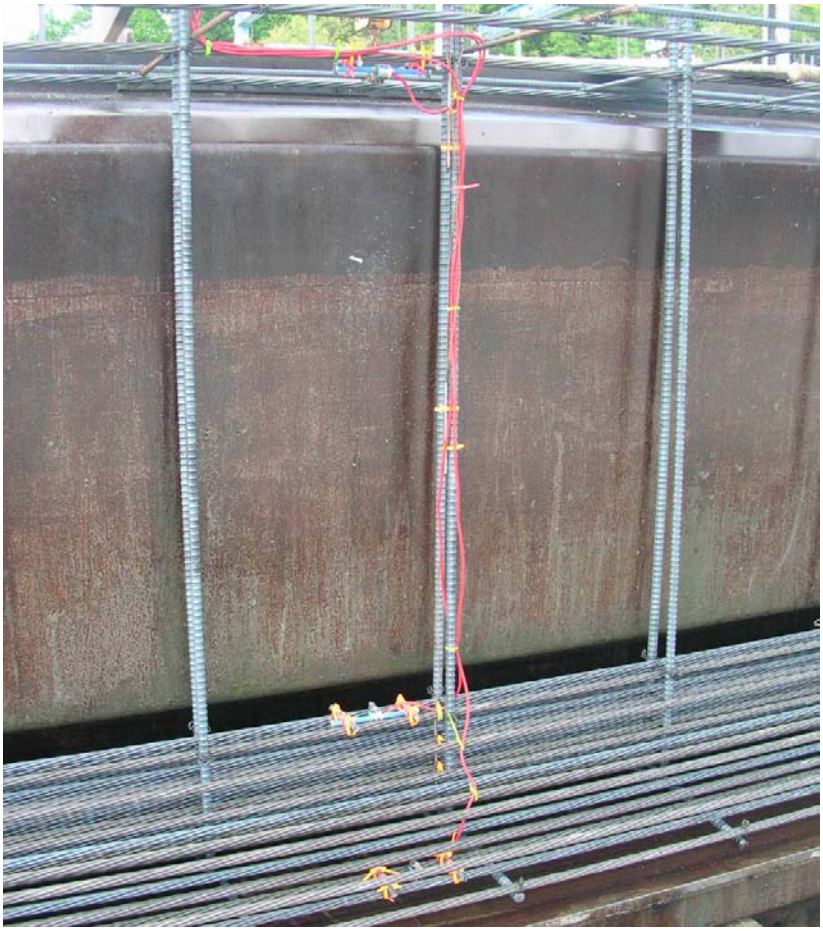

Figure 3.15 Three BT-56 midspan, VWSGs prior to concrete placement

Figure 3.16 Close-up of VWSG prior to concrete placement

3.2.1.5 Data Acquisition Systems

There were two data acquisition systems used by Georgia Tech researchers to obtain and record all data. One system was manufactured by National Instruments (NI) and consisted of a SCXI-1000 chassis, a SCXI-1520 strain gauge based sensor module and a SCXI-1314 strain terminal block. The NI equipment was read using Labview software made by NI. The other system was manufactured by Geokon and consisted of two multiloggers connected to one main datalogger. The Geokon system was read using Multilogger software, also manufactured by Geokon. The NI system was used to read all load cells and all electrical resistance strain gages used during load testing. The Geokon system was used to read all VWSGs and thermistors, in addition to some thermocouples. Figure 3.17 shows both data acquisition systems recording data on the Type IV girder in the Georgia Tech Structures Laboratory.

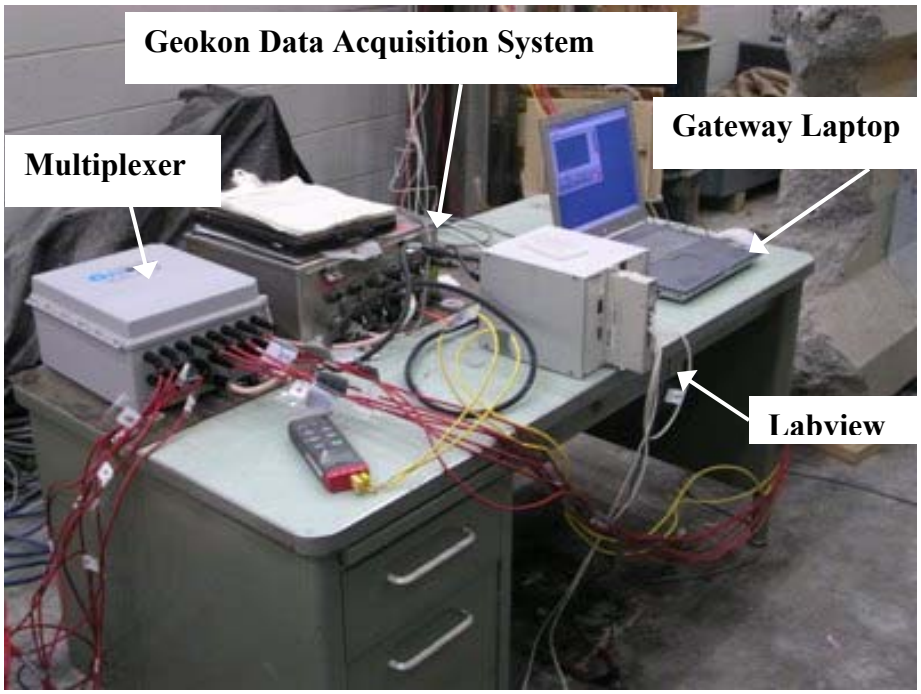

Figure 3.17 Data acquisition systems in use at the Georgia Tech Laboratory

3.2.2 Mix Design

The HPC mix used for both girders was to be the same as that used in the Jonesboro Road Bridge. The mix used in the bridge contained Type I cement, but since that time, SCP had changed to using Type III cement, and therefore, the mix for the laboratory girders used Type III cement. The mix design was classified by the Georgia DOT as a "Class AAA HPC" and was developed as a grade 2 HPC mix. The actual laboratory girder mixes achieved strengths which actually make them grade 3 mixes, but for consistency with past research at Georgia Tech, the mixes are referred to as grade 2 throughout this report. Information on the development of the HPC mix design can be found in "Mix Design and Properties of High Performance Concrete" (Lai, et al. 1999), and the proportions of the actual mix design are given in Table 3.2. The specified 56-day concrete compressive strength was 10,150 psi (70 MPa).

Table 3.2 HPC mix design for both girders

Material	Quantity lb/yd3 [kg/m3]
Cement,Type III	796 [472]
Flyash, Class F	98 [58]
Silica Fume, Force 10,000	70 [41]
Fines, Brown Brothers #2 sand	965 [573]
Coarse, Vulcan #67 stone	1837 [1090]
Water	237 [140]
w/cm	0.25
Material	Quantity oz/yd3 [ml/m3]
AEA, Daravair 1000	7 [271]
Water reducer, WRDA 35	35 [1354]
HRWR, Adva 100	169 [6537]

3.2.3 Formwork Preparation

Formwork preparation began on April 21st, 2005. SCP provided Georgia Tech students access to the formwork prior to casting the girders, to install necessary inserts for several types of measurements. Three types of inserts were installed onto the formwork for each girder. Detachable Mechanical (DEMEC) insert strips used for concrete surface strain (CSS) measurements, inserts for attaching a taut wire used for deflection measurements, and inserts requested by SCP were also placed at specific locations along each form. Figure 3.18 shows installation of a DEMEC insert strip onto the girder formwork.

Figure 3.18 M. Lopez installing DEMEC inserts onto greased formwork

3.2.4 Strand Tensioning

SCP personnel ran all 52 strands for the Type IV girder down the prestressing bed from the live end to the anchor end, shown in Figure 3.19. After the strands were strung

through the dead end of the prestressing bed, Georgia Tech researchers placed load cells on certain strands in the configuration presented in Figure 3.6. Figure 3.20 shows the placing of load cells at the dead end.

Once all the load cells were connected, zeroed, and checked, plant personnel cleared the area and began tensioning the strands. Each 0.6-in. diameter, 270 ksi, low relaxation strand was tensioned in the order shown in Figure 3.20. Each strand was to be tensioned to 75 percent of f_{pu} or 202.5 ksi. The corresponding required force on each strand was approximately 44.5 kips. The average force on each strand according to the Georgia Tech load cells was 44.7 kips which corresponded to an initial stress (f_i) of 206 ksi. The individual load cell readings, and the tensioning force measured by SCP is presented in Appendix A. Figure 3.22 shows SCP personnel getting ready to attach the hydraulic jack to a prestressing strand at the live end and Figure 3.23 shows the device used by SCP personnel to tension the strands. Figure 3.24 shows the prestressing bed with all strands tensioned.

Figure 3.19 SCP personnel installing the 52 strands of the Type IV girder

Figure 3.20 Installation of load cells onto the dead end of the prestressing bed

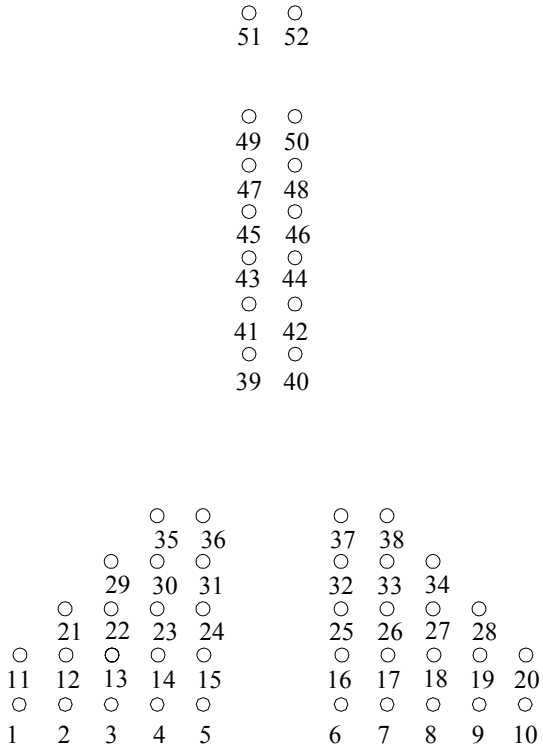

Figure 3.21 Strand tensioning order at live end

Figure 3.22 SCP personnel jacking the prestressing strands

Figure 3.23 SCP personnel tensioning strands

Figure 3.24 Prestressing bed with all strands tensioned

3.2.5 Installation of Vertical Reinforcing Steel

After all 52 strands were tensioned, SCP personnel installed all of the required non-prestressed reinforcing bars. A detailed drawing of the various types of non-prestressed reinforcement is presented in Figures 3.2, 3.3 and 3.4. The vertical reinforcing bars used were # 6 stirrups at the ends of each girder and # 5 stirrups throughout the remainder of each girder. The "doghouse" bars used at both ends of each girder were # 3 bars. The nominal yield strength of the bars was 60 ksi (413.7 MPa); the actual yield strength is presented in Chapter 4. Georgia Tech researchers checked all stirrup spacing to insure correct installation. Figure 3.25 shows the installation of vertical

reinforcing bars and Figure 3.26 shows the checking of stirrup spacing along with spacing of the "doghouse" bars.

Both girders contained 2 lifting hooks at each end so that cranes would be able to lift them on the prestressing yard and in the structural laboratory. Each hook consisted of five unstressed and bundled 0.6 in. prestressing strands. The hooks added a large amount of shear strength to each girder in the critical section. They can be seen at the east end of the Type IV girder in Figure 3.26. More details on these lifting hooks will be given in Chapter 6.

Figure 3.25 Installation of vertical reinforcing bars

Figure 3.26 Checking of stirrup spacing

3.2.6 Installation of Girder Instrumentation

The final task for Georgia Tech researchers before the formwork was put into place was the installation of all of the internal instruments. The two types of instruments installed in the girders were Vibrating Wire Strain Gages (VWSG) and thermocouples. The instruments were placed in both girders at midspan and at quarterspan. A diagram and layout of where these gages were placed is given in section 3.2.1.4. Each instrument was securely attached to the prestressing strand and vertical reinforcing bars with zip-ties at different heights for each girder. Figures 3.27 and 3.28 show the placement of a VWSG and a thermocouple at midspan of the BT-56 girder.

Figure 3.27 Placement of VWSG gages at Type IV midspan bottom flange

Figure 3.28 Installed thermocouple at midspan

3.2.7 Formwork Placement

SCP coated all of the forms with a form releasing agent prior to placement to facilitate the formwork removal from the girders. Care was taken to avoid coating the DEMEC inserts with the release agent. Figure 3.29 shows an oiled BT-56 form being lifted into place. Another detail performed before the formwork was placed was the placement of Teflon bearing pads at each end of each beam. Figure 3.30 shows a Teflon pad prior to formwork placement. The pads were 14-in. long x 26-in. wide and approximately 1/8-in. thick. They were used to reduce the friction between the girder ends and the prestressing bed during the transfer of prestressing force. Also shown in Figure 3.30 is the chamfer block at the end of the girder.

Once the forms were properly aligned, they were moved into place with SCP cranes. Once in place, Georgia Tech researchers double checked the alignment so that all inserts and devices were in the correct locations. SCP personnel then locked the forms into place at the top and bottom of the forms.

Figure 3.29 BT-56 formwork being lifted into place

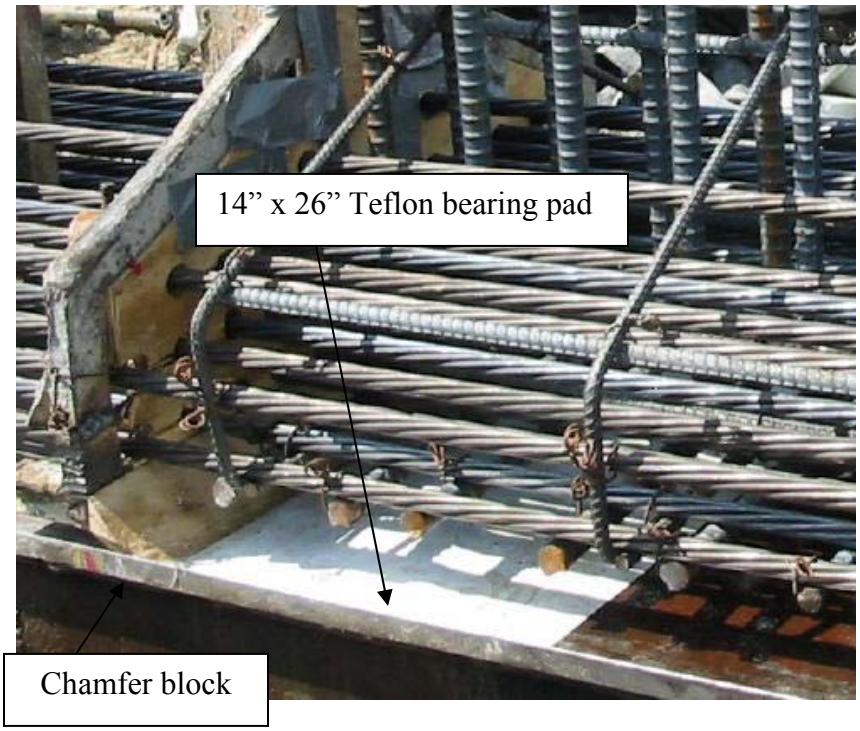

Figure 3.30 Teflon bearing pad prior to form placement

3.2.8 Concrete Placement

Batching of the concrete began as soon as the forms were locked into place. The batching took place in a rotary auger-type mixer in an elevated mix station just east of the prestressing beds. The actual batching was performed according to standard specifications and each batch took an average of 15 minutes to place.

3.2.8.1 Concrete Placement and Finishing

As mentioned before, the girders were cast a day apart, due to the different number and configuration of strands in each girder. Six batches of concrete were required for the completion of each girder. Each batch was dumped into a Tuckerbilt truck and carried to different locations along each girder. Figure 3.31 shows how each batch was placed into each girder cross-section. Figure 3.32 shows a picture of a Tuckerbilt truck placing concrete into the Type IV form.

The pour for the Type IV girder ran into some problems, when one of the Tuckerbilt trucks broke down in between batches 3 and 4. There was a 15-20 minute delay as SCP personnel had to tow the Tuckerbilt out of the way. This delay was not seen as a major problem and batching continued without incidence after the second Tuckerbilt was utilized. The BT-56 pour did not run into any problems, was completed in less time, and had a more normal batching sequence.

SCP personnel used formwork and spud vibrators to properly consolidate the concrete. There were at least two Georgia Tech researchers present at all times during this phase to ensure the protection of all of the instrumentation within the girders.

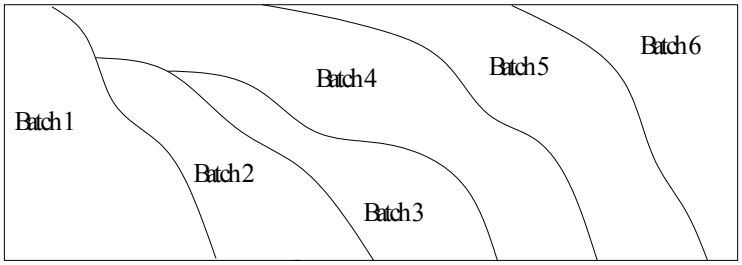

Type IV

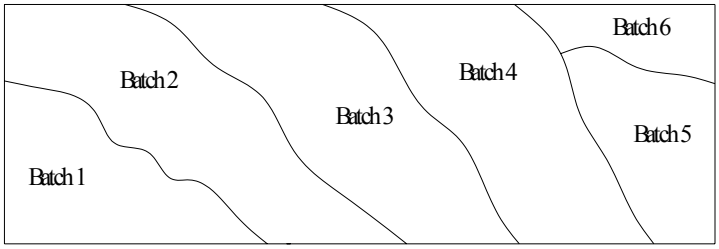

BT-56

Figure 3.31 Batch configurations for each girder

Figure 3.32 Tuckerbilt truck placing concrete into Type IV form

After vibrating the concrete, SCP personnel raked the tops of each girder to provide the required ¼ -in. roughened top surface. As the workers moved from west to east, Georgia Tech researchers followed behind them placing small inserts into the concrete at approximately 3-ft intervals along each girder. The embedded inserts were used to attach the plywood deck formwork to the girders at the Georgia Tech Structures Laboratory. Discussion on the deck construction is presented in Section 3.3.

3.2.8.2 Materials Testing

As each new batch was mixed, a small amount was used to perform quality control tests, conducted by SCP personnel. Slump and air content tests were performed according to ASTM C231 and ASTM C173 to ensure that each batch met the design standards. If the batches did not meet the design criteria, the concrete was discarded, and corrections were made in the batching plant. Upon batch approval, concrete was taken to use in control cylinders, made by Georgia Tech researchers. This procedure was followed for the necessary batches from each girder, until casting was completed.

Control specimens were made from concrete placed in each end and the middle of both girders, as well as additional specimens used for a statistical sampling. They were taken from the three locations to obtain a representative sample of data from each girder. Care was taken to ensure the samples were taken from the appropriate batches.

Some specimens were kept in the open air while others were kept in insulated curing boxes. Previous Georgia Tech research showed that the concrete samples more closely match the actual properties of the girder when allowed to cure in insulated boxes (Saber, 1998). Figure 3.33 shows Georgia Tech researchers placing concrete into

cylinders. SCP personnel also fabricated some quality control specimens and placed them into their match-curing devices. These devices were designed to match the curing temperature in the girders, which was measured by a thermocouple placed in the middle of the bottom flange of each girder. SCP match-cure temperatures and testing results are presented in Chapter 4. Figure 3.34 shows SCP personnel preparing a match-cure sample. Chapter 4 also details the number and organization of all quality control samples, along with the material properties of each sample taken.

Figure 3.33 Georgia Tech researchers placing concrete into cylinders

Figure 3.34 SCP personnel preparing a match cure specimen

3.2.9 Concrete Curing

The curing of the each girder was different. The Type IV girder, which was cast first, was covered with heavy duty tarps and cured with both steam and water at 110°F. The next morning at approximately 10:30 AM, the Type IV tarps were removed and the ten strands not required in the BT-56 were cut so that preparations could begin for casting the BT-56. After casting, the BT-56 was covered with the same tarps and was water cured without steam. The temperatures were monitored by the match-cure thermocouples, the quality control sample thermocouples, and both thermocouples and thermistors in each girder. Plots of girder curing temperatures along with control sample temperatures are presented in Chapter 4, Section 4.3.

SCP quality control personnel performed compression testing on the match-cured samples and on ASTM samples after the beams had been curing for some time. The

Type IV samples were tested 13 hours after the pour, and the BT-56 samples were tested 14.5 hours after the pour. In all cases, the match-cured cylinders were stronger than the ASTM cylinders. The match cure cylinders were more indicative of the actual girder strength because of the temperature matching. The compression results indicated that each girder had gained necessary strength for cutdown, as provided in Chapter 4.

3.2.10 Formwork Removal and Cutdown

The formwork for each girder was removed at different times on different days. Upon arrival at SCP on the morning of April 23rd, Georgia Tech researchers removed all screws and attachments that were holding inserts on the Type IV formwork. Once all inserts were free and clear of the forms, the Type IV girder formwork was removed by SCP cranes. Immediately after form removal, Georgia Tech researchers removed the DEMEC strips from the concrete and took initial or "zero" CSS readings. Figure 3.35 shows initial CSS readings being taken. After initial DEMEC readings were taken, researchers installed the taut wire and an initial camber reading was taken. After the area was cleared, SCP personnel cut and removed the necessary ten strands. The two additional strands for the BT-56 top flange were then placed and tensioned.

After the BT-56 was poured and allowed to cure overnight, the same procedure was followed. Students removed the insert screws, SCP personnel removed the forms, and the DEMEC strips were removed from the concrete. Once the strips were removed, students took "zero" CSS readings, installed the taut wire, and took initial camber readings.

SCP personnel tested more match-cured specimens before cutdown to ensure the concrete had reached the minimum cutdown strength of 8,120 psi (80% of the design strength, 10,150 psi). SCP personnel used oxy-acetylene welding torches to simultaneously flame cut the strands at each girder end. The strands had to be cut at the live end east of the Type IV, in between the two girders, and at the dead end, west of the BT-56. Figure 3.36 shows SCP personnel cutting the strands, at each girder end. After all strands were cut, "release" readings were taken on each girder. These readings included CSS and camber. The internal instruments in each girder were continually taking measurements, so the time of cutdown was recorded, which began at 10:30 AM on April 24th.

Figure 3.35 Georgia Tech researcher taking "zero" DEMEC readings

Figure 3.36 Flame cutting of prestressing strands at east end of Type IV girder

3.2.11 Girder Movement and Storage

After both girders were cut down, they were temporarily placed on dunnage directly south of the prestressing bed. At this time, CSS and camber readings were taken again, as any restraint from the prestressing bed would be removed. The girders remained at this location until Wednesday, April 28th, as storage locations had not been cleared until that time. On that day, the BT-56 was moved to a storage location in the morning, and the Type IV was moved directly beside it in the afternoon. Figure 3.37 shows the moving of the Type IV to storage and Figure 3.38 shows the BT-56 in its location on the SCP yard.

Figure 3.37 Movement of Type IV girder to storage location

Figure 3.38 BT-56 girder in storage at Standard Concrete Products

The Type IV girder remained in storage until May 10th, 2004, when it was transported to the Georgia Tech Structures Laboratory. Figure 3.39 shows the Type IV being delivered to the laboratory. The BT-56 was kept at SCP until August 3rd, 2004. The BT-56 was transported in the same way, with the same truck. Figure 3.40 shows the BT-56 being loaded onto the truck at SCP.

Figure 3.39 Type IV girder being delivered to the structural engineering laboratory

Figure 3.40 BT-56 girder being loaded onto transport truck

3.3 Composite Deck Construction

Both girders had composite decks that were cast in the structural engineering laboratory by Georgia Tech researchers. The Type IV deck was placed on June 30th, 2004 at 4:15 PM and the BT-56 deck was placed 2 months later on September 1st at 10:00 AM.

3.3.1 Mixture Design

The concrete mixture used for both decks was the same as the Jonesboro Rd. Bridge. The mix was classified by the Georgia DOT as a "Class AA HPC" mix and developed as a grade 1 HPC mix. The grade 1 HPC mixture was designed in a study conducted at Georgia Tech in Task 3 (Lai, et al., 1999). Table 3.3 shows the mix design used for both decks.

Table 3.3 Mixture design for both decks

Material	Quantity lb/yd3 [kg/m3]
Cement,Type I	606 [360]
Flyash, Class F, Boral	99 [59]
Silica Fume, Force 10,000	25 [15]
Sand, natural Waugh Marietta	1162 [690]
Coarse, Vulcan #67 stone	1767 [1050]
Water	242 [144]
w/cm	0.34
Material	Quantity oz/yd3 [ml/m3]
Air entrainer, grace AEA-II	19.2 [47]
HRWr, Garace Adva 140	88.16 [213]

3.3.2 Formwork Design and Preparation

It was determined to use a 5-ft wide x 8-in. thick composite deck on each girder, due to laboratory constraints. To accurately represent the conditions of the Jonesboro Rd. Bridge, the deck formwork was supported by the girder.

The formwork design was optimized so that the same formwork could be used for both girders. The material used consisted of primarily nominal 2 in. x 4 in. boards and ¾-in. plywood. The Type IV deck formwork was designed first, as the Type IV girder had a narrower top flange and therefore larger plywood forms. The plywood was attached to the top of each girder and secured by small screws inserts embedded into the girder top flanges. For the Type IV, the plywood extended 19-in. out from each side of the girder to obtain the necessary 5-ft wide deck. For the BT-56, a 9-in. span was all that was required. Two 2 in. x 4 in. supports were used every 4 ft. along the length of the girder to support the plywood for the Type IV and one support was used at 4 ft. on center to

support the plywood for the BT-56. The 2 in. x 4 in. supports were then attached to wooden blocks bonded to the bottom flange of each girder. The wooden blocks were attached to the girders using PL-400 construction adhesive.

Once the bottom section of the formwork was assembled and installed, the 8-in. high sides were constructed and attached. The sides were used for both girders with little modification. Each piece was screwed into the 2 in. x 4 in. horizontal runners that supported the plywood deck. At the top of each side board, a 2 in. x 4 in. runner was installed horizontally to provide added lateral stiffness. Once the runners were installed, both sides were connected together with 5-foot long packing straps to provide the lateral support needed to prevent side blowout. Each strap was screwed to both sides of the vertical plywood sides. Figure 3.41 shows the Type IV formwork design and Figure 3.42 shows the BT-56 formwork design.

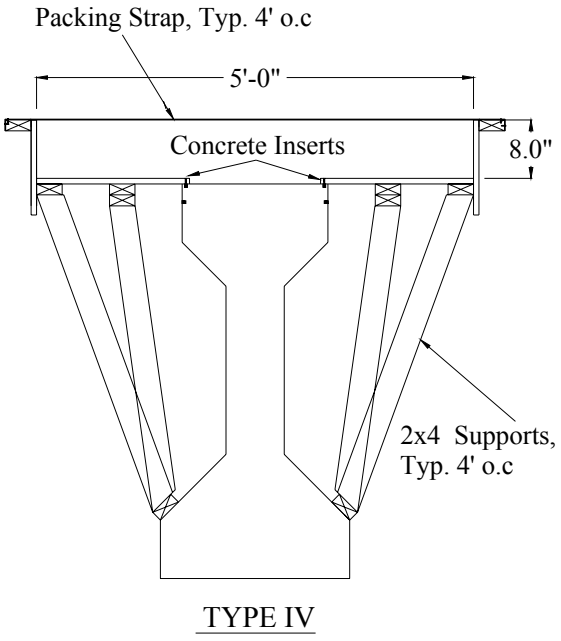

Figure 3.41 Type IV formwork design

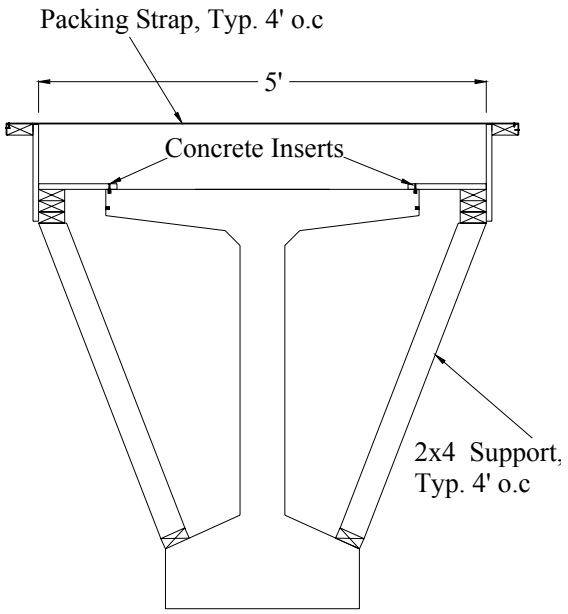

Figure 3.42 BT-56 formwork design

3.3.3 Steel Reinforcement Layout

The steel reinforcement placed in each deck was partially based on the steel reinforcement used in the Jonesboro Rd. Bridge deck. The reinforcement parallel to the girder's centerline was based on the bridge deck design, but the perpendicular reinforcement was not. It was decided to use temperature and shrinkage steel only in the transverse direction, as this steel was only required to support the deck dead load.

Georgia Tech researchers installed all deck steel in the structures laboratory. Different sized chairs were used to obtain the proper heights and spacing. All steel was tied together with wire tie.

The reinforcement consisted of # 4 bars placed longitudinally and transversely. The longitudinal steel was assembled from 20-ft pieces of steel with 18-in. splices. 9

rows of longitudinal steel were placed in two layers; one 2 in. from the bottom of the deck, and one 2 ¾ in. from the top of the deck. There were 6 rows in the bottom layer and 3 rows in the top layer. The transverse steel was placed in two layers, the top bars spaced at 10" on center and the bottom spaced approximately 10 ft on center. The bottom transverse steel was primarily used to support the longitudinal steel. Figure 3.43 shows the reinforcement spacing used in each deck. Figures 3.44 and 3.45 show completed formwork for each deck and Figure 3.46 shows typical steel layout in each deck

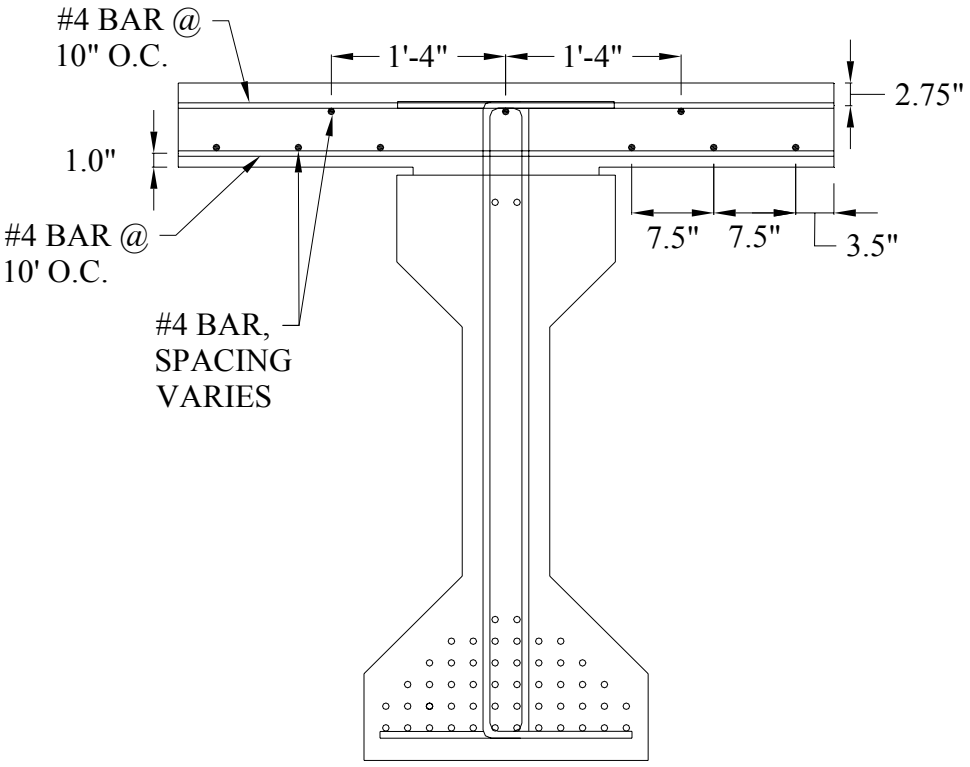

Figure 3.43 Typical deck reinforcement layout for each girder

Figure 3.44 Type IV formwork

Figure 3.45 BT-56 completed formwork

Figure 3.46 Typical steel reinforcement layout

3.3.4 Installation of Deck Instrumentation

Georgia Tech researchers installed instrumentation in each deck at quarterspan and midspan. Each instrument was installed with zip-ties and small pieces of rebar in order to obtain proper placement. Instrumentation was installed in each deck so temperatures and strains could be measured. The strains measured by the deck instrumentation, along with the girder instrumentation would allow for complete strain profiles to be obtained before, during, and after girder flexure tests. The three gages installed in each deck were VWSGs, thermocouples, and electrical resistance strain gages (ERSG).

Eight low modulus VWSGs and two thermocouples were installed in each deck. Four VWSGs were installed at quarterspan and midspan. The VWSGs had a low stiffness in order to obtain the early age strains within the curing concrete. Two thermocouples were installed at midspan for both girders. Both instruments were numbered based on the

previous girder numbering for consistency. Figure 3.46 shows how they were numbered at midspan; Figure 3.48 shows them in place at the midspan of the BT-56; and Figure 3.49 shows a close-up of a VWSG and a thermocouple.

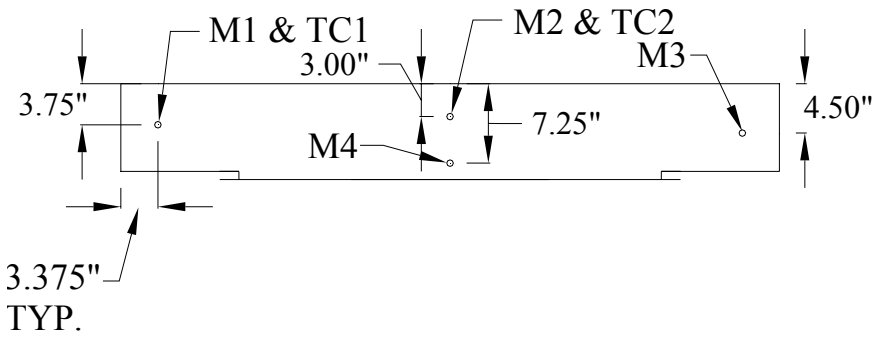

Figure 3.47 Location and labeling of deck VWSGs and thermocouples

Figure 3.48 VWSG at midspan of BT-56

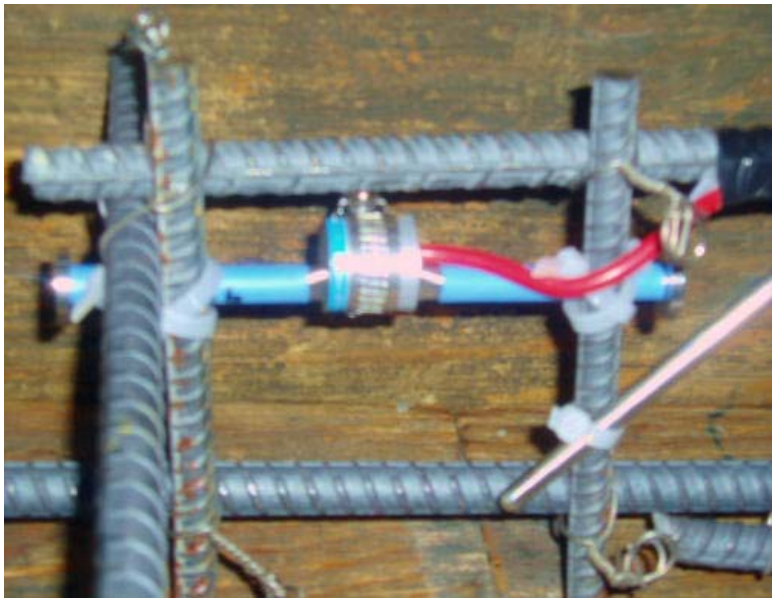

Figure 3.49 Close-up of VWSG and thermocouple in deck formwork

ERSGs were used on both girders to monitor strain at the deck/girder interface and at the top of the finished deck. These gages were 6-in. long electrical resistance strain gages manufactured by Texas Measurements and read by Labview. A total of eight were used in each composite girder. Four were placed at the girder interface, (two at midspan and two at quarterspan), and four more were placed at midspan on top of the finished decks. Figure 3.50 shows the locations of the ERSGs at the interface and top of the deck. The interface gages were zeroed before concrete placement to study the girder surface strain during the deck curing process. The gages on top of the finished decks were installed and zeroed prior to flexure testing.

Georgia Tech researchers installed the interface gages before the reinforcement steel was in place for ease of construction. A smooth and level surface was needed for the placement of each gauge. After gauge positions were marked, researchers used

electric grinders and sandpaper to create the necessary conditions. Dev-con quick drying epoxy was used to fill up any voids in the concrete and to level any unevenness remaining. Researchers placed more epoxy on the smooth surfaces with small brushes and installed the gages. Figure 3.51 shows a researcher putting epoxy over an interface gauge. After the gages were in place, a protective wax was melted and placed over each gauge, which protected each gauge from moisture. Finally, a protective tape was placed over the wax to ensure that the gages would not be damaged by the fresh concrete in any way. Figure 3.52 shows two midspan surface strain gages with the protective wax and tape.

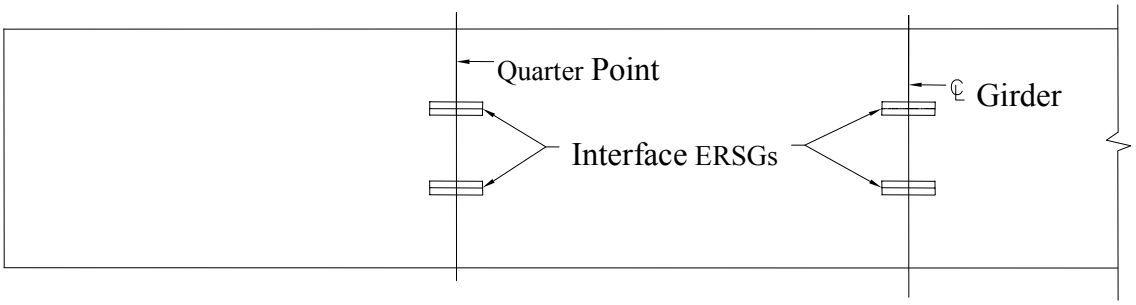

Typical ERSG placement at deck/girder interface

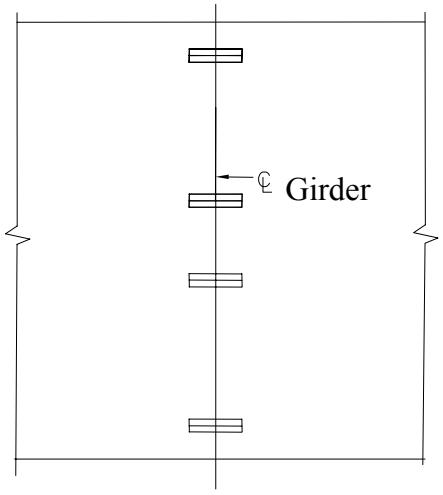

Typical ERSG placement on top of finished deck

Figure 3.50 ERSG locations at interface and top of deck

Figure 3.51 Installation of a concrete surface strain gauge

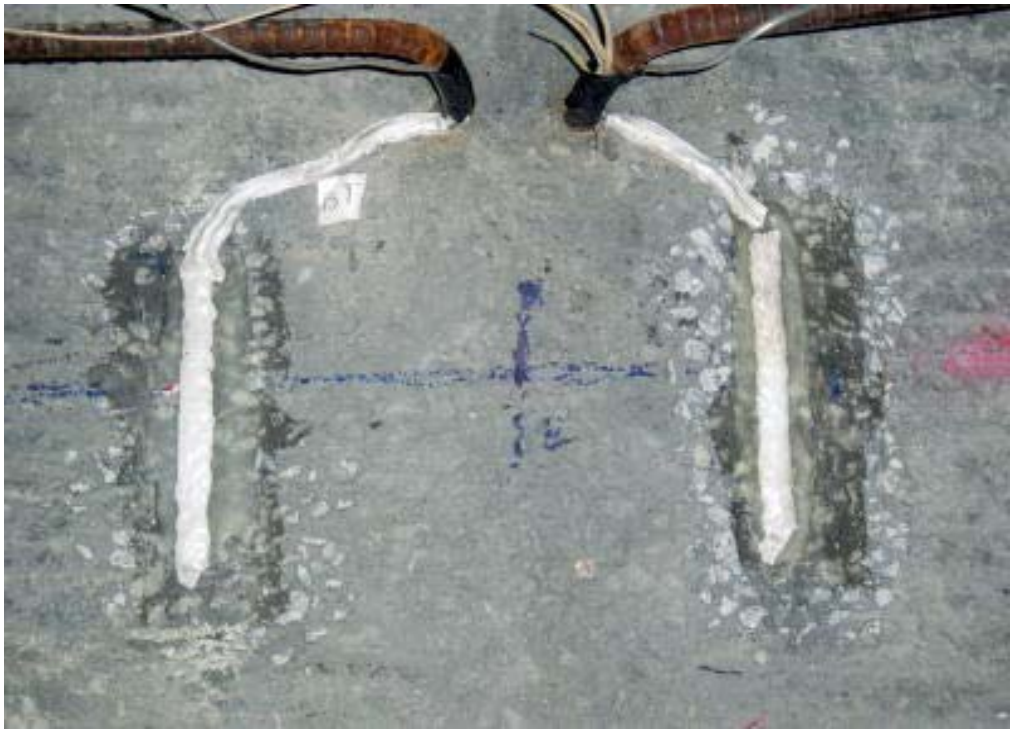

Figure 3.52 Fully installed concrete surface strain gages

3.3.5 Concrete Placement

The concrete placement for each deck was performed in a similar manner. Both decks had the same mix design, with a specified compressive strength of 7,000 psi (48.3 MPa). Lafarge Concrete of Atlanta mixed the concrete at their batching plant and delivered it to the structures laboratory in ready-mix trucks. Both decks required approximately 13 cubic yards of concrete, which was comprised of two batches per deck. Georgia Tech researchers handled and placed all the concrete in the deck and quality control samples.

3.3.5.1 Concrete Placement and Finishing

When the concrete arrived, it was necessary for Georgia Tech researchers to take the slump of each batch to ensure the mix met the required specifications. Only one ready-mix truck from either girder needed additional water to acquire an acceptable slump. After the concrete slump was approved for a given batch, the ready-mix conveyor system was positioned at the end of girder farthest from the laboratory door.

Several Georgia Tech researchers assisted in the placement of the deck concrete after the slump was taken. Two researchers assisted in the actual placing and vibrating of the concrete. One guided and directed the concrete chute while the other followed behind with a spud vibrator ensuring proper compaction. Both decks required two batches. Batch 1 filled approximately half of the Type IV deck, and batch 2 filled the remainder of the deck. Batch 1 of the BT-56 deck filled approximately ¾ of the deck, and the remainder was filled with batch 2 concrete. Two more researchers followed behind the

conveyor to screed and finish the concrete with a long 2 in. x 4 in. board. Figure 3.53 shows the placement and screeding of the concrete as it occurred for both girders.

After the concrete began to set, students troweled the concrete at midspan to ease the process of later attaching ERSGs. The concrete was covered with wet burlap and plastic to hold moisture and aid in the curing process. The burlap was kept wet for 7 days, after which it was removed.

Figure 3.53 Placement and screeding of the BT-56 deck

3.3.5.2 Materials Testing

Georgia Tech researchers made all of the deck quality control samples. Several researchers were needed to scoop, shovel, screed, and rod the concrete in all of the

specimens. Figure 3.53 shows researchers placing the deck concrete in quality control specimens.

The same number of quality control samples were taken from both batches for each deck. 4 in. x 8 in. control cylinders were made for compressive strength and chloride permeability; 6 in. x 12 in. cylinders were made for CTE and modulus of elasticity tests; and 4 in. x 15 in. cylinders were made for shrinkage measurements. All samples were allowed to cure under ASTM conditions.

Figure 3.54 Georgia Tech researchers placing deck concrete into cylinders

Temperatures of the cylinders were monitored using embedded thermocouples and will be discussed in the next section. After 24 hours, the majority of the samples were demolded and taken to the fog room for further curing at the structures laboratory.

The shrinkage cylinders, however, were demolded after 8 hours and placed underneath the tarp on top of each deck to match the actual curing temperatures. Chapter 4 presents all of the material properties of the deck concrete.

3.3.6 Concrete Curing

Each deck was watered daily for a period of six days, and after 7 days from casting, the formwork was removed. Strain and temperature data in the deck and girder were measured continuously inside the decks. Shrinkage and temperature data of the cylinders were taken continuously for seven days, and twice a week for two months after that. The effect of the deck on the girder camber in addition to deck strains during the hydration phase is discussed in Canfield and Kahn (2005). Figure 3.55 shows the deck in the curing process. Each deck was cured under ambient conditions inside the structures laboratory.

Figure 3.55 Type IV deck curing

CHAPTER 4

MATERIAL TESTING AND PROPERTIES

4.1 Introduction

This chapter provides details on the production and testing of quality control specimens for both girders and both decks. Several different methods were used to cure the control specimens; match-curing, insulated-box (accelerated), and ASTM curing are discussed in Section 4.3. All the deck control samples were made at the Georgia Tech Structures and Materials Laboratory, where each deck was cast. The control samples for each deck were all cured according to ASTM C31. Unless otherwise stated, all samples were demolded and stored in the fog room at 70°F and 100 percent RH per ASTM C31 at the Georgia Tech Structures Laboratory.

A total of seven different quality control tests were performed on the concrete in each girder. All tests were performed on a variety of batches from each girder to obtain reliable averages. The seven tests performed were compressive strength, modulus of elasticity, modulus of rupture, chloride permeability, coefficient of thermal expansion (CTE), creep, and shrinkage. All of the above tests were performed on the deck control specimens except modulus of rupture and creep.

The data presented in this chapter present the averages and summaries of all specimen testing. Specific test results are provided in Appendix B.

4.2 Specimen Organization

The organization of specimens was planned to ensure the proper amount of control specimens for each test. The specimen nomenclature was designed so that each sample would be labeled for either girder or deck and location, type of test, and age at testing. Each girder required 6 batches, and each deck required 2 batches. Different numbers of samples were taken from each girder batch depending on the batch location and importance. For example, more control specimens were taken from the middle of each girder because these data were most important for flexure testing and girder deflection. Equal numbers of samples were taken from each deck.

4.2.1 Girder Specimen Nomenclature

Most specimens were taken from the middle and ends of each girder. These locations were chosen because they would provide a representative average for each girder. The batches were labeled BEE, BEW and BM for each girder, which indicated Batch End East, Batch End West, and Batch Middle. For the Type IV girder, batches 1, 3, and 6 were used to represent the three labeled sections. For the BT-56 girder, batches 1, 3, and 5 were used. The batch layout was shown in Chapter 3, Section 3.2.7.1. Table 4.1 shows the number of samples taken from the three main girder locations.

4.2.2 Deck Specimen Nomenclature

Each deck contained two batches of concrete provided by Lafarge Concrete in Atlanta, GA. Each batch was transported in a ready mix truck and was placed directly into the deck formwork. The Type IV deck consisted of approximately equal volumes of

concrete from both batch 1 and batch 2. The BT-56 deck however, contained approximately ¾ of batch 1 concrete and the remaining concrete was from batch 2.

Both the Type IV and BT-56 deck control samples were labeled in the same manner. The specimens were labeled IV-B1 or IV-B2 and BT-B1 or BT-B2 indicating batch 1 or batch 2, along with the test type and testing day. Table 4.2 shows the number of samples taken for each deck.

Table 4.1 Number of samples taken from each girder batch

Type IV			
Test	BEW (West end)	BM (Middle)	BEE (East End)
Compression Testing	9	24	9
Rapid Chloride Permeability		3	
Modulus of Elasticity	3	6	3
CTE Testing		1	
Modulus of Rupture	1	1	1
Creep		3	
Shrinkage		2	
BT-56			
Test	BEW (West end)	BM (Middle)	BEE (East End)
Compression Testing	11	26	11
Rapid Chloride Permeability		3	
Modulus of Elasticity	3	6	3
CTE Testing		3	
Modulus of Rupture	1	1	1
Creep		2	
Shrinkage		3	

Table 4.2 Number of samples taken from each deck

Type IV		
Test	Batch 1	Batch 2
Compression Testing	15	15
Rapid Chloride Permeability	1	1
Modulus of Elasticity	4	4
CTE Testing	2	2
Shrinkage	4	4
BT-56		
Test	Batch 1	Batch 2
Compression Testing	15	15
Rapid Chloride Permeability	1	1
Modulus of Elasticity	4	4
CTE Testing	2	2
Shrinkage	4	3

4.3 Concrete Curing Methods

The three methods of curing used on control samples were match-curing, insulated (accelerated) curing and ASTM curing. Match-cured samples were placed in a housing after casting, which was temperature controlled. The control panel had a thermocouple embedded in the girder bottom flange, at midspan, and it maintained the

same temperature in the match-cure housing. The match-cured samples were assumed to provide the same compressive strength as the girder as a result of the same curing temperature.

Insulated-cured samples were placed in a plywood box lined with polystyrene to prevent heat loss to the environment. One sample in each insulated box had a thermocouple embedded to record temperatures during curing.

The final method of curing was the ASTM method (ASTM C 31), in which each sample was cast and left in ambient conditions alongside the girder of deck during curing. A thermocouple was also placed in at least one ASTM cured sample to record curing temperatures.

The curing method had no bearing on how each sample was stored. Generally, one day after each specimen was made, it was demolded and placed in a fog room at 100% relative humidity and 73° F until time of testing.

As noted in Chapter 3, each girder was cured differently. The Type IV girder was cured with both water and steam at 110 ^{o}F, (43.3°C) whereas the BT-56 girder was water cured without steam. Figure 4.1 compares the curing temperatures obtained from internal thermistors and thermocouples for each girder during the first 24 hours. Figures 4.2 and 4.3 give curing temperature comparisons for each girder and their corresponding control specimens. The ASTM cured BT-56 girder specimens had a high heat of hydration because they were kept near the insulated boxes inside the laboratory truck.

The decks for both girders were cured according to ASTM C31. Wet burlap was placed over the entire deck and was then covered with plastic tarps to ensure proper

curing conditions. Figures 4.4 and 4.5 show the curing temperature comparisons for each deck and their corresponding control specimens.

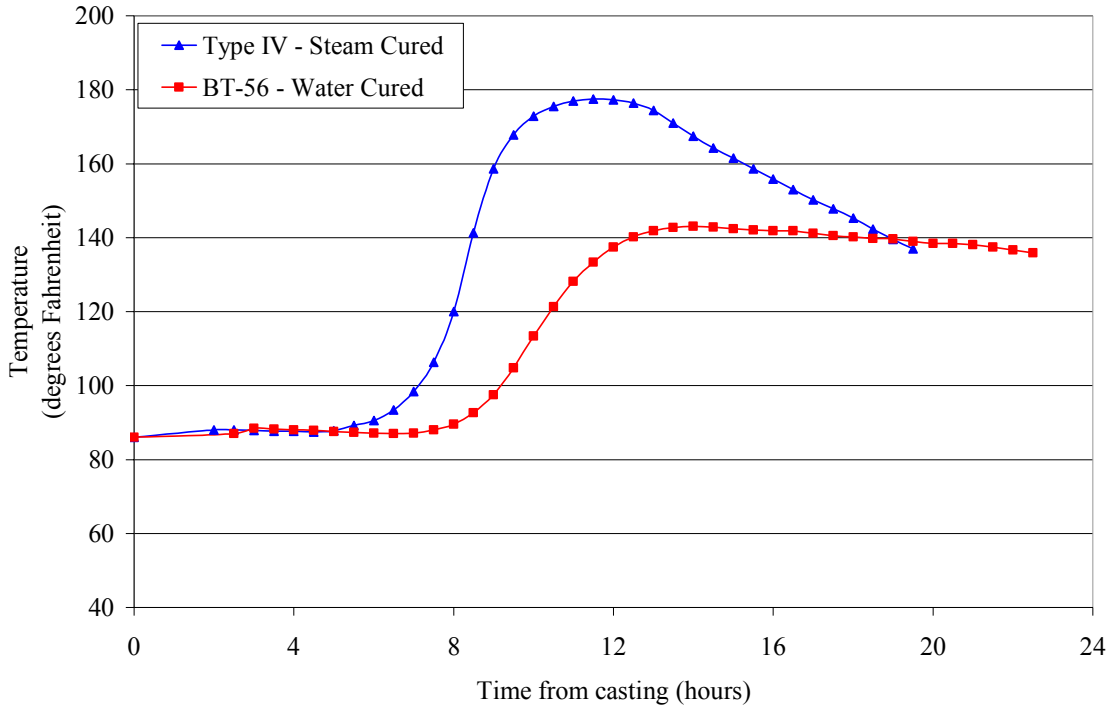

Figure 4.1 Curing temperatures for each girder

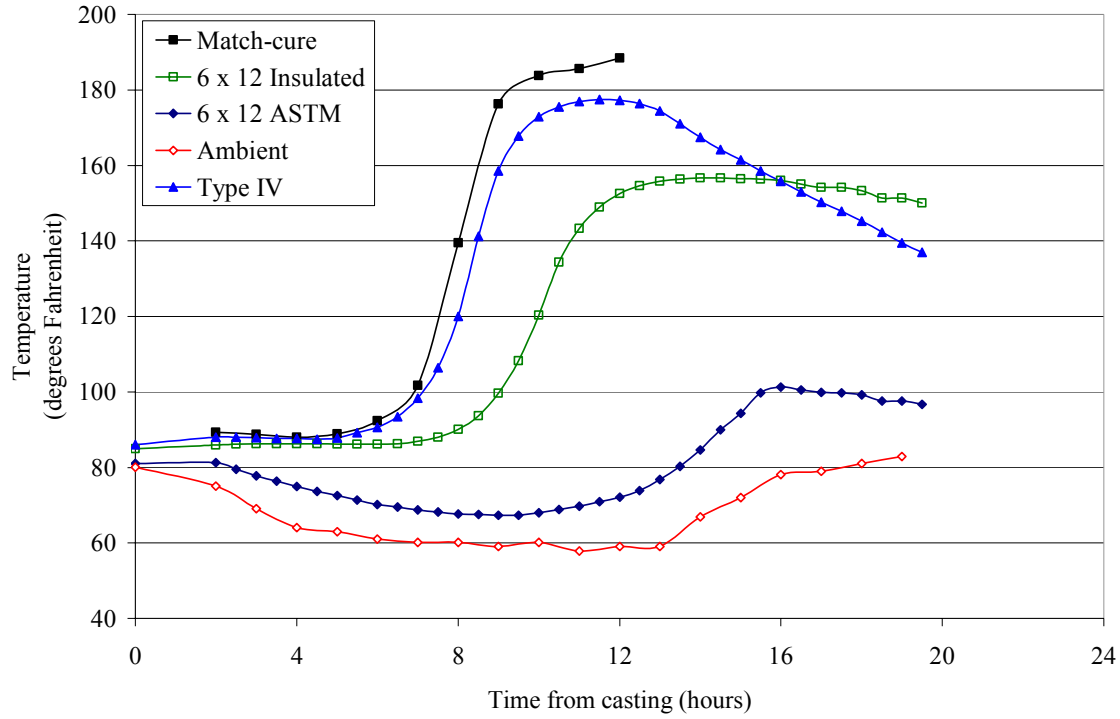

Figure 4.2 Temperature curing curves for the Type IV girder and samples

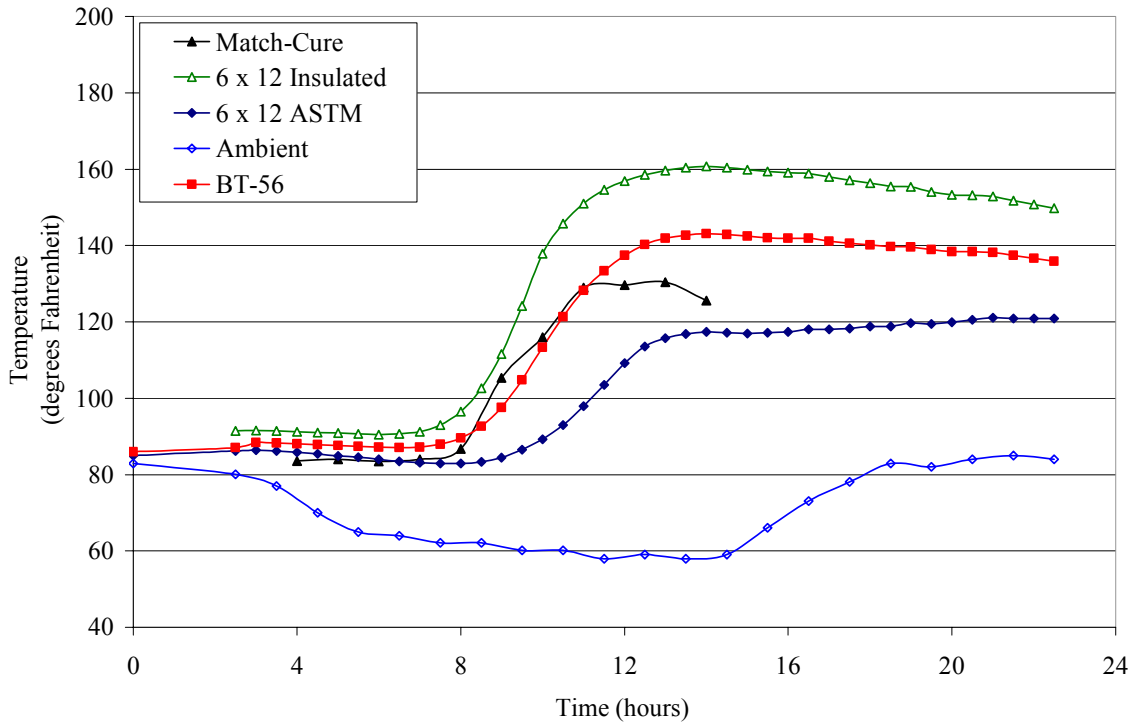

Figure 4.3 Temperature curing curves for the BT-56 girder and samples

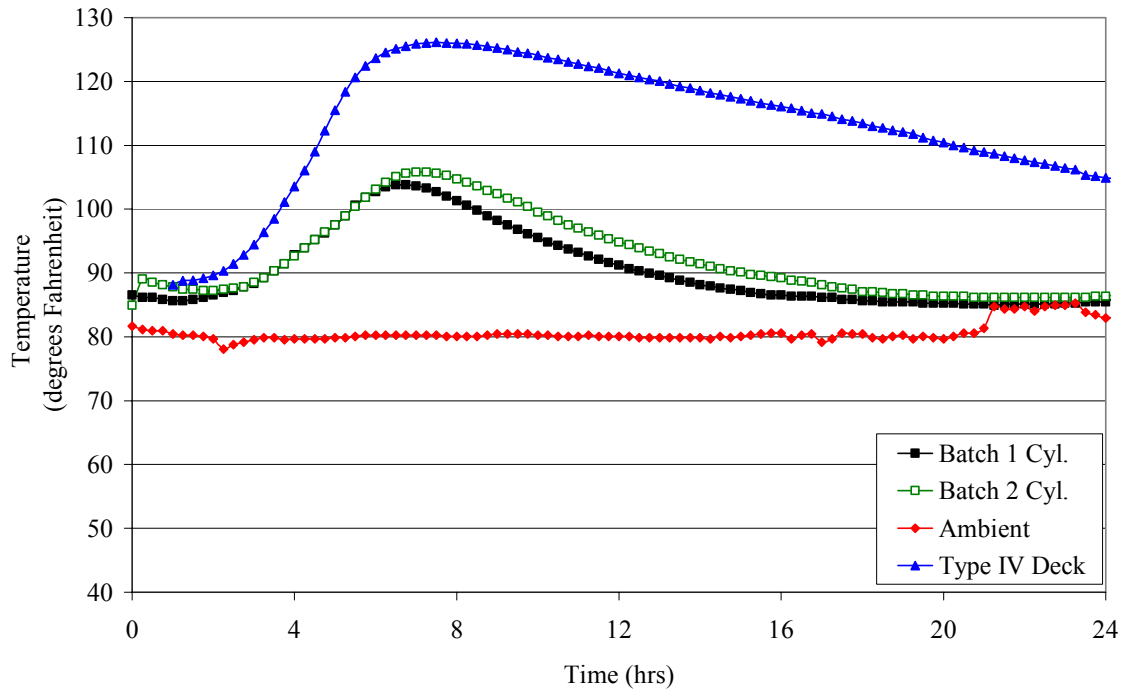

Figure 4.4 Temperature curing curves for the Type IV deck and samples

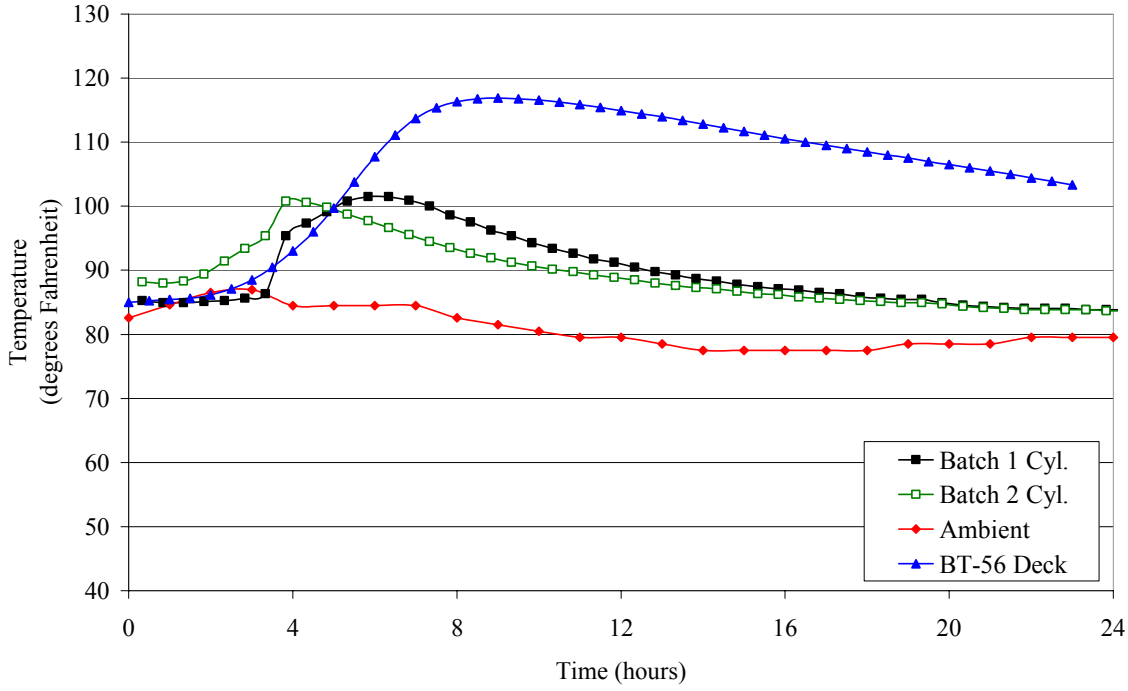

Figure 4.5 Temperature curing curves for the BT-56 deck and samples

4.4 Testing Procedures

A brief overview and description of each test is given in this section. All tests were performed by Georgia Tech researchers according to the applicable ASTM standards. Along with all 6 concrete tests being performed for quality control, this section also details the strand direct pullout test and the testing of all steel reinforcement used in the girders and decks.

Compressive strength for insulated and ASTM cured cylinders was tested at 1, 7, 28, and 56 days and on the girder testing day. The modulus of elasticity was tested for insulated and ASTM cured specimens at 1 and 56 days. The actual times of testing varied slightly due to the one day difference in casting of the two girders and time constraints at the initial testing days. The actual time of testing is presented with testing results in Section 4.4. The modulus of rupture and chloride permeability tests were performed on ASTM cured specimens for each girder at 56 days. The CTE tests were performed on ASTM cured samples at 3.5, 63 and 224 day from casting. Finally, creep and shrinkage data were taken for both girder specimens beginning at approximately 28 hours and 53 hours after casting of the BT-56 and Type IV girders, respectively, and measurements continued for 270 days. Table 4.3 shows the tests for each girder, how many samples were cast, and how they were cured.

Table 4.3 Girder specimen schedule and number of samples

	Specimen	Type IV		BT-56	
Compression Testing	4 in. x 8 in.	Insulated	ASTM	Insulated	ASTM
1 day			3	9	3
2 day		9	3		
7 day		3	3	3	3
28 day		3	3	3	3
56 day		3	9	3	30
Testing day		3		3	
Rapid Chloride Permeability	4 in. x 8 in.	3		3	
56 Day					
Modulus of Elasticity	6 in. x 12 in.				
1 day				3	
2 day		3			
56 day		3	3	3	3
Testing day		3		3	
CTE Testing	6 in. x 12 in.				
3.5 day					2
63 day			1		1
224 day			2		2
Modulus of Rupture	4 in. x 4 in. x 14 in.		3		3
56 day					
Creep	4 in. x 15 in.	3		2	
Shrinkage	4 in. x 15 in.	2		3	

The two girders were cast 1 day apart from each other. The Type IV was cast first and the BT-56 girder was cast second. The Type IV girder specimens were taken back early so that 1 day testing could be performed. Only three compression samples were demolded and tested at 1 day for the Type IV girder. The rest of the Type IV girder specimens were transported on the 2nd day with all of the BT-56 girder specimens. After all of the specimens were labeled and stored, the remaining "1 day" samples from the Type IV girder and all of the 1 day samples from the BT-56 girder were tested according to ASTM C 39. It is important to note that one day testing for the BT-56 girder was

possible, but the "1 day" samples for the Type IV girder were actually tested on day 2, which can be seen in Table 4.3.

Only ASTM curing was used on the control samples for both deck concretes. The insulated curebox method was not used as it was assumed the curebox would produce temperatures greater than that in each deck. Table 4.4 shows the types of tests and number of specimens for each deck batch.

Table 4.4 Deck control specimen schedule and number of samples

	Specimen	Type IV Deck		BT-56 Deck	
Compression Testing		Batch 1	Batch 2	Batch 1	Batch 2
1 day	4 in. x 8 in.	3	3	3	3
7 day		3	3	3	3
28 day		3	3	3	3
56 day		3	3	3	3
Testing day		3	3	3	3
Rapid Chloride Permeability 56 day	4 in. x 8 in.	1	1	1	1
Modulus of Elasticity	6 in. x 12 in.				
1 day		2	2	2	2
56 day		2	2	2	2
Testing day		2	2	2	1
CTE Testing	6 in. x 12 in.				
3 day		1	1	1	1
60 day		1	1	1	1
92 day		1	1	1	1
155 day		1	1	1	1
Shrinkage	4 in.x 15 in.	4	4	3	4

4.4.1 Compressive Strength

The compressive strength for each girder and deck was determined by testing the 4 in. x 8 in. (101.6 x 203.2 mm) cylinders according to ASTM C39. Georgia Tech

researchers used a SATEC MKIII 800RD, 800 kip capacity compression machine to perform all testing.

The specimens were taken out of the fog room at the specified day and tested according to the ASTM specifications. Georgia Tech researchers ground down both ends of each specimen with an electric grinder to obtain a smooth, flat surface. In addition ½ in. (12.7 mm) thick pad-caps ensured uniform load distribution. The cylinders were then loaded at a rate no greater than 40 kips per minute until failure. For each sample location and type of curing, there were at least three cylinders tested and averaged. Figure 4.6 shows a 4 in. x 8 in. (101.6 x 203.2 mm) compression specimen after failure in the SATEC Machine.

Figure 4.6 A 4 in. x 8 in. cylinder compression failure

4.4.2 Modulus of Elasticity

The modulus of elasticity test was performed using 6 in. x 12 in. (152.4 x 304.8 mm) cylinders in accordance with ASTM C 469. The modulus test could not be performed before the 4 x 8 in. (101.6 x 203.2 mm) compression testing was complete. The average compressive strength from each 4 x 8 in. cylinder was needed to determine the loading force required for the modulus testing of the corresponding 6 x 12 in. cylinders.

After the 4 x 8 in. compression tests, the 6 x 12 in. specimens were ground down with an electric grinder to obtain the required flat end surfaces. Pad caps were used on both ends of the 6 x 12 in. cylinders, and the compressometer shown in Figure 4.7 was mounted on the cylinder. Using the previously obtained 4 x 8 in. compressive strength, values were obtained for 40 and 60 percent of that ultimate compressive strength. The cylinders were loaded to the 40 percent compressive strength value to achieve proper seating of the compressometer. Georgia Tech researchers then unloaded the cylinders, zeroed the longitudinal and lateral dial gauges, and they loaded the cylinders to the 60 percent value of the ultimate compressive strength. As the cylinders were loaded, horizontal dial gauge, longitudinal dial gauges, and load readings were taken. The dial gauges have 0.0001-in. accuracy and the compressometer has an 8-in. (203.2 mm) gauge length, which corresponds to a precision of 6.25 με. When the 60 percent load value was obtained, the specimens were unloaded, the compressometer was removed, and the 6 x 12 in. specimens were tested in compression.

Figure 4.7 Modulus of elasticity test set up on a 6 x 12 in. specimen

4.4.3 Modulus of Rupture

The modulus of rupture test was used to estimate the tensile strength of each concrete specimen. The specimens were 4 x 4 x 14 in. (101.6 x 101.6 x 355.6 mm) prisms tested in four point bending, according to ASTM C 78. This four point bending caused a constant moment zone in the middle third of the specimen with zero shear. When the applied load caused an excessive tensile stress at the bottom of the specimen, brittle failure would occur within the constant moment region. Figures 4.8 and 4.9 show the modulus of rupture test before and after failure.

Figure 4.8 Modulus of rupture test set up

Figure 4.9 Modulus of rupture test failure

4.4.4 Creep

Creep tests were performed on specimens from both girders to better understand the behavior of the high performance concrete under constant load. Georgia Tech researchers followed ASTM C 512 to properly test the creep specimens. 4 x 15 in. (101.6 x 381 mm) cylinders were used for all creep testing.

4 x 15 in. cylinders were used instead of the ASTM recommended 6 x 12 in. (152.4 x 304.8 mm) in order to compare with past research on creep conducted at Georgia Tech. DEMEC inserts were installed in four pre-drilled holes on opposing sides of the metal forms. The holes were arranged in two sets of two, spaced at 10 in. on center. Care was taken to ensure that the inserts were not broken or bent when the concrete was being placed. Figure 4.10 shows a 4 x 15 in. metal form with the ends and top disconnected for display.

Figure 4.10 Metal form used to make the 4 x 15 in. creep and shrinkage specimens

The two circular disks at each end of the form contained ¼-inch pins concentric with each disk. The end plates with center holes assured uniform stress and good alignment of the cylinders in the creep racks.

The cylinders were cast on site at SCP by Georgia Tech researchers and were cured in the insulated curing boxes. They were demolded with the rest of the concrete specimens after transport back to the structures laboratory.

It was decided to load the creep specimens as close to one day as possible to observe the creep behavior at an early age, although ASTM recommends loading no sooner than 48 hours. Because the two girders were cast at different times, cutdown occurred when the Type IV girder was 41 hours old and the BT-56 girder was 18.5 hours old. The creep specimens were loaded at 52.6 hours for the Type IV girder and at 30 hours for the BT-56 girder.

The cylinders were placed into the creep racks and initial, unloaded zero measurements were taken with the DEMEC readers. The desired load was 40 percent of each cylinder's initial ultimate capacity according to the ASTM specification. A hydraulic loading jack was used to apply the force, and a 700 kip Strainsert Load Cell was used to monitor the applied load. Three Type IV girder specimens were loaded to 40 percent without incident. However, one of the three BT-56 girder specimens cracked while loading and was used as an extra shrinkage specimen. Because one of the specimens cracked, the two BT-56 specimens were only loaded to 35 percent of their tested ultimate compressive strength. When both racks were loaded, DEMEC readings were taken again to get the initial elastic strain.

Creep readings were taken once a day for the first seven days, once a week for a month, and then periodically until they were unloaded. The same Georgia Tech researchers used the same DEMEC reader for every reading for consistency. The creep room was kept at a constant temperature of 73° F and a relative humidity of 50 percent. The creep room fluctuated in the temperature and relative humidity by as much as 2° F and 6 percent, respectively throughout creep and shrinkage testing. Before every reading, the creep racks were reloaded to the required load value and the nuts were re-tightened. Figure 4.11 shows the girder specimens in the creep racks.

Figure 4.11 Girder specimens in creep racks

4.4.5 Shrinkage

4 x 15 in. (101.6 x 381 mm) shrinkage specimens were fabricated for both girders and both decks. All girder shrinkage specimens were kept in the creep room so the shrinkage strain could be removed from the creep strain. Five specimens were used for girder shrinkage measurements; two from the Type IV girder and three from the BT-56 girder. The specimens were demolded with the rest of the samples for each girder and deck, and DEMEC values were taken immediately after initial creep readings. All shrinkage testing was performed according to ASTM C 157.

The shrinkage specimens for the deck concrete were placed under the tarp on each deck during curing, and kept on top of each deck to match their ambient curing conditions. Eight specimens were cast for each deck; four were unwrapped and four were wrapped in a sealing foil that held in moisture. This was done to separate the autogenous shrinkage from total shrinkage in the specimens. Figure 4.12 shows the measurement of shrinkage strain.

Figure 4.12 Measurement of shrinkage strains on a 4 x 15 in. cylinder

4.4.6 Rapid Chloride Permeability

The rapid chloride permeability test (RCPT)was performed on the concrete from both decks and both girders and used to measure the durability of the high performance concrete. Georgia Tech researchers performed the test according to ASTM C 1202. 4 x 8 in. (101.6 x 203.2 mm) cylinders were cast and stored in the structures laboratory fog room until 56 day testing. The cylinders were cut into four 2-in. (50.8 mm) thick pieces using a diamond blade saw. The two outside pieces were discarded, and the two middle pieces from each cylinder were used for testing. The specimens were prepared in a water vacuum for 18 hours, and then placed in the "Proove-It" system device for chloride testing.

The permeability of a specimen was indirectly assessed by the total charge passed through each sample in 6 hours. There are different classes of permeability defined by ASTM and they are shown in Table 4.5. The ASTM specification for permeability is based on the permeability of a 3.75 in. (95.3 mm) sample. Therefore, recommended correction equations were used so the results from the "Proove-It" system could be compared to the ASTM specifications. The "Proove-It" RCPT system can be seen in Figure 4.13.

Table 4.5 ASTM chloride permeability specifications

Charge Passed (Coulombs)	Chloride Ion Penetrability
> 4,000	High
2,000 - 4,000	Moderate
1,000 - 2,000	Low
100 - 1,000	Very Low
< 100	Negligible

Figure 4.13 "Proove-It" chloride permeability test set up

4.4.7 Coefficient of Thermal Expansion

An average coefficient of thermal expansion (CTE) was taken for both girders and decks. The CTE values were used to make temperature corrections on all obtained strain data.

The test was performed in a manner similar to that specified by the Army Corps of Engineers Specification CRD-C39. 6 x 12 in. (152.4 x 304.8 mm) cylinders were tested in a Thermatron climate chamber. The Army specification states the cylinders be placed in a water bath to prevent any moisture loss, but the climate chamber provided controlled humidity as well as temperature. In addition, each cylinder was sealed with either epoxy or adhesive foil tape to prevent moisture loss. Thermocouples were installed in each CTE sample, and were used to monitor the temperature inside each specimen. The oven was heated to 140° F until each cylinder reached equilibrium, at 95 percent

humidity. Two sets of concrete surface strain (CSS) measurements were taken with DEMEC readers. After the readings were taken, the oven was set to 40° F, and again remained at that temperature until the cylinders reached equilibrium. Then two final sets of DEMEC readings were taken.

4.4.8 Direct Pull-Out Capacity

The direct pull-out capacity or "Moustafa" test of the 0.6-in. diameter, 270 ksi, low relaxation prestressing strands used in both girders was performed at the structures laboratory. The method used was first implemented by Moustafa in 1974 and was modified by Logan in 1997 (Logan, 1997). The pull-out block dimensions, reinforcement details and strand arrangement are presented in Figure 4.14. The formwork was transported to SCP, where six 48-in. (1.22 m) long prestressing strands from the same strand reel as used for the girder strands were tied to the rebar cage. The strands were spaced evenly in the formwork and kept at least 6 in. (152.4 mm) from the edges of the block and adjacent strands. The strands were secured 20-in. (508 mm) deep into the block. A 2-in. (50.8 mm) long PVC tube bond breaker was placed over each strand, at the height of the block top surface prior to casting to prevent surface cracking, leaving an 18-in. (457.2 mm) embedment length. Concrete from the Type IV girder was placed in the formwork, and the block was allowed to cure at SCP in ambient conditions.

Each prestressing strand was tested at 56 days from casting with a hydraulic center-hole jack. A load cell and strand chuck were placed on top of the ram to monitor the load and secure the apparatus, respectively. Two dial gauges were placed on each side of each strand to obtain an average displacement value. Load displacement curves,

as well as the individual strand pull-out loads are presented in Section 4.5.10. Figure 4.14 shows the construction details of the pullout block. Figure 4.15 shows the test set up, and Figure 4.16 shows researchers performing the test.

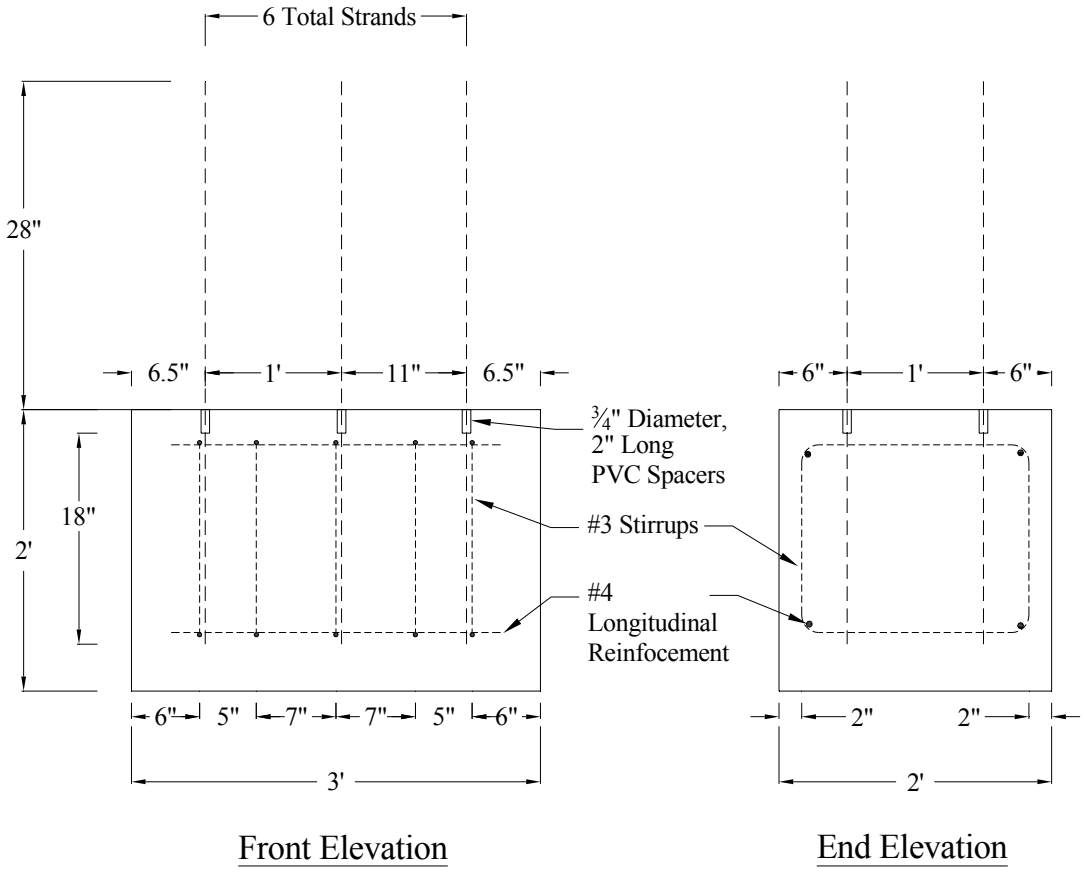

Figure 4.14 Direct pull-out block design

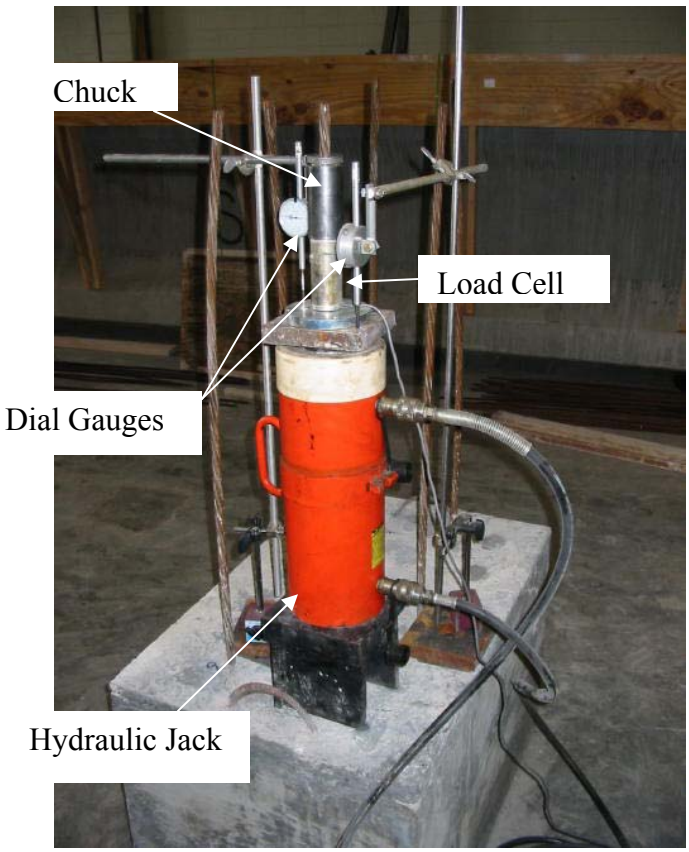

Figure 4.15 Direct pull-out test set up

Figure 4.16 Researchers performing direct pull-out test

4.4.9 Reinforcing Steel Testing

Representative samples of the Grade 60 reinforcing steel were obtained from SCP during girder construction. The girders used # 3 bars for doghouse bars, # 4 bars for horizontal transverse reinforcement, # 5 bars for most shear reinforcement, and # 6 bars for shear reinforcement in the transfer region.

Each length of bar was machined down at its midpoint to remove surface deformations and to ensure failure at a specific location. The diameters of each machined section were measured with calipers and recorded. Georgia Tech researchers performed the tests according to ASTM A 370. Each bar was tested in the Baldwin Universal Testing Machine. An MTS extensometer with 1 με accuracy having a 2-in. (50.8 mm) gauge length was attached to the machined section of each bar, to record displacement, and the load was recorded manually. The extensometer data were recorded by an Optim Data Acquisition System. The load was increased at a slow rate until a strain of 6.0 percent was obtained, at which time the extensometer was removed to prevent damage. Manual strain readings using calipers over a 10-in. (254 mm) gauge length were then taken until the sample fractured. Results are presented in Section 4.5.11. Figure 4.17 shows the test set up.

Figure 4.17 Reinforcing steel test setup

4.5 Girder Concrete Results

Results from the material property tests discussed in Section 4.4 are presented in this section. All values presented are specimen averages and all specific specimen data are presented in Appendix B.

4.5.1 Mixture Requirements and Specifications

The mixture requirements for the girder concrete were matched to the requirements specified by the Georgia DOT for the Jonesboro Road Bridge project. The mixture met "Class AAA HPC" requirements as outlined by the FHWA and "Grade 2 HPC" requirements developed in Task 3 of this study by Lai, et al. (1999). The Class AAA requirements specified a compressive strength of 8,120 psi (56 MPa) at release and a 56 day strength of 10,150 psi (70 MPa). The grade 2 HPC required a 24-hour strength of 7,000 psi (48.3 MPa) and a 56 day strength of 10,000 psi (70 MPa). Both mixture specifications limited the total charge passed in the rapid chloride permeability test to 2,000 coulombs.

The fresh concrete property requirements were also matched with the requirements listed for Task 6 of this study (Slapkus and Kahn, 2002). The "Class AAA HPC" was required to have a slump of 2 to 7 in. (50.8 to 177.8 mm) and an air content of 3.5 to 6.5 percent. The grade 2 HPC required a slump of 4 to 6 in. (101.6 to 152.4 mm) and an air content of 5 to 8 percent. Table 4.6 shows the slump, air content, and temperature values obtained from SCP for both girders. Fresh concrete data were obtained for batches 1, 3, and 6 only for the Type IV girder, as these batches were the critical batches. All but one of the batches from either girder met slump requirements for Class AAA HPC and all but 2 met the requirements for Grade 2 HPC. The air content requirements were also met for all batches.

Table 4.6 Slumps, air contents, and concrete temperatures for each girder

Type IV			
Batch	Slump (in.)	Air Content (%)	Concrete Temp. (°F)
1	5.5	2.8	88.1
3	5.25	2.4	88.2
6	4.75	2.6	88.6
BT-56			
1	6.25	3.6	87.9
2	8	2.9	85.2
3	8.25	3	87.6
4	7	3.4	86.2
5	5.25	3.5	88.2
6	4.75	3.6	88.5

4.5.2 Compressive Strength

The results of compressive strength tests for the concrete in both girders are given in Table 4.7. Every strength value is the average of the number of specimens tested. The average release strength and 56 day strengths were higher than the required values. A statistical analysis was performed on the 56 day strength of 30 ASTM cured specimens for the BT-56. The characteristic strength was found to be 13,040 psi (89.9 MPa). According to Chapter 5 of the ACI 318-02 code, the minimum average required compressive strength, f_{cr}', for the 10,000 psi (68.9 MPa) concrete was 10,737 psi (74 MPa). Based on the characteristic value for the BT-56 girder concrete, the concrete satisfied the requirements for being considered a 10,000 psi design strength mixture. The characteristic strength differs from the mean value (14,756 psi) found in Table 4.7 because the former was obtained from the 5^{th} percentile of the two-parameter Weibull distribution. It is a characteristic value based on a 75 percent confidence bound on the 5^{th} percentile. The calculations for this statistical analysis can be found in Appendix C.

Figures 4.18 and 4.19 show the concrete strength over time for both insulated and ASTM cured samples.

Differences were observed between the insulated, match-cured, and ASTM-cured specimens. The match-cured samples from SCP were stronger than the ASTM-cured samples by 18.5 percent on the Type IV girder and by 56.2 percent on the BT-56 girder at form removal. At cutdown, the Type IV girder match-cured samples were 10.3 percent stronger, and the BT-56 girder match-cure specimens were 30 percent stronger. The insulated cylinders were 10 percent stronger than the ASTM samples at 1 day for the Type IV girder. The BT-56 girder insulated cylinders were 31 percent stronger than the ASTM samples at 1 day. These results are consistent with what was found for the "Class AAA HPC" concrete made by Slapkus and Kahn, (2002). Over time, the ASTM-cured samples gained more strength than the insulated cylinders. At 56 days, the ASTM-cured cylinders were 12 percent stronger than the insulated-cured specimens for the Type IV girder and 7 percent stronger for the BT-56 girder specimens.

The two concrete strength plots show that the insulated cylinders for each girder achieved strength gain more quickly than the ASTM cured cylinders, but actually lost strength after 35 days. The ASTM cylinders continued to gain strength well after the insulated cylinders tapered off. These results suggest that ASTM curing may overestimate the strength of concrete girders at 28 days and beyond. The insulated specimens more closely match the temperatures inside the girders, which makes them the more reliable specimens to use for actual girder concrete strengths.

Table 4.7 Compression test results for girder concrete

Girder	Event	Age (days)	Curing type	Average Compressive Strength (psi)	Average Strength (MPa)	Number of Tests	Coefficient of Variation (%)
Type IV	Form Removal (13 hours)	0.54	Match (SCP)	10,526	72.6	1	n/a
Type IV	Form Removal (13 hours)	0.54	ASTM (SCP)	8,887	61.3	1	n/a
Type IV	26 hours	1	ASTM	10,416	71.8	3	12.2
Type IV	Cutdown	1.65	Match (SCP)	11,700	80.7	1	n/a
Type IV	Cutdown	1.65	ASTM (SCP)	10,600	73.1	1	n/a
Type IV	49 Hours	2	Insulated	11,727	80.9	9	10.4
Type IV	49 Hours	2	ASTM	10,660	73.5	3	3.9
Type IV	7-Day	7	Insulated	12,194	84.1	3	5.1
Type IV	7-Day	7	ASTM	12,617	87.0	3	4.2
Type IV	28-Day	28	Insulated	14,056	96.9	3	2.3
Type IV	28-Day	28	ASTM	14,644	101.0	3	1.2
Type IV	56-Day	56	Insulated	13,660	94.2	3	1.9
Type IV	56-Day	56	ASTM	15,287	105.4	9	5.9
Type IV	Test-Day	160	Insulated	14,353	99.0	3	7.7
BT-56	Form Removal (14.5 hours)	0.6	Match (SCP)	9,171	63.2	1	n/a
BT-56	Form Removal (14.5 hours)	0.6	ASTM (SCP)	5,872	40.5	1	n/a
BT-56	Cutdown	0.73	Match (SCP)	10,350	71.4	1	n/a
BT-56	Cutdown	0.73	ASTM (SCP)	8,005	55.2	1	n/a
BT-56	26 hours	1	Insulated	11,755	81.0	9	5.7
BT-56	26 hours	1	ASTM	8,986	62.0	3	1.0
BT-56	7-Day	7	Insulated	11,982	82.6	3	4.4
BT-56	7-Day	7	ASTM	12,443	85.8	3	2.2
BT-56	28-Day	28	Insulated	13,969	96.3	3	6.2
BT-56	28-Day	28	ASTM	14,284	98.5	3	3.9
BT-56	56-Day	56	Insulated	13,819	95.3	3	4.0
BT-56	56-Day	56	ASTM	14,756	101.7	30	4.9
BT-56	Test-Day	184.2	Insulated	15,145	104.4	3	4.1

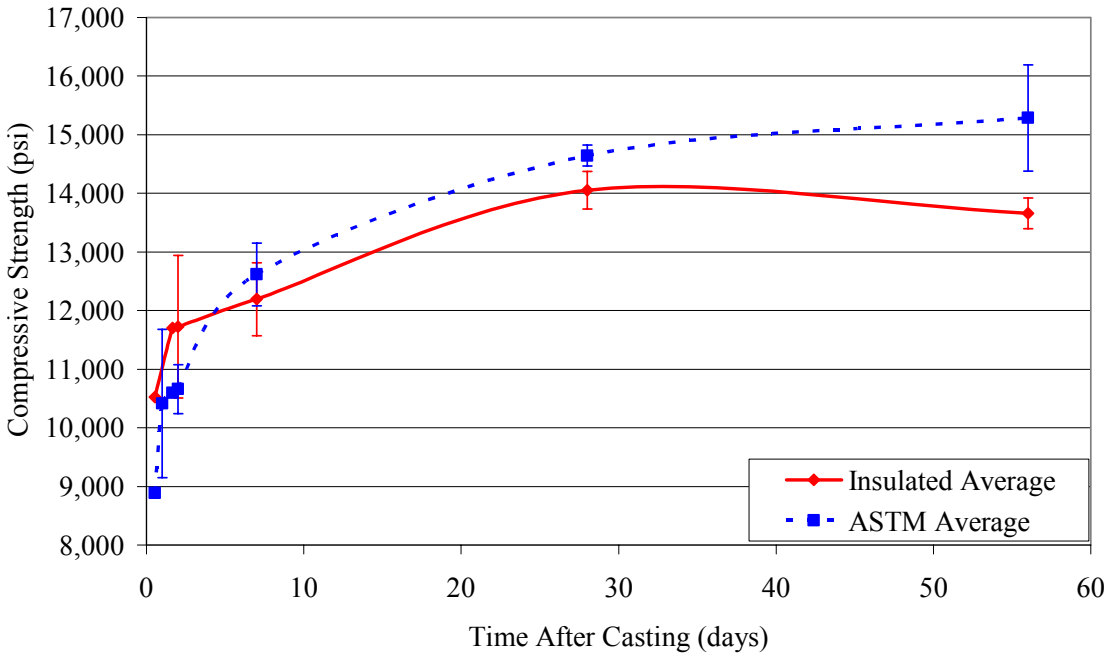

Figure 4.18 Type IV strength vs. time plot with standard deviations

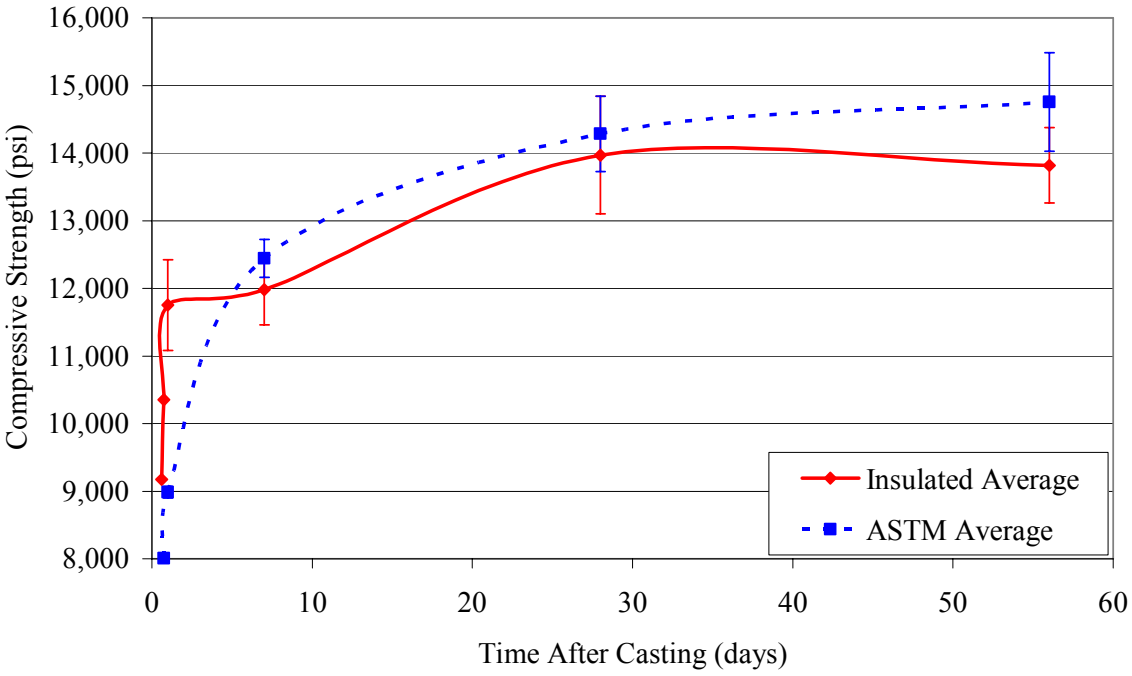

Figure 4.19 BT-56 strength vs. time plot with standard deviations

4.5.3 Modulus of Elasticity

Modulus of elasticity tests were performed on the concrete from each girder at 1 day and 56 days. The modulus was calculated using the secant slope of the stress-strain curve for each sample. Three insulated specimens were tested on both days and three ASTM cured specimens were tested at 56 days for each girder. Table 4.8 shows the average modulus and average 6 in. x 12 in. compressive strength of each girder for each day.

Table 4.8 Modulus of elasticity results for both girders

Girder	Time of Test	Curing Type	Average 6 in. x 12 in. Compressive Strength (psi)	Experimental Modulus (ksi)	Number of Tests	Coefficient of Variation %
Type IV	2-Day	Insulated	11,897	4,672	3	0.3
Type IV	56-Day	Insulated	13,081	4,717	3	2.0
Type IV	56-Day	ASTM	14,302	5,108	3	4.2
BT-56	1-Day	Insulated	12,278	4,771	3	3.6
BT-56	56-Day	Insulated	12,713	4,834	3	4.1
BT-56	56-Day	ASTM	13,471	4,876	3	8.7

The experimental values were compared to the values obtained from three existing prediction equations to determine which one was the most accurate. The first and most commonly used equation to predict modulus of elasticity comes from ACI 318 (2002), presented as Eqn. 4.1 and 4.2.

$$E_c = w_c^{1.5} * 33\sqrt{f_c'} \qquad \text{(psi)} \qquad (4.1)$$

or

$$E_c = 57{,}000\sqrt{f_c'} \qquad \text{(psi)} \qquad (4.2)$$

where,

w_c = unit weight of concrete, pcf

f_c' = concrete strength at time of testing, psi

According to ACI 363, Eqn. 4.1 is not accurate for concrete over 6,000 psi (27.6 MPa). According to Slapkus and Kahn, (2002), it seems to grossly overestimate the modulus when the concrete strengths become extremely high. Eqn. 4.3 is recommended by Nawy (2003) and Eqn. 4.3b is recommended by the State-of-the-Art Report on High Strength Concrete by ACI Committee 363 for high strength concrete (ACI 1992). Equations 4.3 and 4.3b are essentially the same, as the unit weight of HPC is typically taken as 145 pcf.

$$E_c = (40{,}000\sqrt{f_c'} + 1{,}000{,}000) * \left(\frac{w_c}{145}\right)^{1.5} \quad \text{(psi)} \qquad (4.3)$$

$$E_c = (40{,}000\sqrt{f_c'} + 1{,}000{,}000) \quad \text{(psi)} \qquad (4.3b)$$

The final equation predicting modulus is an equation suggested by Lai, et al. (1999). The equation was obtained through research with HPC development in Georgia and is shown as Eqn. 4.4,

$$E_c = (38{,}000\sqrt{f_c'} + 730{,}000) * \left(\frac{w_c}{145}\right)^{1.5} \quad \text{(psi)} \qquad (4.4)$$

Comparisons between the experimental modulus values and the prediction equations are shown in Table 4.9. The equation used to estimate the percent difference between each equation and the experimental values is given as Eqn. 4.5.

$$\frac{(\text{Pred. E} - \text{Exp. E})}{\text{Exp. E}} * 100 \qquad \text{(percent)} \qquad (4.5)$$

It can be seen how much each equation overestimates the actual, tested modulus of elasticity. Eqn. 4.1 overestimates the experimental modulus by an average of 35.8 percent and should not be used for high performance concrete. Eqn. 4.3 is better than Eqn. 4.1, with an average overestimation of 15 percent. Eqn. 4.4 is the most accurate equation, with an average difference of 4.7 percent. The results from the Jonesboro Road Bridge agree with the results produced here for all three prediction equations (Slapkus and Kahn, 2002).

Table 4.9 Comparisons between predicting equations and experimental results

Girder	Time of Test	Curing Type	Equation 4.1	Equation 4.3	Equation 4.4	% Difference Eqn. 4.1 vs Exp.	% Difference Eqn. 4.3 vs Exp.	% Difference Eqn. 4.4 vs Exp.
Type IV	2-Day	Insulated	6,285	5,363	4,875	34.5	14.8	4.3
Type IV	56-Day	Insulated	6,590	5,575	5,076	39.7	18.2	7.6
Type IV	56-Day	ASTM	6,891	5,784	5,274	34.9	13.2	3.3
BT-56	1-Day	Insulated	6,384	5,432	4,941	33.8	13.9	3.6
BT-56	56-Day	Insulated	6,497	5,510	5,015	34.4	14.0	3.7
BT-56	56-Day	ASTM	6,688	5,643	5,140	37.2	15.7	5.4

Poisson's ratio was recorded for each modulus test performed. The Type IV girder concrete had an average value of 0.16 for 9 samples, and the BT-56 girder concrete

had an average value of 0.18 for 12 samples. Their coefficients of variation were 11.2 percent and 9.3 percent, respectively. The values were consistent throughout each beam and each sample. The standard value for high performance concrete was approximately 0.15 according to Slapkus and Kahn (2002).

4.5.4 Modulus of Rupture

The modulus of rupture results were consistent for each girder and are reported in Table 4.10. Samples were taken from three different batches in each girder to obtain a representative sample. Specimens were ASTM cured and tested at 56 days.

Table 4.10 Experimental results for modulus or rupture

Girder	Time of Test	Curing Type	Average Compressive Strength (psi)	Experimental Modulus of Rupture (psi)	Number of Tests	Coefficient of Variation %
Type IV	56-Day	Insulated	13,660	974	3	3.2
BT-56	56-Day		13,819	1,010	3	1.2

The standard modulus of rupture equation given by Eqn. 4.6 underestimates the experimental results.

$$f_r = 7.5\sqrt{f_c'} \qquad \text{(psi)} \qquad (4.6)$$

ACI committee 363 (1992) found that Eqn. 4.6 was not accurate for high performance concrete. They suggest that concrete can have a range of tensile strengths

from $7.5\sqrt{f_c'}$ to $12\sqrt{f_c'}$ depending on the strength of the concrete. For high performance concrete, Eqn. 4.7 was suggested.

$$f_r = 11.7\sqrt{f_c'} \qquad \text{(psi)} \qquad (4.7)$$

In general, the modulus of rupture can be calculated using Eqn. 4.8.

$$f_r = \lambda\sqrt{f_c'} \qquad \text{(psi)} \qquad (4.8)$$

where,

λ = a constant

All three equations are tabulated and compared to the experimental modulus of rupture in Table 4.11. Eqn. 4.6 was conservative on average by 15 percent and Eqn. 4.7 was un-conservative on average by 30 percent. These results indicate that Eqn. 4.6 can be used for design purposes because it is conservative and more accurate than Eqn 4.7. Equation 4.8 determines the actual constant value, λ, based on the experimental modulus of rupture. From the modulus of rupture results, an average λ value of 8.74 is needed to match the experimental figures.

Table 4.11 Comparisons between predicting equations and experimental results

Girder	Experimental Modulus of Rupture (f_r) (psi)	Predicted f_r, Eqn. 4.6 (psi)	Predicted f_r, Eqn. 4.7 (psi)	λ Based on M.O.R. Tests Eqn. 4.8
Type IV	974	877	1,370	8.33
BT-56	1,010	882	1,380	8.60

4.5.5 Creep

Creep specimens were loaded in the Structures and Materials Laboratory temperature and humidity controlled creep room after obtaining the 4 in. x 8 in. cylinder compressive strengths for each girder. The Type IV girder cylinders were 22 hours older than the BT-56 girder cylinders upon loading. The Type IV girder cylinder was loaded to 40 percent of the maximum compressive strength corresponding to a stress of 5,100 psi (36.2 MPa). The BT-56 girder was loaded to 35 percent of its maximum compressive strength corresponding to a stress of 4,250 psi (29.3 MPa), due to previously encountered cracking in similar specimens.

The strains measured during all creep testing included elastic, thermal, total creep, and shrinkage. Shrinkage samples were kept in the same room so shrinkage strains could be subtracted from the total creep strain data. Thermal corrections were made to the shrinkage cylinders to account for the heat of hydration and temperature variation. Figure 4.20 shows elastic and total creep strain for each girder corrected for thermal and shrinkage strains. The Type IV girder creep specimens showed higher early age creep values despite the 22 hour maturity difference. The creep strain after 150 days converges for both girders and shows that they both have the same long term creep values. Because the loads used were different for each girder's creep samples, a better comparison of the creep data is shown in Figure 4.21, which shows the specific creep. Specific creep was found by dividing the creep strain by the stress applied to the specimens. The figure shows that the BT-56 samples experienced more specific creep than the Type IV girder samples, which is explained by the difference in age at loading.

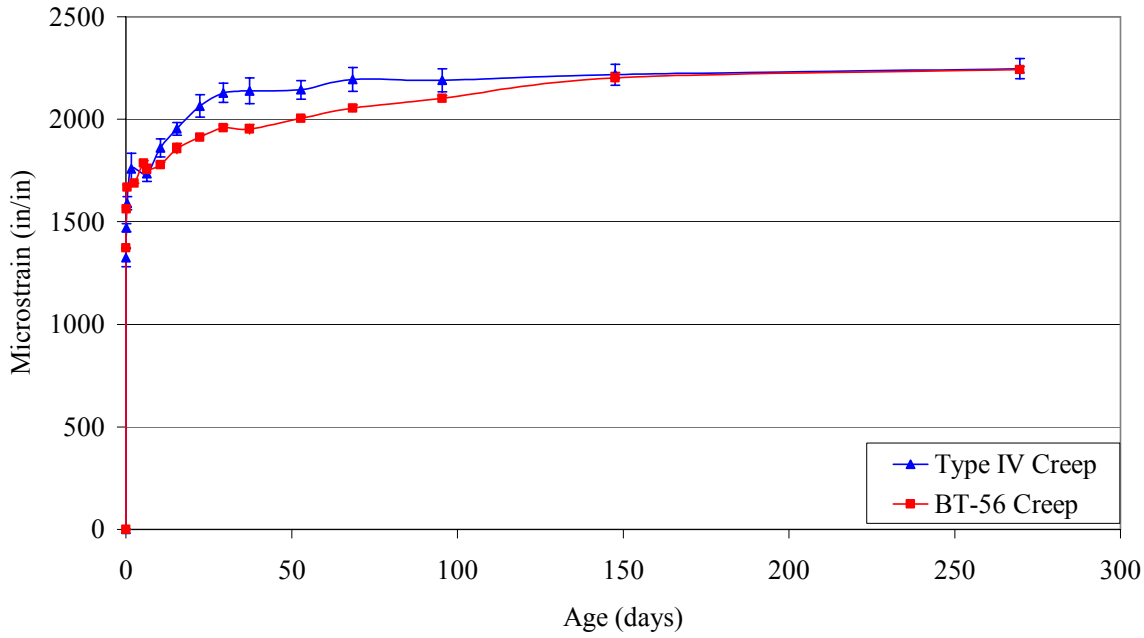

Figure 4.20 Average elastic plus creep strain for each girder's samples with standard deviations

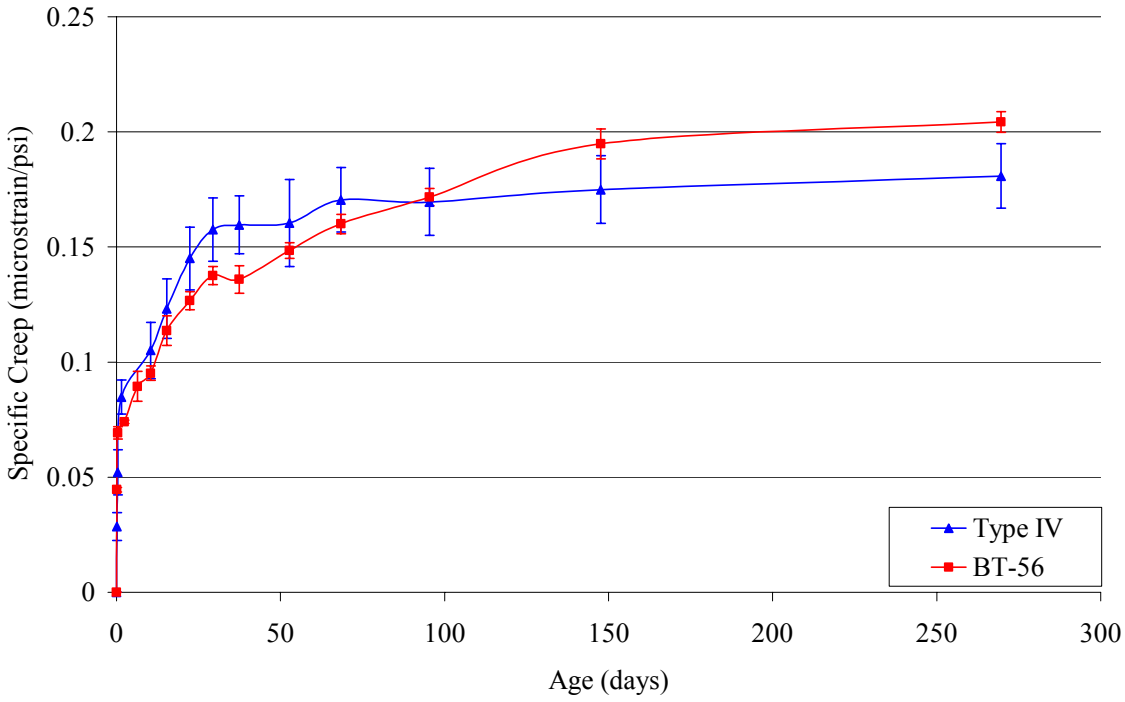

Figure 4.21 Average specific creep for each girder's samples with standard deviations

The creep data obtained from both girders were compared to other studies on high performance concrete, including data obtained from the Jonesboro Rd. Bridge Project. The data were compared using the creep coefficient, which was defined as the creep strain divided by the elastic strain. The creep coefficient was used to normalize the data and to create a standard method of comparison. Lai, et al. (1999), Shams and Kahn (2000), Slapkus and Kahn (2002), and ACI committee 209 (1997) all predicted creep coefficients. The general form for the creep coefficient, ϕ_t, at time t (days) recommended by ACI Committee 209 is given by Eqn. 4.9.

$$\phi_t = \frac{t^{0.6}}{d + t^{0.6}} \phi_u \qquad \text{(unitless)} \qquad (4.9)$$

where,

d = days after load application when 50 percent of ultimate creep occurs

ϕ_u = ultimate creep coefficient

When predicting creep coefficients, ACI-209 (1997) suggests using a base ultimate creep coefficient of 2.35. This value is adjusted based on the specific properties of the concrete mixture. These adjustments include loading age, relative humidity, volume to surface ratio, slump, fine aggregate content, and air content. After these factors were taken into account, each girder had a slightly different creep coefficient because of their different ages. However, both were averaged together to obtain an ACI-209 creep coefficient of 2.53. It is important to note that each girder had a slightly different ACI predicted value, but the two were averaged together to obtain one value for

both girders. Lai, et al. (1999), Slapkus and Kahn (2002), and Shams and Kahn (2000) found ultimate creep coefficients of 1.23, 1.42, and 1.69, respectively, for grade 2 HPC. The ultimate creep coefficient for this study was found by a best fit line and was determined to be 0.88. Table 4.12 gives the values for d and ϕ_u that define Eqn. 4.9.

Table 4.12 Values of d and ϕ_u that define the creep coefficient versus time curves

	Lai et al., 1999	Slapkus and Kahn, 2002	Shams and Kahn, 2000	ACI-209, 1997	Best Fit
d	4.0	3.8	7.1	10.0	6.4
ϕ_u	1.23	1.69	1.42	2.53	0.88

Figure 4.22 graphically compares all the prediction methods with the measured values from both girders. The ACI-209 (1997) prediction overestimates the creep coefficient for high performance concrete significantly. The long term values for the Type IV and BT-56 girders were similar, but were significantly lower than all other prediction methods. The values should have matched the values of Slapkus and Kahn (2002), because the same mixture was used. The only difference was that Type III cement was used for the test girders, and Type I cement was used for actual bridge girders. Besides the different cement and possible humidity variations, the low creep coefficients cannot be explained.

Because the Type IV girder was 22 hours older than the BT-56 girder when the specimens were loaded, it should have had smaller specific creep values and smaller creep coefficients. The Type IV girder did not have smaller specific creep values at an early age, but did show less overall specific creep. The Type IV girder showed larger creep coefficients than the BT-56 girder throughout the loading process. The unusual

creep coefficients could have been caused because the initial elastic strains for both sets of specimens were almost identical. A possible reason for this was that the more mature Type IV girder specimens were more heavily loaded than the BT-56 girder specimens. Therefore, the older and stiffer Type IV girder specimens experienced the same elastic strain as the younger, weaker, and less loaded BT-56 girder specimens. Because of the same initial elastic strain of both girder specimens, the creep coefficient data in Figure 4.22 were very similar to the total creep strain data presented in Figure 4.20.

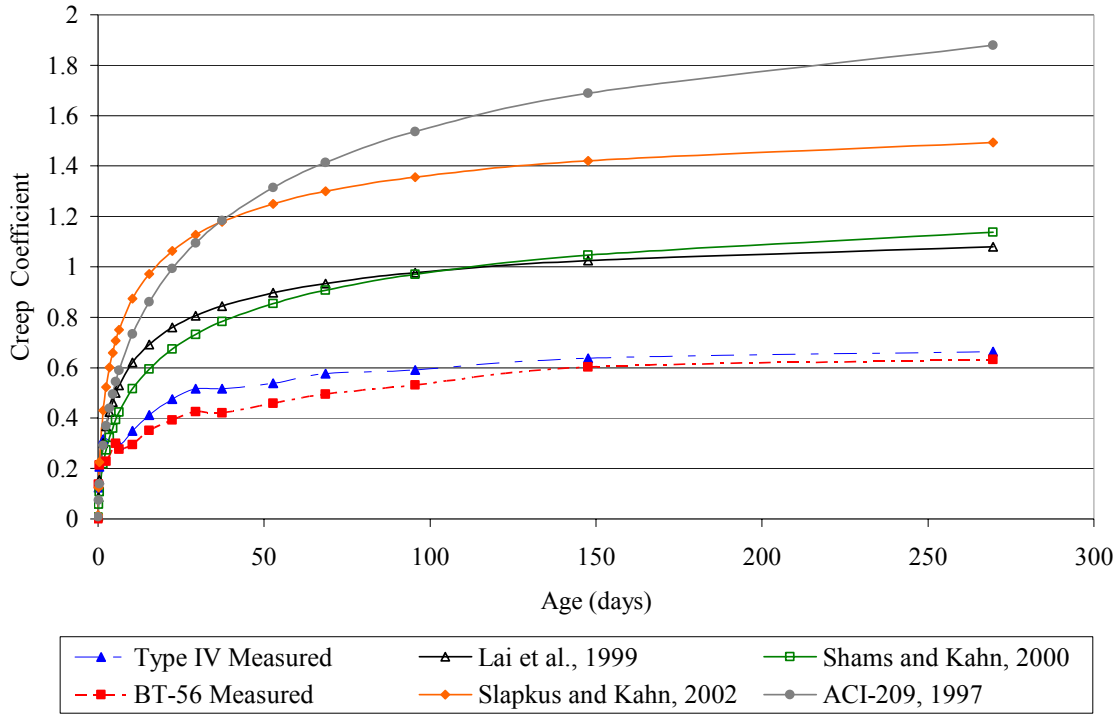

Figure 4.22 The creep coefficient versus time, compared to prediction methods

4.5.6 Shrinkage

The shrinkage specimens for each girder were placed inside the structures laboratory creep room. ASTM C 157 specifies that shrinkage should not be started until after 28 days. To examine early age shrinkage and to provide companion shrinkage specimens for the creep data, Georgia Tech researchers began shrinkage measurements as early as 1 day after casting. Thermal variations were present due to the heat of hydration of the specimens. They were eliminated by using the coefficient of thermal expansion for each girder. Figure 4.23 shows the temperature corrected shrinkage strains for both girders. The variations in the shrinkage up to 100 days could not be explained except for possible variations in the temperature and humidity in the creep room.

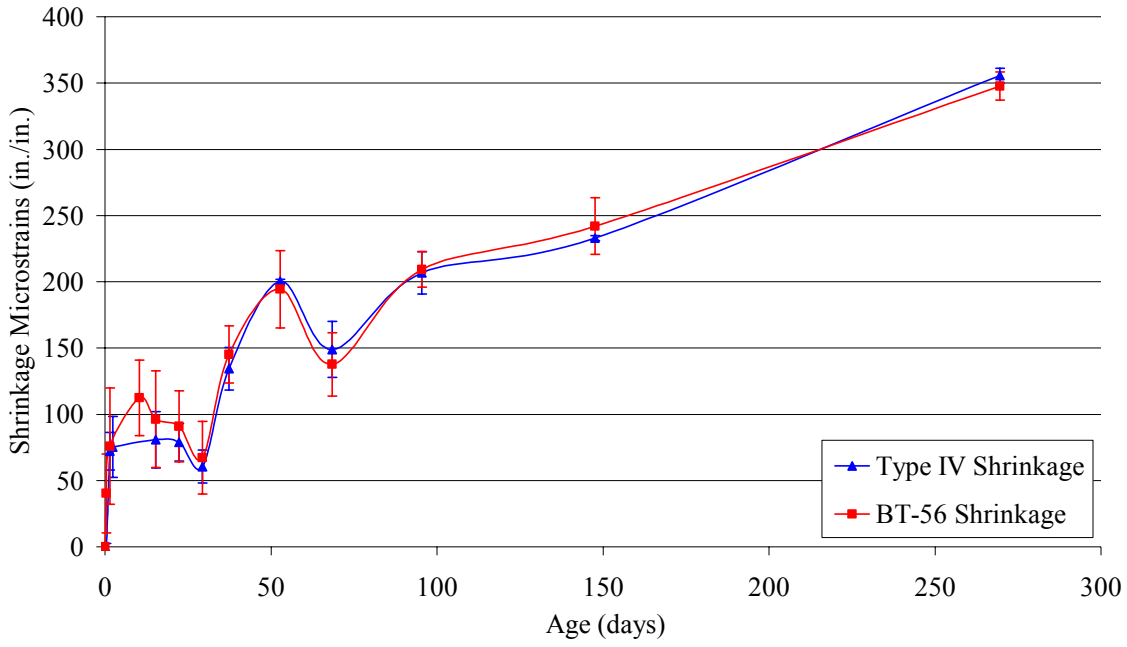

Figure 4.23 Shrinkage strain for both girders with standard deviations

The shrinkage strains obtained from the two girders were compared to the same four prediction methods as the creep strains. Lai, et al. (1999), Shams and Kahn (2000), Slapkus and Kahn (2002), and ACI committee 209 (1997) all predicted shrinkage strain over time. The general form that the four methods used for time dependant shrinkage prediction, (ε_{sh}), at time t (days) is given by Equation 4.10.

$$\varepsilon_{sh} = \frac{t}{f+t}(\varepsilon_{sh})_u \qquad \text{(unitless)} \qquad (4.10)$$

Where,

f = days after load application when 50 percent of ultimate shrinkage occurs

$(\varepsilon_{sh})_u$ = ultimate strain value

When predicting time dependant shrinkage, ACI-209 suggests an f value of 55 days and a base ultimate strain value of 780 microstrain. The ultimate strain value is subject to adjustment factors including relative humidity, volume to surface ratio, slump, fine aggregate content, air content, and total cementitious material per cubic yard. After all adjustments were made for the two girders, the average suggested prediction value was 855 microstrain. The ultimate shrinkage values found by Lai, et al. (1999), Shams and Kahn (2000), and Slapkus and Kahn (2002), were 536, 500, and 627 microstrain, respectively for grade 2 HPC. The data in this report had a best-fit ultimate shrinkage strain of 325. Table 4.13 shows the values for f and $(\varepsilon_{sh})_u$ that define Equation 4.10.

Table 4.13 Values of f and $(\varepsilon_{sh})_u$ that define the shrinkage strain versus time curves

	Lai et al., 1999	Shams and Kahn, 2000	ACI-209, 1997	Slapkus and Kahn, 2002	Best Fit
f	20.0	71.0	55.0	32.0	52.0
$(\varepsilon_{sh})u$	500.00	536.00	863.00	627.00	325.00

Figure 4.24 graphically compares all the prediction methods with the measured shrinkage strain values from both girders. The ACI-209 prediction equation is overly conservative in predicting time dependant shrinkage for high performance concrete. The specimens for each girder have shrinkage values that are lower than all of the prediction values.

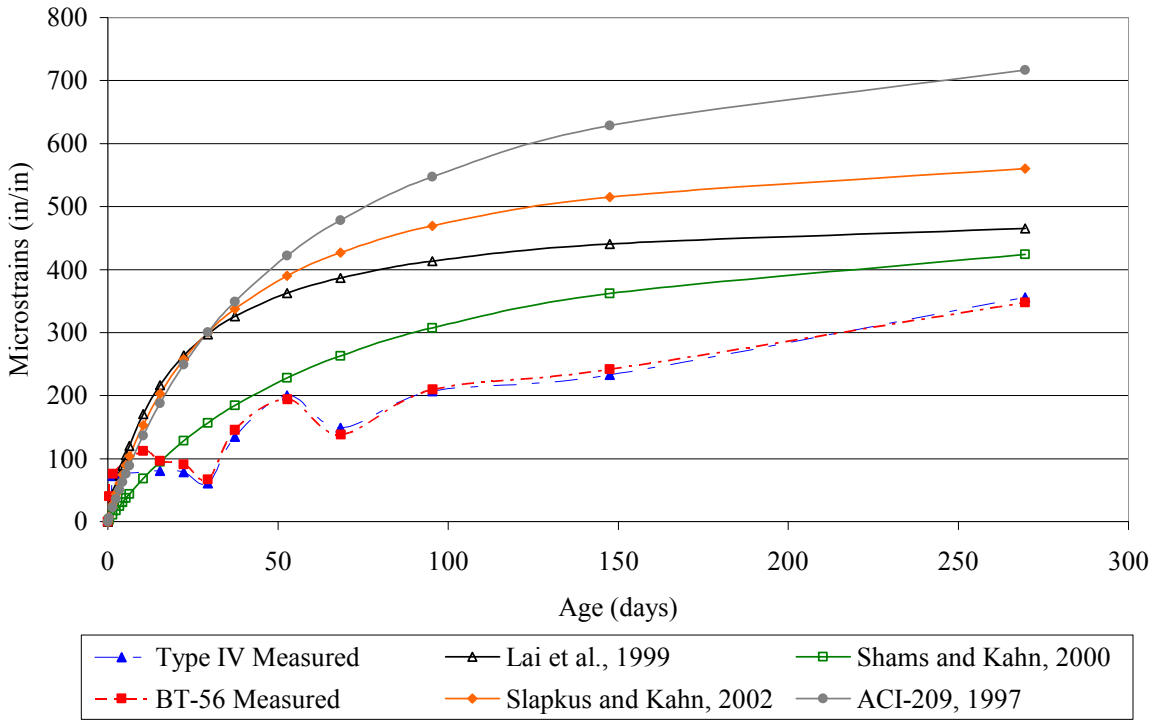

Figure 4.24 Shrinkage strain versus time, compared to prediction methods

4.5.7 Rapid Chloride Permeability

RCPT was performed on concrete from both girders to determine if they met the durability requirements of "Class AAA HPC" and the grade 2 HPC. Tests were done on 4 specimens from each girder. They were cured in insulated (accelerated) boxes to match the performance of the actual girders. The tests were performed after the specimens had been curing in the fog room for 56 days. Table 4.14 shows the results of the chloride permeability tests for both girders. The HPC in both girders met the requirements for both classes of concrete.

Table 4.14 Results of the rapid chloride permeability tests for concrete used to cast both girders

Type IV		
Specimen	Charge (Coulombs)	Permeability
1	225	very low
2	319	very low
3	303	very low
4	197	very low
Average	261	very low
BT-56		
Specimen	Charge (Coulombs)	Permeability
1	252	very low
2	261	very low
3	238	very low
4	268	very low
Average	255	very low

4.5.8 Coefficient of Thermal Expansion

No specific requirements or specifications were given for the coefficient of thermal expansion. The CTE values for each girder were taken and averaged to get a standard CTE equation to be used for all temperature corrections. A total average was used because the strength and modulus of elasticity data indicated there was no statistical difference between girder concretes. The CTE was found according to Eqn. 4.11.

$$CTE = \frac{L_{140°F} - L_{40°F}}{G\Delta T} \qquad (\mu\varepsilon/°F) \qquad (4.11)$$

Where,

$L_{140°F}$ = gauge length at 140°F, inches

$L_{40°F}$ = gauge length at 40°F, inches

G = original gauge length

ΔT = the difference in temperature between the two readings

Table 4.15 shows the average CTE values at different days. Figure 4.25 shows a plot of the CTE values versus time. Instead of using a single value for all temperature corrections, CTE tests were performed at several points in time to obtain an approximate value.

The values for the two girders were close to the values found by Shams and Kahn (2000) and Slapkus and Kahn (2002). Their average values were 5.13 με/°F (9.25 με/°C) and 5.91 με/°F (10.6 με/°C), respectively, at 56 days.

Table 4.15 Average CTE values for both girders

Day	CTE	
	με/°C	με/°F
4	10.48	5.84
63	12.54	6.97
224	13.98	7.76

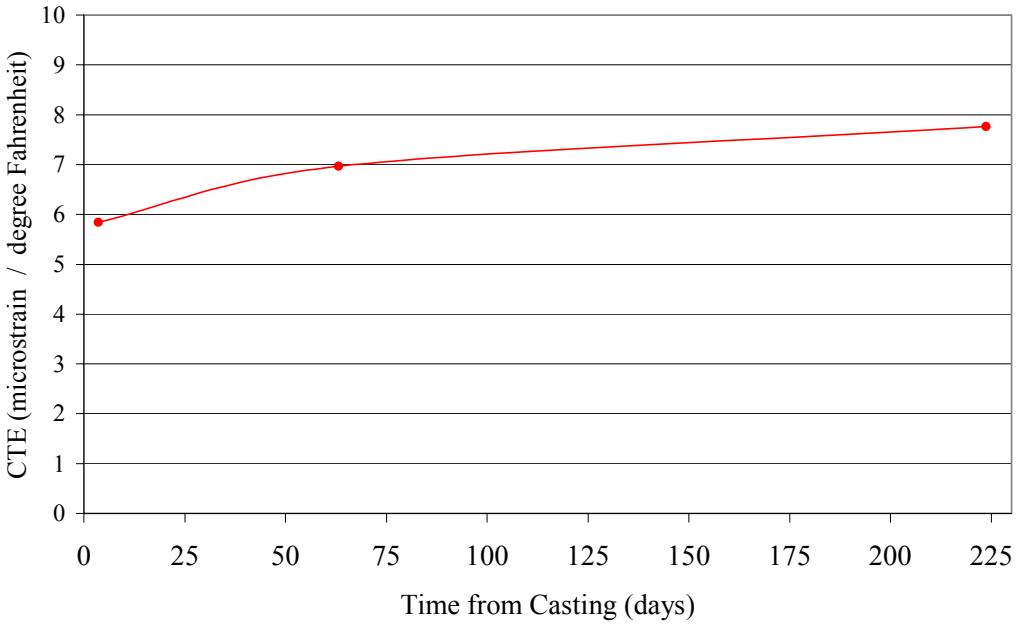

Figure 4.25 Average girder CTE vs. time

4.5.9 Prestressing Strand Properties

The 0.6-in. diameter, 270 ksi, low relaxation prestressing strands were provided by Insteel Wire Products and actual manufacturer strand test results were received at the time of the girder construction. No tests were performed by Georgia Tech researchers. The manufacturer data are presented in Table 4.16, and the actual stress versus strain data is given in Appendix A.

Table 4.16 Prestressing strand properties

0.6-inch Diamater Grade 270 ksi Low-Relaxation Strand		
Property	Value	Units
Strand Diameter, d_b	0.6	in.
Cross Sectional Area, A_{ps}	0.2181	$in.^2$
Modulus of Elasticity, E_{ps}	29,682	ksi
Yield Strain, ε_y	0.01	in/in
Yield Stress, f_y	261.3	ksi
Ultimate Strain, ε_{su}	0.0547	in/in
Ultimate Stress, f_{su}	283.3	ksi

4.5.10 Direct Pull-out Capacity

The direct pull out capacity for the 0.6-in. diameter prestressing strands was measured at the Georgia Tech Structural Laboratory at 56 days. The minimum acceptable pull out capacity for 0.5 in diameter prestressing strands, was 36 kips (Logan, 1997). The bond stress corresponding to that load was 995 psi (6.9 MPa). The bond stress is determined by Eqn. 4.12 and was used to determine the minimum acceptable pull out capacity for the 0.6-in. diameter prestressing strands used in this study. The corresponding minimum acceptable pull-out capacity for 0.6-in. diameter strands was calculated to be 43.2 kips, and Table 4.17 gives the results for each strand.

$$\sigma = \frac{P}{\frac{4}{3}\pi DL} \qquad \text{(psi)} \qquad (4.12)$$

where:

P = pullout force, kips

D = nominal diameter of the strand, inches

L = embedment length (18 inches)

Table 4.17 Results of direct pull-out capacity for six strands

Strand	Direct pull-out capacity (kips)	Max Bond Stress (psi)
1	48.57	1,070
2	47.20	1,040
3	48.90	1,080
4	42.12	931
5	46.40	1,030
6	45.35	1,000
Average	46.42	1,030

Each strand was loaded in increments until the maximum capacity was obtained. The maximum pull out capacity was often characterized by a loud "pop" and an immediate drop in load. After this pop, 0.5 to 0.85 in. of previously unexposed strand was visible above the top surface of the block. There was no visible damage to the outer wires of each strand, but two strands had the center wire protrude beyond the strand end after testing, as shown in Figure 4.26. Although this phenomenon was visible in two strands, all strands were assumed to experience a bond failure, because of the load at failure and the slip of each strand. The load at failure for each strand was below the strand yield force.

Figure 4.26 Slippage of center wire of a pull-out capacity specimen after testing

The average pull out capacity for the strands was 46.42 kips, which was higher than the minimum defined by Logan (1997). The average values found by Reutlinger (1999) and Slapkus and Kahn (2002) were 56.3 kips and 56.9 kips. Figure 4.27 shows resistance – pullout curves for the 6 strands.

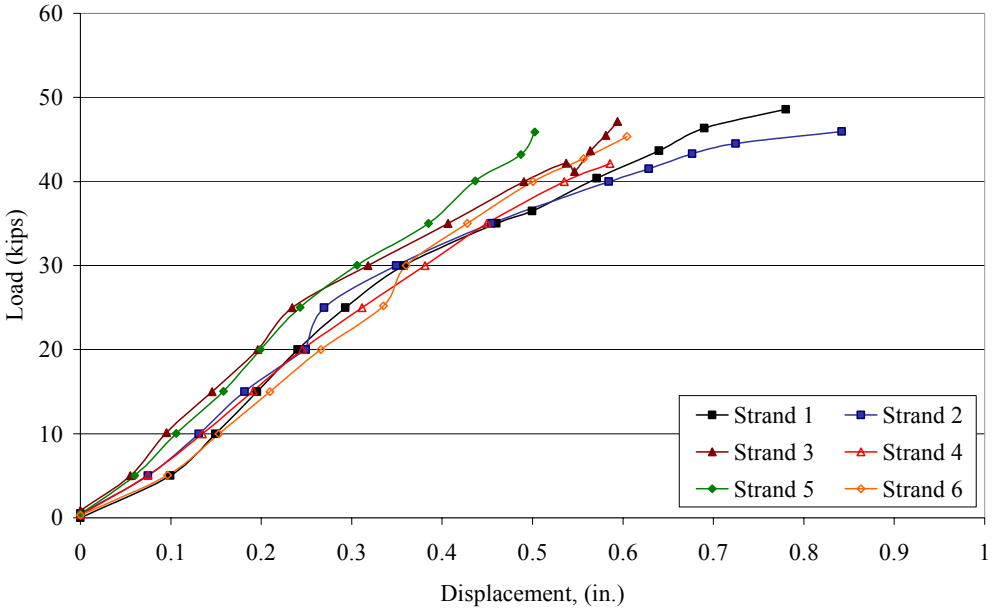

Figure 4.27 Strand resistance – pullout curves

4.5.11 Reinforcing Bar Testing

Two # 4, # 5, and # 6 bars were tested to determine the yielding and rupture strength of reinforcing bars used in both girders. Table 4.18 shows the average experimental yield stress, strain, and modulus of elasticity for each bar size. Figures 4.28, 4.29, and 4.30 show the average stress-strain curves for each reinforcing bar size.

Table 4.18 Nominal and experimental properties of reinforcing bars

Bar Size	Nominal			Experimental		
	σ_y (ksi)	ε_y (in/in)	E (ksi)	σ_y (ksi)	ε_y (in/in)	E (ksi)
# 4	60	0.00207	29,000	75.0	0.00256	29,253
# 5				74.0	0.00248	29,861
# 6				73.0	0.00251	29,097

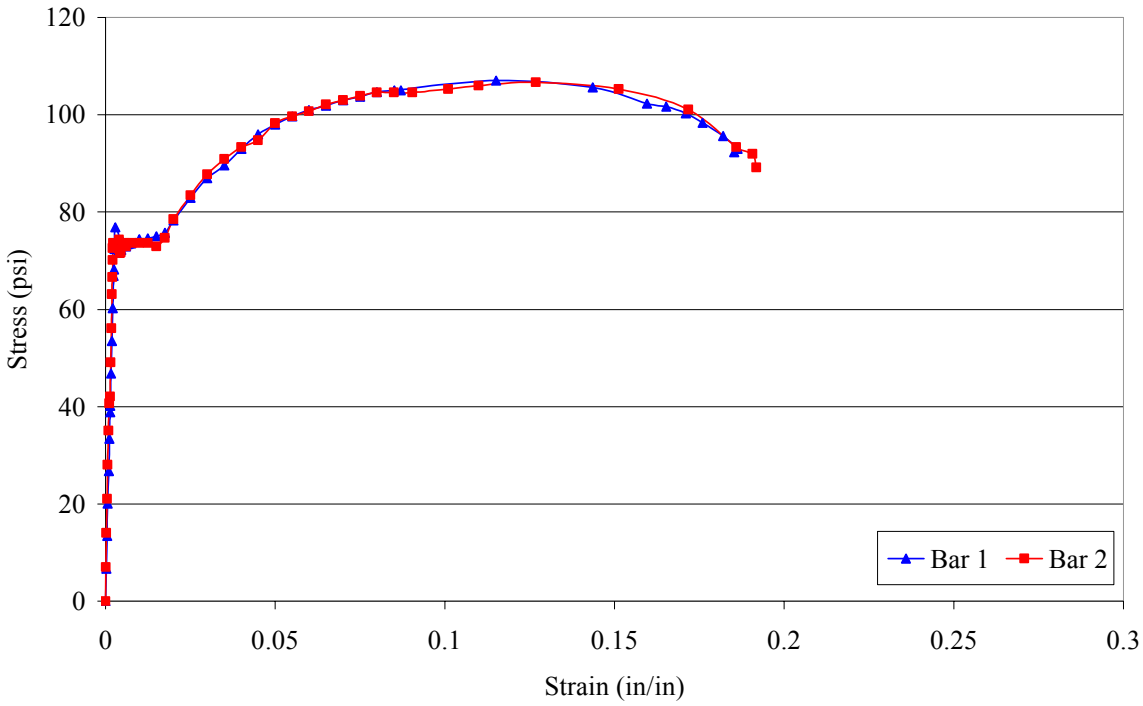

Figure 4.28 Stress versus strain plots for # 4 bars

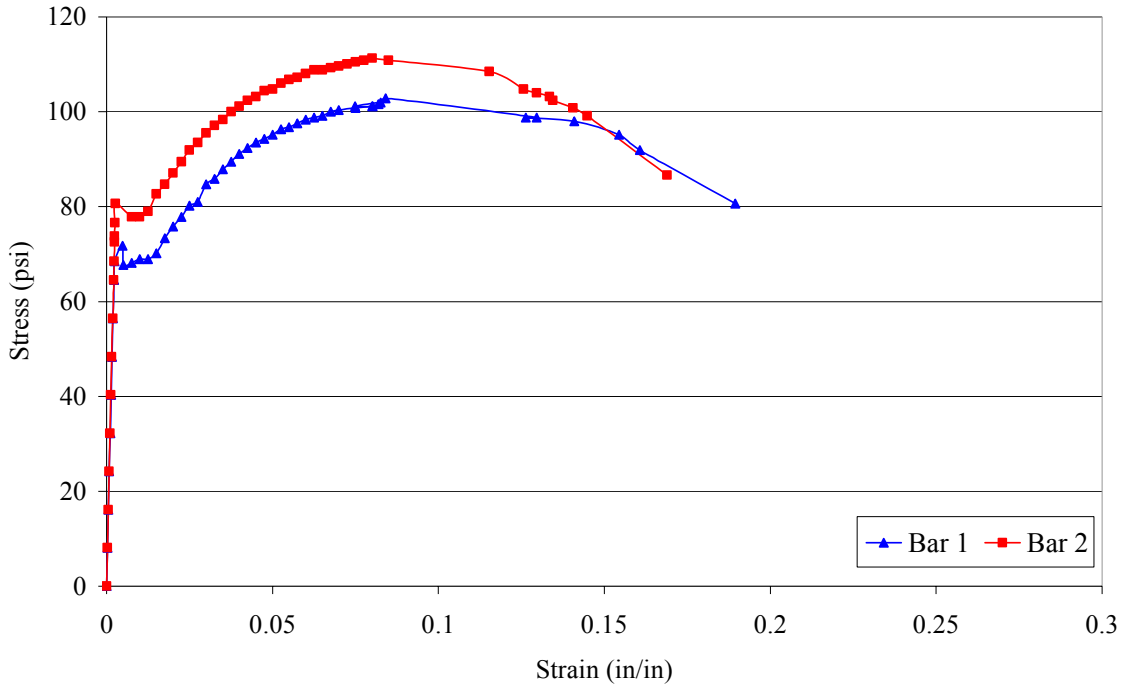

Figure 4.29 Stress versus strain plots for # 5 bars

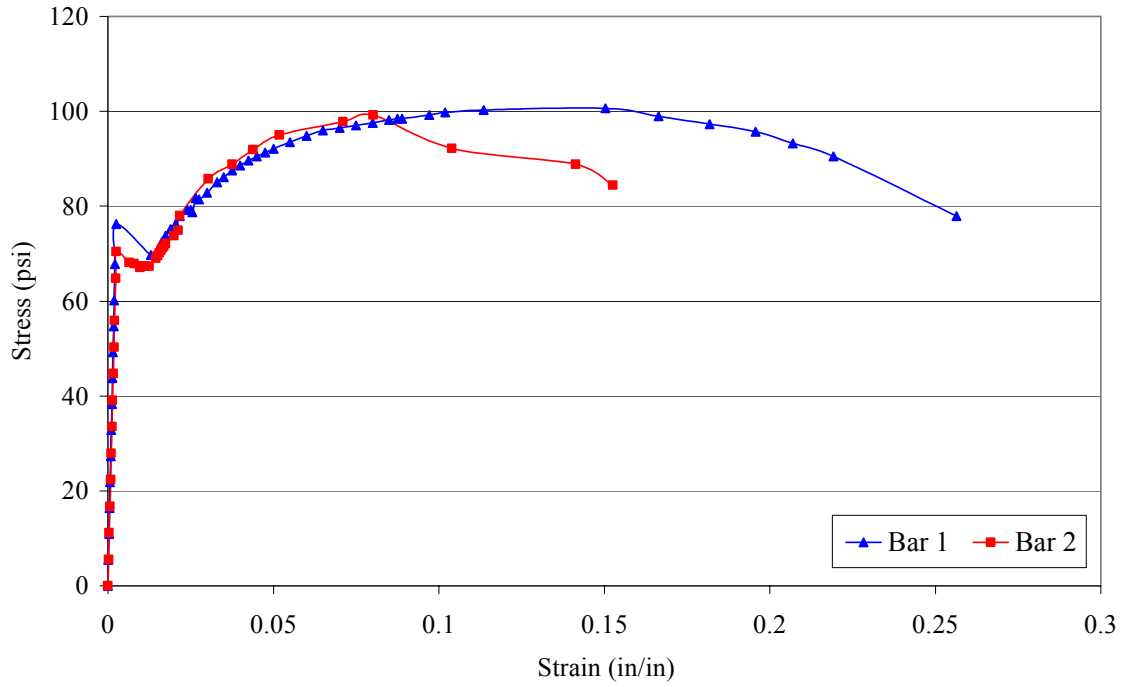

Figure 4.30 Stress versus strain plots for # 6 bar

4.6 Deck Concrete Results

Results from compression testing, modulus of elasticity, shrinkage, chloride permeability, and coefficient of thermal expansion will be presented in this section. All values were obtained from specimen averages, and all individual test data are presented in Appendix B.

4.6.1 Mix Requirements and Specifications

The mixture requirements for the deck concrete were matched to the requirements specified by the Georgia DOT for Task 6, the Jonesboro Road Bridge Project. The mixture was to meet "Class AA HPC" requirements specified by the FHWA and "Grade 1 HPC" requirements developed in Task 3 of this study by Lai, et al. (1999). The Class AA requirements specified a 56 day strength of 7,240 psi (50 Mpa). The grade 1 HPC required a 56 day strength of 7,000 psi (48.3 MPa). Both mixture specifications limited the total charge passed in the chloride permeability test to 2,000 coulombs.

The fresh concrete property requirements were also matched with the requirements listed for Task 6 of this study. The "Class AA HPC" was required to have a slump of 2 to 5 in. (50.8 to 122 mm) and an air content of 3.5 to 6.5 percent. The grade 1 HPC required a slump of 2 to 4 in. (50.8 to 102mm) and an air content of 5 to 8 percent. Table 4.19 shows the slump values for both decks. The slump values were all higher than that required by the two specifications. The air content was not measured for either deck.

Table 4.19 Slump values for both deck batches

Type IV Deck	
Batch	Slump (in.)
1	5.5
2	6.25
BT-56 Deck	
Batch	Slump (in.)
1	6.5
2	4.75

4.6.2 Deck Compression Results

The results of compression testing for both decks are given in Table 4.20. The average 56 day strengths for the Type IV deck concrete and BT-56 deck concrete were 7,165 psi (49.4 MPa) and 6,700 psi (46.2 MPa), respectively. The Type IV deck met the strength requirements of grade 1 HPC, but the BT-56 deck did not. Slapkus and Kahn (2002) also found that all of the deck concrete placed at the Jonesboro Road Bridge was below the minimum strength requirements for grade 1 HPC. Figures 4.31 and 4.32 show graphs of the concrete strength vs. time for each deck.

Table 4.20 Results of compression tests for both decks

Deck	Testing Day	Curing Type	Average Compressive Strength (psi)	Average Strength (MPa)	Number of Tests	Coefficient of Variation (%)
Type IV Batch 1	1	ASTM	3,539	24.4	3	9.8
Type IV Batch 2	1	ASTM	2,414	16.6	3	8.4
Type IV Batch 1	7	ASTM	4,526	31.2	3	5.1
Type IV Batch 2	7	ASTM	4,204	29.0	3	7.5
Type IV Batch 1	28	ASTM	6,755	46.6	3	3.8
Type IV Batch 2	28	ASTM	6,001	41.4	3	5.5
Type IV Batch 1	56	ASTM	7,411	51.1	3	5.3
Type IV Batch 2	56	ASTM	6,920	47.7	3	3.1
Type IV Batch 1	91 (test day)	ASTM	7,829	54.0	3	4.6
Type IV Batch 2	91 (test day)	ASTM	7,929	54.7	3	5.3
BT-56 Batch 1	1	ASTM	2,669	18.4	3	4.2
BT-56 Batch 2	1	ASTM	2,036	14.0	3	3.5
BT-56 Batch 1	7	ASTM	3,987	27.5	3	5.8
BT-56 Batch 2	7	ASTM	4,188	28.9	3	10.8
BT-56 Batch 1	28	ASTM	5,732	39.5	3	3.2
BT-56 Batch 2	28	ASTM	6,682	46.1	3	3.5
BT-56 Batch 1	53 (test day)	ASTM	6,051	41.7	3	6.2
BT-56 Batch 2	53 (test day)	ASTM	7,256	50.0	3	4.0
BT-56 Batch 1	56	ASTM	6,286	43.3	3	4.6
BT-56 Batch 2	56	ASTM	7,117	49.1	3	3.5

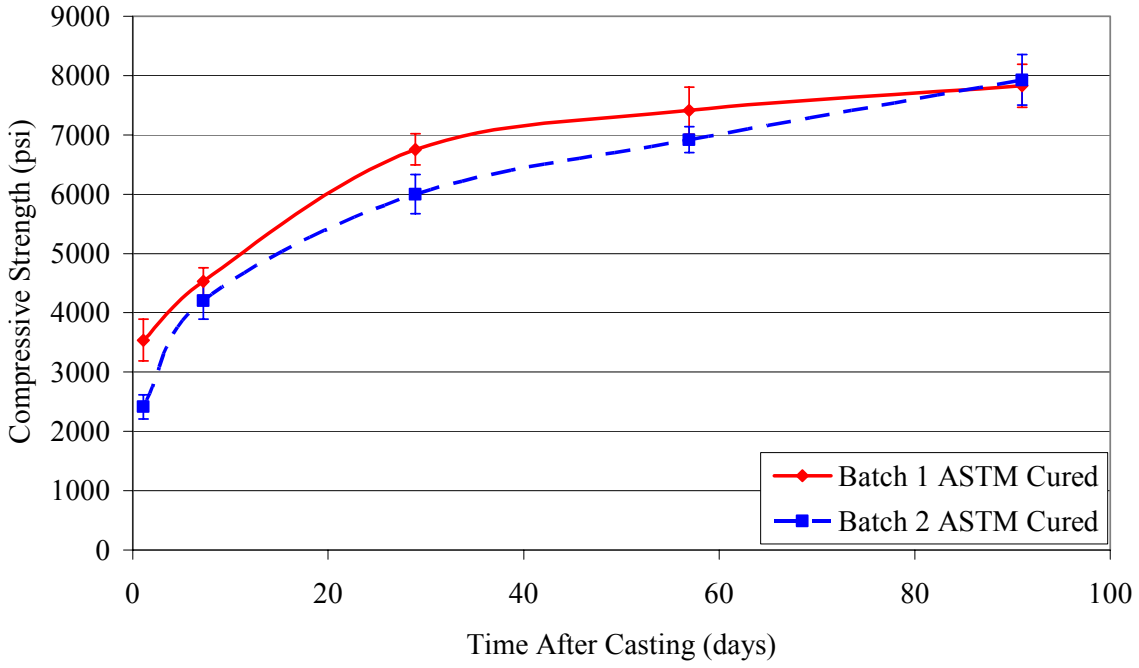

Figure 4.31 Type IV deck compressive strength vs. time plots with standard deviations

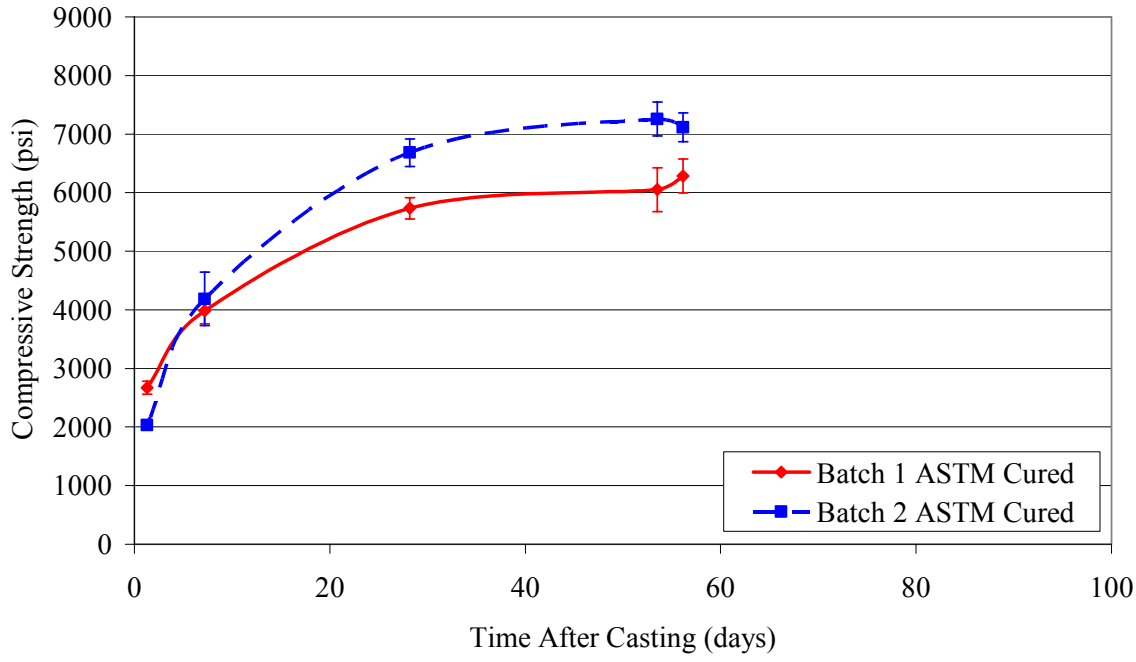

Figure 4.32 BT-56 deck compressive strength vs. time plots with standard deviations

4.6.3 Modulus of Elasticity

Table 4.21 shows the average experimental modulus of elasticity for each deck. Each deck's average modulus had large coefficients of variation because the respective batches for each deck varied significantly. Table 4.22 compares the experimental modulus with the prediction equations obtained from Eqns. 4.1, 4.3, and 4.4. Eqn. 4.1 overestimates the elastic modulus for the decks by an average of 30 percent. Eqns. 4.3 and 4.4 overestimate the deck modulus by 23.22 and 11.24 percent, respectively

Table 4.21 Modulus of elasticity results for both decks

Girder	Time of Test	Curing Type	Average 6 in. x 12 in. Compressive Strength (psi)	Experimental Modulus (ksi)	Number of Tests	Coefficient of Variation %
Type IV	1-day	ASTM	2,977	2,568	4	16.9
Type IV	56-day	ASTM	7,166	3,561	4	5.2
Type IV	91 (test day)	ASTM	7,879	3,546	4	3.6
BT-56	1-day	ASTM	2,352	2,469	4	6.9
BT-56	56 (test day)	ASTM	6,653	3,506	7	4.8

Table 4.22 Comparisons between modulus of elasticity prediction equations and experimental results

Experimental Modulus (ksi)	Predicted E_c, Eqn. 4.1	Predicted E_c, Eqn. 4.3	Predicted E_c, Eqn. 4.4	% Difference Eqn. 4.1 vs Exp.	% Difference Eqn. 4.3 vs Exp.	% Difference Eqn. 4.4 vs Exp.
2,568	3,144	3,182	2,803	22.4	23.9	9.1
3,561	4,877	4,386	3,947	37.0	23.2	10.8
3,546	5,114	4,550	4,103	44.2	28.3	15.7
2,469	2,795	2,940	2,573	13.2	19.1	4.2
3,506	4,700	4,263	3,830	34.0	21.6	9.2

4.6.4 Shrinkage

Shrinkage tests were performed on both batches of each deck. Eight specimens were made for each girder. All specimens were cured on top of the freshly poured decks. The initial shrinkage measurements were taken eight hours after each deck was placed to examine early age shrinkage. Four specimens from each deck were wrapped in a sealing tape to prevent moisture loss, while the remaining four were unwrapped. This was done to isolate the autogenous shrinkage from the total drying shrinkage. Figure 4.32 shows both types of shrinkage for both girders.

Figure 4.33 shows the total drying shrinkage strain versus time compared to previously mentioned prediction methods. The general form for the prediction of time-dependant shrinkage was given by Eqn. 4.10 and the values used for each prediction method are given in Table 4.23. ACI Committee 209 (1997) provided a general value of 780 microstrains for the ultimate shrinkage strain. This value was changed to 886 based on relative humidity, volume to surface ratio, slump, fine aggregate content, air content, and total cementitious material per cubic yard. Ultimate shrinkage strains found by Lai et al. (1999), Shams and Kahn (2000), and Slapkus and Kahn (2002) for Grade 1 HPC were 500, 536, and 676, respectively. The average ultimate shrinkage strain found for the two decks was 940 microstrain and this value was used in the prediction equation to obtain a best fit line. All the prediction methods underestimated the shrinkage strain found in both decks.

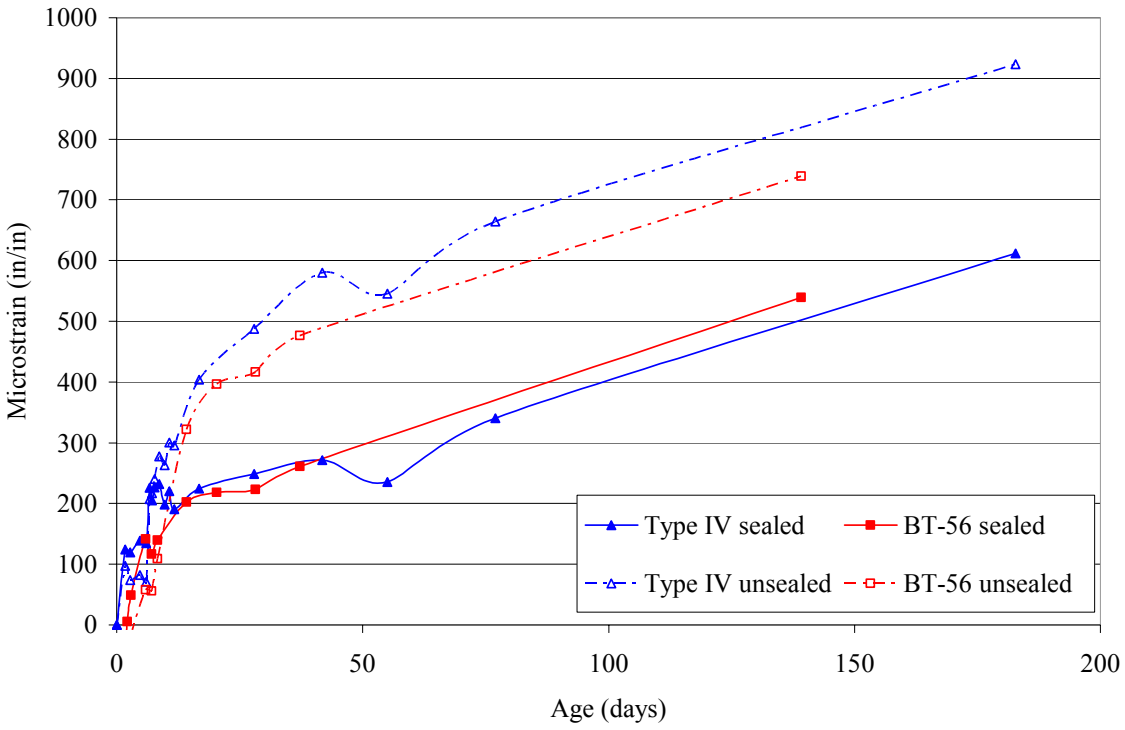

Figure 4.32 Total drying and autogenous shrinkage for both decks

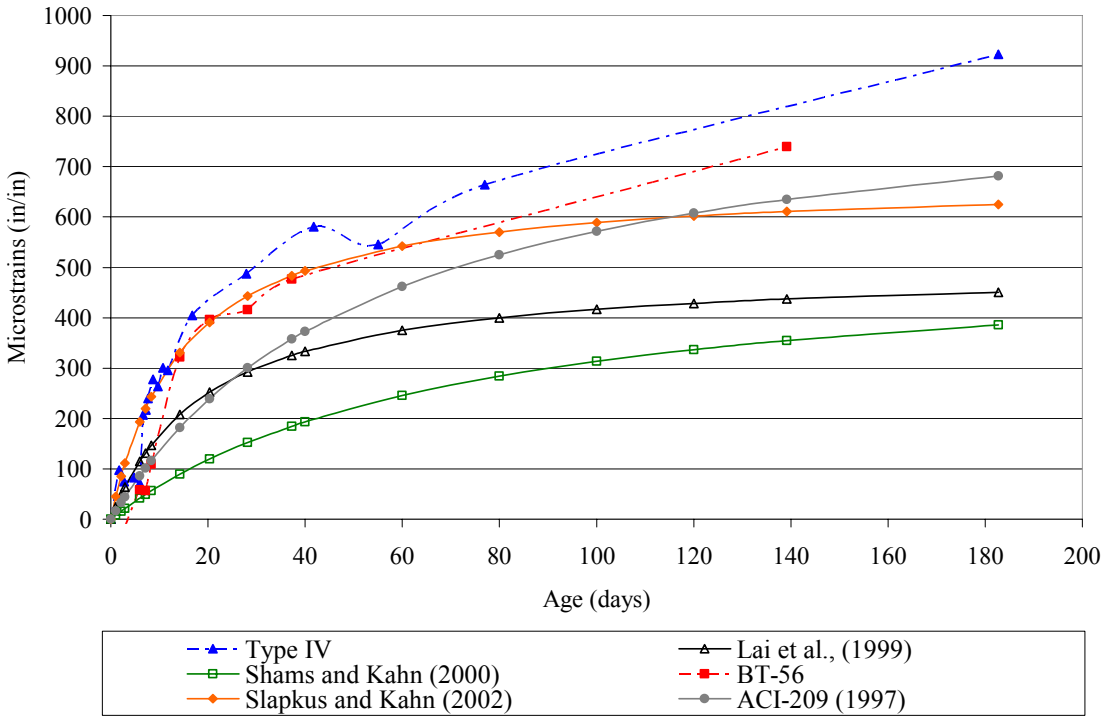

Figure 4.33 Shrinkage strain versus time, compared to prediction methods

Table 4.23 Values of f and $(\varepsilon_{sh})_u$ that define the shrinkage strain versus time curves

	Lai et al., 1999	Shams and Kahn, 2000	ACI-209, 1997	Slapkus and Kahn, 2002	Best Fit
f	20	71	55	14.83	28
$(\varepsilon_{sh})u$	500	536	886	676	940

4.6.5 Rapid Chloride Permeability

RCPT tests were performed on four specimens from each deck, two from each batch. Results are given in Table 4.24. The average chloride ion penetration values for the Type IV and BT-56 decks met the required mixture specifications.

Table 4.24 Results of the rapid chloride permeability tests for concrete used to cast both decks

Type IV		
Specimen	Charge (Coulombs)	Permeability
1	2052	moderate
2	1838	low
3	2094	low
4	1839	low
Average	1956	low
BT-56		
Specimen	Charge (Coulombs)	Permeability
1	2370	moderate
2	1158	low
3	1445	low
4	1013	low
Average	1496	low

4.6.6 Coefficient of Thermal Expansion

The coefficient of thermal expansion was measured for both decks at 3, 60, 92, and 155 days. Measurements were taken in the same manner as used for girder CTE tests discussed in Section 4.5.8. Table 4.25 shows the average CTE values for both decks for each day in με/°C and με/°F. A plot was used to determine the CTE value at any given time for the deck concretes. This is shown in Figure 4.34, which plots the average CTE values versus time. Slapkus and Kahn (2002) found the CTE for the Jonesboro Road Bridge deck samples to be 6.35 με/°F (11.430 με/°C) at 56 days, which is slightly higher than the values obtained in this study.

Table 4.25 Average CTE values for both girders

Day	CTE	
	με/°C	με/°F
3	8.90	4.93
59	9.35	5.19
92	10.36	5.76
155	10.86	6.03

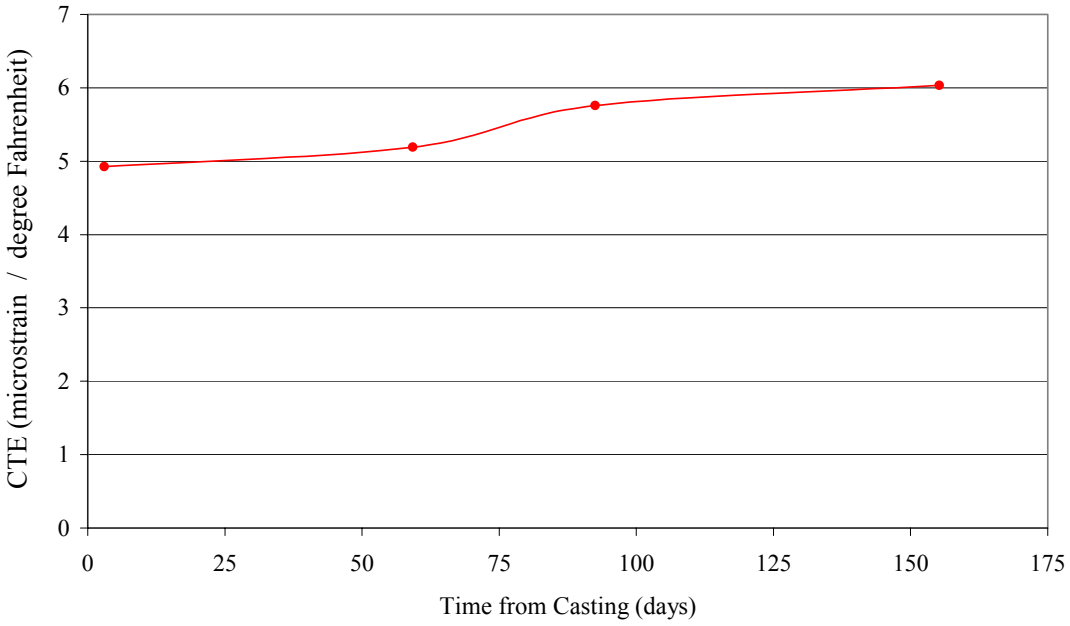

Figure 4.34 Average deck CTE versus time

CHAPTER 5

SHEAR TEST SET-UP AND PROCEDURE

5.1 Introduction

The two girders discussed in Chapters 3 and 4 were both tested in flexure by Canfield and Kahn (2005). The Type IV girder was ruptured and was not tested in shear. The BT-56 girder was tested in flexure and not ruptured. Therefore, this chapter discusses the test set-up for three shear tests performed on the AASHTO BT-56 girder. Shear tests were performed on both ends of the girder, along with one performed 12 ft. inside the west end. The tests were labeled E1, W1, and W2; and the shear reinforcement was spaced at 7 in., 9.5 in., and 24 in. on center, respectively, in the critical sections. In this research, shear/bond failure was not desired. Therefore, AASHTO Standard (2002) development length equations were used so that the shear spans used on the BT-56 girder would be outside the development length. The specifications predicted a development length of 93.4 in. The test was also designed so that there would not be a direct strut from the load to the support. That is, the shear span would be greater than two times the effective depth of the composite member (128 in.). Shear spans of approximately 143 in. were used. The girder details and test set-up are discussed for each test.

5.2 Test Set-Up

All of the testing components used in the shear testing were taken from the flexure test set-up (Canfield and Kahn, 2005) and used for all three shear tests. The BT-56 girder was positioned for the shear tests on two 40 in. tall concrete supports with roller supports

at each end as illustrated in Figure 5.1. At the end of the girder closest to the loading point, the roller was blocked to create a pinned support. The far support was allowed to roll. The flexure test left no damage at either end of the girder. Therefore, there was no change needed to the girder's position and neither the supports nor the girder were moved. Figures 5.2 and 5.3 show the girder supports prior to girder placement. An 800 kip capacity load frame was used for all shear testing, and it was post-tensioned to the structural laboratory's floor with 16 Dywidag bars for each shear test. Figure 5.4 shows the load frame before testing. A 1,000 kip hydraulic loading ram was used to load the girder. Figure 5.5 shows the loading ram with the load cell and steel plates prior to shear testing. Figure 5.6 shows the typical set-up of the frame, jack, load cell, spreader beam, and roller supports. Figures showing each specific test set-up are presented in the following sections.

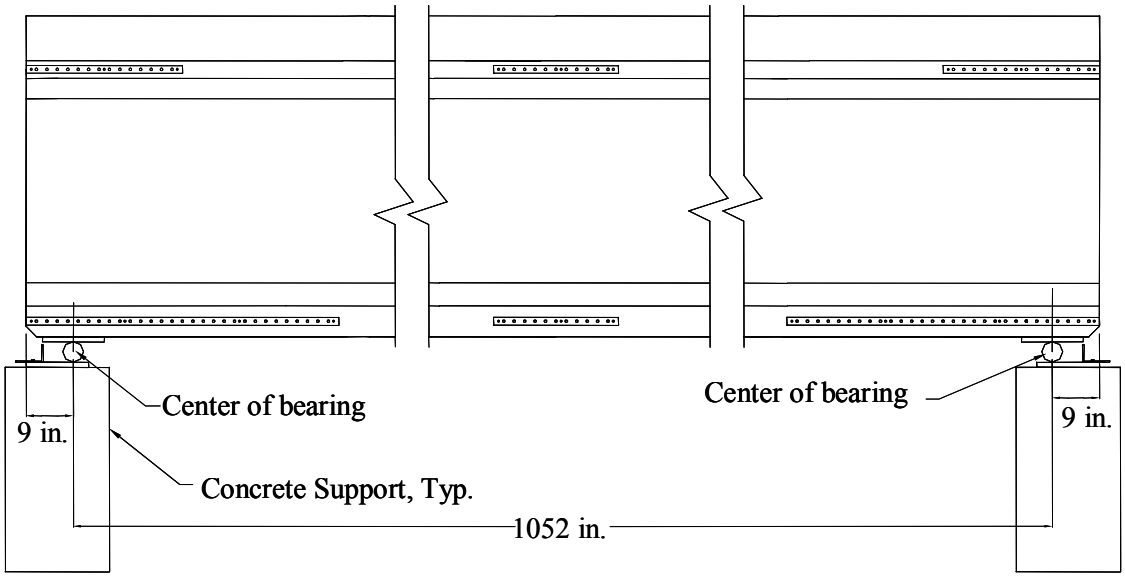

Figure 5.1 BT-56 girder on concrete supports

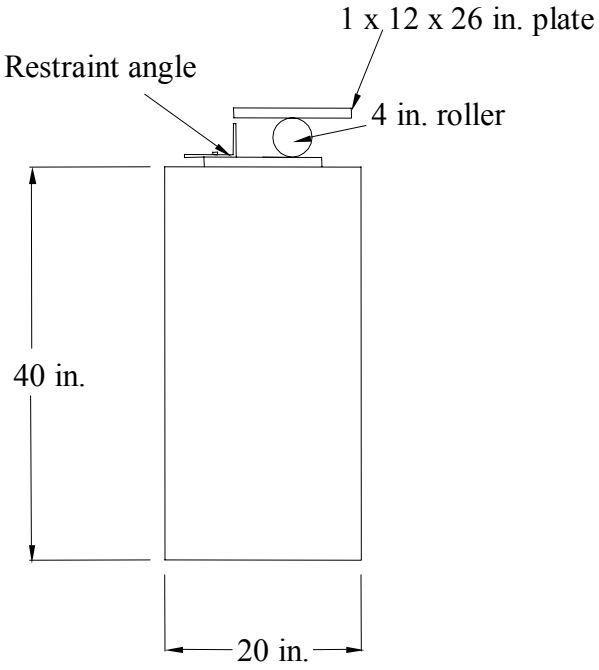

Figure 5.2 Typical girder support

Figure 5.3 BT-56 girder roller supports: Typical at both ends

Figure 5.4 Shear test 800 kip load frame

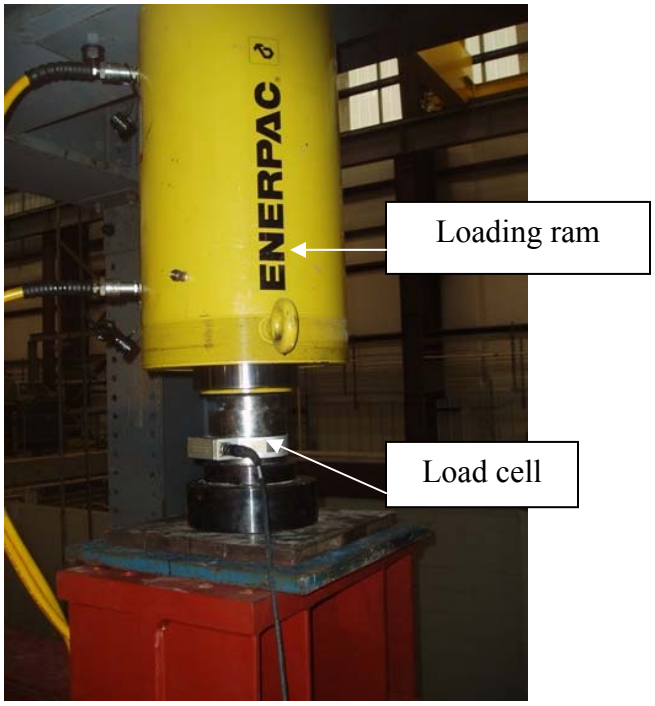

Figure 5.5 1,000 kip hydraulic loading ram with load cell and steel plates

Figure 5.6 Typical shear test set-up

5.2.1 Shear Test E1

Test E1 was the first shear test conducted on the BT-56 girder. The east end had the least amount of cracking due to the flexure testing and the closest shear spacing. The shear span was the distance from the center of bearing, pin support, to the center of load, midway between the two loading rollers, which were 12 in. apart. For test E1, the shear span was 143.5 in. causing the embedment length to be 152.5 in. The shear span was chosen so that there would be no development length failure or strand slip at the end of the girder. The stirrup spacing varied within the shear span due to design considerations.

Figure 5.7 shows the total test set-up for Test E1, and Figure 5.8 gives detailed drawings of the test set-up and shear reinforcement provided for Test E1.

Figure 5.7 Test E1 set-up

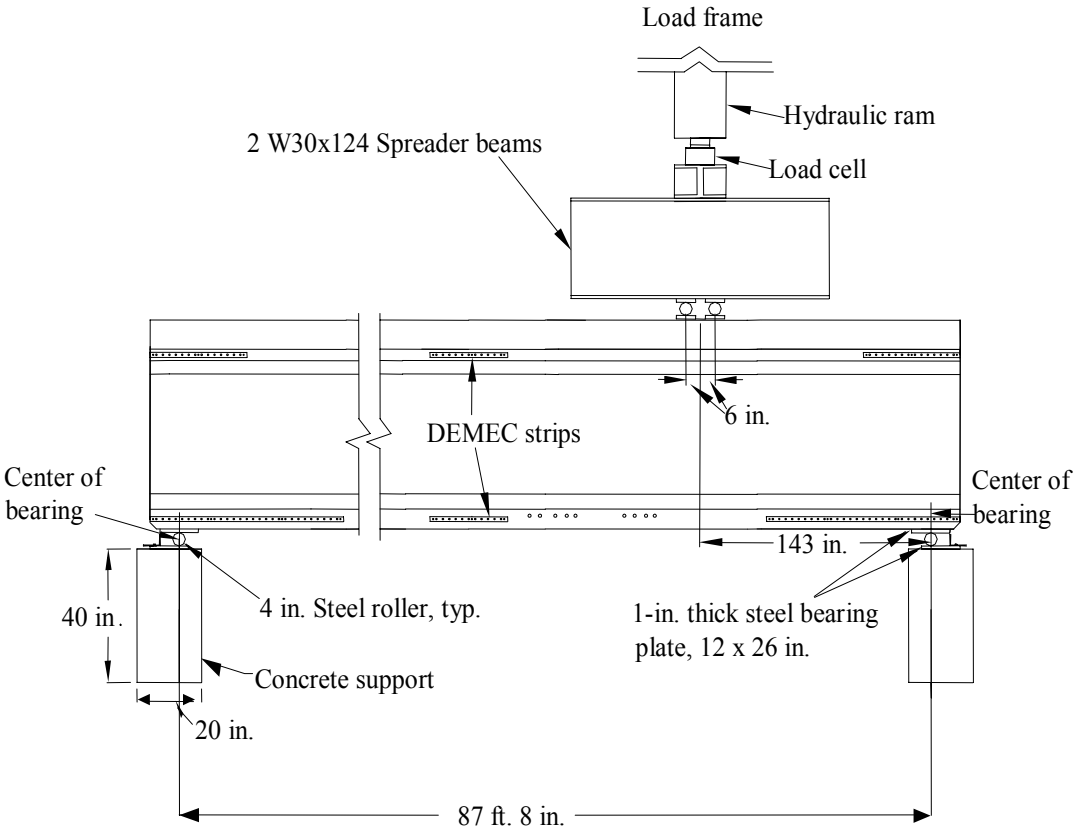

Test E1 set-up

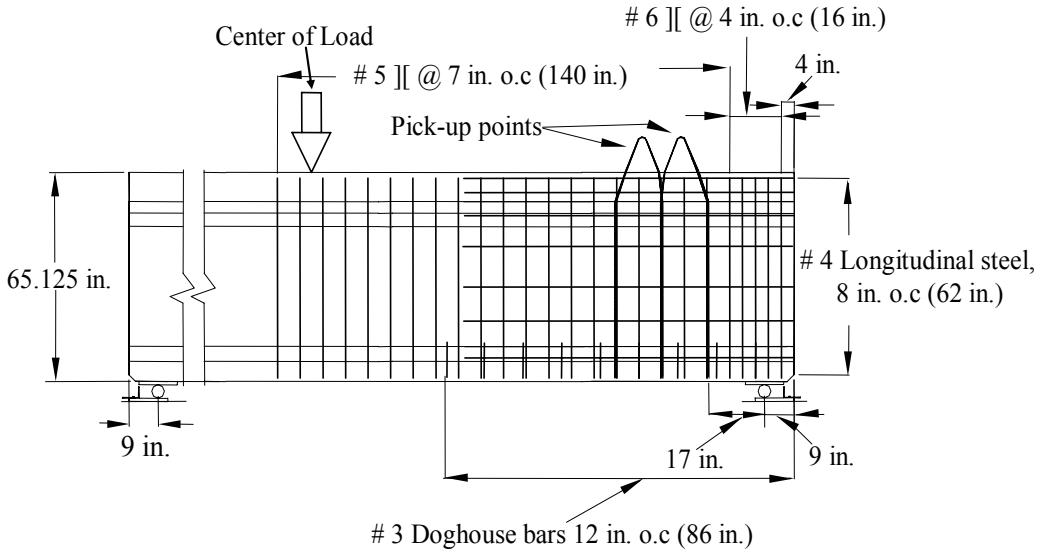

Test E1 stirrup spacing

Figure 5.8 Test E1 set-up and stirrup spacing

5.2.2 Shear Test W1

Test W1 was the second shear test conducted on the BT-56 girder. Shear flexure cracks from Canfield's flexure tests extended farther towards the west end due to larger stirrup spacing. However, there were no cracks within the shear span of the west end. The shear span for the test was 142.5 in. causing the embedment length to be 151.5 in. The shear span mirrored the E1 test and is shown in Figure 5.9. The stirrup spacing varied due to design considerations and is shown in Figure 5.10.

Figure 5.9 Test W1 set-up

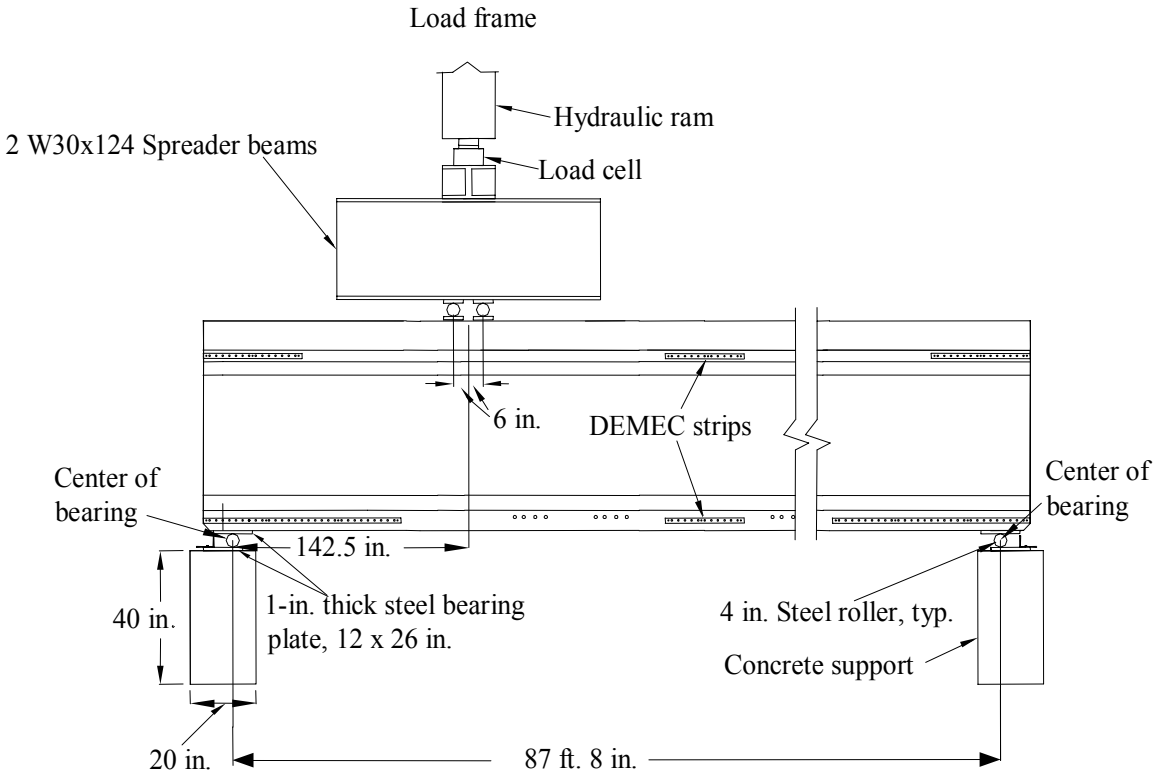

Test W1 set-up

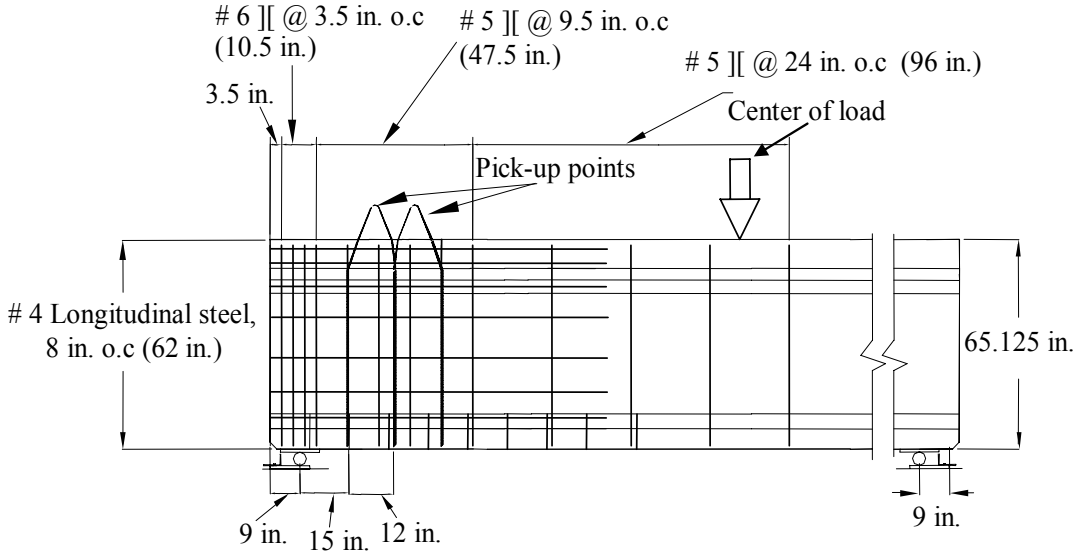

Test W1 stirrup spacing

Figure 5.10 Test W1 set-up and stirrup spacing

5.2.3 Shear Test W2

Test W2 was the third and final shear test conducted on the BT-56 girder. It was performed because ultimate failure was not reached in either of the first two tests. It was thought that the first two tests did not reach failure because of the pick-up loops located at both ends of the girder. Therefore, it was necessary to test the girder so that the shear forces would not have to transfer through the pick-up loops. The girder support was located 8 ft. from the end of the girder to clear the pick-up loops as illustrated in Figure 5.11. The prestress and dead load forces were calculated to ensure that the cantilevered 8 ft. section would not crack or fail. Figure 5.12 shows drawings of the set-up and shear spacing at that section.

Figure 5.11 Test W2 set-up

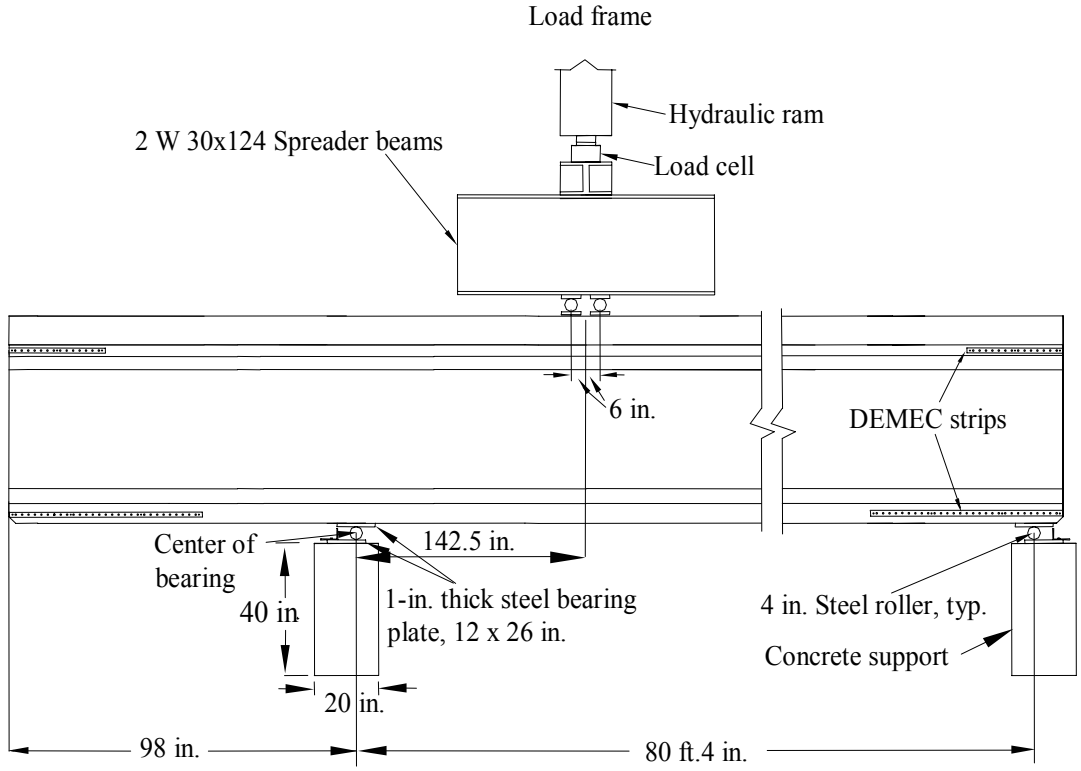

Test W2 set-up

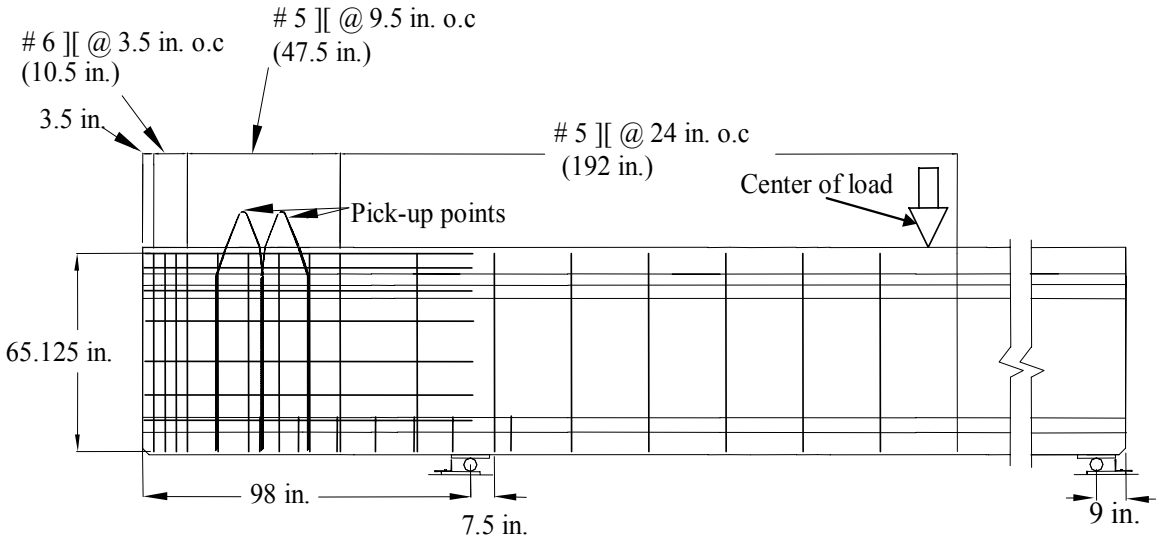

Test W2 stirrup spacing

Figure 5.12 Test W2 set-up and stirrup spacing

5.3 Test Instrumentation

The instrumentation used in each of the shear tests was identical. A load cell was used to monitor the applied load. The DEMEC points on both sides of the girder were read to monitor the strain in the prestressing strands at the girder ends. To monitor and record strand slip, linear spring potentiometers were placed on seven strands at each end of the girder. A dial gage was placed at the shear span center to monitor any horizontal shear slip between the deck and the girder. To measure and obtain strain profiles throughout the loading sequence, string potentiometers were placed at the bottom, middle, and top of the girder. Finally, to determine stirrup strain and principle stresses, 5 LVDTs were placed at the shear span center of each test. This section details and discusses each instrument's characteristics, installation, placement, and the data acquisition systems used to record the data.

5.3.1 Load

The load cell used to monitor the applied load was a Strainsert 700 kip load cell. The model number was (CLC-FB) Q14928, and it had a voltage rating of 2.0 mV/V. The load cell had a full-bridge configuration that required ten volts of direct current excitation. It was calibrated and tested with the SATEC compression machine at Georgia Tech, and it was not perfectly linear. Therefore, a correction equation was applied after all data were recorded in order to obtain accurate loading results. The load cell was centered and placed between the spreader beam and the hydraulic loading jack.

5.3.2 Surface Strains

DEMEC strips placed at both ends of the bottom of the girder were monitored and recorded at various loads in order to determine the strain in the prestressing strands and the partial development length. Only partial development length was possible because the DEMEC points extended just 60 in. from the end of the girder, and the calculated development length was 93.4 in. Zero readings were taken before any loads were placed on the BT-56 girder. After this was done, DEMEC readings were taken at every 100 kips up to cracking, and then at about 30 kip load increments. The DEMEC gages and development length were relevant for Tests E-1 and W-1, but not for Test W-2. Test W-2 was conducted outside the DEMEC points, and thus they were not used. Locations of the DEMEC points are shown in Figures 5-8, 5-10, and 5-12.

5.3.3 Strand Slip

Spring potentiometers were used in the shear tests to monitor and determine if any strand slip had occurred at the end of the girder. A total of 7 spring potentiometers were used for each test. They were mounted to a ¼ in. steel plate and connected to the strands using a U-bolt. Figure 5.13 shows two spring potentiometers mounted on the strands. Figure 5.14 shows the configuration of the 7 gages for each test. Tests by Dill and Kahn (2000) showed that maximum strand slip occurred on bottom strands located at the sides of the section. Therefore, four of the gages were placed at these locations.

Figure 5.13 Spring potentiometers

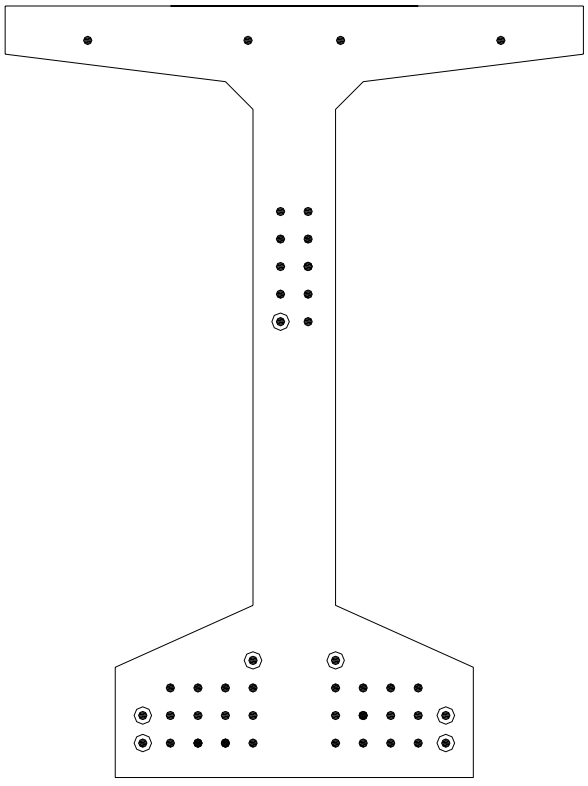

Figure 5.14 Spring potentiometer locations (circled)

5.3.4 Deck-Girder Interface Shear

A single dial gage was mounted to the bottom of the deck and to the side of the girder in order to monitor horizontal shear slip between the deck and the girder. It was placed at the center of the shear span at the deck/girder interface. The gage was zeroed before load was placed, and it was monitored throughout the test for any movement. Figure 5.15 shows the installed dial gage.

Figure 5.15 Horizontal shear slip dial gage

5.3.5 Longitudinal Strain and Vertical Displacement

A total of four string potentiometers were used for each shear test. The string potentiometers were Ametek Linear Motion Transducers, with 2 in. and 40 in. measurement lengths. One 40 in. potentiometer was used to monitor the vertical deflection of the girder with an accuracy of 0.001 in. The string potentiometer was placed directly under the loading point. It was anchored with a heavy steel plate and attached to a wooden block glued to the underside of the girder.

The other three potentiometers had 2 in. length change capacities and were used to obtain longitudinal, flexural strain profiles beneath the load center throughout each shear test. Figure 5.16 shows a close-up of the top two string potentiometers. The center of the gage length corresponded to the center of the load point. They were mounted horizontally on the girder and were attached to predrilled and pre-installed inserts. The gage length between the inserts was 36 in. Care was taken to ensure that the strings were level so the movement of the strings corresponded exactly to the movement of the girder. The potentiometers were mounted at the bottom layer of the strands, at the top layer of strands, and at the top of the deck. Figure 5.17 shows the typical location of the four string potentiometers. The horizontal potentiometers were accurate to 0.001 in. which resulted in a strain accuracy of 28 με over the 36-in. gage length.

Figure 5.16 Top two string potentiometers used for strain profile

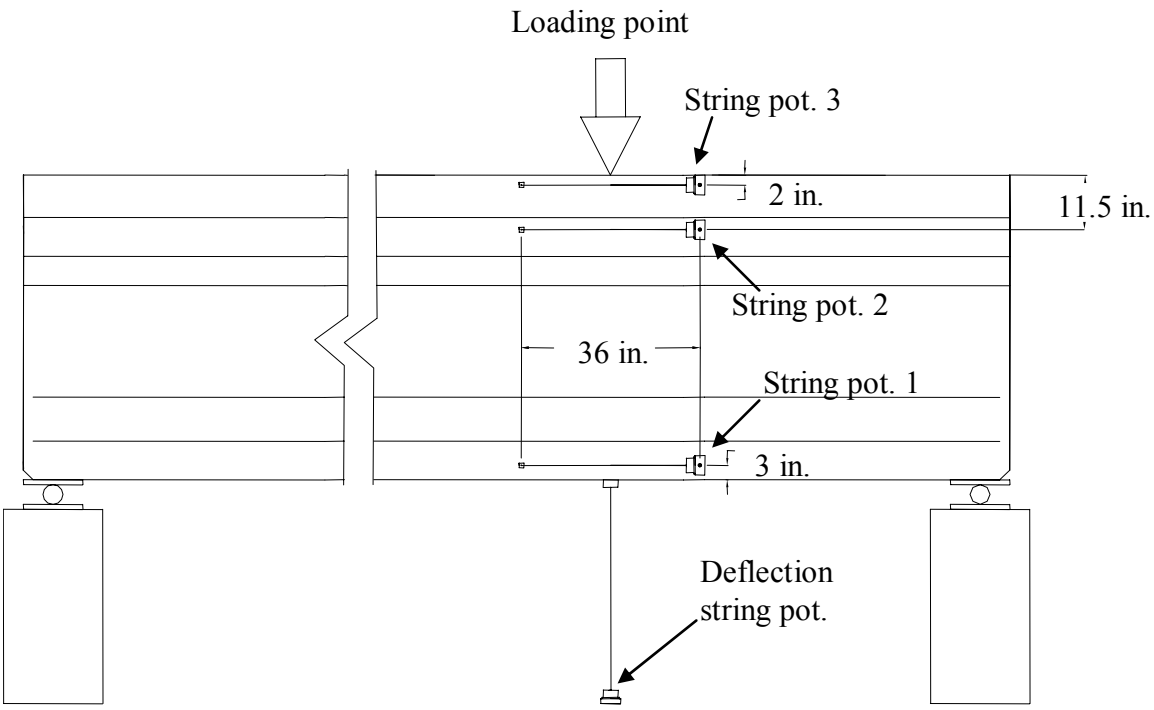

Figure 5.17 Typical string potentiometer layout for shear tests

5.3.6 Principal Web Strains and Stirrup Strains

Linear Variable Displacement Transducers (LVDTs) were manufactured by the RDP Group and were model number DCTH 500; each was accurate to 0.0001 in. displacement. Five were used for each shear test; three for a strain rosette and two more for vertical strain at stirrup locations. The LVDTs were all six inches long with a range of ± 0.5 in. Threaded rods with $^{5}/_{32}$ in. diameters were used to extend the length of the LVDT rods so they could reach their required gage lengths, generally 18 in. The LVDTs were mounted onto the concrete by drilling holes in the concrete at the pre-measured locations and by gluing DEMEC inserts into them. Brackets were fabricated to hold both the LVDTs and the threaded rod at the opposite end. The LVDT brackets were designed to slightly pivot to take into account the curvature of the girder as it was loaded. Figure

5.18 shows a typical LVDT and its brackets. All of the LVDTs required a minimum of ± 12 volts up to a maximum of ±15 volts. The voltage requirement was bi-polar, and two external power sources were required to provide the adequate voltage. The external power sources were 2 BK Precision DC Power Supplies that were wired directly to the LVDTs. The LVDTs were each calibrated by Georgia Tech researchers to read accurately down to 0.0001 in., which corresponded to approximately 10 με accuracy.

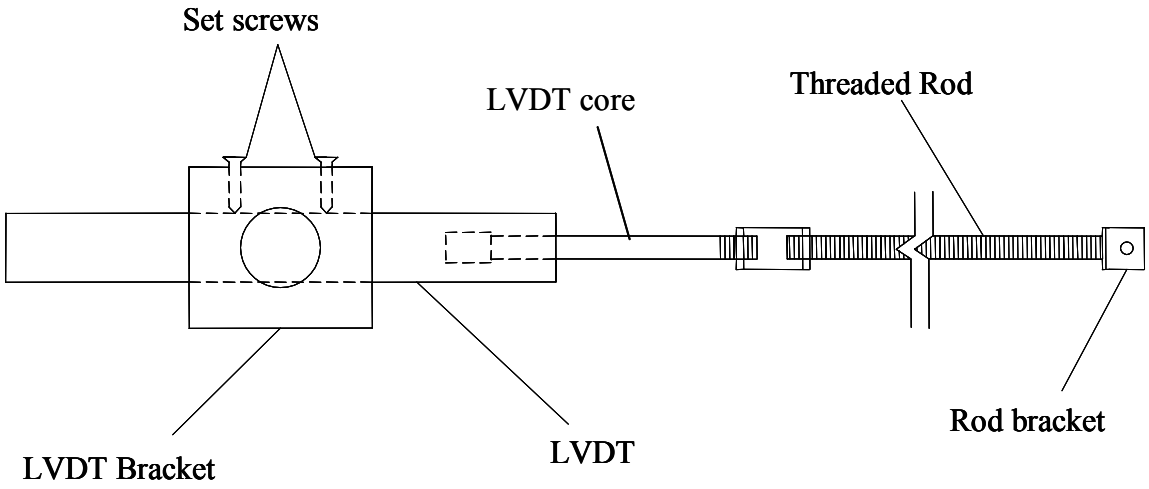

Figure 5.18 Typical LVDT brackets and extensions

On tests E-1 and W-1, the three LVDTs that were vertical and the one horizontal had gage lengths of 18 in., and the LVDT at 45° had a gage length of 25.5 in. Test W-2 had gage lengths of 20 in. for the four vertical and horizontal LVDTs. The 45° LVDT had a gage length of 28.25 in. The 20 in. gage length was used to avoid concrete voids that made installing the gages at 18 in. impossible.

The center of the strain rosette for each test was installed to be at the center of the shear span. The vertical LVDTs were installed so that they were directly in line with the vertical stirrups. The stirrup locations were determined by using the as-built drawings

and drawing vertical lines on the outside of the girder at both ends. The location and configuration of the LVDTs can be seen in Figure 5.19. It is important to note that the configuration of the strain rosette differed at each end of the girder due to the opposite direction of shear cracks. The 45° LVDT was set so that it crossed the web shear cracks seen in each test. Figures 5.20 and 5.21 show the LVDT set-up for the three shear tests.

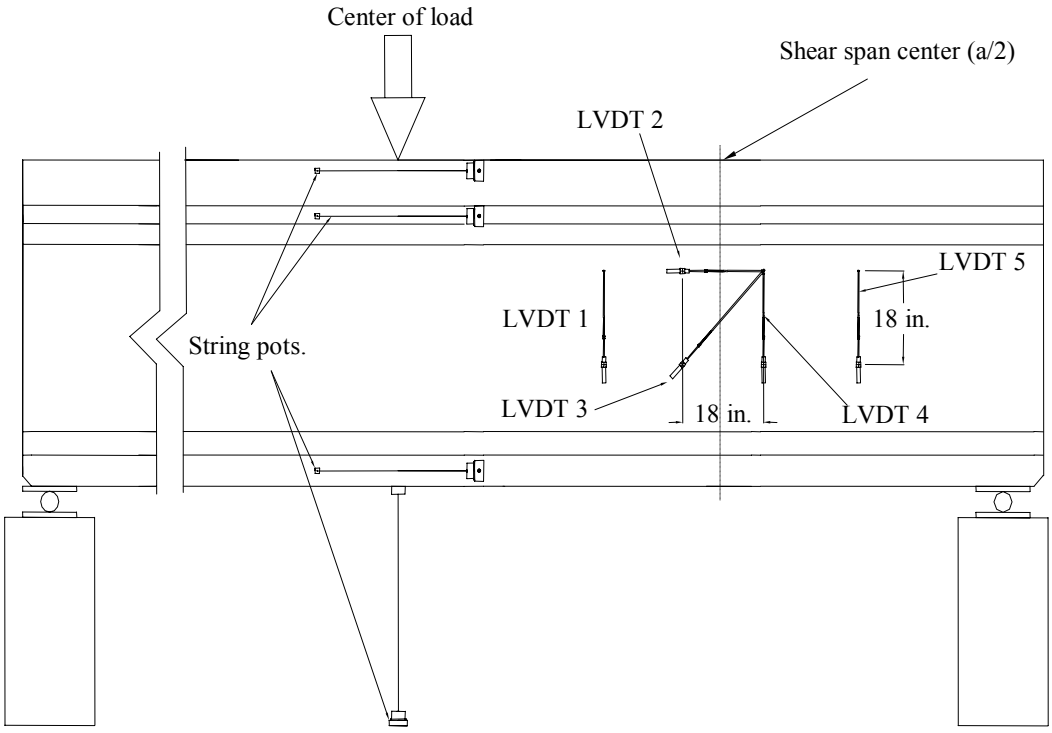

Figure 5.19 Typical LVDT and string potentiometer configuration (Test E-1 shown)

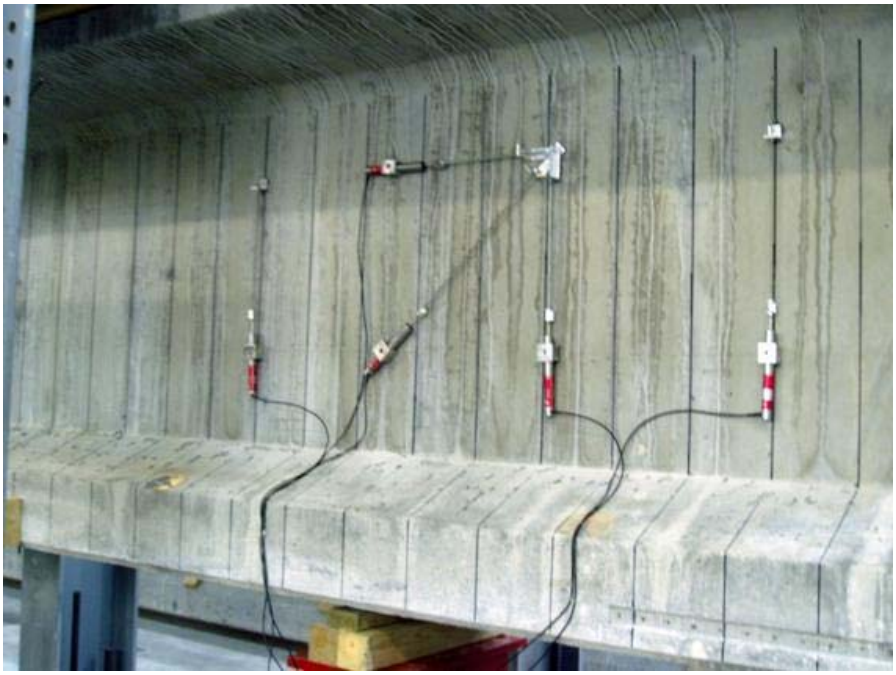

Figure 5.20 Test E-1 LVDT configuration

Figure 5.21 Test W-1 and W-2 LVDT configuration

5.3.7 Data Acquisition Systems

Two separate data acquisition systems were used to record all of the data for each shear test. The two systems, National Instruments Labview, and Optim Electronics MEGADAC, were started at the same time and their clocks were synchronized for the combination of the data after testing was complete. NI Labview was used to record the 7 strand-slip string potentiometers and the load cell, and MEGADAC was used to record the three longitudinal strain potentiometers, the one vertical displacement string potentiometer, and the five LVDTs.

All 8 instruments that used the Labview system were configured as strain gages and connected to an NI SCXI-1314 terminal block. The terminal block was connected to an NI SCXI-1520 input module which was mounted in an NI SCXI-1000 chassis. The 7 string potentiometers were connected as quarter-bridge strain gages with an excitation of 10 volts. The load cell was installed as a full bridge strain gage with 10 volts of excitation. All of the instrumentation was connected to a laptop computer. Labview software was used to monitor and record the data as the tests were performed. Figure 5.22 shows a picture of the National Instruments chassis and set-up.

Figure 5.22 National Instruments Labview and laptop computer used for shear testing

The Optim Electronics MEGADAC system was used to record the 5 LVDTs and 4 string potentiometers. The LVDTs required an excitation voltage of ± 15 volts, as previously mentioned. They were wired to the external power supplies and to a CB-808 terminal block which was connected to an AD-808 FB-1 module inside the MEGADAC chassis. The Optim system had calibration curves for all the string potentiometers used in the shear tests from previous experiments. They were connected to an 808 FB-1 terminal block that was connected to an AD-808 FB module inside the MEGADAC chassis. The MEGADAC system was connected to a personal computer in a rolling cabinet located in the structural laboratory. Figure 5.23 shows Optim system and the BK Precision voltage sources.

Figure 5.23 Optim Electronics Data Acquisition set-up

5.4 Testing Procedure

All three of the shear tests performed on the BT-56 girder were performed in a similar fashion. For tests E-1 and W-1 the load frame and all subsequent pieces were simply moved from one end to the other. For test W-2, the girder was lifted at one end and the concrete support was moved 8 ft. closer to the opposite support. The moving of all testing equipment was handled with two 30 ton cranes. When all testing equipment was in place and all gages were mounted, the tests were performed as detailed below.

5.4.1 Initial Readings

Prior to applying load, initial measurements were taken on all LVDTs and string potentiometers to obtain actual gage lengths and initial readings for each instrument. Initial readings were taken from the DEMEC strips on both sides of the girder for Tests E1 and W1. Also, initial, "zero" readings from both data acquisition systems were recorded by hand in order to determine the amount of strain in the bottom strands and in the vertical stirrups at any given load. Manual deflection and strain measurements were taken directly underneath the point load to verify the electronic data. When all of the initial readings were recorded, load was applied to the girder with the hydraulic loading ram. Figure 5.24 shows researchers taking initial DEMEC readings.

Figure 5.24 Researcher taking initial DEMEC readings

5.4.2 Loading Method and Experimental Data

The load was applied in increments of 100 kips until first cracking was observed. After first cracking, the load was increased about 50 kips at a time. At each loading increment, an approximate ten minute pause was observed while manual measurements were taken. During this time no efforts were made to maintain load. The first two minutes of the pause were to let the girder stabilize. The rest of the time was used to record DEMEC values, manual strain data, and manual deflection data. Many Georgia Tech researchers were used to take the readings. For consistency, the same researchers performed the same measurements at each load increment. Notes were taken regarding deflection, end slip, any significant cracking, or other noticeable testing events. After web shear cracking occurred, the cracks and corresponding loads were marked on the girder using felt-tip markers. Figure 5.25 shows a researcher marking cracks for Test E-1. As the load and cracking increased, the additional cracks and crack propagation were marked as well.

Figure 5.25 Researcher marking shear cracks

After the load was above the calculated ultimate strength, the test continued on a deflection-controlled basis. At deflection changes of 0.25 in., loading was stopped and manual measurements were taken. The loading was stopped when the girder either failed, or when the ultimate capacity of the testing equipment was reached. Two of the tests resulted in reaching the capacity of the loading equipment. The final test, W-2, resulted in a web-crushing shear failure, which is shown in Figure 5.26.

Figure 5.26 Web-crushing shear failure, Test W-2

5.4.3 Unloading Procedure

Once the maximum load was reached, it was reduced gradually so that the data acquisition systems could record the decreasing load curve. No manual readings were taken until the beam was completely unloaded. A final set of manual readings was then taken in order to determine any elastic or inelastic behavior in the BT-56 girder. After the final reading, the load frame and instruments were removed and prepared for the next test.

CHAPTER 6

SHEAR BEHAVIOR

6.1 Introduction

This chapter presents the predicted and experimental shear behavior of the BT-56 girder. The BT-56 girder was tested in flexure by Canfield and Kahn (2005) before any shear tests were performed. The east (Test E1) and west (Test W1) ends remained uncracked after the flexure test, but flexure shear cracks developed in the section used for Test W2 (near quarterspan). The BT-56 girder was tested at the three separate locations to provide an understanding of shear behavior with different stirrup spacing. The vertical steel reinforcement was spaced at 7.5, 16.75, and 24 in. for Tests E1, W1, and W2, respectively. Tests E1 and W1 did not reach ultimate shear failure because the capacity of the testing equipment was surpassed. Consequently, Tests E1 and W1 were used to determine and analyze the concrete shear strength, V_c, and Test W2 was used to determine the ultimate shear capacity of the BT-56.

This chapter discusses the methods suggested by AASHTO Standard (2002), ACI Alternate, AASHTO LRFD (2004), and the Variable Angle Truss Model for predicting shear capacity. The four different prediction methods were used to calculate shear capacities based on the measured properties. The measured properties were based on physical measurements performed by Georgia Tech researchers, including concrete strengths and mild reinforcement yield strengths. When test-to-predicted values were compared to other research, all calculations used measured properties. The measured

section properties are shown in Figure 6.1. All shear capacity calculations were performed at the code-specified critical sections, which are discussed in section 6.2.

This chapter also provides experimental results of each shear test, comparisons with the four prediction methods, and comparisons with previous research on the shear capacity of prestressed high performance concrete bridge girders.

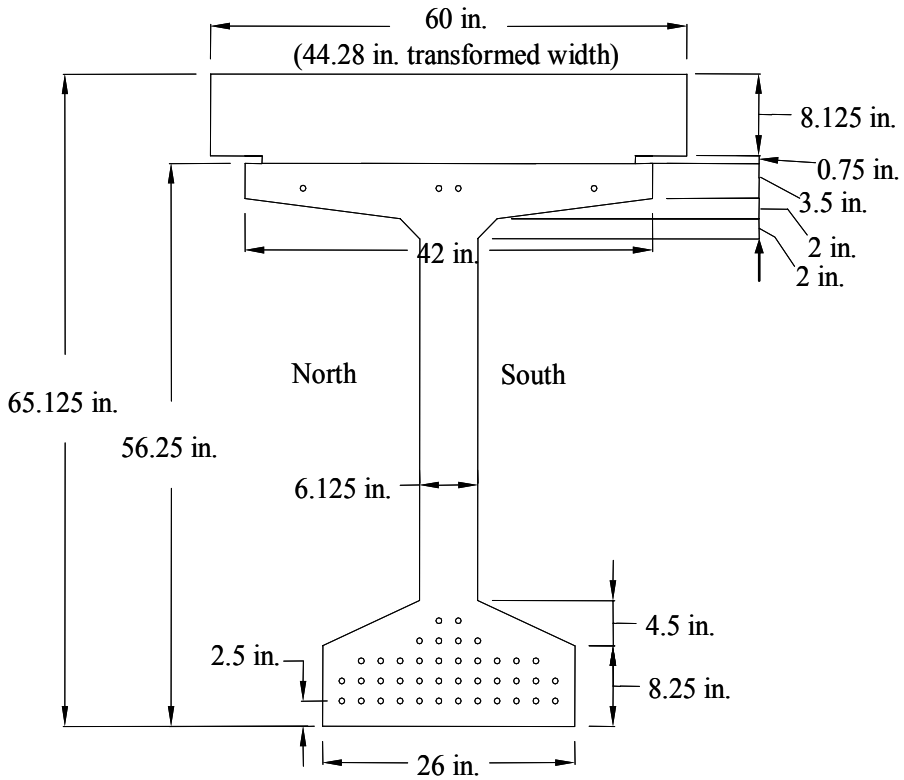

BT-56 Measured Transformed section

Girder Properties		**Composite Transformed Properties***	
Area, A_g =	717.5 in^2	Area, A_c =	1092 in^2
Moment of inertia, I_g =	312529 in^4	Moment of inertia, I_c =	578420 in^4
Centroid from bottom, y_b =	27.54 in.	Centroid from bottom, y_{bc} =	39.09 in.
Concrete Properties†		**Steel Properties**	
Girder concrete strength, f_c' =	13819 psi	Strand area, A_{ps} =	9.5964 in^2
Girder modulus of elasticity, E_c =	4834 ksi	Strand yield stress, f^*_y =	252 ksi
Deck concrete strength, f_c' =	7256 psi	Strand ultimate stress, f'_s =	280 ksi
Deck modulus of elasticity, E_{cd} =	3500 ksi	Mild reinforcement yield stress, f_y =	69 ksi
Modular ratio, n =	0.724		

•deck transformed based on the nominal ratio of deck E_{cd} to girder E_c (no steel transformed)
† concrete properties are on day of girder testing

Figure 6.1 Measured cross section properties

6.2 Shear Prediction Methods

This section details the four previously mentioned shear prediction methods and how they were used to calculate the shear capacities of each tested section. How and where each analysis was performed is also discussed. The calculated predictions for each method and test are presented. Sample calculations and properties for all methods are given in Appendix D.

6.2.1 AASHTO 2002 Standard Shear Design Approach

The 2002 AASHTO Standard Specifications were exactly the same as the ACI 318-02 detailed shear calculations. The shear capacity for this method was calculated along the length of the shear span using both nominal and measured properties. The calculated values that were compared to experimental results were obtained at the code specified distance of h/2. For Test W2, shear capacity was also examined at the center of the shear span ($a_s/2$), because that was the region of failure. The following sections outline the process for calculating the concrete shear strength, V_c, the shear strength provided by the stirrup reinforcement, V_s, and the total shear strength, V_n.

6.2.1.1 Concrete Strength, V_c

According to AASHTO Standard, concrete shear strength was the minimum of the flexure shear strength, V_{ci}, and the web shear strength, V_{cw}. Both strengths were calculated and compared for all three shear tests. The shear spans and properties in this research caused the web shear strength, V_{cw}, to always control.

The flexure shear strength was calculated using AASHTO equation 9-27 which is given as Equation 6.1:

$$V_{ci} = 0.6\sqrt{f'_c}\,b_w d + V_d + \frac{V_i M_{cr}}{M_{\max}} \geq 1.7\sqrt{f_c'}\,b_w d \qquad (6.1)$$

The girder concrete strength, f_c', was nominally 10,000 psi and determined on testing day as 13,819 psi. The value b_w was taken as the web thickness of the BT-56 girder, which was measured as 6.125 in. The code specified that d was the distance from the topmost compression fiber to the centroid of the prestressing strands. The value could not be taken as less than 0.8h, where h was the height of the total composite section. V_d was the shear caused by the dead load at a specific section. V_i and M_{max} were the maximum applied moment and shear at the section in question. These values could not be determined because the maximum live load was not known. However, the single point load located at the shear span of each test allowed for a ratio of V_i / M_{max} to be calculated so that the actual loads weren't needed. M_{cr}, which was the estimated cracking moment, was calculated using AASHTO equation 9-28 which is given as Equation 6.2:

$$M_{cr} = \frac{I}{y_t}\left(6\frac{\sqrt{f_c'}}{1000} + f_{pe} - f_d\right) \qquad (6.2)$$

where:

f_d = Stress due to unfactored dead load, at extreme fiber of section where tensile stress is caused by externally applied loads, psi
f_{pe} = Compressive stress in concrete due to effective prestress forces only at extreme fiber of section where tensile stress is caused by externally applied loads
y_t = Distance from centroidal axis of gross section, neglecting reinforcement, to extreme fiber in tension

Composite section properties were used in calculating M_{cr} because the load that caused cracking was applied to the total composite section. The cracking stress of the concrete, determined by $6\sqrt{f_c'}$, was the conservative value used by this code to approximate the allowable tensile stress. The terms f_{pe} and f_d were the stresses in the girder due to prestressing action and dead load, respectively. They were determined using non-composite girder properties.

The web-shear strength was calculated using AASHTO equation 9-29, which is given as Equation 6.3:

$$V_{cw} = \left(3.5\sqrt{f_c'} + 0.3 f_{pc}\right) * b_w d + V_p \tag{6.3}$$

Where:

b_w = web width
d = Distance from extreme compression fiber to centroid of longitudinal tension reinforcement, but need not be less than 0.8h
f_{pc} = Compressive stress in concrete at centroid of composite section due to both prestress and moments resisted by precast member acting alone
V_p = Vertical component of effective prestress force at section

The term in parenthesis is a quantification of the estimated principal tensile stresses of the concrete, derived from Mohr's circle. V_p was the vertical effect of the draped strands located in the BT-56 girder. The term f_{pc} was defined as the compressive stress in the concrete at the centroid of the cross section resisting externally applied loads. For non-composite girders, this was simply F_{se}/A_g. However, for composite sections, the centroid was higher than in the original girder. Equation 6.4 gives an approximation of the compressive stresses due to prestressing and dead load at the new composite centroid.

All terms in Equation 6.4 are considered positive and the equation properly accounts for the tensile and compressive stresses, where compression is positive.

$$f_{pc} = \frac{F_{se}}{A_g} - \frac{F_{se} e (y_{bot-c} - y_{bot-nc})}{I_g} + \frac{M_d (y_{bot-c} - y_{bot-nc})}{I_g} \quad (6.4)$$

where:

A_g = Gross cross sectional area of non-transformed girder
e = Eccentricity of prestressing strands
f_{pc} = compressive stress at centroid of composite section
F_{se} = Total prestressing force at section
M_d = Total dead load moment due to girder and composite deck
y_{bot-c} = Distance from centroid to extreme tension fiber for composite section
y_{bot-nc} = Distance from centroid to extreme tension fiber for girder alone

The term F_{se} was obtained by multiplying the area of prestress, A_{ps}, by the effective prestressing force, f_{pe}, after losses. The effective prestressing force was reduced when the section being examined was inside a distance equal to the transfer length from the end of the girder (21.4 to 27.8 in.). The transfer lengths of the BT-56 were determined by Canfield and Kahn (2005). The dead load moment, M_d, was obtained from the dead load produced by both the girder and the composite deck.

6.2.1.2 Transverse Reinforcement Shear Strength, V_s

The transverse reinforcement shear strength was calculated using AASHTO equation 9-30, which is given by equation 6.5:

$$V_s = \frac{A_v f_y d}{s} \leq 8\frac{\sqrt{f_c'}}{1000} b_w d \qquad (6.5)$$

For all three shear tests, the shear area, A_v, was 0.62 in^2 for double # 5 bar stirrups. The measured values for the yield stress of the stirrups are given in Figure 6.1. The experimental stress strain curves for the shear steel are given in Chapter 4. The maximum value for the shear reinforcement strength, given as the second term of the equation was ignored because the measured properties were used. The maximum was exceeded in Test E1 due to stirrup spacing and girder pick-up loops. The maximum value was exceeded in Test W1 due to the added strength of the girder pick-up loops.

6.2.1.3 Total Shear Strength

Then total shear strength was calculated using AASHTO equation 9-26 which is given as Equation 6.6:

$$V_n = V_c + V_s \qquad (6.6)$$

There was no maximum limit to the AASHTO Standard Specifications ultimate shear capacity. The only limit was imposed on the strength of the steel reinforcement.

Table 6.1 provides calculated values for all three tests. Unless otherwise noted, all values were calculated at the code defined critical section of h/2 (32.56 in. from the center of bearing). AASHTO Standard calculations are given in Appendix D.1.

Table 6.1 AASHTO Standard (2002) shear capacity predictions

Test	Cracking shear (kips)	Ultimate shear (kips)	
Test E1	308	623*	698†
Test W1	306	539*	614†
Test W2	299	390	392‡

* Values calculated neglecting the pick-up strands

† Values calculated with the pick-up strands using f_y=69 ksi

‡ Values calculated at center of shear span

6.2.2 ACI Alternate Approach for Calculating V_{cw}

ACI 318-02 Section 11.4.2.2 provides an alternate technique for calculating V_{cw}. It states that V_{cw} shall be computed as the shear force corresponding to dead load plus live load that results in a principal tensile stress of $4\sqrt{f_c'}$ at the centroidal axis of the member. In composite members, the principal tensile stresses shall be computed using the cross section that resists live load. This technique was addressed by Lin and Burns (1981), and they provided the following equations which came directly from the application of Mohr's circle. Equation 6.7 gives an approximation of the predicted concrete shear strength based on the principal tensile stress of the concrete.

$$V_{cw-\mathrm{Pr}ed} = \left(f''_{t-\mathrm{Pr}ed} \sqrt{1 + \frac{f_{pc}}{f''_{t-\mathrm{Pr}ed}}} b_w d \right) + V_p \qquad (6.7)$$

The ACI code specified the f''_{t-Pred} value to be $4\sqrt{f_c'}$. The value f_{pc} was calculated at the AASHTO Standard specified critical section. It is important to note that the first term accounts for the concrete strength, V_c, and the vertical prestressing force V_p must be added to get the actual predicted cracking shear capacity, V_{cw}.

In order to determine the accuracy of the ACI Alternate method, the experimental diagonal tensile strength, f''_{t-Exp}, was determined based on $V_{cw\text{-}exp}$. This value was the experimental cracking load determined by visual inspection and confirmed by strain rosettes. When no draped strands were present in a prestressed girder and $V_p = 0$, the experimental diagonal tensile stress was calculated using Equation 6.8:

$$f''_{t-Exp} = \sqrt{\left(\frac{V_{cw-\exp}}{b_w d_p}\right)^2 + \left(\frac{f_{pc}}{2}\right)^2} - \frac{f_{pc}}{2} \tag{6.8}$$

However, in the ACI and AASHTO Standard Specifications, the concrete cracking strength takes the vertical prestressing force, V_p, into account. Therefore, for the BT-56 girder, the vertical prestressing force, V_p had to be subtracted from $V_{cw\text{-}Exp}$ in order to obtain the concrete principal tension stress. The equation used to get the experimental concrete diagonal tensile stress for the BT-56 girder is given in Equation 6.9:

$$f''_{t-Exp} = \sqrt{\left(\frac{(V_{cw-\exp} - V_{p)}}{b_w d_p}\right)^2 + \left(\frac{f_{pc}}{2}\right)^2} - \frac{f_{pc}}{2} \tag{6.9}$$

Once the experimental diagonal tensile stress was determined, it was normalized so that it could be compared directly to the ACI Alternate value of 4. This was done using Equation 6.10:

$$\xi_t = \frac{f''_{t-Exp}}{\sqrt{f_c'}} \tag{6.10}$$

A normalized value, ξ_t, less than 4 was an indication that the ACI Alternate principal stress provided an unconservative prediction of the tensile stresses at which initial web shear cracking occurred. Table 6.2 gives the predicted concrete shear capacities for Tests E1, W1, and W2 using the code specified diagonal tension factor of 4. The normalized diagonal tension factors obtained from the experimental results are presented in section 6.4.7.2. ACI Alternate calculations are given in Appendix D.2.

Table 6.2 ACI Alternate method cracking shear predictions

Test	Cracking shear (kips)
Test E1	344
Test W1	344
Test W2	330

6.2.3 2004 AASHTO LRFD Shear Design Approach

The AASHTO LRFD (2004) shear design method was much different than the AASHTO Standard method. The LRFD capacities were calculated using the measured

properties of the BT-56 girder. The distance from the center of bearing for Tests E1, W1 and W2 was 46.89 inches as defined by the LRFD equation for d_v, displayed in Equation 6.11. Test W2 was analyzed at the defined critical section and at the center of the shear span, which was where the shear failure occurred. Shear capacities were not calculated along the shear span length due to the iterative nature of the code.

6.2.3.1 Concrete Shear Strength, V_c

The LRFD method for calculating concrete shear strength was complex and iterative. This method was mainly used for design, and when used for analysis, it became a doubly iterative process requiring spreadsheets and computer programs for efficiency. Calculations were made using both nominal and measured properties. The concrete shear contribution was not meant to predict the cracking shear strength of prestressed girders. The term, V_c, was derived based on the amount of shear force that could be carried across a cracked concrete section. Therefore, the concrete shear contribution was only intended to more accurately predict the ultimate shear capacity, V_n. However, in this research, comparisons were made between the experimental cracking shear strength and the LRFD concrete shear contribution, V_c to demonstrate that V_c did not accurately predict concrete cracking shears and to compare the data to previous research. The comparisons are presented later in this chapter.

The first step of the LRFD code was to calculate the effective shear depth, d_v, using equation 6.11:

$$d_v = \max\left(d_p - \frac{a}{2},\ 0.9d_e,\ 0.72h\right) \tag{6.11}$$

where:

a = Concrete rectangular stress block depth at ultimate capacity
d_e = Effective distance from the top fiber in compression to the centroid of tensile force at the section in question
d_p = Distance from the top fiber in compression to the centroid of prestressing steel at the maximum moment
h = Total height of composite section

For the calculations, a "c" value (depth from compression surface to neutral axis) was obtained from the experimental strain profiles. The "a" value was then calculated using $a = \beta_1 c$, where $\beta_1 = 0.65$ (based upon girder properties). In the LRFD Specifications, it was assumed that the prestressing strands were at their ultimate flexural capacity. It was seen from the experimental strain profiles that the strands were not near ultimate or yielding stresses. Therefore, no LRFD Specification equation was used to estimate the "c" value.

The average stress in the prestressing strands at ultimate, f_{ps}, was needed for the LRFD shear calculations. The ultimate stress in the strands, f_{ps} was derived from the total experimental strain profiles. The experimental stresses are presented in Section 6.3. The experimental strain profiles showed that the girder was not at ultimate flexural capacity, as assumed by the LRFD Specifications. Therefore, no LRFD Specifications equation was used to estimate f_{ps}.

Once the above values were obtained, it was necessary to determine the critical section for each test. To determine the critical section, Equation 6.12 was used.

$$\text{Critical Section} = C_s = d_v \tag{6.12}$$

Once the critical sections were defined, the LRFD equation for development length was used to determine if the critical section was within that length. Equation 6.13 gives the LRFD equation for development length.

$$l_d = \left(f_{ps} - \left(\frac{2}{3} \right) f_{pe} \right) d_b \tag{6.13}$$

where:

d_b = Diameter of prestressing strand
f_{pe} = Effective prestressing force after losses
f_{ps} = Force in prestressing strands at nominal ultimate moment

If the critical section was within the development length, the prestressing force at ultimate, $f_{ps,}$ was reduced. The reduced value, $f_{psred,}$ was determined assuming a linear relationship between the initial prestressing force, f_{se}, and the ultimate prestressing force, $f_{ps.}$ Equation 6.14 gives the method used to determine f_{psred}. The ratio of (f_{psred} / f_{ps}) was obtained and used as a reduction factor, $R_{d,}$ to obtain the effective area of prestressing. The prestressing steel located in the flexural region, A_{pse}, was specified by the LRFD shear equations and is discussed later in this section.

$$f_{psred} = f_{pe} + \left(\frac{f_{ps} - f_{pe}}{l_d - l_t} \right) \left(C_s + b_e - l_t \right)$$

Once f_{psred} was determined, the reduction ratio, R_d was taken as (6.14)

$$R_d = \left(\frac{f_{psred}}{f_{ps}} \right)$$

where:

b_e = Distance from the center of bearing to the end of the girder
l_t = Measured girder transfer length

In all three tests, b_e was the distance from the center of bearing to the end of the girder. For Tests E1 and W1, b_e was 9 in.; for Test W2, the reduction equation was not needed because the critical section was not within the development length.

The LRFD Specifications utilized the modified compression field theory, which required a compression strut angle, θ to be used to calculate the ultimate shear capacity of a section. In this research, the values of θ were obtained in two different ways. The values of θ were first calculated and interpolated using the LRFD Specifications. Secondly, the compression angles were physically measured during testing and confirmed by strain rosettes. Both values and resulting shear capacities are presented in Table 6.3.

An ultimate shear was required to start the iterations for the LRFD Specifications. For normal bridge design, the ultimate shear loads were known before construction. However, for this research, the ultimate shear loads were unknown and had to be assumed.

The assumed ultimate live load shear was added to the dead load shear and was used to obtain the ultimate shear force, V_u. The concrete shear stress was then calculated using LRFD equation 5.8.2.9-1 shown as Equation 6.15. Because the ultimate shear value was assumed, it had to equal the ultimate calculated shear force, V_n at the end of all iterations.

$$v = \frac{V_u - \phi V_p}{\phi b_v d_v} \tag{6.15}$$

The resistance factor for shear given in the LRFD code, ϕ, was taken as 1 for both the nominal and measured calculations for consistency. The value, b_v, was taken as the web width of the BT-56 girder.

To obtain θ and the ultimate shear capacity, the LRFD Specifications required the calculation and interpolation of the tensile strain and shear stress in the section of interest. The strain in the tensile reinforcement on the flexural tension side of the specimen, ε_x, was calculated using LRFD equation 5.8.3.4.2-1, given as Equation 6.16.

$$\varepsilon_x = \frac{\frac{M_u}{d_v} + 0.5N_u + 0.5(V_u - V_p)\cot\theta - A_{pse}f_{po}}{2(E_s A_s + E_p A_{pse})} \tag{6.16}$$

Since there was no non-prestressed reinforcement or axial load in the test girder, Equation 6.16 simplified to Equation 6.17. The reduction term R_d was inserted to account for the critical section being within the development length.

$$\varepsilon_x = \frac{\frac{M_u}{d_v} + 0.5(V_u - V_p)\cot\theta - R_d A_{pse}f_{po}}{2(E_p R_d A_{pse})} \tag{6.17}$$

The value f_{po} was defined by the LRFD code as $0.7*f_{pu}$ and was taken as such. The area of prestressing steel on the flexural tension side of the girder, A_{pse}, was defined as the

area of prestressing steel below the mid-height of the girder. If the strain in the flexural tension side of the member was negative, LRFD Specifications required a different strain calculation given as Equation 6.18.

$$\varepsilon_{x\,adj} = \frac{\frac{M_u}{d_v} + 0.5(V_u - V_p)\cot\theta - R_d A_{pse} f_{po}}{2(E_c A_c + E_p R_d A_{pse})} \tag{6.18}$$

The value A_c was the area of concrete on the flexural tension side of the girder and E_c was the nominal and measured modulus of elasticity.

Using the values of υ/f_c' and ε_x, θ and β values were linearly interpolated from LRFD figure 5.8.3.2-1. The first iterative step was to properly guess a value of θ that matched the value interpolated from the LRFD figure. When the physically measured angles were used, the θ value was set and not interpolated. Once the value of θ was determined, a value of β was linearly interpolated from the same figure. The β value was used to determine the concrete shear contribution, V_c. The equation used to calculate V_c was obtained from LRFD equation 5.8.3.3-3 and is shown as Equation 6.19.

$$V_c = 0.0316\beta\sqrt{f_c'}\,b_v d_v \tag{6.19}$$

where:

β = Interpolated value from LRFD figure 5.8.3.2-1
b_v = Web width
f_c' = Nominal and measured concrete strengths, ksi

6.2.3.2 Transverse Steel Shear Strength, V_s

The strength of the shear reinforcing steel was calculated with LRFD equation C5.8.3.3-1 and is shown as Equation 6.20:

$$V_s = \frac{A_v f_y d_v \cot\theta}{s} \tag{6.20}$$

where:

A_v = Area of shear reinforcement within a distance s
f_y = Specified yield strength of prestressing tendons (69 ksi)
s = Spacing of shear reinforcement in the direction parallel to longitudinal reinforcment

The abbreviated version of the equation was used because the stirrups were placed vertically. The spacing, as previously mentioned, changed for each shear test.

6.2.3.3 Nominal Shear Strength, V_n

The nominal shear strength of the girder was then calculated by combining LRFD equations 5.8.3.3-1 and 5.8.3.3-2 to one equation as Equation 6.21.

$$V_n = V_c + V_s + V_p \le 0.25 f_c' b_v d_v + V_p \tag{6.21}$$

The second term of Equation 6.23 was the LRFD maximum allowable shear capacity of a section. This limit was neglected when the girder pick-up loops were considered.

Because the LRFD method was used for analysis, and the initial loads were not known, iterations were performed until the initial assumed shear, V_u, matched the total

shear capacity, V_n. This method was suggested by Kulicki et al. (1997) in the reader comments to Shahawy and Batchelor (1996). When both the compression strut angle and ultimate shear values were matched, the iterative process was stopped and the shear value was considered correct.

Table 6.3 provides LRFD Specification predictions for cracking and ultimate shear strengths. All calculations were performed at the code defined critical section unless otherwise noted. Measured LRFD properties and calculations are given in Appendix D.3. The measured crack angle w was determined from physical measurements and strain rosettes, as discussed in Section 6.4.4.

Table 6.3 AASHTO LRFD (2004) shear capacity predictions

Test		Concrete Shear Contribution, V_c (kips)	Ultimate shear, V_n (kips)		θ (degrees)	β
E1†	LRFD Angles	89	696		28.5	2.517
	Measured Angles	93	612*	902†	31.5	2.811
W1†	LRFD Angles	91	601		24.75	2.688
	Measured	96.5	565*	866†	26.2	2.94
W2	LRFD Angles	141	425		19.85	3.9
	Measured Angles	150	373*	369‡	23.4	4.516

* Values calculated neglecting the pick-up strands

† Values calculated with the pick-up strands

‡ Values calculated at center of shear span

† Section did not fail or reach ultimate strength

6.2.4 Variable Angle Truss Model

The variable angle truss model (VATM) was the final method used to analyze the shear capacities for each test. It was used to determine the ultimate shear capacity of each test only. It was also used to approximate forces in the bottom strands near the girder ends. This helped approximate the bond stress that occurred in each tested section. None of the shear tests in this research experienced strand slip. This indicated that the bond stresses were below the maximum allowable bond stresses at all times.

The VATM assumed that the girder experienced shear and flexure failure simultaneously. It also neglected the self weight of the girder and considered only the concrete strength to transfer the stirrup forces. The stirrups resisted the entire shear force and were assumed to be at yield stress. The method was similar to the strut and tie models suggested by ACI 318-02. The model was addressed in *Prestressed Concrete Structures*, by Michael P. Collins and Denis Mitchell (1991).

6.2.4.1 Shear Force

In this model, a single shear force was determined, and the value was used to determine the compressive stress in the concrete strut and how many stirrups were required to hold the total load. The ultimate shear capacity (V_{ult}) was calculated based on Figure 6.2 and Equation 6.22.

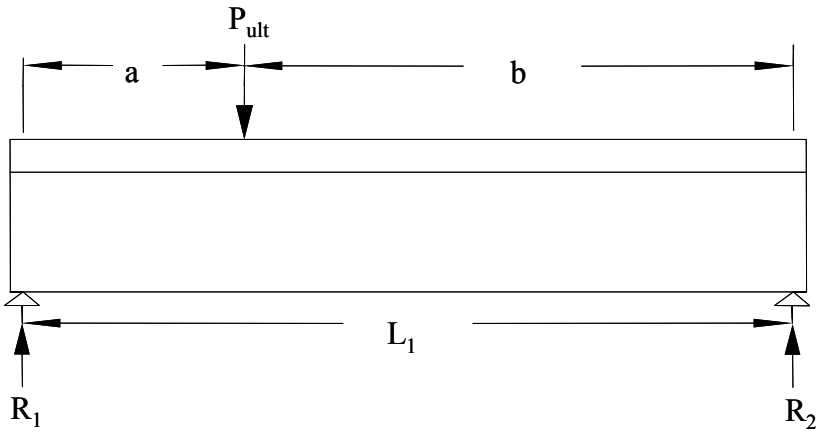

Figure 6.2 Diagram for calculation of V_{ult}

$$V_{ult} = R_1 = R_{1-dead} + P_{ult}\frac{b}{L_1} \tag{6.22}$$

6.2.4.2 Stirrup Force

The force in each shear stirrup, $F_{stirrup}$, was calculated using equation 6.23.

$$F_{stirrup} = A_v f_y \tag{6.23}$$

To obtain the predicted shear capacity from the VATM method, it was necessary to use maximum and minimum specified angles to determine how many stirrups would be used to contribute to the shear capacity of the girder. The maximum recommended angle was 70° and the minimum acceptable angle was 25°. Figures 6.3, 6.4, and 6.5 were used to determine how many stirrups would be crossed for the ultimate capacity of each test. It was determined that Tests E1, W1, and W2 would have 13, 5, and 4 stirrups contribute to the shear capacities of the sections. The amount of compression in each strut was then calculated to determine if the allowable stress in the struts was exceeded.

The allowable forces in the struts are discussed later in this section. Many of the compression struts were carried by the girder pick-up loops in Tests E1 and W1. After shear capacities were determined without the loops, the capacities were then estimated including the added shear capacity given by the pick-up loops. The predicted VATM shear capacities are shown in Table 4 and were based on the number of stirrups that the compression field crossed.

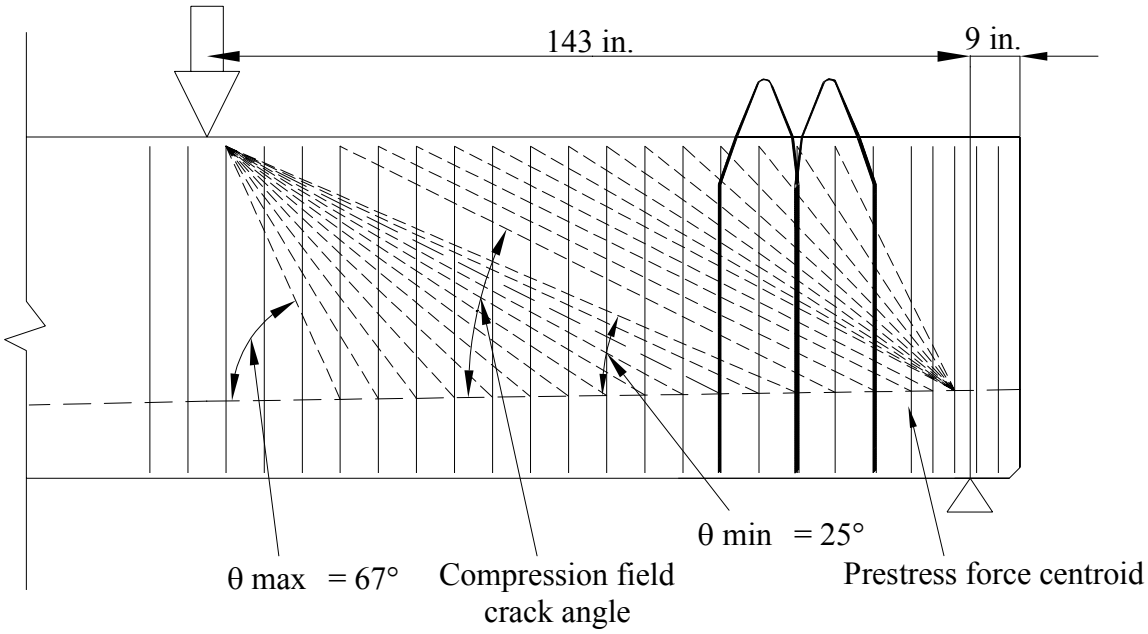

Figure 6.3 Test E1 Variable Angle Truss Model

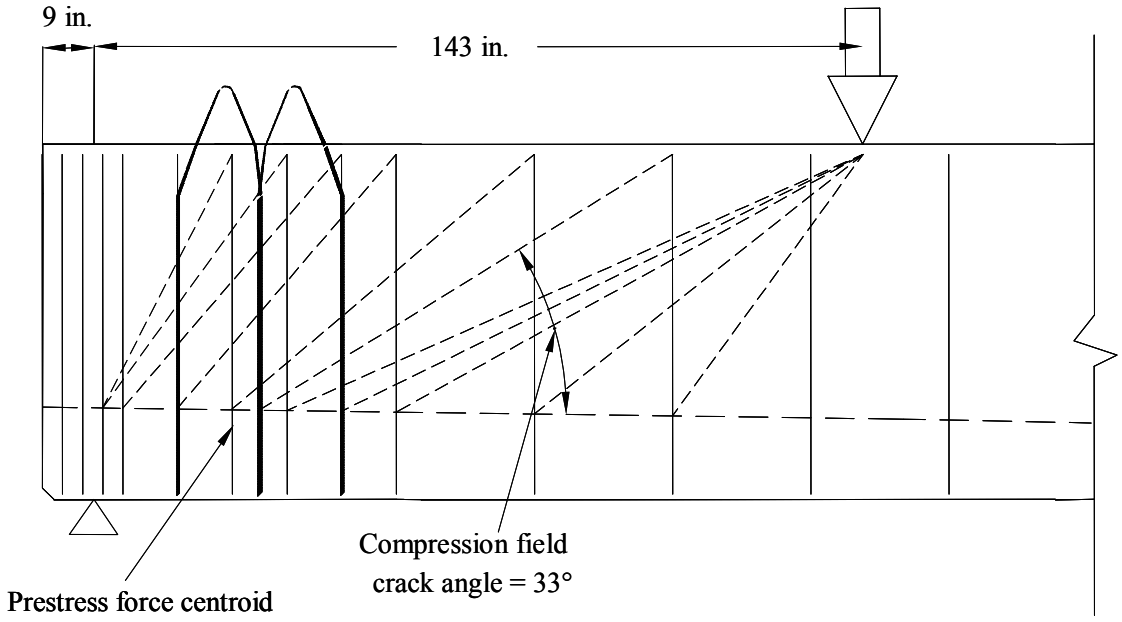

Figure 6.4 Test W1 Variable Angle Truss Model

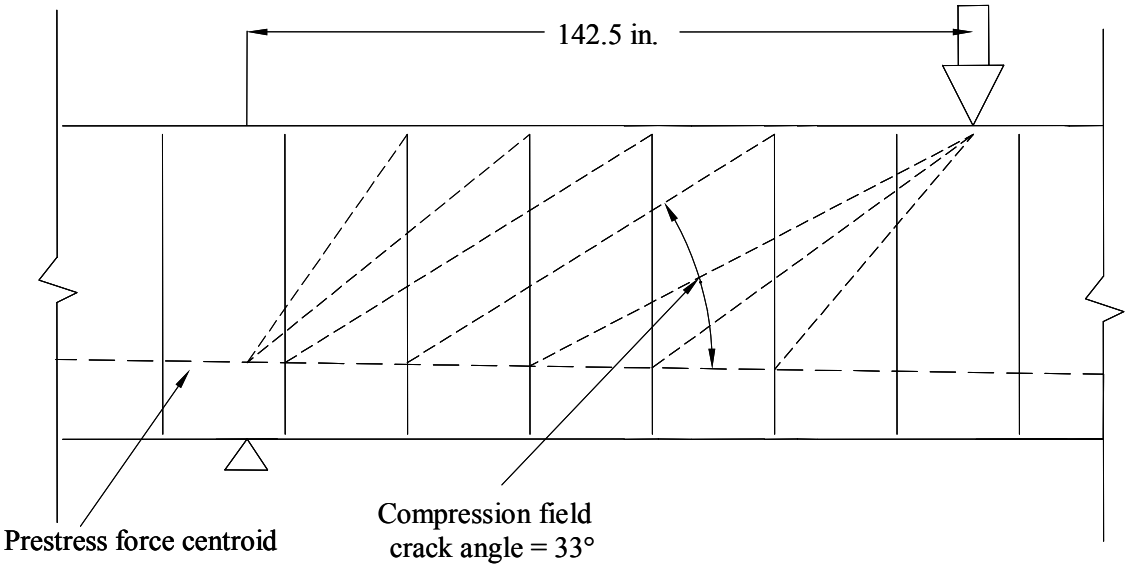

Figure 6.5 Test W2 Variable Angle Truss Model

Table 6.4 VATM shear capacity predictions

Test	Stirrups crossed	Ultimate Shear Capacity, Vn (kips)	Maximum Shear, Vu (kips)
E1	13	593	653
		*832	
W1	5	254	569
		*577	
W2	4	169	580

* Values were calculated using pick-up loops

6.2.4.3 Stirrups Required to Carry V_{ult}

After determining the ultimate predicted capacities of the three tests, it was necessary to determine how many stirrups it would take to carry the ultimate load. The number of stirrups required, $\#_{stirrups}$, to carry V_{ult} was calculated with Equation 6.24:

$$\#_{stirrups} = \frac{V_{ult}}{F_{stirrup}} \tag{6.24}$$

The number of stirrups calculated determined the number of compression struts required to transfer the loads to the stirrups. In addition, the number of stirrups required determined the angle of the compression field. There was a minimum angle of 25° specified by this method. Therefore, it was possible to have an insufficient amount of stirrups to carry the applied load. For all three tests, the minimum compression strut angle limited the number of stirrups available to carry load. When the pick-up loops

were used to add extra capacity, Test E1 showed that it had the required capacity. Due to large stirrup spacings, tests W1 and W2 did not have the required capacity to carry the applied shear force.

6.2.4.4 Internal Moment Arm

The internal moment arm, jd, was calculated using Equation 6.25.

$$jd = d_p - \frac{a}{2} \tag{6.25}$$

Because of the draped strands, jd varied throughout the shear spans of each test. However, for all calculations, jd was taken as the distance directly under the point load at the maximum moment. This allowed the compression struts to cross the largest number of stirrups possible. The value of "a" was determined by using strain compatibility at the point of maximum moment.

6.2.4.5 Compression Field Crack Angle

The compression field crack angles for each test are labeled in Figures 6.3, 6.4, and 6.5. The angles were determined based on a "carryover strut". A carryover strut was defined as a strut that neither began at the loading point nor ended at the support. It was used to determine the compression field crack angle, how many stirrups were crossed for ultimate capacity, and for concrete stress checks that are discussed in the next section.

6.2.4.6 Stress in Compression Strut

The stress compression check that was most commonly used with the VATM considered the entire compression field that fanned from the point load as one strut, and stresses were calculated accordingly. This calculation is shown in Equation 6.26.

$$f_{strut} = \frac{V_{ult}}{jd\cos(\theta)b_w\sin(\theta)} \leq 0.85\beta_1 f_c' \tag{6.26}$$

The denominator of this equation calculated the angular surface area of the compressive strut. The value β_1 was 0.6 based on the use of HPC without adequate confinement to resist splitting forces. The compressive stress in the concrete strut stayed lower than the maximum allowable stress in all three tests, even when the capacity of the pick-up strands was included.

6.2.4.7 Forces in Strands at Point of Loading

Since the VATM assumed the girder to be at flexural and shear failure simultaneously, the strands were predicted to be near failure. Therefore, the value, f_{ps} was assumed to be 268.5 ksi for all three tests. The top strands were considered to be at effective prestressing forces, with an f_{se} of 168 ksi. To obtain the total initial strain force at the maximum moment, Equation 6.27 was used.

$$\text{Strand force} = F_s = (f_{ps}A_{psb} + f_{se}A_{pst}) \tag{6.27}$$

The values A_{psb} and A_{pst} represent the area of prestressing steel on the flexural tension side and the area of prestressing steel in the top flange.

6.2.4.8 Strand Force Reduction

At each intersection of the strand force centroid with a stirrup, some of the strand force was reduced and carried by truss action through the concrete to the support. Equation 6.28 gave a proper estimate for strand reduction taking into account the angle of each strut and the force in each stirrup.

$$F_r = \frac{x}{jd} F_{stirrup} \tag{6.28}$$

The value x indicated the distance the stirrup was from the point of loading. As the distance increased, the amount of reduction in the strands decreased. Figures 6.6, 6.7, and 6.8 provide the plots of strand force reduction from the point of loading to the support with the pickup straps included.

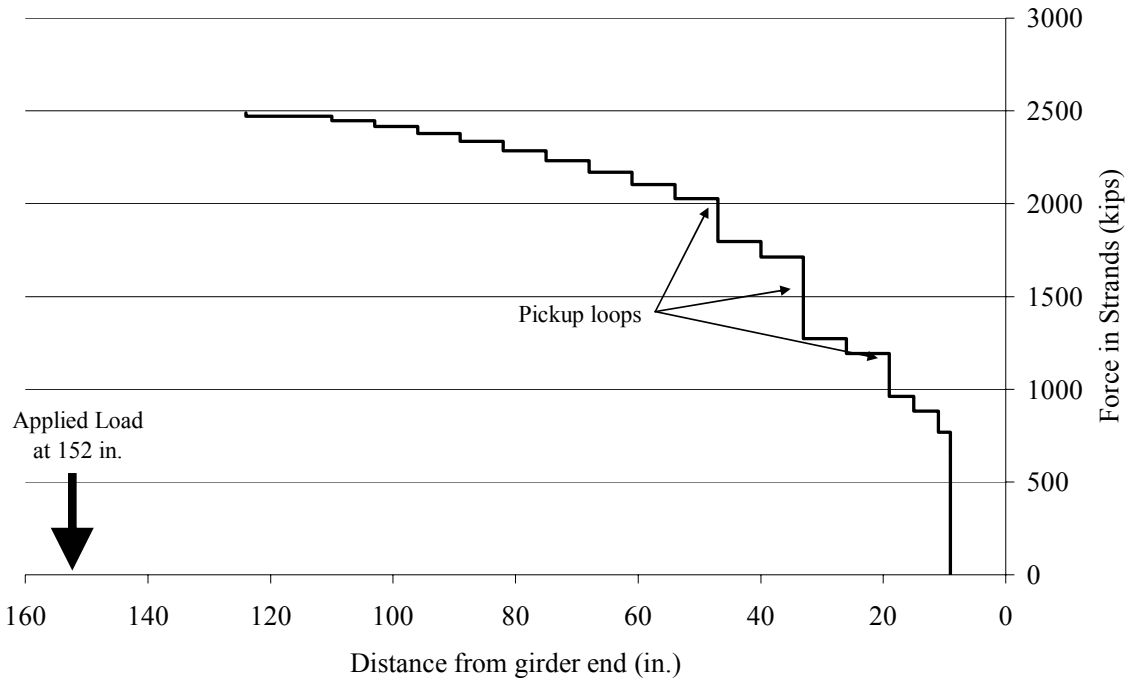

Figure 6.6 VATM strand force reduction plot for Test E1

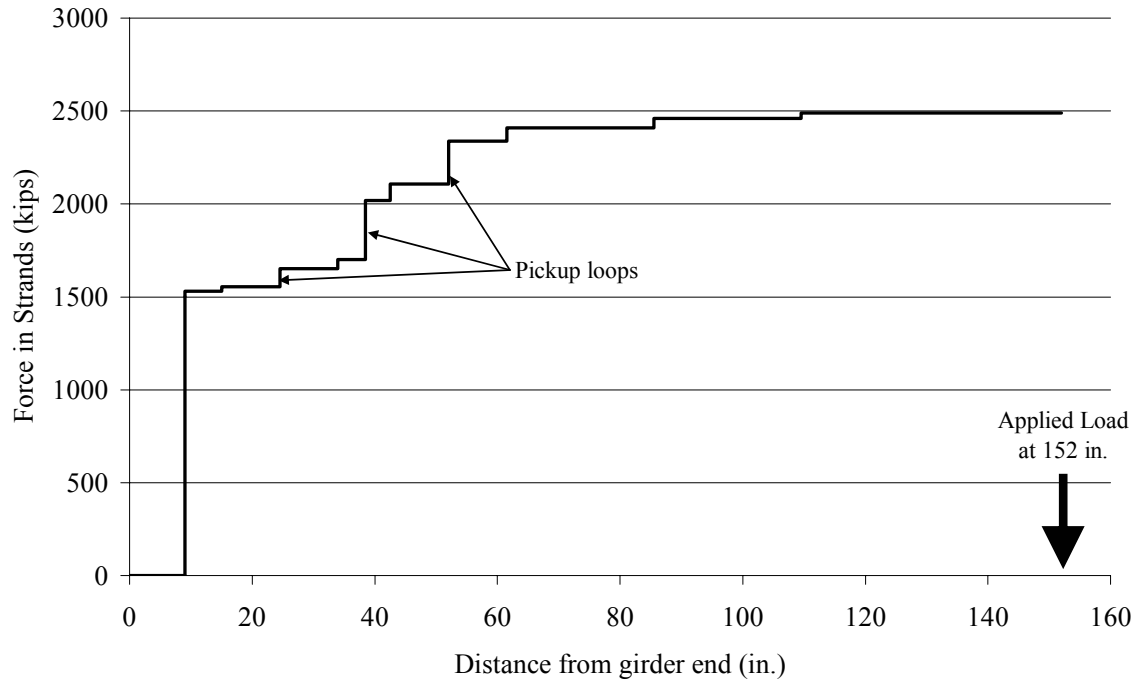

Figure 6.7 VATM strand force reduction plot for Test W1

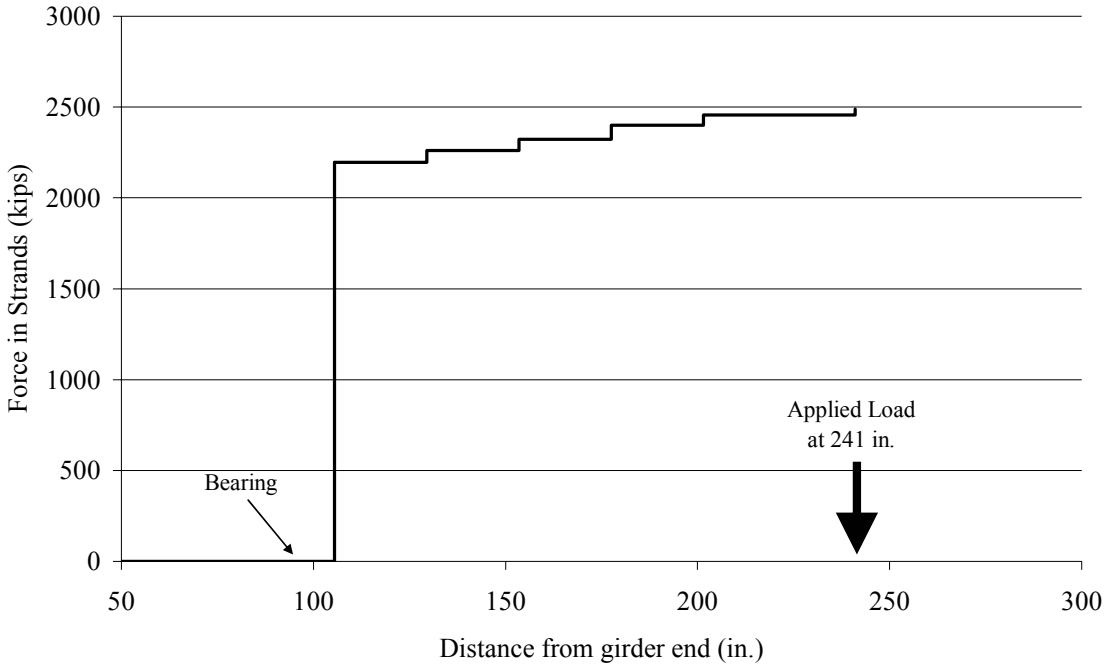

Figure 6.8 VATM strand force reduction plot for Test W2

6.2.4.9 Strand Bond Stress

The strand bond stress was calculated based on the force remaining in the strand, F_{strand}, the length of embedment at the point, l_e, and the nominal circumference, πd_b, of the strand using Equation 6.29, which was suggested by Logan (1997).

$$f_{bond} = \frac{F_{strand}}{\frac{4}{3} l_e \pi d_b} \tag{6.29}$$

Bond stress plots from the point load to the support are given for Tests E1 and W1 in Figures 6.9 and 6.10. Bond stresses were not calculated for Test W2 because the test

was not performed near the end of the girder. The bond stresses due to loading were compared with the calculated bond stresses over the transfer length due to the effective prestressing. Finally, the straight dotted line on each plot shows the experimental maximum bond stresses obtained from the Mustafa direct pull-out tests. Details of those tests are provided in Chapter 4. Test E1 showed that the bond stresses did not exceed the maximum allowable stress, even at its ultimate flexural capacity, which indicated a prediction of no strand slip. Test W1 indicated that strand slipping and bond failure was possible if the girder approached its ultimate flexural capacity. However, from test results, which are discussed in the next section, it was seen that none of the three tests were near ultimate flexural capacity.

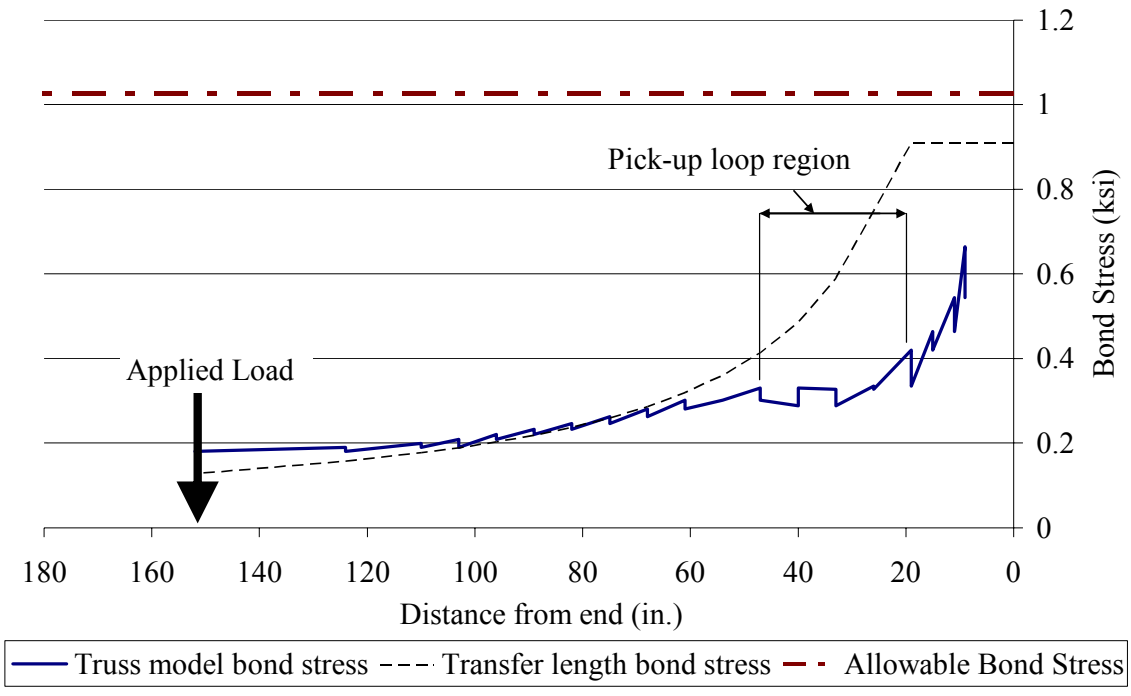

Figure 6.9 Bond stress plot for Test E1

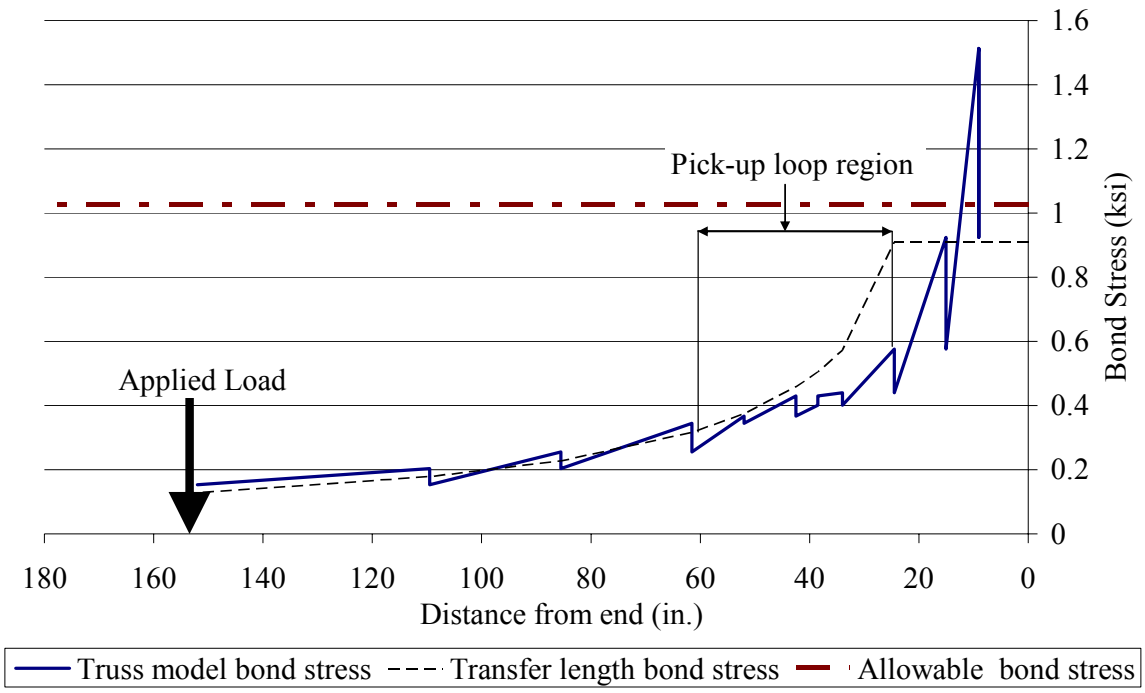

Figure 6.10 Bond stress plot for Test W1

6.3 Experimental Shear Results

This section provides results from the three shear tests performed on the BT-56 girder. The shear test set-up for all testing is provided in Chapter 5. This section discusses experimental prestress losses and how they were determined for the three shear tests. It also details girder deflection, cracking, stirrup strains, rosette strains, principal tension angles, strand slip, flexural strain profiles, and partial development length results for each of the three shear tests.

6.3.1 Prestress Losses

In order to properly calculate properties and shear capacities of the BT-56 girder at different locations, the initial stresses in the girder were needed. These initial stresses were obtained from Vibrating Wire Strain Gages (VWSGs) that were located at the quarterspan and midspan of the girder. Details of the placement and installation of the gages are presented in Chapter 3. The VWSGs were zeroed directly before girder cutdown so that all strains in the concrete would be seen. They were corrected for temperature variations to obtain the load related strain. The final strain profile from the VWSGs was taken before the initial flexure test performed by Canfield and Kahn (2005). The strain profiles obtained from the quarterspan of the BT-56 girder are given in Figure 6.11. Profiles are given at cutdown, after deck placement, and immediately before the flexure test. Tests E1, W1, and W2 were performed 66, 82, and 113 days after the last strain profile was taken.

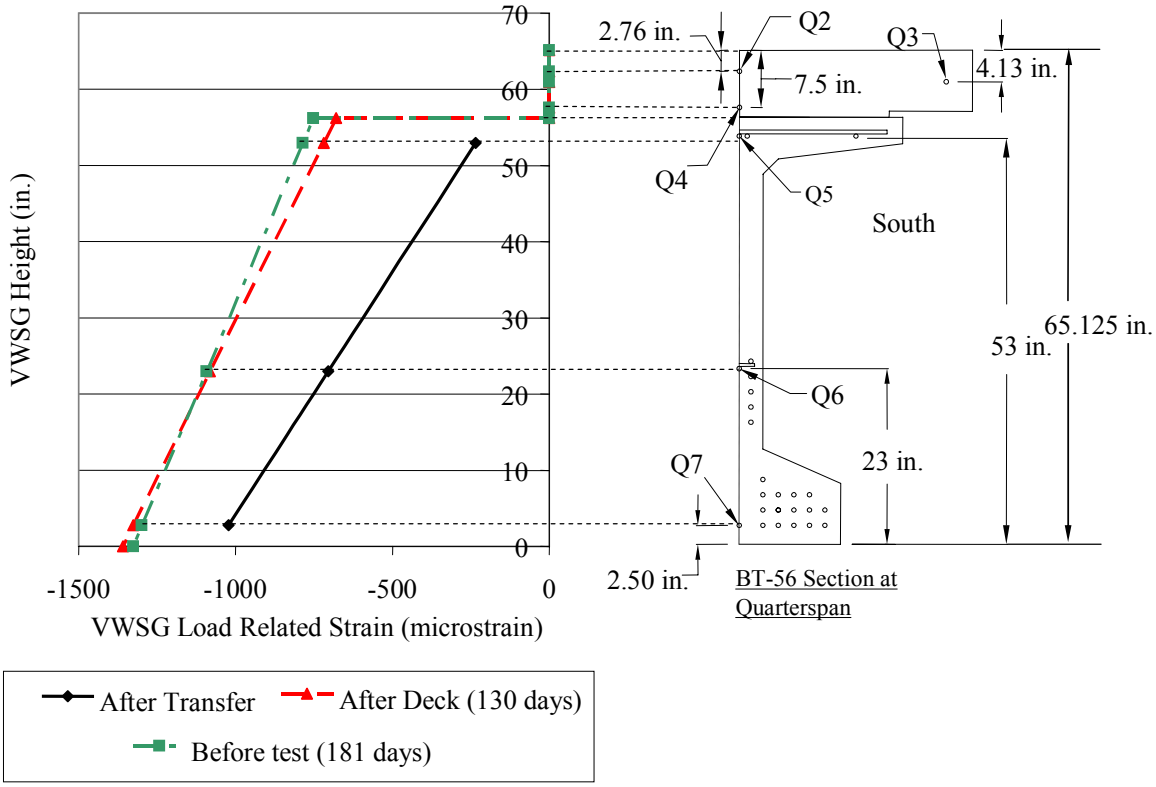

Figure 6.11 Initial concrete strain profile at quarterspan

An average effective prestressing stress, f_{pe}, was obtained using the 181 day strain profile shown in Figure 6.11. From the strain profile, it could be seen that the concrete had compressive strains due to creep, shrinkage, and prestressing. The strain was determined at the centroid of the prestressing force, which was 14 in. from the bottom of the girder. After the strain was linearly determined at 14 in., a stress in the strand was calculated based on the modulus of elasticity of the prestressing strands. After stresses due to the dead load moment at the quarter point were accounted for, the remaining stress was considered to be the measured prestress loss in the BT-56 girder. It was known that the initial jacking stress used at Standard Concrete Products (SCP) was 206 ksi. The initial effective prestressing, f_{pe}, was obtained by subtracting the VWSG stress from the initial jacking stress. This calculation is shown in Equation 6.30.

$$f_{pe} = f_{pi} - \varepsilon_c E_{ps} \tag{6.30}$$

The term f_{pi} was the jacking stress obtained during construction, ε_c was the strain in the concrete found from the VWSG and located at the center of force (14 in.) after dead load moment stresses were taken into account, and E_{ps} was the measured modulus of elasticity of the prestressing strands. The prestress losses were determined to be 38 ksi for the BT-56 girder. Therefore, the BT-56 girder had an experimental effective prestressing force of 168 ksi, and it was used for calculations in all three shear tests. Comparisons of the measured prestress losses to the calculated losses obtained from the AASHTO Standard Specifications (2002) are presented by Canfield and Kahn (2005). Calculated and experimental initial and loading strain profiles are given for each test later in this section.

6.3.2 Results for Test E1

Test E1 was the first shear test performed on the BT-56 girder, and is shown in Figure 5.7. It was performed on November 22nd, 2004 on the eastern end of the girder, where the stirrup spacing was 7 in. The section was loaded up to 695 kips (shear force of 653 kips) and then stopped because the capacity of the load cell was reached. At a load of 675 kips (V_{exp} = 635 kips), large shear flexure cracks were noticed near the midspan of the girder. Because of the large cracks near midspan, it was difficult to say if the beam would have failed near midspan with a stirrup spacing of 24 in. or if it would have failed within the shear span, where stirrup spacing was 7 in.

6.3.2.1 Deflection

The deflection of Test E1 was obtained directly under the point load throughout the loading process. The ultimate deflection seen during this test was 2.5 inches at 695 kips and the predicted ultimate deflection was 2.84 in. The deflection curve changed slope at approximately 400 kips, which indicated that the shear cracks became wide enough for a reduction in stiffness. Figure 6.12 shows the load deflection plot for Test E1.

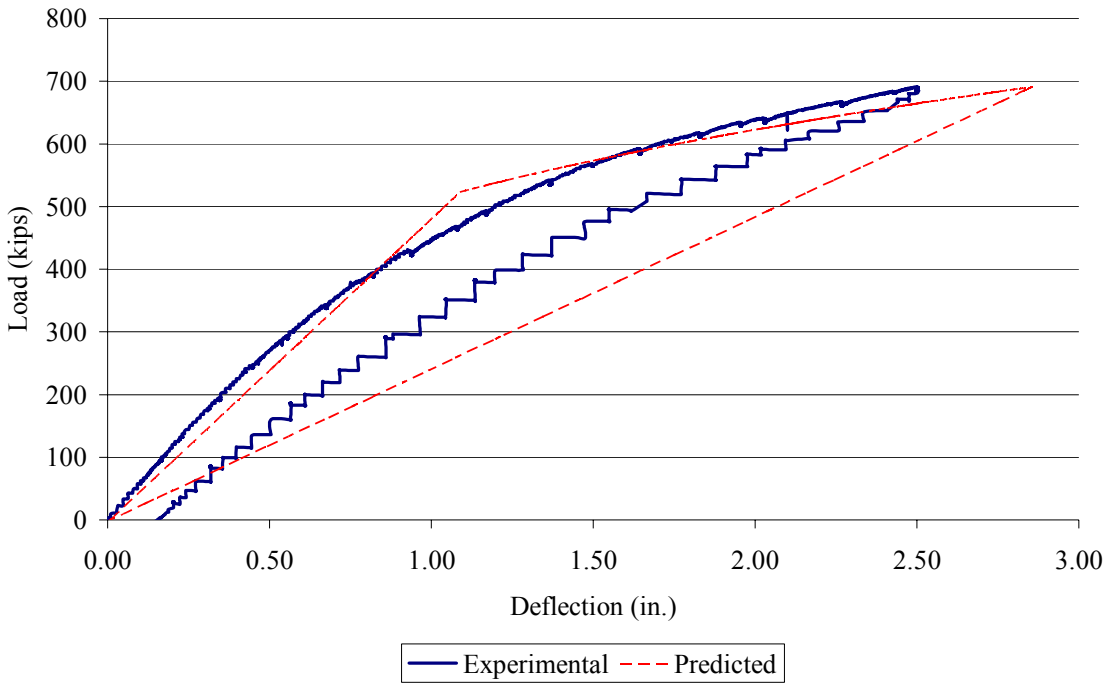

Figure 6.12 Load deflection plot for Test E1

The predicted load deflection curve was calculated in two sections. The first section was calculated assuming an un-cracked elastic section, and it accounted for the shear deformations using virtual work. Equation 6.31 shows the method used.

$$\Delta_t = \frac{Pa_s{}^2 b^2}{3E_c I_c l} + \int_0^{143} K\left(\frac{v_1 V_1}{GA}\right)dx + \int_0^{909} K\left(\frac{v_2 V_2}{GA}\right)dx \qquad (6.31)$$

where:

A = Area of the web
a_s = Shear span
b = Length minus the shear span
E_c = Modulus of elasticity of the concrete
G = Shear modulus of elasticity, $G = \frac{E_c}{2(1+\nu)}$
I_c = Composite section moment of inertia
K = 1 for wide-flange and I-beams
l = span length, bearing to bearing
ν = Poisson's ratio, 0.187
v_1 = Internal virtual shear in the member, expressed as a function of x and caused by the external virtual load integrated from the eastern support to the point load
V_1 = Internal shear in the member, expressed as a function of x and caused by the real loads integrated from the eastern support to the point load
v_2 = Internal virtual shear in the member, expressed as a function of x and caused by the external virtual load unit integrated from the western support to the point load
V_2 = Internal shear in the member, expressed as a function of x and caused by the real loads integrated from the western support to the point load

The first part of the equation was the standard flexural deflection calculation for an elastic structural shape and was obtained from the *Manual of Steel Construction*, LRFD 3rd edition. The second and third terms used virtual work to determine the shear deformations that occurred in the BT-56 girder according to R.C. Hibbeler's *Structural Analysis* book.

The second part of the curve was calculated assuming an effective moment of inertia, I_e based on a cracked concrete section. The effective moment of inertia was determined using Edward G. Nawy's *Prestressed Concrete* book. Equation 6.32 shows the equation used to determine the effective moment of inertia.

$$I_e = I_{cr} + \left(\frac{M_{cr}}{M_a}\right)^3 \left(I_c - I_{cr}\right) \leq I_c \tag{6.32}$$

where:

I_{cr} = Cracked moment of inertia = $n_p A_{ps} d_p{}^2 \left(1 - 1.6\sqrt{n_p \rho_p}\right)$

A_{ps} = Total area of prestressing strands
d_p = Depth from extreme compression fiber to centroid of prestressing steel
I_e = Effective moment of inertia
M_{cr} = Live load moment causing flexural cracking
M_a = Actual applied live load moment

$$n_p = \frac{E_{ps}}{E_c}$$

$$\rho_p = \frac{A_{ps}}{b_w d_p}$$

The effective moment of inertia was applied once the live load moment, M_a, exceeded the calculated live load cracking moment, M_{cr}. As the live load moment, M_a increased, the effective moment of inertia, I_e, decreased.

6.3.2.2 Cracking

Before testing of the eastern end of the BT-56 girder, there were no cracks present within the shear span. The section was loaded in 100 kip increments until initial shear

cracking occurred. As previously mentioned, the first cracks appeared at a point load of 342 kips. The cracks appeared near the shear span center at the top of the web, extending down at an angle of 23° as seen in Figure 6.13. A majority of the cracks examined in this test were located at the center of the shear span, and not at the critical sections defined by the AASHTO Standard (2002) and AASHTO LRFD (2004) codes. The centroid of the composite section was approximately at the level of the top, horizontal LVDT in Figure 6.14.

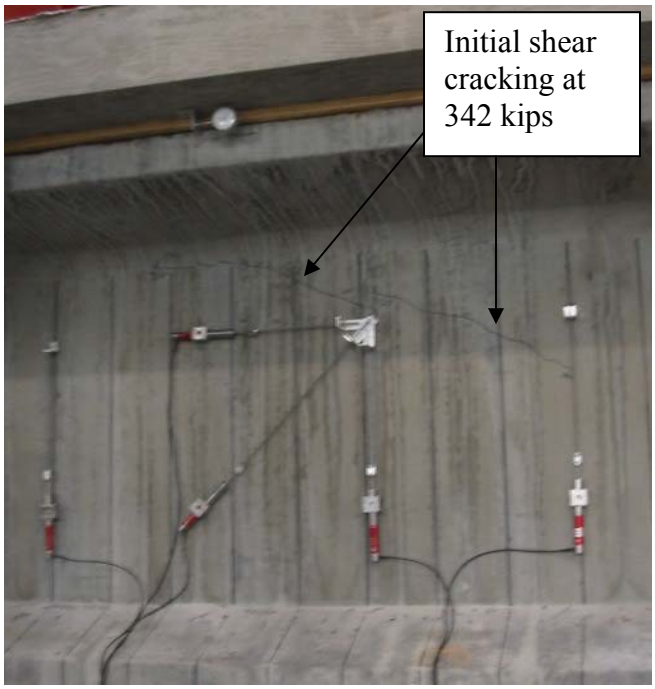

Figure 6.13 Initial shear cracks of Test E1

The widths of the cracks were measured with crack comparators at various loadings in order to physically estimate the strain in the stirrups. At 433 kips, crack widths were 0.005 in. and at angles of 26° to 31°. Web-shear cracks appeared at loads up to 600 kips before any flexure-shear or flexure cracks occurred. The cracks extended

outward in both directions from the shear span center as the load was increased. After 600 kips, flexural cracks began to appear under the point load and flexural shear cracking began to appear along the beam on the midspan side of the point load. Web-shear cracks at 600 kips were observed as large as 0.016 in. The spacing between the cracks was about 4 in. At loads approaching 695 kips (shear force = 653 kips), large shear flexure cracks were seen near the midspan of the girder. The cracks at midspan were near 0.04 in. and the cracks in the shear span were as large as 0.02 in. The large crack widths indicated that most stirrups in the shear span had yielded and that the girder should have been approaching failure at both midspan and within the shear span. It was suspected that the pick-up loops within the shear span were significantly contributing to the strength of the section. Figures 6.14 and 6.15 show Test E1 cracking patterns at 550 and 700 kips, where the test was stopped.

The pick-up loops were seen to have an effect on the shear capacity of the tested section. The web shear cracks extending from the center of the shear span were large and became smaller as they approached and crossed the pick-up loop region. From Figure 6.15, it can be seen that there were also fewer cracks across the pick-up loop region than there were at the center of the shear span.

Figure 6.14 Shear cracking at a shear force of 527 kips (550 kip load) through the shear center for Test E1

Figure 6.15 Final shear cracking at a shear force of 653 kips (695 kip load) for Test E1

6.3.2.3 Stirrup Strains

Vertical LVDTs were placed at stirrup locations so that stirrup strains could be estimated. The placement and gage lengths of the LVDTs are listed in Chapter 5. The strains in the stirrups represent the change in strain resulting from externally applied load and do not account for the small strains due to dead load and temperature variation. Figures 6.16 and 6.17 provide the stirrup strains and stresses for Test E1. A diagram of where the stirrups were located is provided in Figure 6.17.

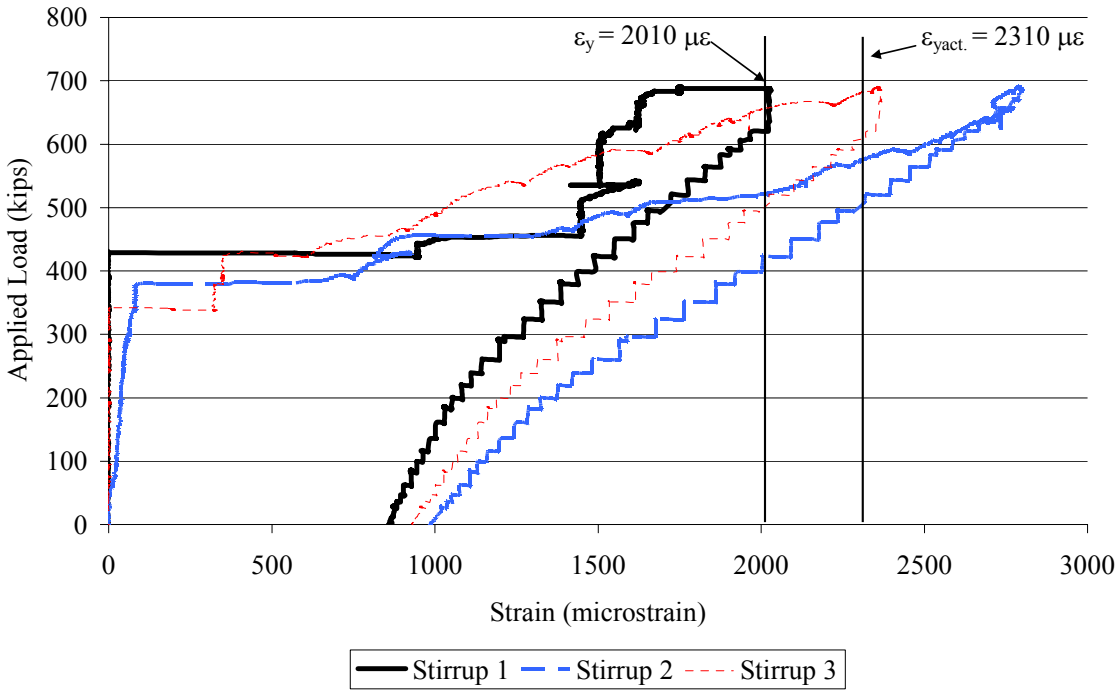

Figure 6.16 Strain in stirrups for Test E1

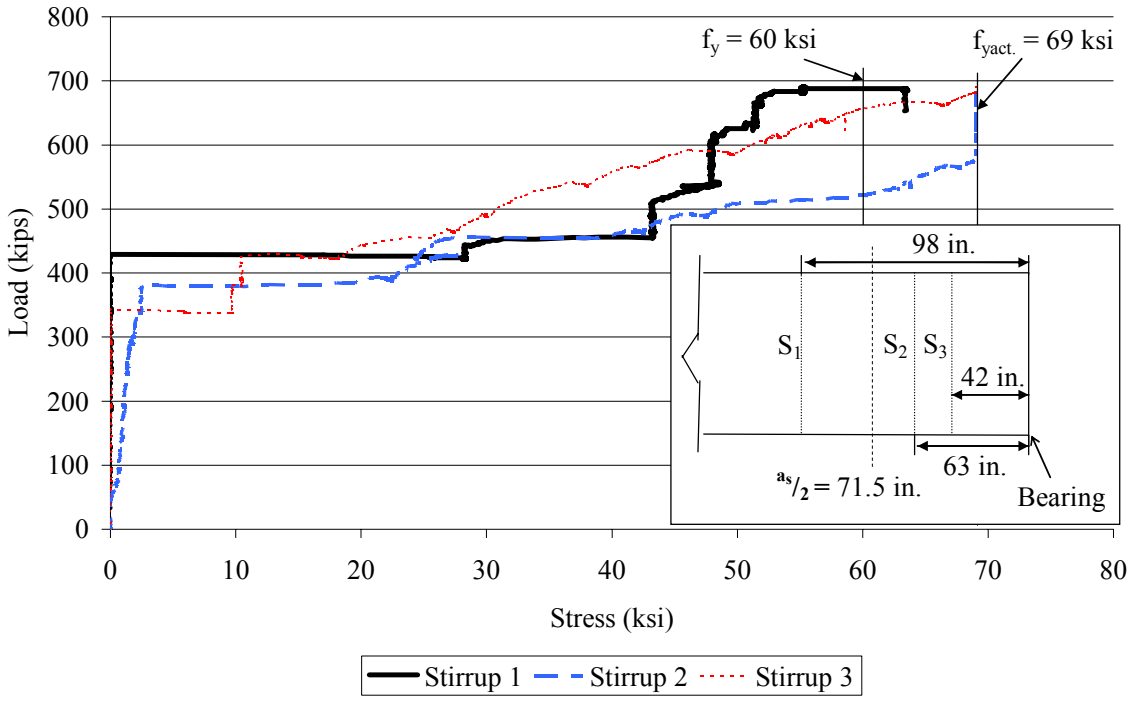

Figure 6.17 Stress in stirrups for Test E1

All stirrups obtained initial strains at different loading values. This was expected because the stirrup strains were not significant until cracks crossed through the gage lengths of the LVDTs. Figure 6.13 shows that the initial cracks were above the LVDTs for stirrups 1 and 2, but crossed through the stirrup 3 LVDT. This caused stirrup 3 to experience cracking strain at the earliest point load of 342 kips. Cracks extended through stirrups 1 and 2 at 390 and 420 kips, respectively. As the load increased, the strain in stirrup 1 reached a plateau because all cracking began extending from the shear span center to the bearing. Stirrup 1 obtained a maximum loading strain of 2,020 microstrain. The strain in stirrups 2 and 3 continually increased as the load increased. The maximum strains for stirrups 2 and 3 were 2,800 and 2,360 microstrain. It was observed that the stirrup with the most strain was the one closest to the center of the shear span; not the one closest to the critical section. The yield stress in the stirrups was limited to the

maximum yield stress measured during reinforcement testing (f_{yact} = 69 ksi). The specific yield strains and stresses are provided in Chapter 4.

6.3.2.4 Concrete Rosette Strains and Principal Angles

The concrete strain rosette for Test E1 was located at the center of the shear span. Details on the installation and placement of the strain rosette are located in Chapter 5. The rosette consisted of three arms which measured strains at 0°, 45°, and 90° to the horizontal. It was used to determine the principal tensile and compressive strains within the web of the girder. The strains were determined using a derived equation based on Mohr's circle from Richard G. Budynas's *Advanced Strength and Applied Analysis* given as Equation 6.33.

$$\varepsilon_{p1,}\varepsilon_{p2} = \frac{\varepsilon_A + \varepsilon_C}{2} \pm \frac{1}{2}\sqrt{(\varepsilon_A - \varepsilon_C)^2 + (2\varepsilon_B - \varepsilon_A - \varepsilon_C)^2} \qquad (6.33)$$

Where,

ε_A = Horizontal Strain
ε_B = Strain at 45°
ε_C = Vertical Strain
ε_{p1} = Principal tensile strain
ε_{p2} = Principal compressive strain

Figure 6.18 shows the experimental principal tensile and compressive strains for Test E1. The strains were plotted against applied shear.

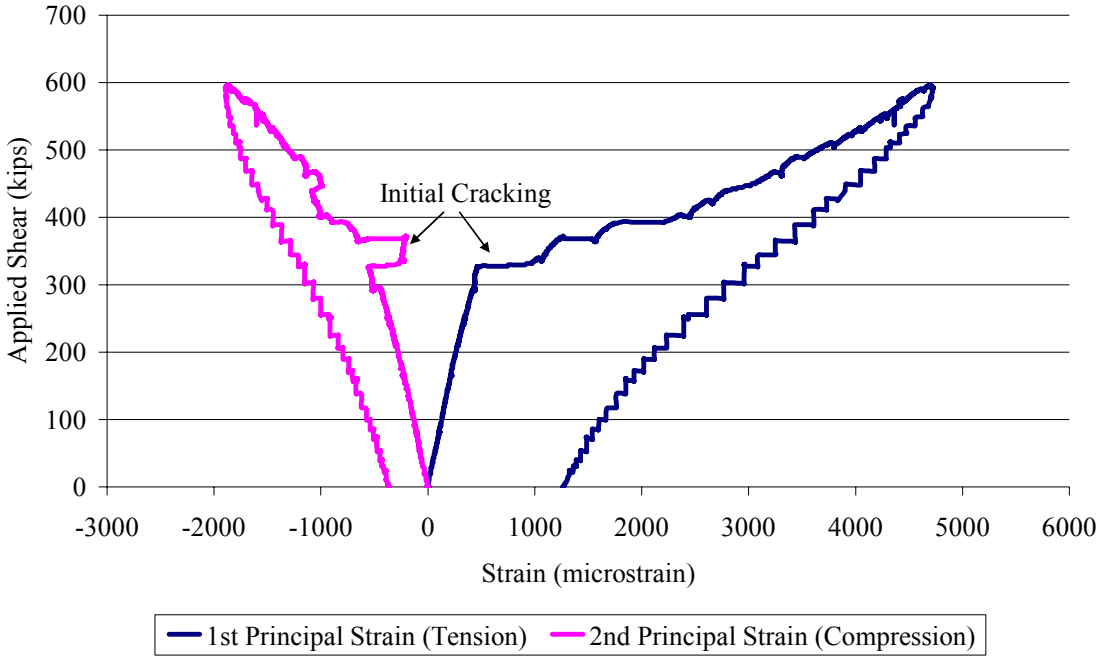

Figure 6.18 Plot of applied shear vs. principal strains for girder Test E1

The point at which initial cracking shear occurred was where the two principal strain plots flattened and separated. The plot shows initial shear cracking at approximately 320 kips of applied shear which corresponded to an applied load of 380 kips. The rosette encountered cracking at a higher load than visually recorded because the initial shear cracks did not pass through the strain rosette. The rosette began measuring cracking when cracks propagated through its region.

Another useful aspect of the principal strain data was a plot of how principal angles varied during the test. Equation 6.34 was used to determine the principle compression angles throughout loading.

$$\theta_p = \frac{1}{2}\tan^{-1}\left(\frac{2\varepsilon_B - \varepsilon_A - \varepsilon_C}{\varepsilon_A - \varepsilon_C}\right) \tag{6.34}$$

Where,

ε_A = Horizontal Strain
ε_B = Strain at 45°
ε_C = Vertical Strain
θ_p = principal compression strain (crack) angle

Figure 6.19 provides the plot of the second principal strain (compression strain) angle, which indicated the angle of shear cracking through the LVDT rosette. Angles were physically measured at different loads to compare to the strain rosette values. For AASHTO LRFD (2004) calculations, average principal strain angles were taken from the rosettes and physical measurements. Predicted and experimental cracking angles are compared in section 6.4.

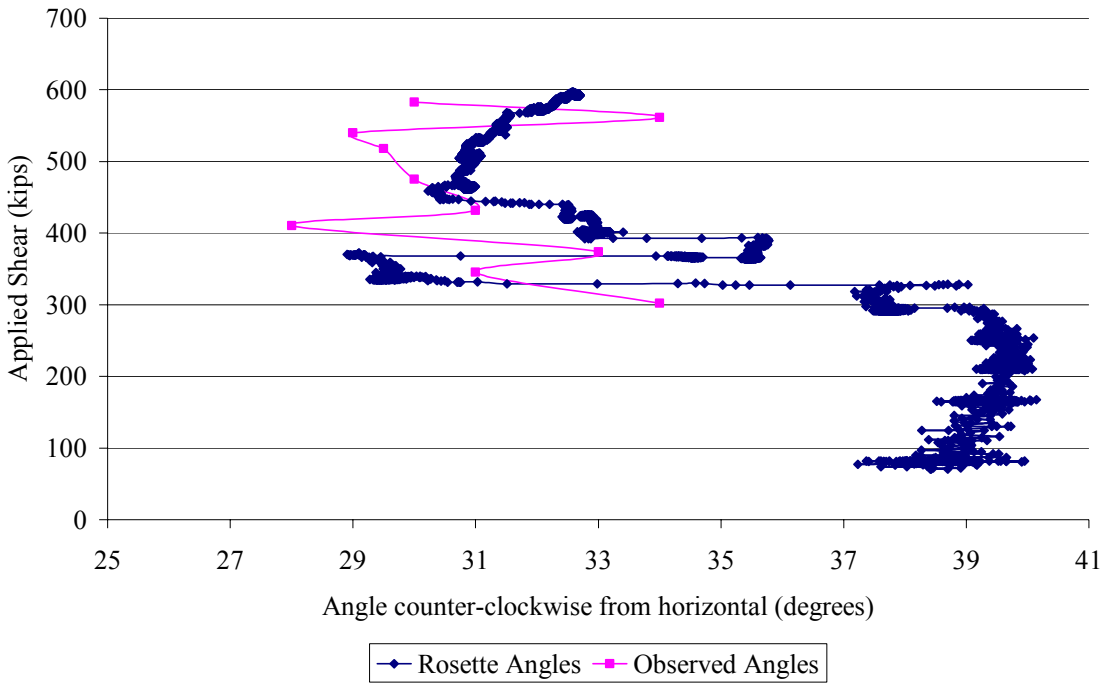

Figure 6.19 Second principal strain direction (cracking angle) for Test E1

The jump from approximately 39° to 29° in Figure 6.19 indicated initial cracking through the rosette. This value corresponded to the principal strain cracking shear of 320 kips obtained from Figure 6.18. Figure 6.19 showed the angle to be consistent before cracking, and then vary from 29° to 33° after cracking. The crack angle stabilized at approximately 31° and reached 33° at ultimate. The overall average experimental compression crack angle taken from physical measurements and the LVDT strain rosette was 31.5° for Test E1.

6.3.2.5 Strand Slip

The strand slip was measured for Test E1 as shown in Chapter 5. There was no strand slip measured on any of the instrumented strands at any time during the testing of section E1.

6.3.2.6 Flexural Strain Profiles

The flexural strain profiles obtained through experimental measurement were taken using VWSGs and 3 string potentiometers that are detailed in Chapter 5. Figure 6.20 gives the experimental and calculated initial strain profiles for Test E1.

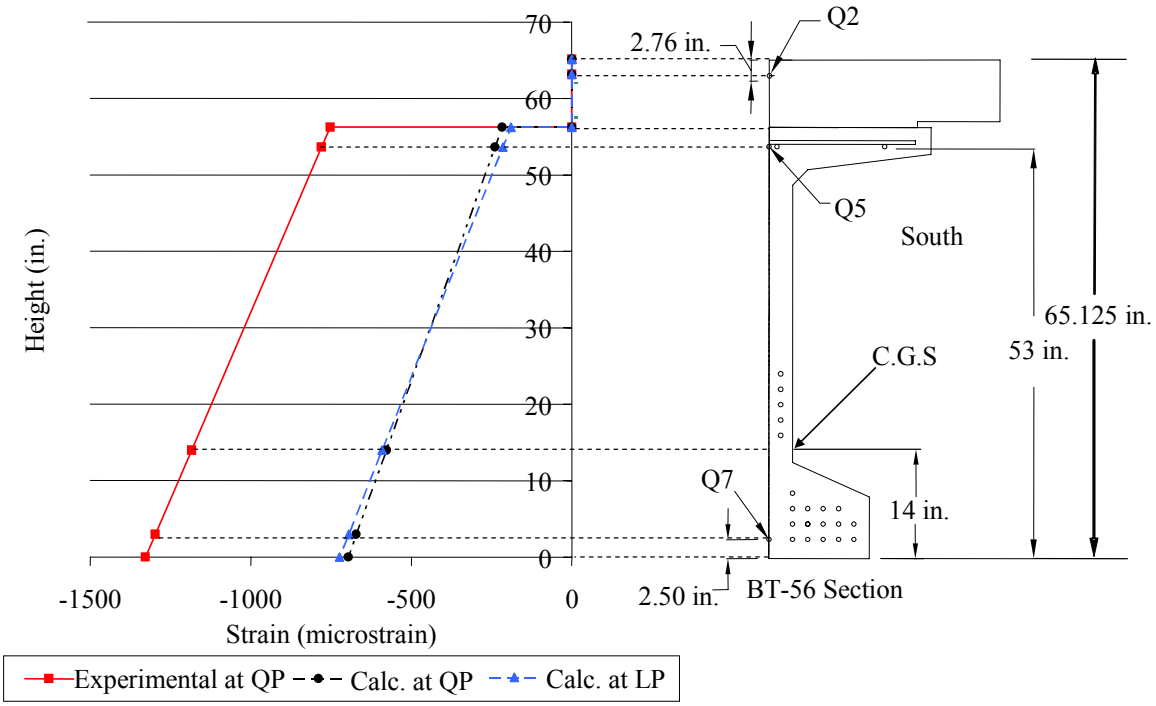

Figure 6.20 Initial strain profiles for Test E1

The experimental strain profile was obtained from the VWSGs approximately 66 days prior to Test E1. The experimental strain profile showed temperature compensated strain based on prestressing, dead load, creep, and shrinkage within the girder. The 66 days were considered insignificant because most of the creep and shrinkage strain had already taken place in the girder. Two calculated profiles were determined at the girder quarter point and at the girder loading point. Equation 6.35 shows the method used to obtain strains used in the calculated strain profiles.

$$\varepsilon_b = \left(\frac{-\frac{F_{se}}{A_g} - \frac{F_{se} e y_b}{I_g} - \frac{(M_D + M_{SD}) y_b}{I_g}}{E_c} \right) \tag{6.35}$$

The two profiles, which were calculated using the measured effective prestressing stress, (f_{se} = 168 ksi), show a difference of 535 microstrain at the top of the girder and a difference of 625.5 microstrain at the bottom. This difference was attributed to the effects of creep and shrinkage throughout the lifetime of the girder. The total age of the girder at the time of Test E1 was 247 days. From specific creep data obtained from Figure 4.21, it was determined that the creep would account for an average of 450 microstrain. From Figure 4.23, the unrestrained shrinkage of the girder concrete was approximately 340 microstrain after 247 days. The actual shrinkage strain in the girder was considered less than the unrestrained shrinkage. When these approximate strains were added to the calculated strain profiles, the measured strain profile obtained from the VWSGs became more reasonable.

The loading strains for Test E1 were obtained from three horizontal string potentiometers mounted directly beneath the point load. Figure 6.21 shows the loading strain profile at 700 kips.

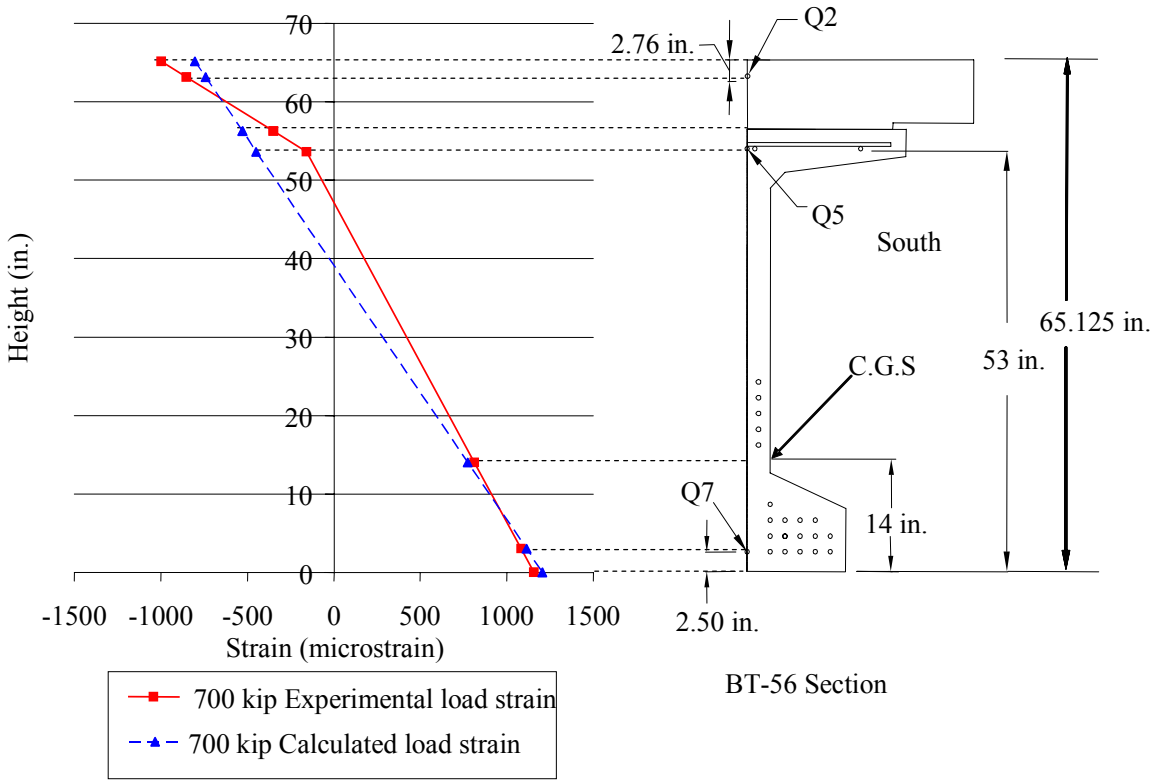

Figure 6.21 Loading strain profile for Test E1

Although not completely linear, the experimental loading strain profile closely matched the calculated loading strain profile. The calculated strain profile was determined by calculating the stress induced by the live load at different locations throughout the tested section and dividing it by the concrete modulus of elasticity. At the bottom layer of strands, the average tension strain was 1,113 microstrain, and at the C.G.S, the average tension strain was 795 microstrain. Equation 6.38 was used to determine the strain at the bottom of the BG-56 girder.

$$\varepsilon_b = \frac{\frac{M_L y_{bc}}{I_c}}{E_c} \tag{6.38}$$

Both the experimental and calculated load strain profiles were used to determine the prestressing force in the strands at maximum loading, f_{ps}. The measured and calculated values for f_{ps} were determined to be 192 ksi and 210 ksi, respectively. It was clear to see that the strands were not near yielding or ultimate stresses. The method used to find f_{ps} is shown as Equation 6.39.

$$f_{ps} = f_{pe} + \varepsilon_{cl} E_{ps} \tag{6.39}$$

where:

ε_{cl} = Measured or calculated strain in concrete due to load at C.G.S
E_{ps} = Modulus of elasticity of prestressing steel = 29,682 ksi
f_{pe} = Measured effective prestressing force

The total strain profiles obtained from experimental and calculated strains are presented in Figure 6.23. The total experimental strain profile was obtained by adding the experimental initial strain profile to the experimental loading profile. The experimental initial profile was obtained from VWSGs and the experimental loading profile was obtained from the string potentiometers. The total experimental strain profile showed a compressive strain of 170 microstrains at the bottom of the girder. Visible flexural cracks were seen in the bottom of the girder at loads exceeding 600 kips. Therefore, the strain in the bottom of the girder had to have a tensile strain higher than the cracking strain of the concrete, which was 180 microstrains. The reason for this inconsistency cannot be explained, except that the initial measured profile was not as accurate as expected.

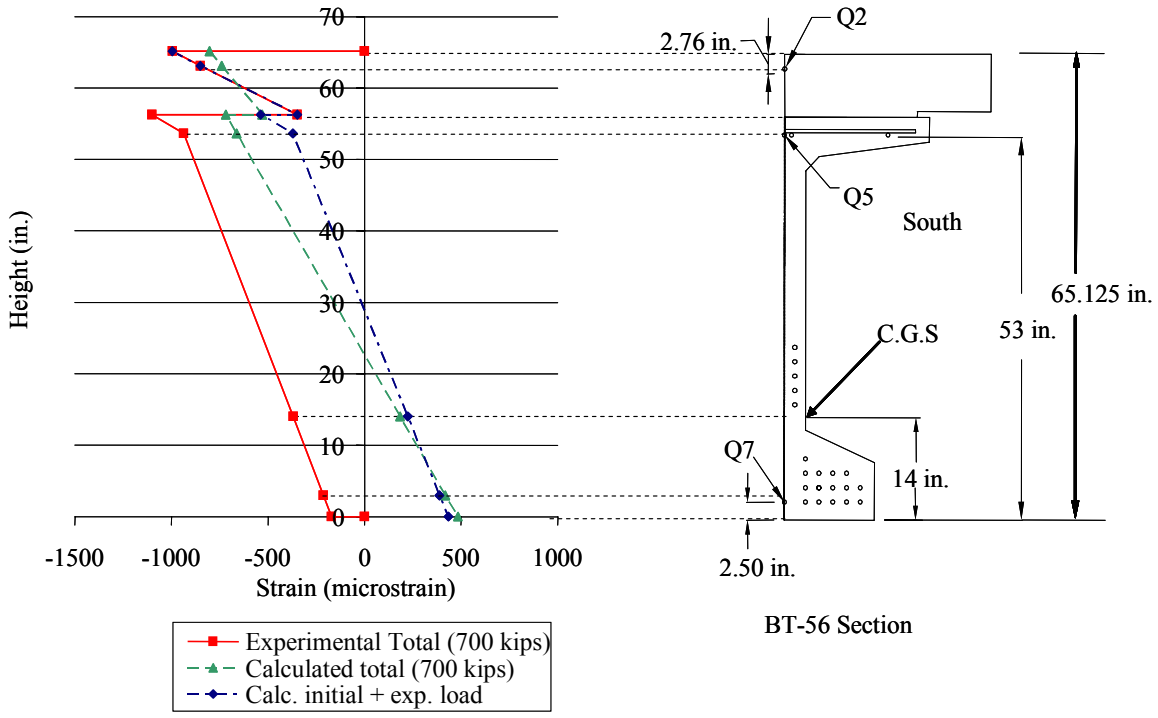

Figure 6.22 Total strain profile for Test E1

The calculated strain profile, obtained by adding the calculated initial to the calculated loading profile showed that there should have been at least 500 microstrains tension in the bottom of the girder at 700 kips. The experimental loading profile was also added to the calculated initial profile. This method more closely matched the calculated total strain profile. The non-linearity of the data obtained from the string potentiometers cannot be explained except for possible instrumentation variations.

6.3.2.7 Partial Development Length Results

During loading of Test E1, DEMEC readings were taken in order to estimate the partial development length for the prestressing strands. Figure 6.23 shows a running average of the strains measured at the different loading points. The strains obtained

during loading were added to the initial transfer length plots, which were obtained from Canfield and Kahn (2005). The final partial development length plot is shown in Figure 6.24. Raw data from the DEMEC readings are included in Appendix E.

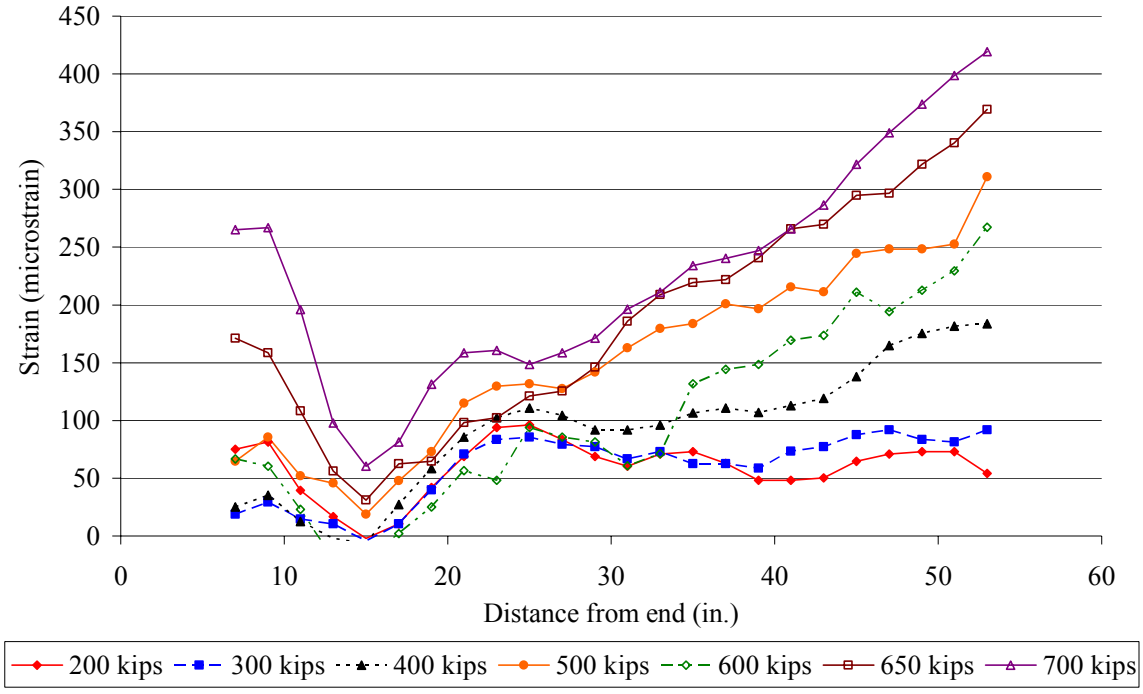

Figure 6.23 Running average of CSS at different loading points for Test E1

In Figure 6.23, a dip in concrete strain directly over the center of bearing was observed on both sides of the girder. The dip was more severe on the northern side of the girder. As the load and distance from the end of the girder increased, the strain increased. At ultimate loading, the maximum strain for Test E1 was 420 microstrains.

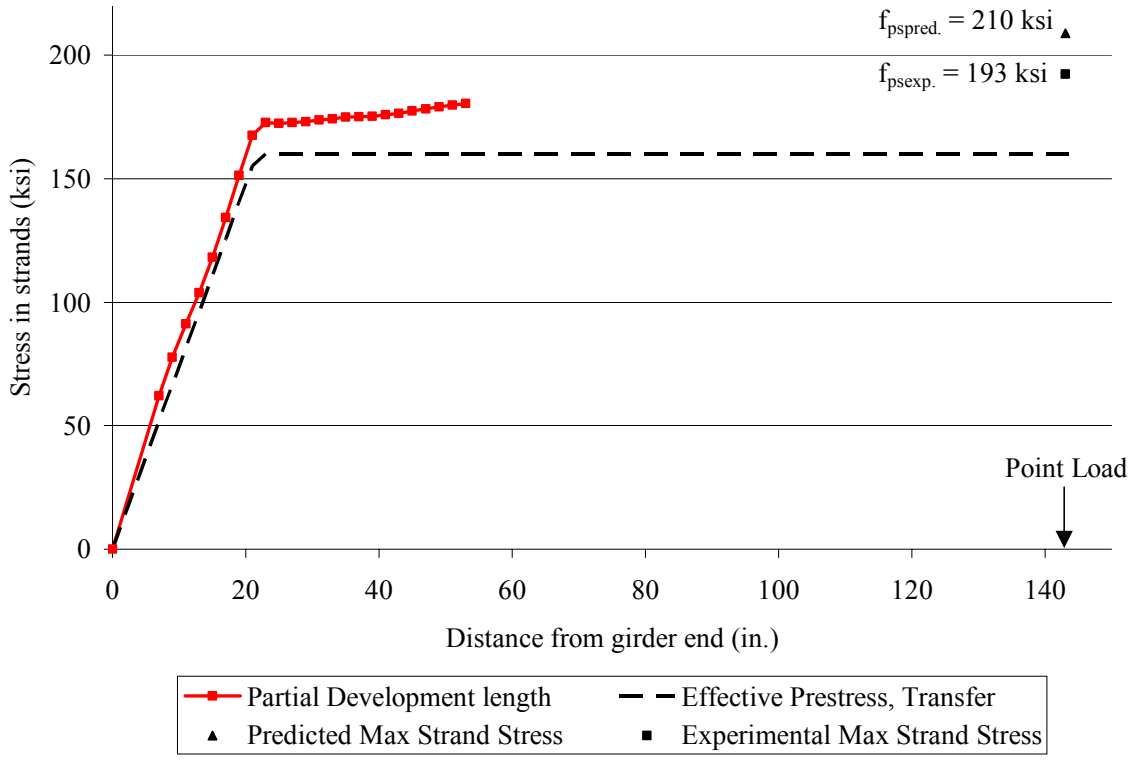

Figure 6.24 Partial development length plot for Test E1

When the running average development length strain was added to the original transfer length plots, the beginning of the development length was determined, as shown in Figure 6.24. The steeper slope of the development length curve indicated that additional stresses were present in the transfer length section. The predicted and experimental strand stresses were given to provide a better estimate of how the rest of the development length curve would look.

6.3.3 Results for Test W1

Test W1 was the second shear test performed on the BT-56 girder. It was performed on December 8th, 2004 on the western end of the BT-56 girder in a similar

fashion to Test E1. The only difference between the two tests was that Test W1 had stirrup spacing varying from 9.5 in. to 24 in. The test set-up and stirrup spacing can be found in Chapter 5. There were some shear-flexure cracks from the flexure test that extended underneath the point load for the shear test. Figure 6.25 shows the cracks that were present before testing. The cracks were not significant and did not reopen during any part of the Test W1.

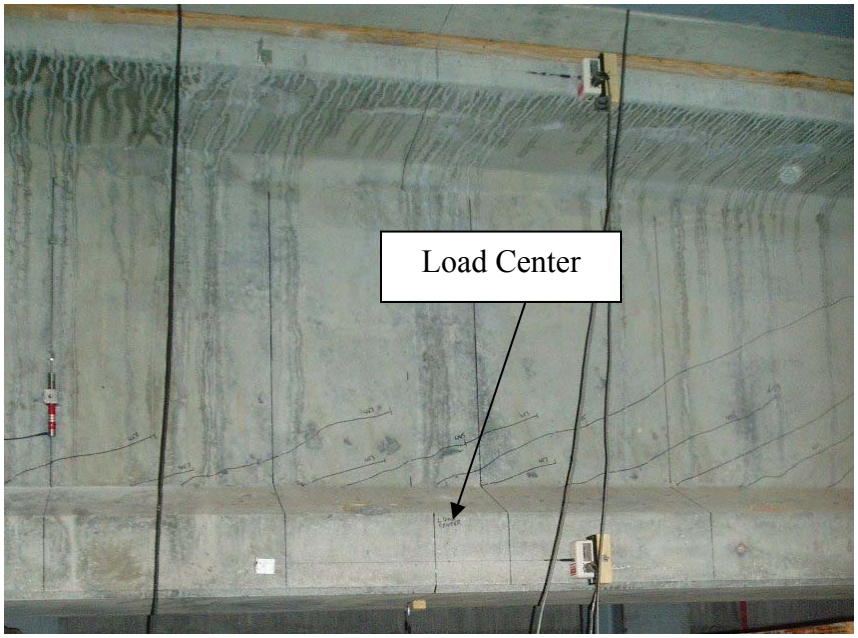

Figure 6.25 Shear-flexure cracks present before Test W1

Test W1 was loaded up to 590 kips before it was determined that there was not sufficient capacity to reach shear failure. The maximum shear, V_{max}, corresponding to the 590 kip point load was 570 kips. At that shear, all instrumented stirrups were beyond yield strain, and crack widths were significant. All indications were that the beam was near failure. However, the section of the girder that contained the pick-up loops remained in-tact with relatively small cracks. Because the pick-up loops were

prestressing strands with a yield stress (f^*_y) of 253 ksi, the shear force required to yield them was determined to be beyond the capacity of the laboratory testing equipment.

6.3.3.1 Deflection

The load-deflection curve for Test W1 was similar to the one observed for Test E1 and can be seen in Figure 6.26. The section of the experimental curve below 300 kips indicated un-cracked section behavior. At a load of approximately 310 kips, the stiffness of the section began to decrease, which indicated initial shear cracking. The predicted curve was calculated using Equations 6.31 and 6.32. The maximum deflection reached for Test W1 was 1.95 in. and the ultimate predicted deflection was 1.66 in. Because the effective moment of inertia from Equation 6.32 was only effective after flexural cracking, the predicted equation slightly underestimated the total deflection.

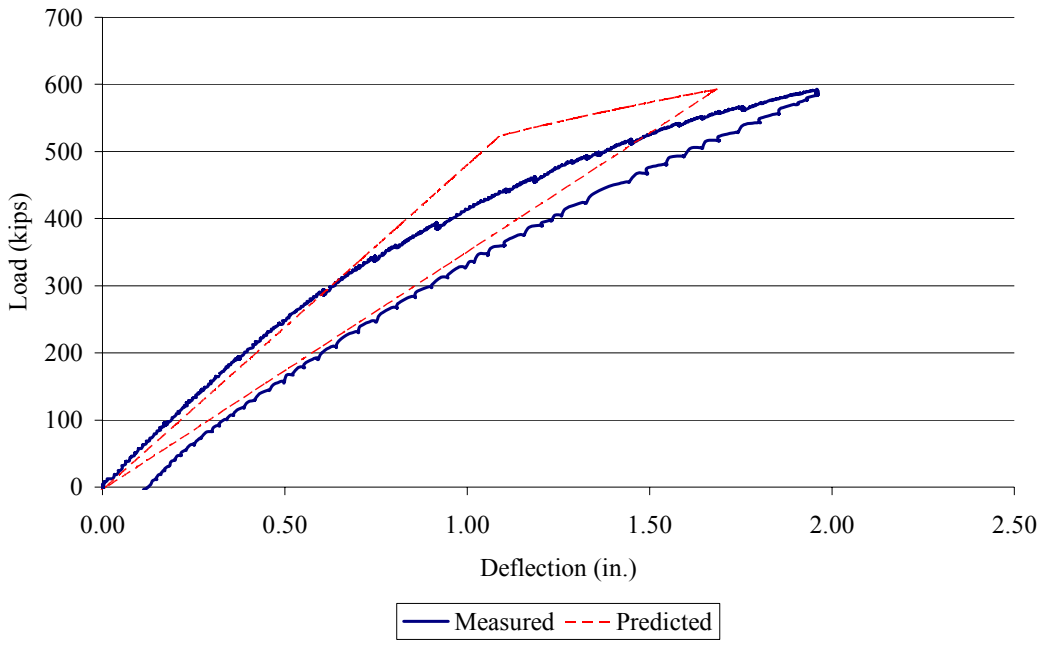

Figure 6.26 Load deflection curve for Test W1

6.3.3.2 Cracking

Initial shear cracking for Test W1 was seen at a load of 300 kips. The corresponding cracking shear force (including dead load shear) on the section was 311 kips. The first cracks were observed near the center of the shear span. The first cracks began extending outwards in both directions as the load increased. By a load of 400 kips, a few of the cracks had fully extended from top to bottom flange and had widths of 0.02 in. One crack extended through the bottom flange directly to the bearing plate at a load of 467 kips. The rest of the cracks were arrested once they reached either flange. At a load of 506 kips, most of the cracks at the center of the shear span were around 0.025 in. wide. At a load of 560 kips, the first flexure cracks were observed directly underneath the point load. At 600 kips, there were still no shear-flexure cracks within the shear span, but some did develop closer to the midspan of the girder. The shear-flexure cracks near midspan began extending from flexure cracks that occurred during the original flexure test. Figures 6.27 and 6.28 show the cracked section for Test W2. Figure 6.29 shows the shear flexure cracks extending from previous flexure cracks. The dotted lines within the figure indicated new shear flexure cracks from Test W1.

As with Test E1, the pick-up loops were seen to have an effect on the shear capacity of the tested section. The web shear cracks extending from the center of the shear span were large and became smaller as they approached and crossed the pick-up loop region.

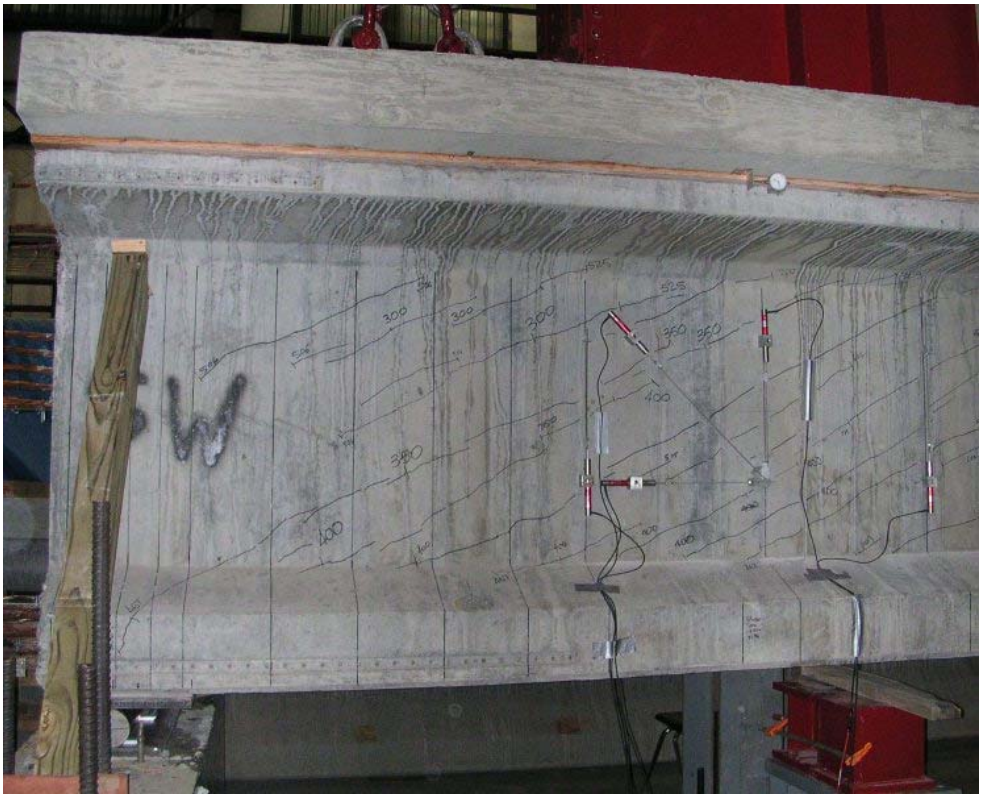

Figure 6.27 Shear cracks at 590 kips for Test W1

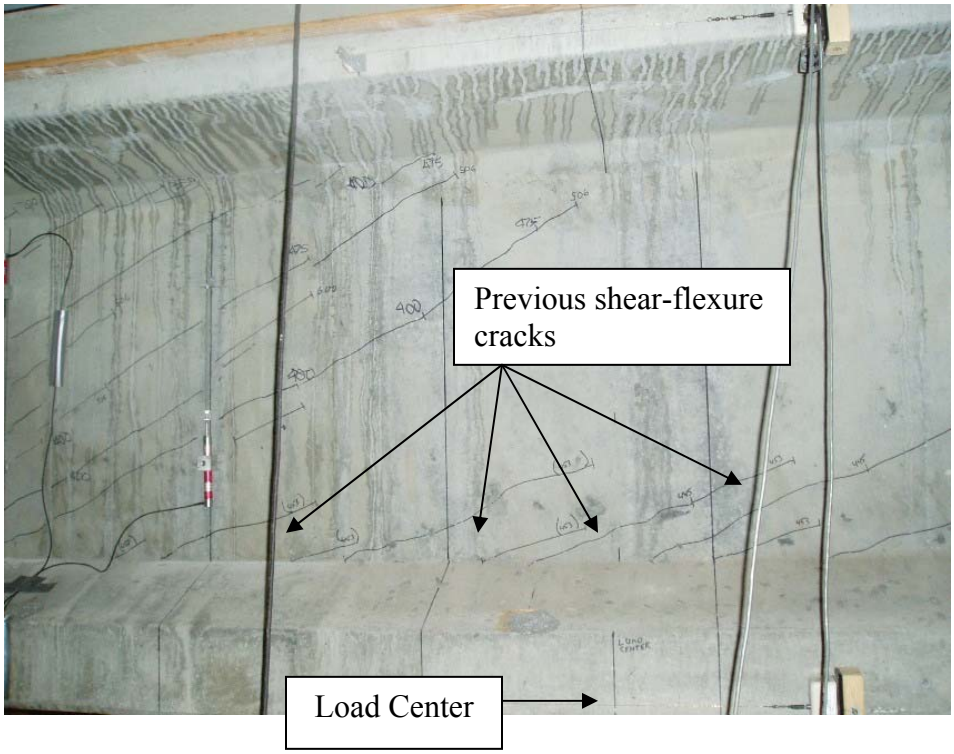

Figure 6.28 Shear cracks at 590 kips for Test W1

Figure 6.29 Flexure shear cracks extending towards midspan for Test W1 (dotted lines)

6.3.3.3 Stirrup Strains

Vertical LVDTs were placed at stirrup locations so that stirrup strains could be estimated. Figures 6.30 and 6.31 provide the stirrup strains and stresses for Test W1. A diagram of where the stirrups were located is provided in Figure 6.31.

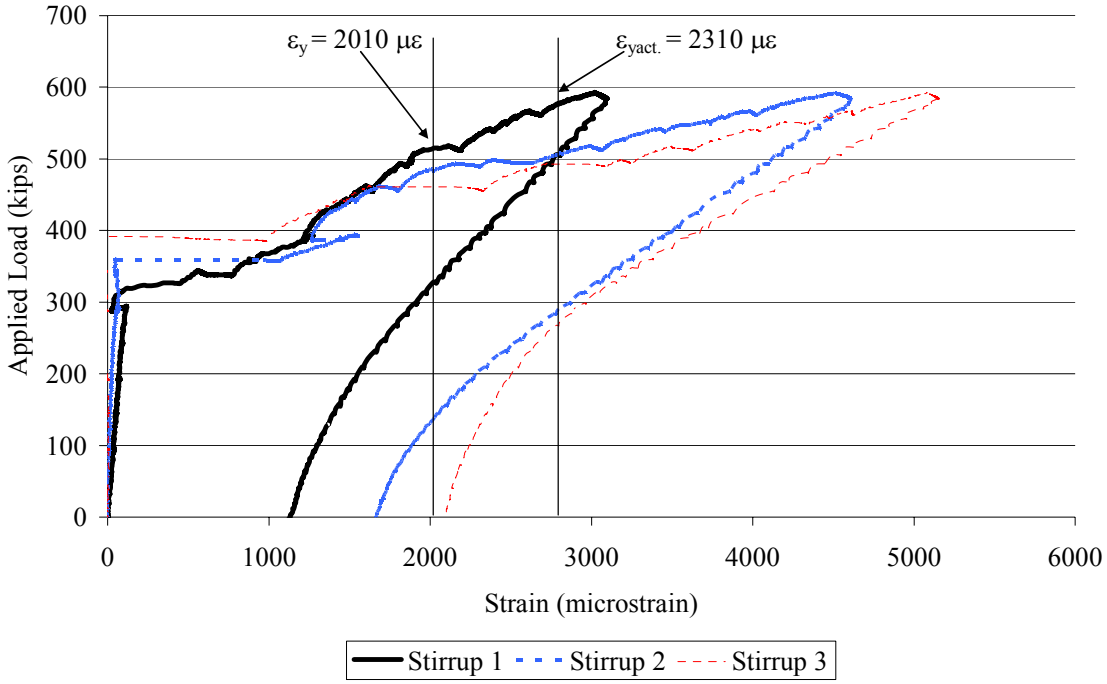

Figure 6.30 Strain in stirrups for Test W1

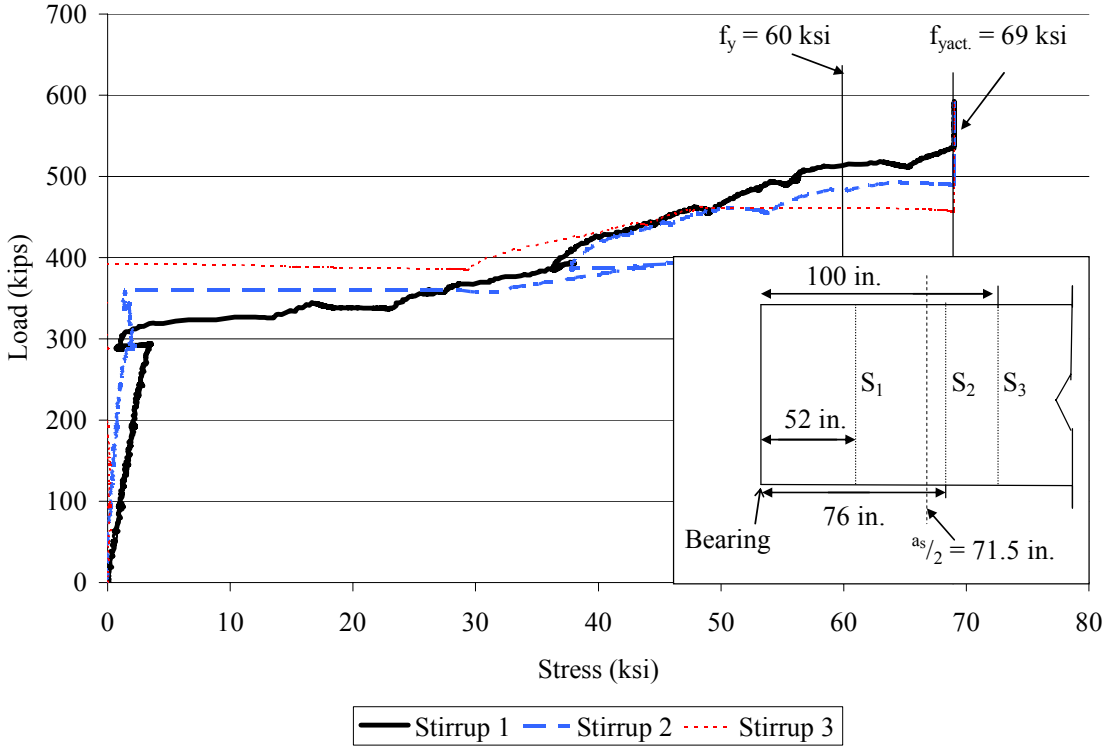

Figure 6.31 Stress in stirrups for Test W1

The strain in all stirrups greatly exceeded the experimental yield stress of 2,310 microstrains. Initial cracking was observed in stirrup 1, which was close to the critical section as defined by AASTHO Standard (2002) and AASHTO LRFD (2004). The initial cracking was seen in stirrup 1 at a load close to 300 kips, which coincided with the visible observations. By a load of 590 kips, stirrups 1, 2, and 3 experienced total loading strains of 3,100, 4,600, and 5,100 microstrains, respectively. The stirrup closest to the point load experienced the highest strain; with the stirrup at the center of the shear span experiencing close to the same strain. The latter stirrups were at 24-in. spacing. Stirrup 1 encountered the least amount of strain despite the fact that initial cracking occurred across it; stirrup 1 was at 9.5-in. spacing. All three stirrups reached yielding stresses in between loading of 450 and 550 kips.

6.3.3.4 Concrete Rosette Strains and Principal Angles

The concrete strain rosette for Test W1 was located at the center of the shear span. The rosette consisted of three arms which measured strains at 0°, 45°, and 90° to the horizontal. It is important to note that the LVDTs were configured oppositely from Test E1 so that the principal tension cracks would cross through the rosette. All principal strains and angles were calculated using Equations 6.33 and 6.34. Figures 6.32 and 6.33 show the principal strains and principal angles determined for Test W1.

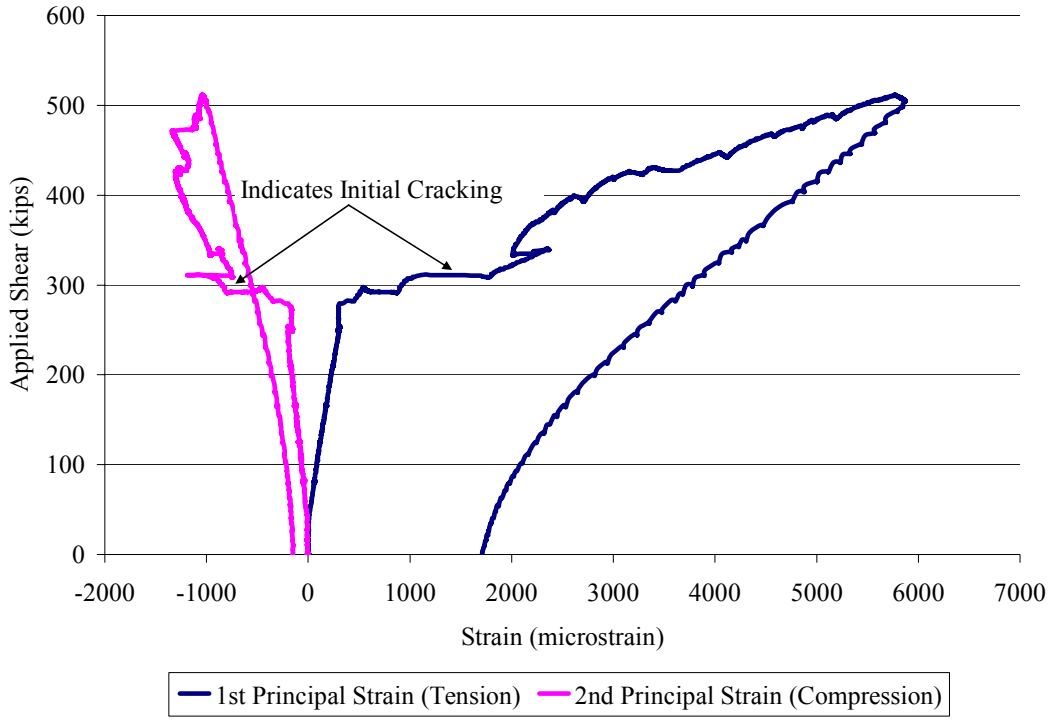

Figure 6.32 Plot of applied shear vs. principal strains for girder Test W1

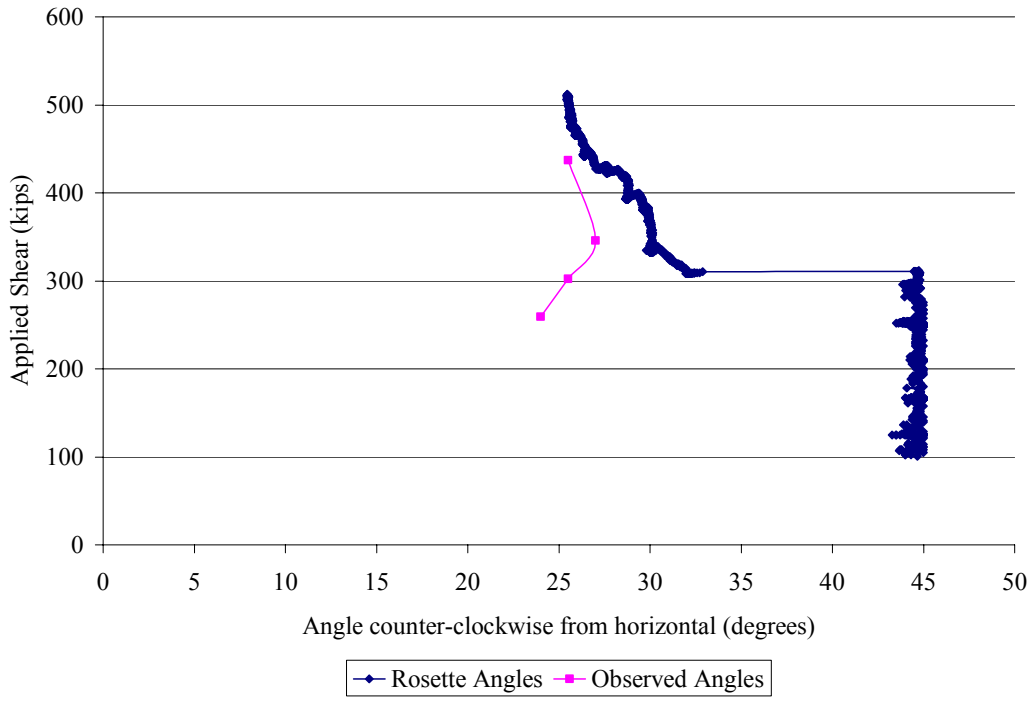

Figure 6.33 Second principal strain direction (cracking angle) for Test W1

Both strain rosette figures show that initial cracking occurred at an applied shear of 311 kips, which corresponded to a point load of 360 kips. The cracking load was higher than what was seen visually because the first cracks did not intersect the strain rosette area. The maximum principal tensile strain was 5,800 microstrains and the maximum principle compression strain was 1,283 microstrains. The principle tension angle obtained from the strain rosette closely matched the physical measurements taken after testing. It was clear to see when the cracks intersected the strain rosette because of the jump from 45° to 30°. The overall average experimental compression crack angle taken from physical measurements and the LVDT strain rosette was 26.2° for Test W1.

6.3.3.5 Strand Slip

The strand slip was measured for Test W1 as shown in Chapter 5. There was no strand slip measured on any of the instrumented strands at any time during the testing of section W1.

6.3.3.6 Flexural Strain Profiles

The flexural strain profiles obtained through experimental measurement were taken using VWSGs and 3 string potentiometers that are detailed in Chapter 5. Figure 6.34 gives the experimental and calculated initial strain profiles for Test W1.

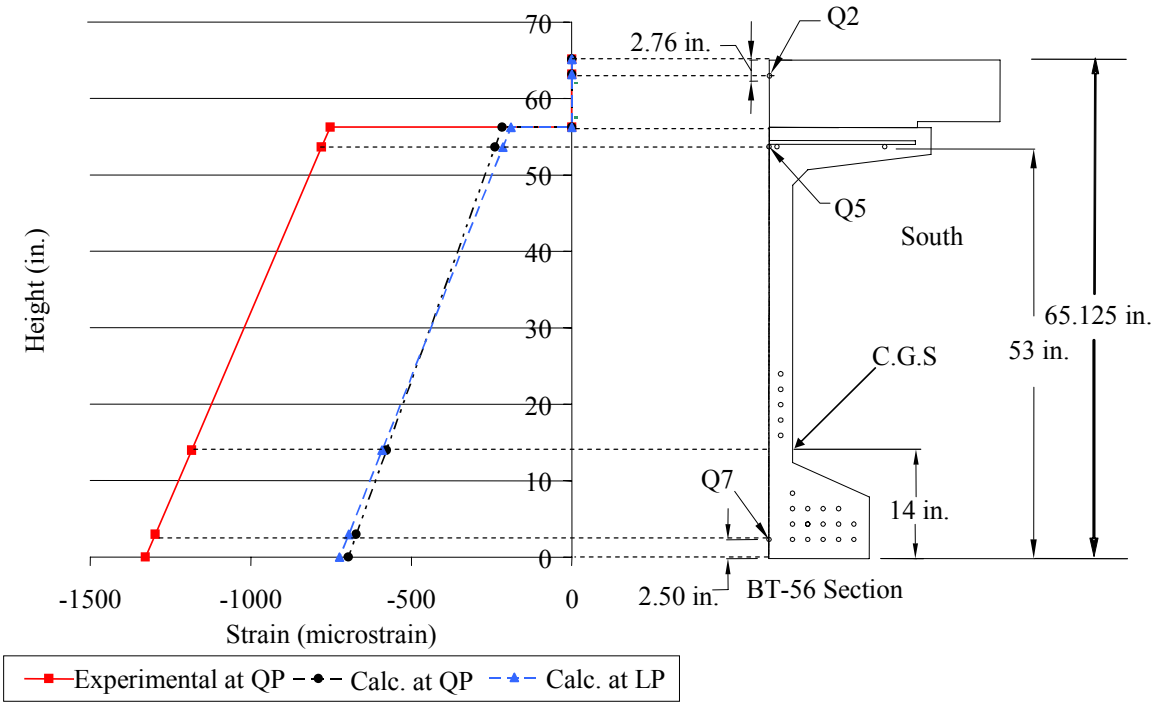

Figure 6.34 Initial strain profiles for Test W1

The initial experimental strain profile was obtained approximately 82 days before Test W2 and was similar to the initial profile for Test E1. The calculated initial profiles were also similar. Equation 6.34 was used to determine the calculated plots. The difference between the two plots was attributed to the creep and shrinkage measured by the VWSGs. The effective prestressing force was taken as 168 ksi, which was the same as in Test E1.

The loading strains observed in Test W1 were slightly different than the ones found in Test E1. Figure 6.35 shows the experimental and calculated loading strains.

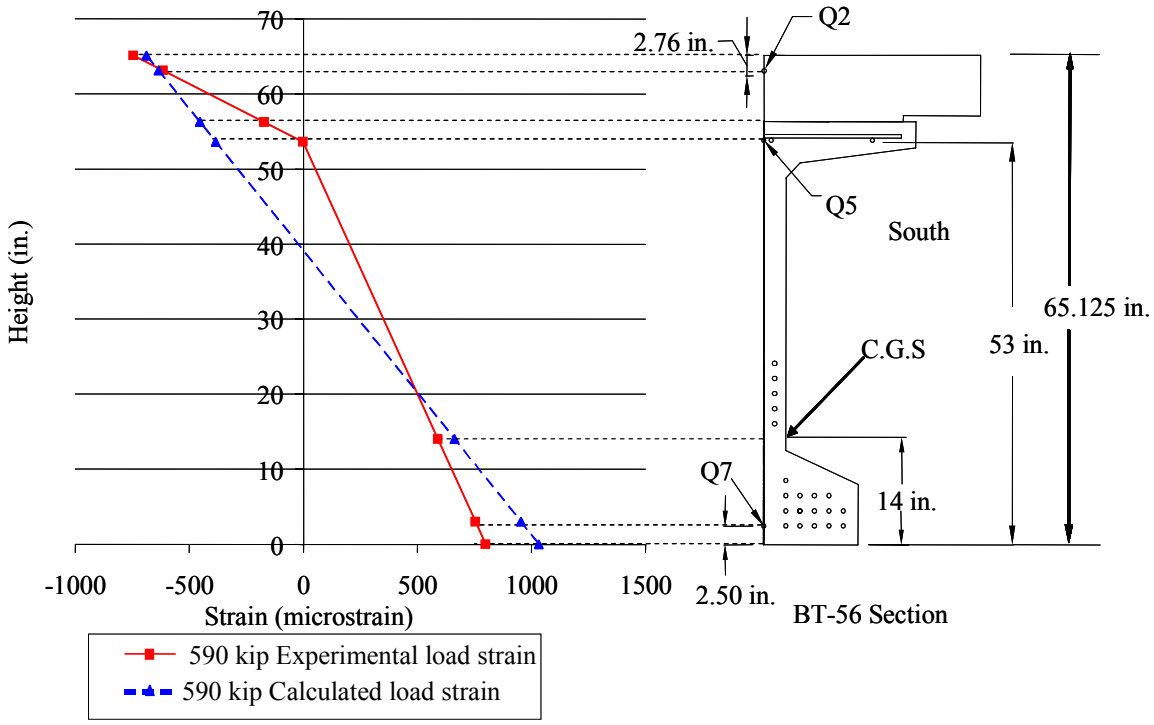

Figure 6.35 Loading strains for Test W1

The experimental loading strain was obtained from the three horizontal string potentiometers detailed in Chapter 5. The calculated load strain was obtained using Equation 6.38. At the bottom layer of strands, the tension strain was 800 microstrains for the measured load profile and 1,000 microstrains for the calculated profile. At the C.G.S, the tension strain was 590 microstrains for the experimental load profile and 660 microstrains for the calculated profile.

Both the experimental and calculated load strain profiles were used to determine the prestressing force in the strands at maximum loading. For Test W1, the maximum loading was 590 kips and the prestressing force at "ultimate", f_{ps}, was found using Equation 6.37. The experimental and calculated values for f_{ps} were determined to be 186 ksi and 206 ksi, respectively. It was clear to see that the strands were not near their yield or ultimate stresses.

The total strain profiles obtained from experimental and calculated strains are presented in Figure 6.36. The total experimental strain profile was obtained by adding the experimental initial strain profile to the experimental loading profile. The total measured strain profile showed a compressive strain of 530 microstrains at the bottom of the girder. This indicated that there was an inconsistency in the measured data, just as with Test E1. Visible flexural cracks were seen in the bottom of the girder at loads exceeding 560 kips. Therefore, the strain in the bottom of the girder had to be at least 180 microstrains in tension. The reason for this inconsistency cannot be explained, except that the initial measured profile was not as accurate as expected.

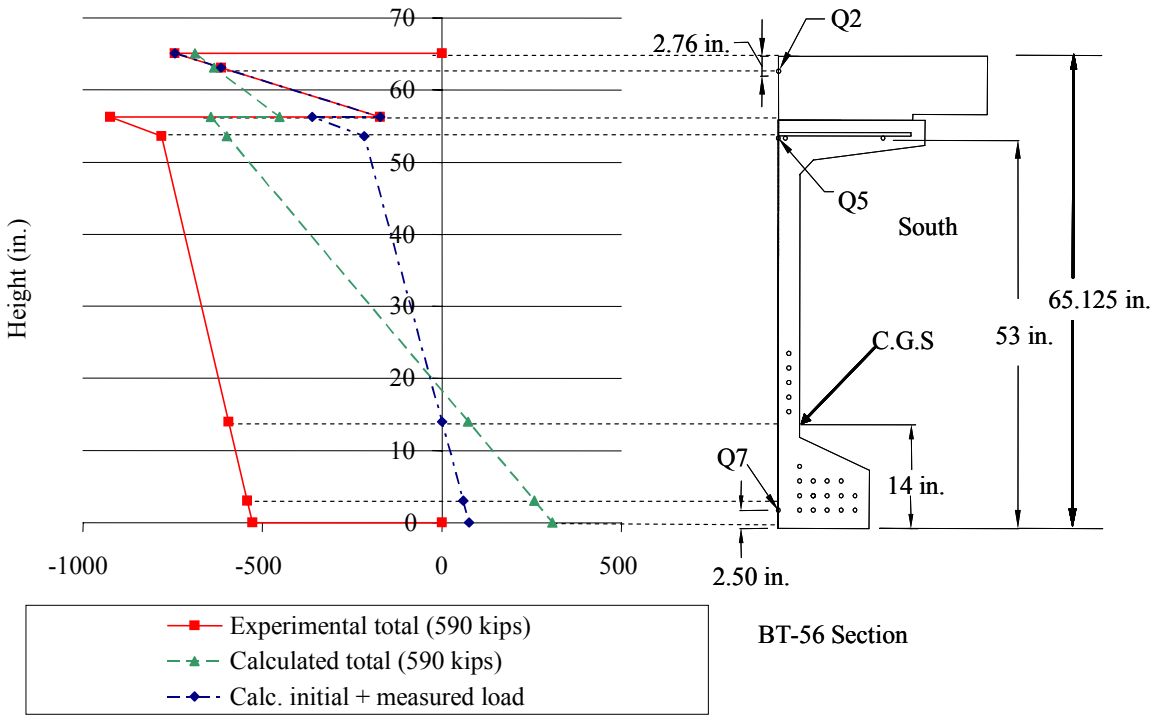

Figure 6.36 Total strain profile for Test W1

The calculated strain profile, obtained by adding the calculated initial to the calculated loading profile shows that there was at least 300 microstrains in the bottom of

the girder at 590 kips. Finally, the measured loading profile was added to the calculated initial profile. Using this method, it was seen that the bottom of the girder had a tensile strain of 75 microstrains and the top of the deck had compressive strains of 744 microstrains. The tensile strain of 75 microstrains was not enough to crack the bottom of the girder. The bottom of the girder was cracked, which showed that the calculated total strain profile may have been the most accurate.

6.3.3.7 Partial Development Length Results

During loading of Test W1, DEMEC readings were taken in order to estimate a partial development length for the prestressing strands. Figure 6.37 shows a running average of the strains measured at the different loading points. The strains obtained during loading were added to the initial transfer length plots, which were obtained from Canfield and Kahn (2005). The final partial development length plot is shown in Figure 6.38. Raw data from the DEMEC readings are included in Appendix E.

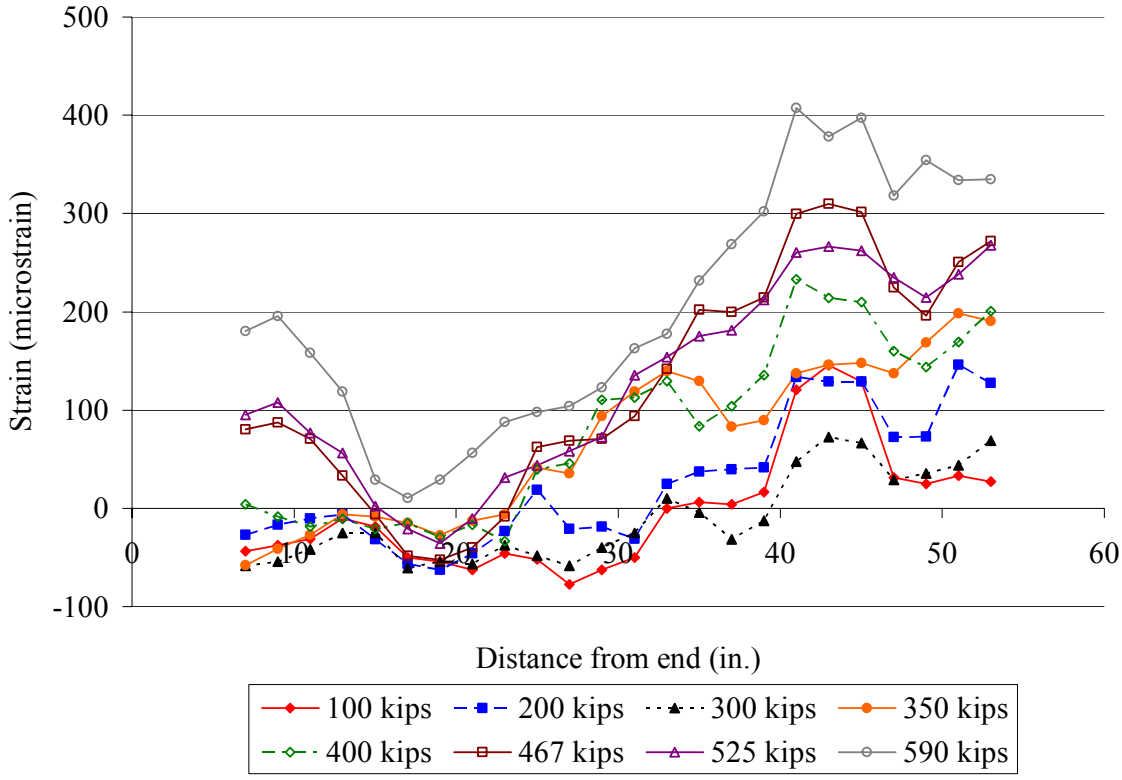

Figure 6.37 Running average of CSS at different loading points for Test W1

In Figure 6.37, a dip in concrete strain directly over the center of bearing was observed on both sides of the girder. The dip was more severe on the southern side of the girder. Despite the dip in strain over the load support, as the distance and load increased, so did the concrete surface strain.

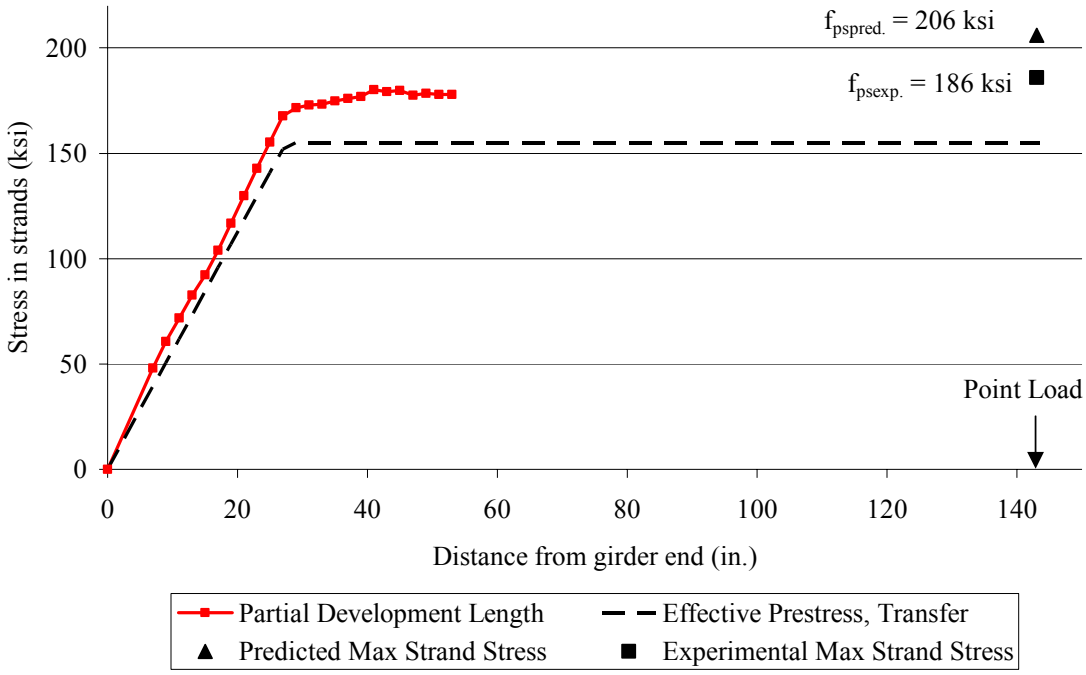

Figure 6.38 Partial development length plot for Test W1

When the running average development length strain was added to the original transfer length plots, the beginning of the development length was determined, as shown in Figure 6.38. The steeper slope of the development length curve indicated that additional stresses were present in the transfer length section. The predicted and experimental strand stresses were given to provide a better estimate of how the rest of the development length curve would look.

6.3.4 Results for Test W2

Test W2 was the third and final test preformed on the BT-56 girder. It was performed on January 5th, 2005. The tested section was located close to the western

quarter-span of the girder. In order to develop a shear failure, the western support was moved in a distance of 8 ft. so that the section could be tested without the influence of the pick-up loops. The stirrup spacing within the shear span was 24 in. The set-up and stirrup spacing for Test W2 is detailed in Chapter 5.

The section was initially cracked because of shear Test W1 and the flexure test performed by Canfield and Kahn (2005). Therefore, the cracking strength of the concrete was unattainable. Figure 6.39 shows the shear span of Test W2 before testing.

Figure 6.39 Cracks prior to loading of Test W2

Test W2 was performed solely to obtain the ultimate shear capacity of the BT-56 girder. The load was applied in 100 kip increments up to 400 kips; and then it was

loaded in 50 kip increments. When new cracks formed, they were marked and measured. The BT-56 experienced a web-crushing shear failure at a point load of 628 kips, which corresponded to an ultimate shear, V_{ult}, of 578 kips. When the failure occurred, an immediate drop in load was observed. The load dropped from 628 kips to 300 kips. The 300 kip load remained until the section was unloaded. With the girder maintaining 300 kips of load, it was determined that the shear failure was more ductile than expected and the section remained largely intact.

6.3.4.1 Deflection

The load-deflection curve for Test W2 is shown in Figure 6.40. Despite the amount of initial cracking present in Test W2, it deflected as a stiff, un-cracked section until a load of 200 kips. After 200 kips, the section deflected as a cracked section, which can be seen by the deviation from the predicted curve. The predicted curve was calculated using Equations 6.31 and 6.32. The ultimate deflection for Test W2 was 2.18 in. while the predicted ultimate deflection was 1.98 in. Because the effective moment of inertia from Equation 6.32 was only accounted for after flexural cracking, the predicted equation slightly underestimated the total deflection. The immediate drop in load at the ultimate deflection indicated the ultimate web-shear failure for Test W2.

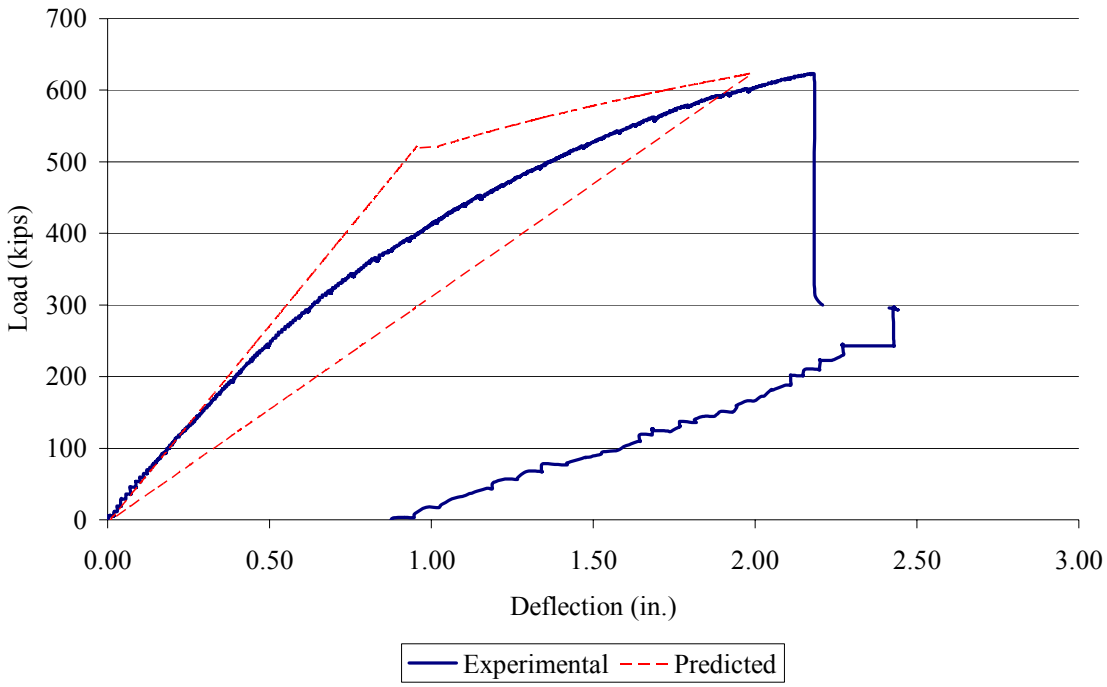

Figure 6.40 Load deflection curve for Test W2

6.3.4.2 Cracking

Because Test W2 was previously cracked, it was not exactly known when the section would have experienced initial cracking. However, new diagonal cracks were seen at a load of 365 kips, which corresponded to an ultimate shear value of 311 kips. Figure 6.41 shows the additional cracking seen during the test. All cracks marked through the strain rosette were new cracks that appeared during loading for Test W2. Not many new cracks were formed before ultimate failure of the section. The section failed along each of the new cracks, as shown in Figure 6.42. All of the cracks extended from the point load and through the center of the shear span. The cracks were arrested when they reached the bottom flange. It was clear to see that the failure was a web shear compression failure that occurred within 30 in. of either side of the shear span center.

Figure 6.41 Cracking at 450 kips for Test W2

Figure 6.42 Cracking at ultimate loading (628 kips) for Test W2

6.3.4.3 Stirrup Strains

Vertical LVDTs were placed at stirrup locations so that stirrup strains could be estimated. Figures 6.43 and 6.44 provide the stirrup strains and stresses for Test W2. A diagram of where the stirrups were located is provided in Figure 6.43.

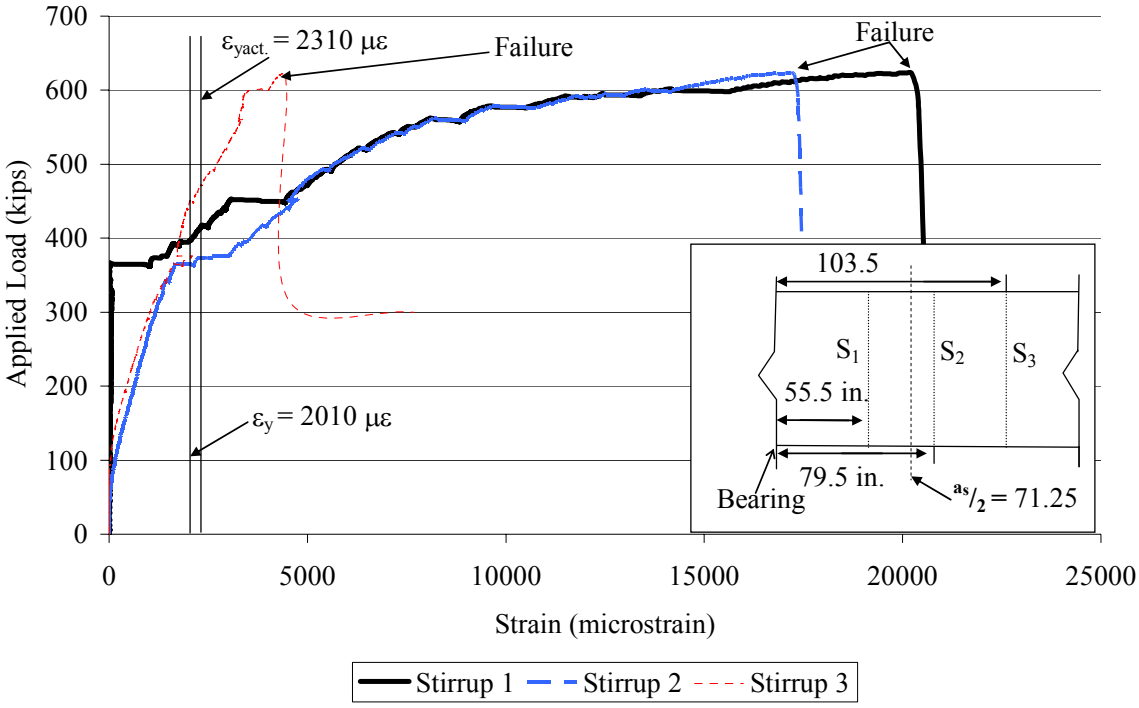

Figure 6.43 Stirrup strains for Test W2

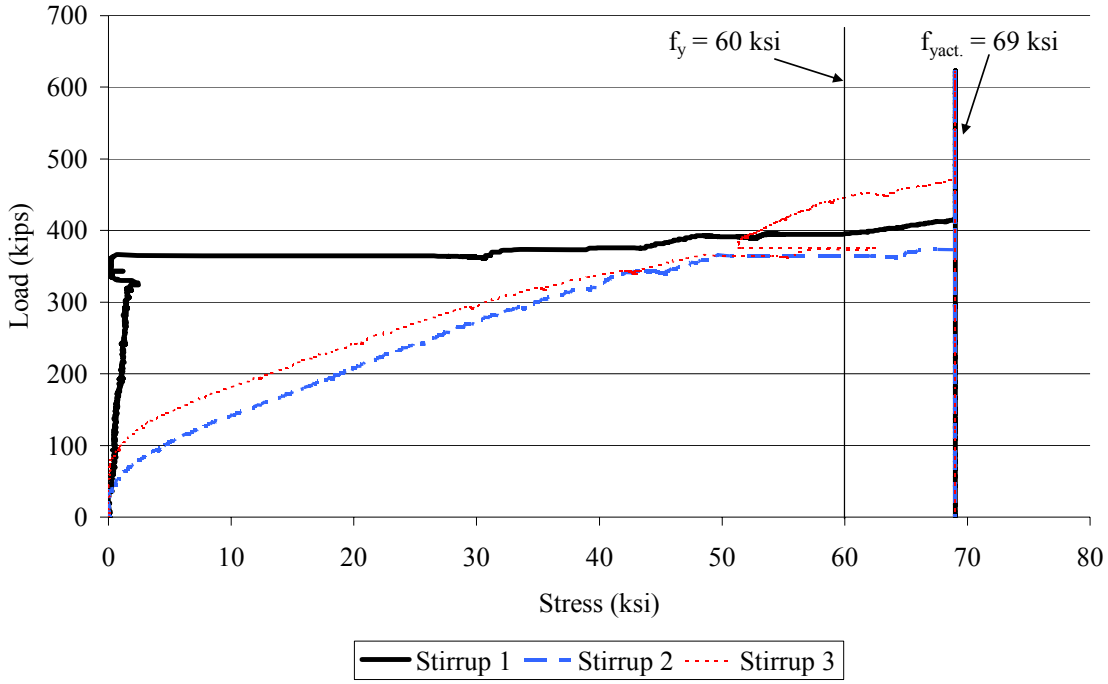

Figure 6.44 Stirrup stresses for Test W2

The strain in all stirrups greatly exceeded the experimental yield strain of 2,310 microstrains. Stirrup 1 indicated that the section was un-cracked until a load of 365 kips, which corresponded to a shear force of 311 kips. Stirrups 2 and 3 experienced strains from the beginning of loading. This indicated that the cracks that crossed the two stirrups began to increase in size from the very beginning of the test. Stirrups 1, 2, and 3 experienced total loading strains of 4,500, 17,263, and 20,227 microstrains, respectively. Stirrups 2 and 3 experienced much higher loading strains than stirrup 1. Stirrup 1 was located 55 in. from the center of bearing and was located in a relatively un-cracked section. Stirrups 2 and 3 were farther from the center of bearing, closer to the shear span center, and had more initial cracking. This was a possible reason for the observed difference in strain.

The yield stress in all three stirrups was reached at approximately the same load. This indicated that if failure was defined by yielding of the stirrups, it would have occurred at a load of approximately 400 kips, which corresponded to a shear force of 390 kips. Failure did not occur, however, until a load of 628 kips, which corresponded to an ultimate shear 583 kips. This indicated that the cracked concrete and vertical component of prestressing provided a considerable amount of shear strength.

6.3.4.4 Concrete Rosette Strains and Principal Angles

The concrete strain rosette for Test W2 was located at the center of the shear span. The rosette consisted of three arms which measured strains at 0°, 45°, and 90° to the horizontal. The LVDTs in Test W2 were installed in the same configuration as Test W1. All principal strains and angles were calculated using Equations 6.33 and 6.35. Figures 6.45 and 6.46 show the principal strains and principal angles determined for Test W1.

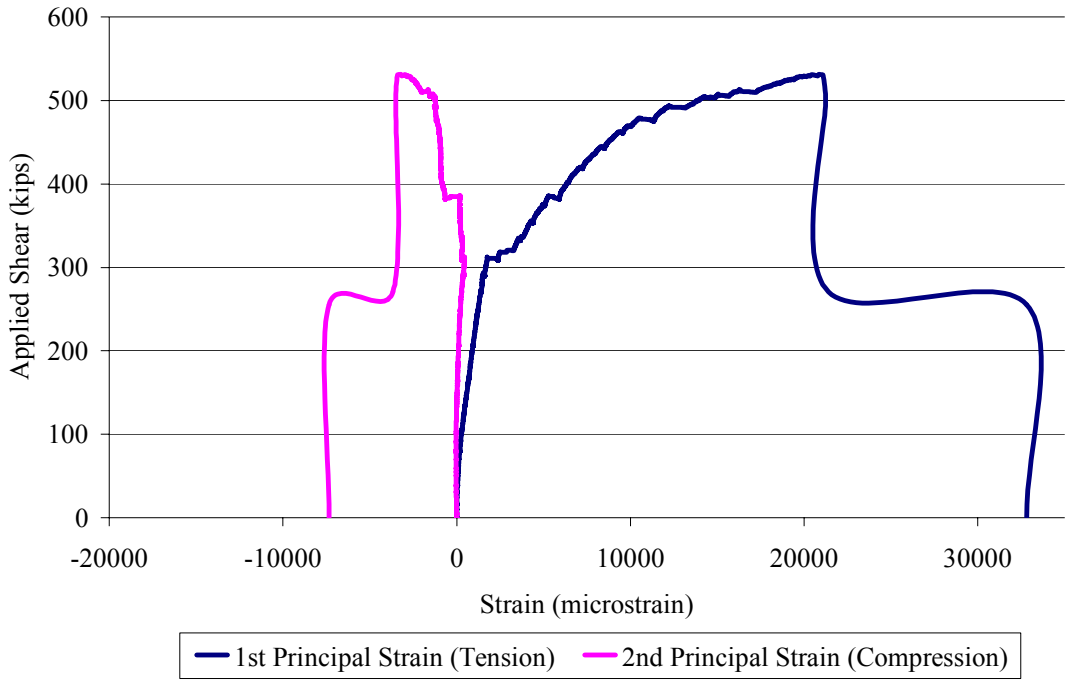

Figure 6.45 Plot of applied shear vs. principal strains for girder Test W2

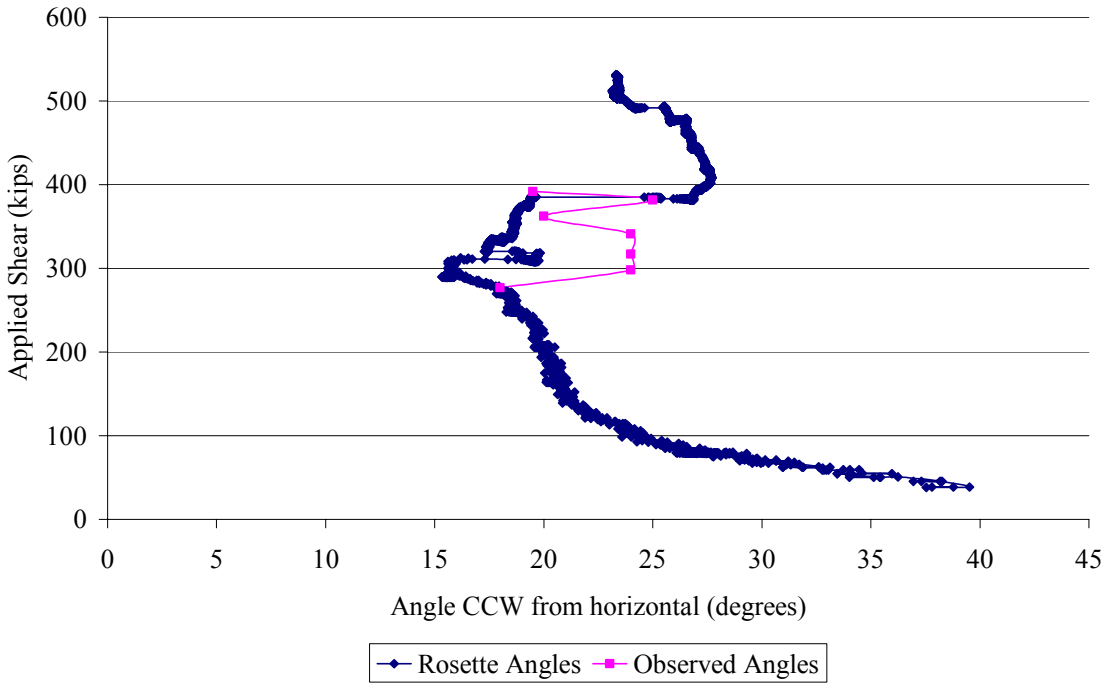

Figure 6.46 Second principal strain direction (cracking angle) for Test W2

The principal tension strains present during Test W2 were similar to the strains found in the other two tests. Because the principal tensile and compressive strains separated from a very small load, it was apparent that the section behaved as an initially cracked section. The drop in load at 530 kips of applied shear corresponded with the ultimate failure at the maximum point load of 628 kips. The difference in tensile and compressive strains was attributed to the stiffer concrete and the minimum amount of transverse reinforcement in the section.

The principal compression angles presented in Figure 6.46 behaved differently than the previous principal angle plots from Tests E1 and W1. From a small amount of applied shear, the angle changed from an initial 40° to an angle as small as 15° at 300 kips of applied shear. At 400 kips shear, the angle jumped back to 27° and finally reached an angle of 23° at 530 kips. The physically measured angles during loading were not exactly the same as the strain rosette angles. The measured angles were, on average, taken as 22.5°. The variability of the strain rosette was attributed to the randomness of the cracking that occurred within its region. An average of both the strain rosette and physically measured angles was taken to obtain the final crack angle. It was calculated to be 23.4°, which was below the AASHTO Standard (2002) minimum crack angle.

6.3.4.5 Strand Slip

The strand slip was measured for Test W2 as shown in Chapter 5. There was no strand slip measured on any of the instrumented strands at any time during the testing of section W2. This was expected for Test W2 because the load point was more than 20 ft. from the end of the girder.

6.3.4.6 Flexural Strain Profiles

The flexural strain profiles obtained through experimental measurement were taken using VWSGs and 3 string potentiometers that are detailed in Chapter 5. Figure 6.47 gives the experimental and calculated initial strain profiles for Test W2.

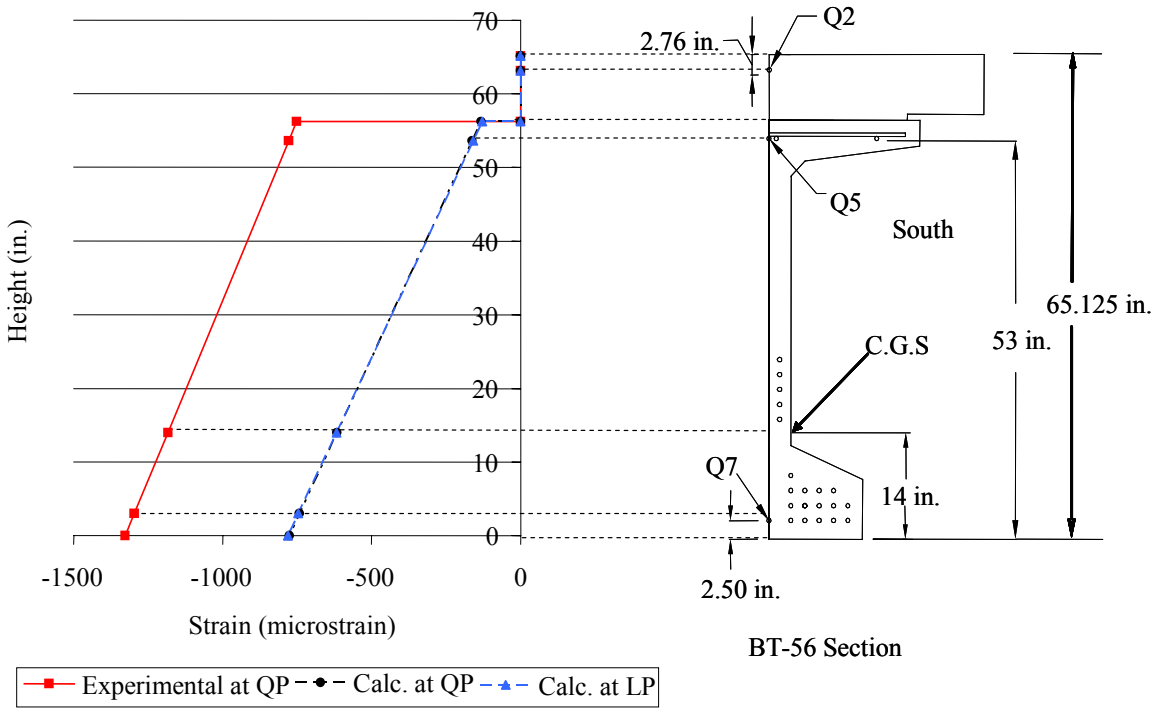

Figure 6.47 Initial strain profiles for Test W2

The initial experimental strain profile was obtained approximately 113 days before Test W2 and was the same exact profile used for Tests E1 and W1. The calculated initial profile directly under the point load was slightly different due to the cantilevered dead load section and the different eccentricities that were encountered. Because the load was much closer to the quarterspan of the girder, the quarter point and load point calculations matched. There was still a difference between the experimental and calculated initial strains of 550 microstrains at the bottom and 623 microstrains at the top.

Equation 6.35 was used to determine the calculated plots. The difference between the two plots was attributed to the creep and shrinkage measured by the VWSGs. As with the other two tests, the effective prestressing force was taken as 168 ksi.

The experimental loading strain was obtained from the three horizontal string potentiometers detailed in Chapter 5 and is shown in Figure 6.48. The calculated load strain was obtained using Equation 6.36. At the bottom layer of strands, the tension strain was 1,120 microstrains for the measured load profile and 1,065 microstrains for the calculated profile. At the C.G.S, the tension strain was 856 microstrains for the experimental load profile and 683 microstrains for the calculated profile. The compressive strains in the top of the deck were at approximately 750 microstrains.

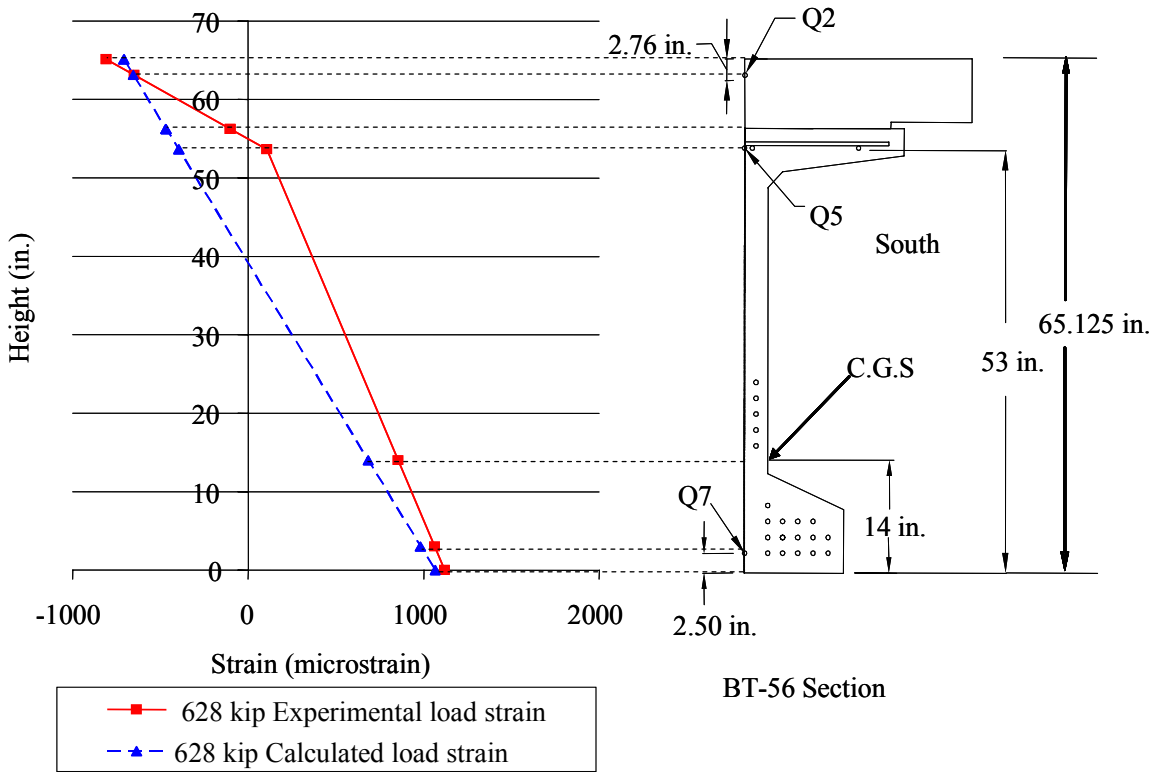

Figure 6.48 Loading strain profiles for Test W2

Both the experimental and calculated load strain profiles were used to determine the prestressing force in the strands at maximum loading. For Test W2, the maximum loading was 628 kips and the prestressing force at "ultimate", f_{ps}, was found using Equation 6.38. The experimental and calculated values for f_{ps} were determined to be 194 ksi and 206 ksi, respectively. It was clear to see that the strands were not near yield or ultimate stresses.

The total strain profiles obtained from experimental and calculated strains are presented in Figure 6.49. The total experimental strain profile was obtained by adding the experimental initial strain profile to the experimental loading profile. The total experimental strain profile showed a compressive strain of 206 microstrains at the bottom of the girder. Just as with the two previous tests, this was considered inaccurate because there were flexure cracks present near ultimate loading. However, Test W2 was previously cracked and it was impossible to tell when flexure cracking would have occurred in the section.

The calculated strain profile, obtained by adding the calculated initial to the calculated loading profile shows that there was a tensile strain of 284 microstrains in the bottom of the girder at 628 kips. Finally, the experimental loading profile was added to the calculated initial profile. Using this method, it was seen that the bottom of the girder had a tensile strain of 340 microstrains and the top of the deck had compressive strains of 800 microstrains. Total profiles for Test W2 show that even at ultimate shear failure, the girder was not near a flexural failure.

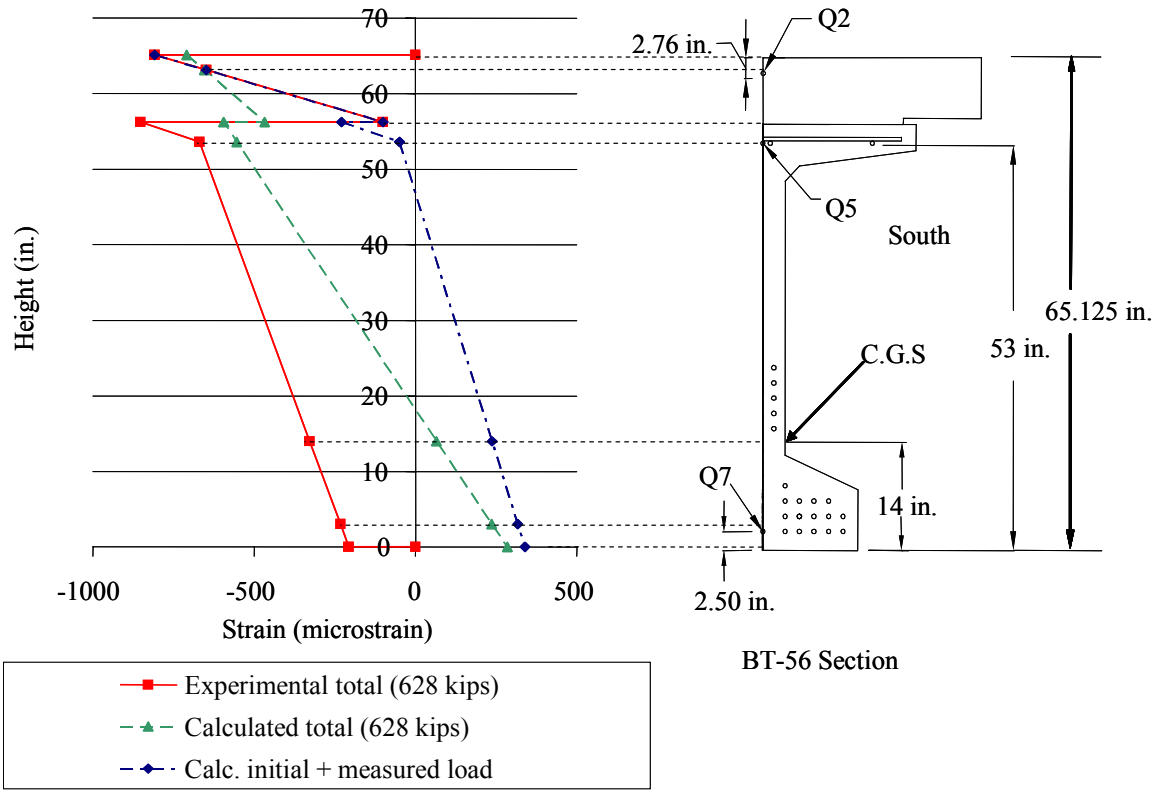

Figure 6.49 Total strain profiles for Test W2

6.3.4.7 Ultimate Failure

Test W2 was the only test to reach ultimate shear failure. Figures 6.50 and 6.51 show the final cracking and web crushing for the north and south sides of Test W2. Figure 6.52 shows the shear cracks extending into the BT-56 top flange just before failure. The BT-56 girder was still holding 300 kips when it was unloaded and further damage and shear cracking would have occurred if the loading continued.

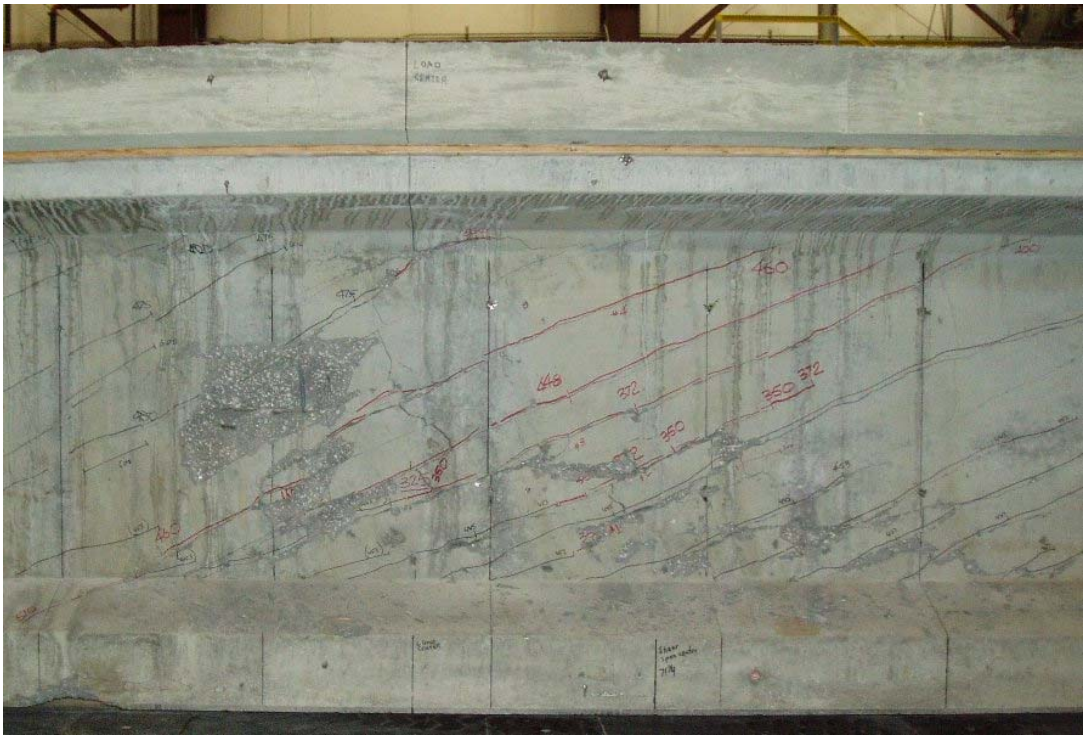

Figure 6.50 South side web-shear compression failure for Test W2

Figure 6.51 North side web-shear compression failure for Test W2

Figure 6.52 Shear cracks extending into the top flange prior to failure in Test W2

6.4 Discussion of Results

This section summarizes the results and trends among the three shear tests. The load deflection curves, initial crack patterns, stirrup strains, crack angles, and flexural strain profiles are compared and discussed for the three shear tests. Also, the cracking and ultimate strengths of all three shear tests are compared to the predicted capacities obtained from AASHTO Standard (2002), ACI Alternate (2002), AASHTO LRFD (2004) and the VATM. Finally, the results from the three shear tests are compared with the results from other research.

6.4.1 Load-Deflection Curve Comparison

The deflection of the girder was taken directly under the point load for each shear test. The girder was pinned at the end of the shear span and allowed to freely roll at the far end. The details of the test set-ups are provided in Chapter 5. Figure 6.53 shows a comparison of the load deflection curves for each test. Test E1 demonstrated a higher stiffness than both of the other tests. This was attributed to the larger amount of shear steel that was present at the east end of the girder. Test W1 had an average stirrup spacing of 16.75 in. and was un-cracked while Test W2 was initially cracked and had stirrups spaced at 24 in. Despite their differences, the plot shows that Tests W1 and W2 had a similar stiffness throughout loading. The ultimate deflections for Tests E1 and W1 were limited by the testing equipment.

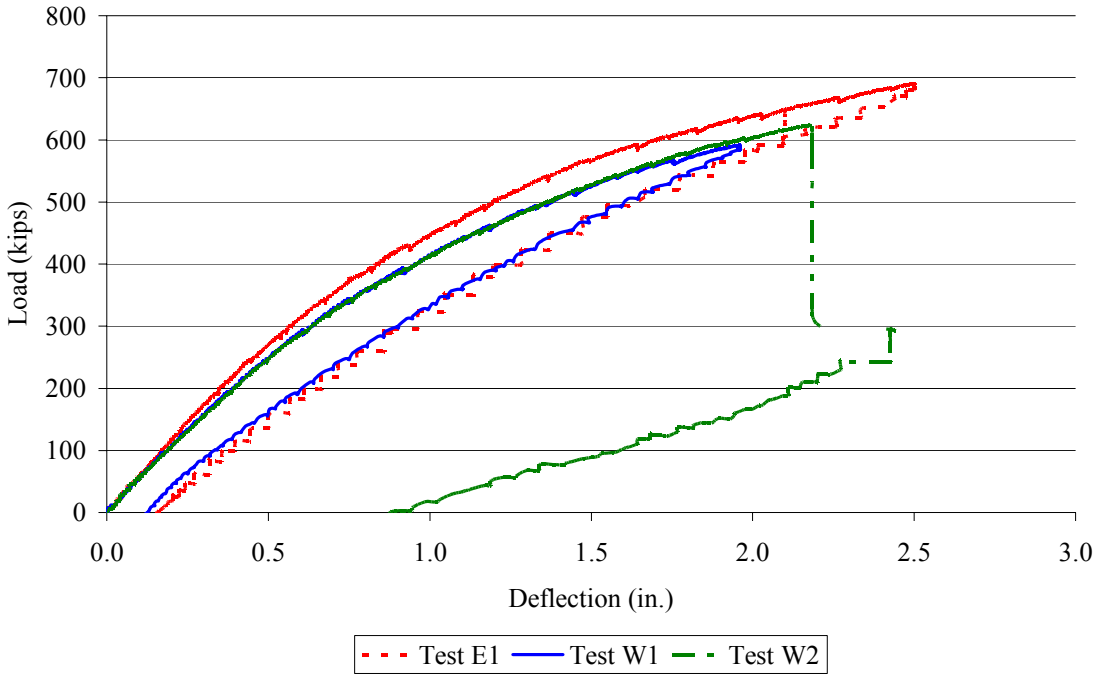

Figure 6.53 Load-Deflection curve comparison

6.4.2 Initial Crack Pattern Comparisons

The cracking patterns for all three tests were very similar. Tests E1 and W1, which were initially un-cracked, experienced diagonal web-shear cracking that extended out from the shear center in both directions. The cracks for both tests were arrested when they reached the top and bottom flanges. The initial cracking shears for both tests were similar, and shear flexure cracks developed outside of the shear span at close to the same load. Cracks and crack widths were limited in the pick-up loop regions for both tests. Despite Test W2 being initially cracked near the bottom flange, it exhibited the same type of cracking behavior as the first two tests. Table 6.5 shows the ultimate shear value for initial cracking, shear-flexure cracking, and flexure cracking.

Table 6.5 Shear cracking forces

	Initial web shear cracking (kips)	Shear flexure cracking (kips)	Flexure Cracking (kips)	$\rho_v f_y$ (psi)
Test E1	350	614	570	1008
Test W1	311	538	573	420
Test W2	311	na	na	294

The cracking pattern for Test W2 was the same as seen for the previous two tests. The new cracks that developed started near the center of the shear span and extended in both directions. The existing cracks began to increase in size from the onset of loading. Shear flexure cracks began extending from previous flexure cracks near the midspan of the girder. This behavior was pronounced due to the closer proximity of Test W2 to the midspan of the girder. Finally, the shear cracks extended into the top flange when the

section was near ultimate loading. This was not seen in the Tests E1 and W1 because they were not tested to failure.

6.4.3 Stirrup Strain Comparison

The amount of strain that occurred in the stirrups for each test depended on the spacing of the stirrups and the maximum load. It was clear from all tests that the ultimate capacity was not defined by the yielding of the stirrups. All instrumented stirrups yielded in each test, but only one test reached ultimate failure.

The stirrups for E1 were numbered from midspan to bearing plate, and it was seen that the stirrup closest to the bearing plate experienced the most amount of strain. Test E1 stirrups experienced the least amount of strain because of the smaller stirrup spacing and insufficient loading.

The stirrups for Tests W1 and W2 were numbered from bearing plate to midspan. From both tests it was seen that the stirrup closest to the point of loading experienced the highest strain. It seemed that the cracks initiated at the stirrup closest to the bearing plate; but the larger, more significant cracks developed in between the shear span center and the point load where the stirrup spacing was 24 in. The stirrup strains for Test W2 were significant because the test reached ultimate failure. A large amount of strain was required in the stirrups before the section actually failed. For Test W2, the shear force causing yield strain was about 400 kips, but the calculated capacity of the section was 638 kips. This difference was attributed to the large amount of draped strands that provided added vertical shear capacity, V_p. The calculated V_p equaled 22.8 kips. The strain difference between stirrup 1 and stirrups 2 and 3 indicated that the section was failing very close to the shear span center.

From the results of all three shear tests, the highest amount of strain occurred close to the center of the shear span. Also, the amount of strain in the stirrups depended on the load and the stirrup spacing. Comparing the ultimate strains of the stirrups in the different tests was not applicable because Tests E1 and W1 were not tested to failure. Table 6.6 provides a comparison of the maximum stirrup strains for each test, along with the stirrup spacing and maximum shear force.

Table 6.6 Maximum stirrup strains

	Maximum shear force, V_u (kips)	Spacing (in.)	Stirrup 1 (με)	Stirrup 2 (με)	Stirrup 3 (με)
Test E1*	654	7	2022	2361	2797
Test W1*	570	16.75	3090	4600	5150
Test W2	583	24	4470	17263	20277

* Tests did not reach ultimate failure

6.4.4 Experimental and Predicted Crack Angle Comparison

The crack angles were physically measured at different loading points during the three tests and the predicted crack angles were calculated using the AASHTO LRFD Specifications (2004) and the VATM. The methods for calculating the angles are presented in sections 6.2.3 and 6.2.4. As previously mentioned, the measured angle for each test was taken as an overall average of the physically measured angles and the strain rosette angles after cracking. Table 6.7 provides a comparison of the experimental and predicted cracking angles along with the number of stirrups that were crossed for each test.

Table 6.7 Crack Angle Comparison

		Experimental		AASHTO LRFD (2004)		VATM		Test / Predicted	
Test	s (in.)	θ (deg.) (crack angle)	Stirrups crossed	θ (deg.) (crack angle)	Stirrups crossed	θ (deg.) (crack angle)	Stirrups crossed	LRFD $\theta_{exp} / \theta_{pred.}$	VATM $\theta_{exp} / \theta_{pred.}$
E1*	7.5	31.5	12	28.5	13	28	13	1.11	1.13
W1*	16.75	26.2	7	24.75	8	33	5	1.06	0.79
W2	24	23.4	5	19.85	6	33	4	1.18	0.71

* Tests did not reach ultimate failure

As the stirrup spacing increased, the angle of cracking decreased. This trend was seen in the experimental results along with both prediction methods. The AASHTO LRFD method had an average test-to-predicted value of 1.11 and the VATM had an average test-to-predicted value of 0.88. Both prediction methods used the measured BT-56 girder properties to determine the compression angles. The average difference in experimental and predicted angles (LRFD) was 2.25°.

Figure 6.55 shows the compression angles plotted versus applied shear for all three shear tests. As the load was applied, the compression angle for each test decreased. Test E1 experienced cracking angles from 40° to 29°; Test W1 experienced angles from 45° to 25°; and Test W2 experienced angles from 40° to 16°. At ultimate loading, the bigger stirrup spacing led to smaller compression angles.

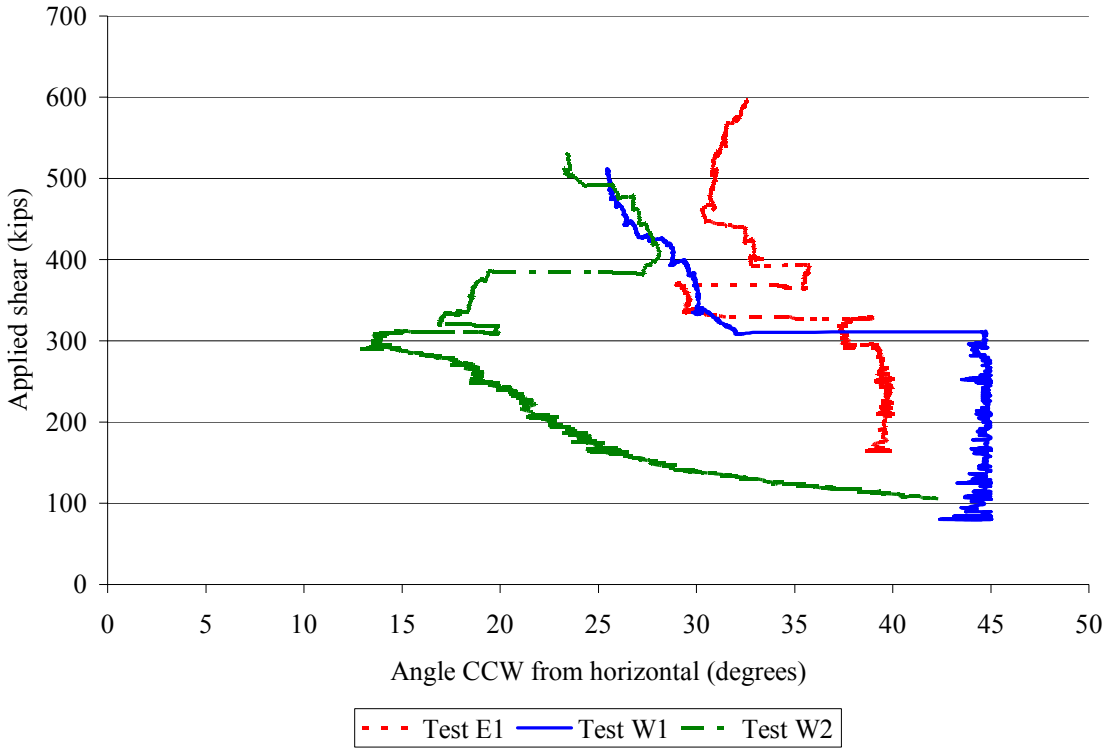

Figure 6.54 Compression crack angle comparison

6.4.5 Flexural Strain Profile Comparison

The flexural strain profiles for each test varied depending on the ultimate load that was placed on the section. They were used to determine the initial strain in the strands, f_{pe}, and the strain in the strands at ultimate, f_{ps}. However, there were some irregularities in the experimental data that were present in all three tests.

The first irregularity was seen in the loading strain profiles. The measured profiles for each test were non-linear. The loading profiles for Tests E1, W1 and W2 can be seen in Figures 6.21, 6.35, and 6.48. The bottom and top strains were consistent with the calculated loading profiles for all three tests. However, the strain obtained from the middle string potentiometer under-predicted the compression strain at the top of the

girder in each test. Because the same phenomenon was seen in all three tests, it was concluded that the middle string potentiometer was inaccurate.

The second irregularity was seen when the initial and loading profiles were added together. When the measured initial profile was added to the measured loading profile, the strain in the bottom of the girder was shown to be in compression. This was impossible because flexural cracking was seen in each test. Because the calculated loading strains were similar to the measured loading strains, the error was assumed to be in the initial measured profile. The profile was taken some time before the shear testing began, and the flexure test could have changed the internal strains in the girder. Because this error existed, the strain in the strands at ultimate loading was taken using both the measured and the calculated strain profiles. Table 6.8 shows the measured and predicted stress that existed at the C.G.S of the prestressing strands for each test along with the strain predicted at the bottom of the girder.

Table 6.8 Comparison of measured and predicted strand stress at ultimate, f_{ps}

	Experimental		Predicted	
	Bottom Strain (με)	f_{ps} (ksi)	Bottom Strain (με)	f_{ps} (ksi)
Test E1*	-170	192	482	210
Test W1*	-530	186	308	207
Test W2	-286	194	204	206

* Tests did not reach ultimate failure

6.4.6 Partial Development Length Comparisons

The partial development length was determined for Tests E1 and W1 only. Test W2 was performed more than 8 ft. from the end of the girder; no DEMEC gage points were located in the bottom flange.

The concrete surface strains (CSS) that were measured for both tests are shown in Figures 6.23 and 6.37. The CSS for both tests displayed similar behavior. As the load and distance along the girder increased, so did the strain values. Both tests demonstrated a large drop in strain over the 12-in. bearing plates. The north side of Test E1 experienced a much larger decrease than the southern side; and the southern side of Test W1 experienced a larger decrease than the northern side. This phenomenon can be seen in the data presented in Appendix E. One possible explanation for this behavior was cracking on the bottom flange of the girder inside of the bearing plate causing excessive strains at the very edge of the girder. Another possible explanation was that the friction caused by the bearing plate on the girder caused a drop in strain over the 12 inch region. The decreases were on opposite sides of the girders at each end. Again, no cracking or strand slip was observed in the CSS regions.

The partial development lengths for Tests E1 and W1 were very similar. They can be seen in Figures 6.25 and 6.39. Both tests experienced an increase in stresses in the transfer length region (l_t = 21.4 and 27.8 in., respectively), which indicated that additional stresses could be developed within that region. At 53 in. from the end of the girder, Test E1 had strand stresses of 180 ksi and Test W1 had strand stresses of 178 ksi. Both stresses were assumed to continue increasing until the maximum stress at the point load was obtained. Because the strands in each test were not near yield or ultimate stresses,

the flexural bond stresses were not exceeded. This indicated that there was no danger of bond failure or strand slip. Dill and Kahn (2000) and Meyer et al. (2002) found that the bond stresses near the end of the specimens exceeded allowable bond stresses found from the Mustafa test. There was considerable bond slip encountered in their test specimens.

6.4.7 Shear Model Comparison

This section discusses experimental girder capacity as compared to the calculated capacities obtained from the methods and models discussed in section 6.2. The girder measured properties are given in Figures 6.1. Appendix D includes assumptions and calculations for each method.

The methods used in calculating shear capacity were the AASHTO Standard Specifications (2002), the ACI Alternate procedure, the AASHTO LRFD Specifications (2004), and the Variable Angle Truss Model (VATM). All load and resistance factors were taken as unity. The shear capacities were calculated at the specified critical sections, which are discussed in section 6.2 and given in Table 6.9. For Test W2, calculations were performed at the defined critical sections and at the center of the shear span. The experimental shear values were calculated at the same critical section for comparison.

Finally, pick-up loops were located within the shear spans of Tests E1 and W1. Ultimate strength calculations were performed with and without the pick-up loops to understand their estimated effect on the capacity of the sections. For shear calculations, the pick-up loops were given an assumed yield stress of 69 ksi, which was the yield stress

of the stirrups. Because neither of the two tests was tested to failure, the total effect of the pick-up loops was not known.

Table 6.9 Critical locations for shear calculations, distance from center of bearing

	AASHTO Standard (2002) (in.)	ACI Alternate (in.)	AASHTO LRFD (2004) (in.)	VATM (in.)
Test E1	32.56	71.5	46.89	71.5
Test W1	32.56	71.5	46.89	71.5
Test W2*	32.56	71.25	46.89	71.25
Test W2†	71.25		71.25	

* Calculations performed at critical section for AASHTO Standard and AASHTO LRFD

† Calculations performed at the center of the shear span

6.4.7.1 AASHTO Standard (2002)

The AASHTO Standard method was accurate and conservative for all cracking predictions. The Specifications accurately predicted web-shear cracking for both tests. The average test-to-predicted value was 1.08 for the cracking strength. The Specifications predicted the same cracking shear capacities for Tests E1 and W1. However, the experimental cracking shear for Test E1 was 36 kips higher than the experimental cracking shear for Test W1. Their only difference was stirrup spacing, which was not taken into account by the AASHTO Standard Specifications concrete shear strength equations. Table 6.10 shows the experimental and predicted concrete shear values for the three tests.

Table 6.10 AASHTO Standard cracking shear, $V_{c\text{-}pred}$ vs. $V_{c\text{-}exp}$

Test	Stirrup spacing s (in.)	$V_{c\text{-}exp.}$ (kips)	$V_{c\text{-}pred.}$ (kips)	$V_{c\text{-}exp}$ / $V_{c\text{-}pred}$
Test E1	7	350	308	1.14
Test W1	16.75	311	306	1.02
Test W2*	24	311	299	1.04

* Test was initially cracked

Table 6.11 shows the experimental and predicted ultimate shear values for the three tests. The accuracy of the AASHTO Standard ultimate shear predictions could only be determined for Test W2. The other two sections were not tested to failure.

Test E1 was loaded 1.05 times the predicted ultimate shear capacity, V_n. The maximum experimental shear was lower than the capacity of the section when the strength of the pick-up loops was added. When the pick-up loops were ignored, Test E1 showed that the AASHTO Standard Specifications provided a test-to-predicted value of at least 1.05.

Test W1 showed that the test-to-predicted value was, at a minimum, 1.06. Once again, the ultimate shear was lower than the capacity predicted when the pick-up loops were considered as shear reinforcement.

Test W2 was tested to failure and the AASHTO Standard Specifications were conservative. The test did not contain pick-up loops, and the stirrup spacing at 24 in. was at the maximum spacing permitted. From Test W2, the ratio of test-to-predicted strength was 1.48 at the center of the shear span.

Table 6.11 AASHTO Standard ultimate shear, $V_{n\text{-}pred}$ vs. $V_{u\text{-}exp}$

Test	Pick-up loops considered	$V_{u\text{-}exp.}$ (kips)	$V_{n\text{-}pred.}$ (kips)	$V_{u\text{-}exp}$ / $V_{n\text{-}pred}$
Test E1	no	653	623	1.05
	yes		698*	0.94
Test W1	no	569	539	1.06
	yes		614*	0.93
Test W2	N/A	580	390	1.49
	N/A		392†	1.48

* Values calculated with pick-up loop capacity

† Value obtained at $a_s/2$

Figures 6.55, 6.56, and 6.57 show the AASHTO Standard shear strength (V_n) calculations along one half the length of the girder for the three different tests. The predictions were based on measured properties with the added capacity of the pick-up loops at the appropriate sections. The shears at visible cracking, V_{cr}, and maximum loading, $V_{u,}$ were included on each graph

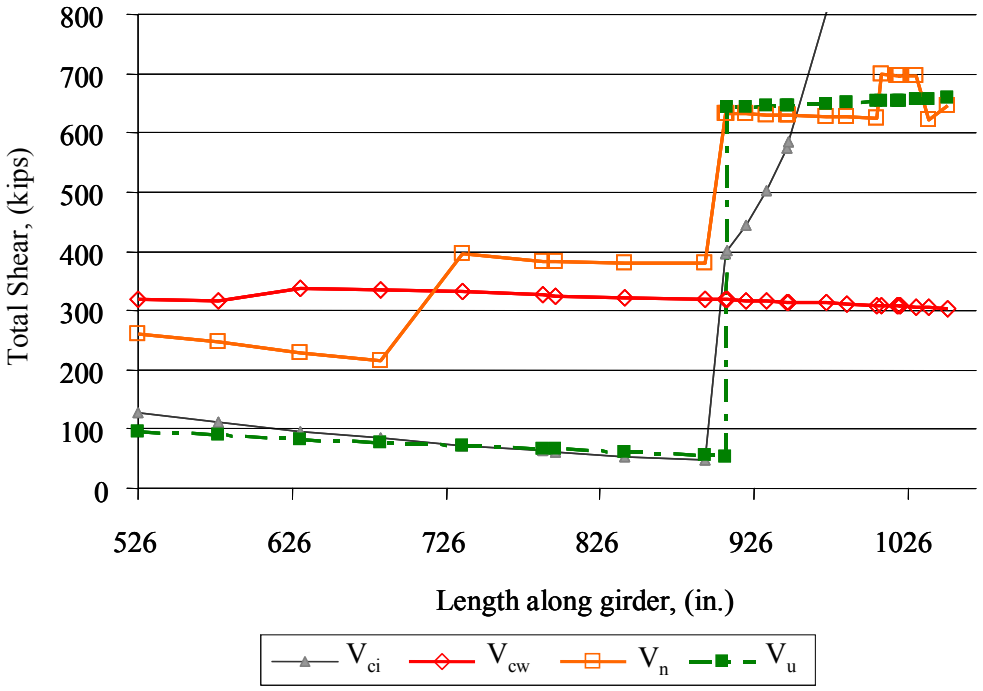

Figure 6.55 AASHTO Standard shear force diagram for Test E1.
(The center of bearing at the east end was 1052 in. from the west bearing.)

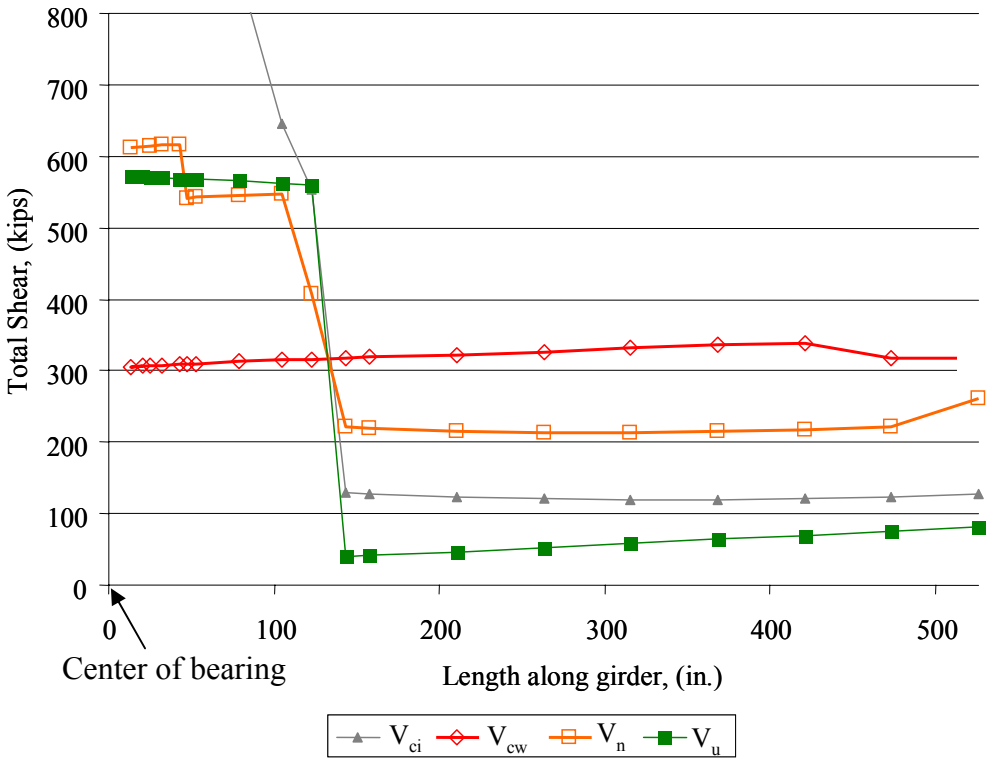

Figure 6.56 AASHTO Standard shear force diagram for Test W1.

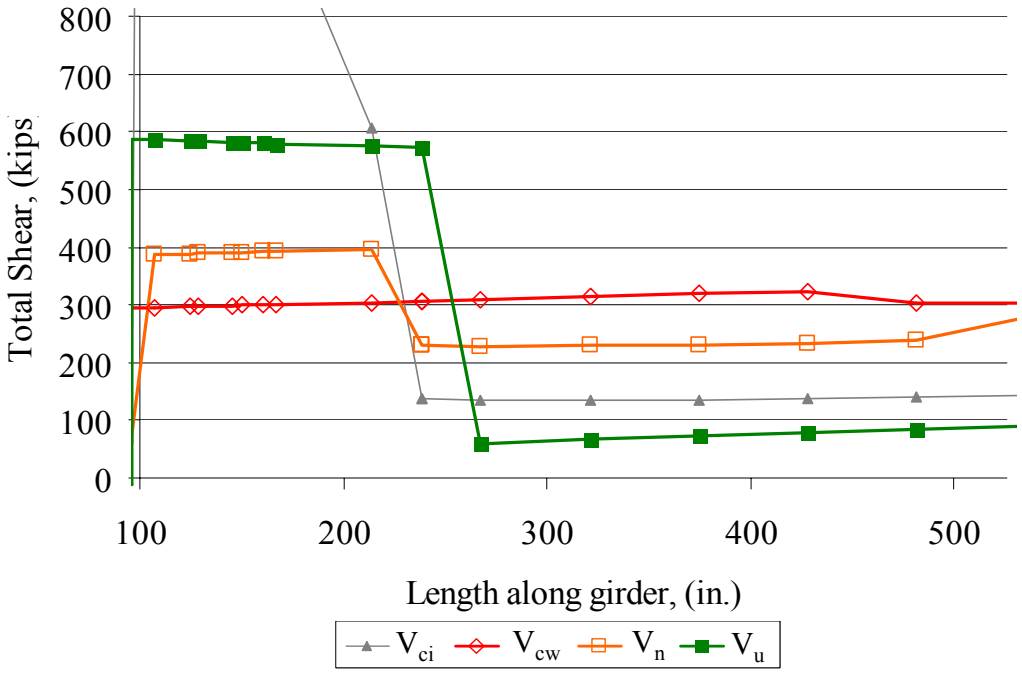

Figure 6.57 AASHTO Standard shear force diagram for Test W2.
(The center of bearing was 98 in. from the west end.)

6.4.7.2 ACI Alternate Method

The ACI alternate method, specified in ACI 318-02, was used to estimate the cracking strength of the girder. The prediction method is discussed in section 6.2.2. When measured properties were used, the method had a test-to-predicted ratio of 1.02 for Test E1, 0.90 for Test W1 and 0.94 for Test W2. Table 6.12 shows the concrete cracking capacities obtained from the ACI Alternate method when the tensile strength was taken as $4\sqrt{f_c'}$. The mean test-to-predicted ratio for cracking strength was 0.95.

Table 6.12 ACI Alternate cracking shear, $V_{c\text{-}pred\ vs.}\ V_{c\text{-}exp}$

Test	$V_{c\text{-}exp.}$ (kips)	$V_{c\text{-}pred}$ (kips)	$V_{c\text{-}exp}$ / $V_{c\text{-}pred}$
Test E1	350	344	1.02
Test W1	311	344	0.90
Test W2	311	330	0.94

Table 6.13 provides an overview of predicted diagonal tension strengths, experimental diagonal tension strengths, and the normalized diagonal tension factors, ξ_t. Figure 6.58 plots the diagonal tension factors versus stirrup spacing for the three tests. Because Test W1 had half of the shear span with stirrup spacing at 9.5 in. and the other half at 24 in., an average spacing of 16.75 in. was used. Figure 6.58 showed that when the stirrup spacings became large, the ACI Alternate predictions for Tests W1 and W2 became unconservative. Meyer et al. (2002) found that as concrete strengths and stirrup spacings increased, the ACI Alternate method became unconservative for lightweight concrete. From Figure 6.58, it was confirmed that the increase in stirrup spacing caused the apparent diagonal tensile strength to decrease for the HPC with a strength of 13,820 psi.

Table 6.13 Normalized diagonal tension strength factors, ξ_t

Test	Stirrup Spacing (in.)	ACI Alternate predicted diagonal tension strength $f_{t\text{-}Pred}$" (psi)	Experimental diagonal tension strength $f_{t\text{-}Exp}$" (psi)	Normalized diagonal tension strength factor ξ_t
Test E1	7	470	485	4.128
Test W1	16.75	470	395	3.362
Test W2	24	470	370	3.148

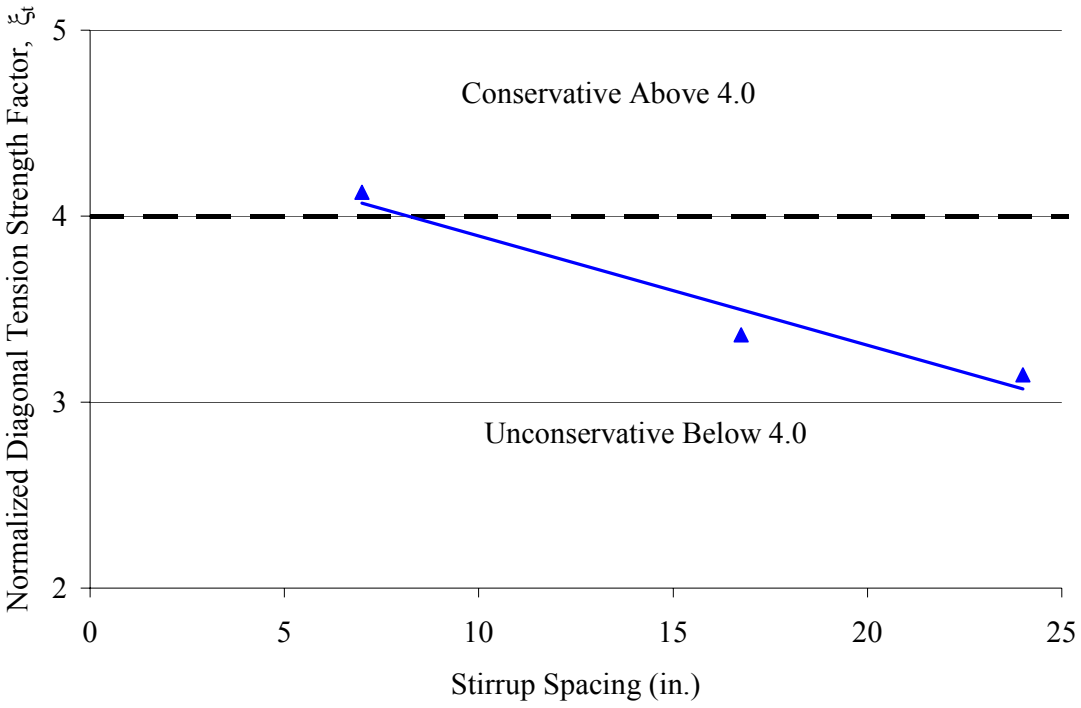

Figure 6.58 Normalized diagonal tension strength factor, ξ_t, vs. stirrup spacing

6.4.7.3 AASHTO LRFD (2004)

The AASHTO LRFD (2004) method predicted concrete shear contributions that were not close to cracking shears seen experimentally. As the stirrup spacing increased, higher concrete shear contributions were predicted. Table 6.14 shows the experimental and predicted cracking shears obtained from the LRFD Specifications. The concrete shear contributions were determined using the LRFD interpolated angles and the physically measured angles. The LRFD Specifications predicted similar concrete shear contributions for Tests E1 and W1 because they had similar stirrup spacings at their critical locations. However, the concrete shear contribution of Test W2 was much higher due to the large stirrup spacing across the critical section. It is important to note that the concrete shear contributions were not intended to relate to the experimental cracking shears. The values were compared in Table 6.14 so that they could be compared with the results from previous research and to confirm that the LRFD concrete shear contribution was not intended to predict the cracking shears of prestressed girders.

Table 6.14 AASHTO LRFD (2004) concrete shear, $V_{c\text{-}pred}$ vs. $V_{c\text{-}exp}$

Test		$V_{c\text{-}exp.}$ (kips)	Concrete Shear Contribution, V_c (kips)	$V_{c\text{-}exp}$ / $V_{c\text{-}pred}$
Test E1	LRFD Angle	350	89	3.93
	Measured Angled		93	3.76
Test W1	LRFD Angle	311	91	3.42
	Measured Angled		96.5	3.22
Test W2	LRFD Angle	311	141	2.21
	Measured Angled		150	2.07

The LRFD Specifications were conservative for predicting ultimate shear capacities. The accuracy of the ultimate shear predictions given by the AASHTO LRFD Specifications could only be compared with an experimental shear failure for Test W2. Table 6.15 shows the shear capacities determined by the AASHTO LRFD Specifications compared to the experimental shear capacities. Ultimate capacities were calculated using LRFD interpolated angles, and physically measured angles with and without the added capacity of the pick-up loops.

When the pick-up loop capacity was added to the total shear capacity, it became clear that the E1 section was not close to ultimate failure. The same results were seen for Test W1.

Test W2 was tested to failure, and it showed the AASHTO LRFD Specifications to be conservative for all three calculated predictions. The test did not contain pick-up

loops, and the stirrup spacing was at a 24 in. It was seen that the AASHTO LRFD Specifications had a test-to-predicted value of 1.36 when the interpolated angle was used and a test-to-predicted value of 1.55 was obtained when the physically measured angles were used. Finally, the shear capacity was calculated at the center of the shear span because the region of failure was located there.

Table 6.15 AASHTO LRFD ultimate shear, $V_{n\text{-}pred}$ vs $V_{u\text{-}exp}$

Test		$V_{u\text{-}exp.}$ (kips)	$V_{n\text{-}pred.}$ (kips)	$V_{u\text{-}exp}$ / $V_{n\text{-}pred}$
Test E1*	LRFD Angle	653	696	0.94
	Measured Angled		612	1.07
			902†	0.73
Test W1*	LRFD Angle	569	601	0.95
	Measured Angled		565	1.01
			866†	0.66
Test W2	LRFD Angle	580	425	1.36
	Measured Angled		373	1.55
			369‡	1.57

* Tests did not reach ultimate failure, values shown are maximum shears

† Values calculated with pick-up loop capacity

‡ Value obtained at $a_s/2$

6.4.7.4 Variable Angle Truss Model (VATM)

The VATM did not take into account any concrete strength or vertical prestressing steel. It was used to estimate the ultimate capacity of each section along with determining the stress in the prestressing strands. The method and results of the VATM are presented in section 6.2.4 and Figures 6.6 – 6.10. Table 6.16 gives the experimental and predicted results for the VATM.

As the stirrup spacing increased, the VATM became overly conservative. For Test E1, its test-to-predicted value was 1.10 at the time of unloading. For Test W1, the VATM had a test-to-predicted value of 2.24 at the time of unloading. Finally, for Test W2, the VATM had a test-to-predicted value of 3.43 at ultimate failure. Despite the inability to reach failure in the first two tests, it was seen that the VATM began greatly under-estimating the capacity of the sections as the stirrup spacing increased.

When the pick-up loop strength was added to the first two tests, the capacity of the sections greatly increased. This caused the test-to-predicted values for Tests E1 and W1 to be 0.79 and 0.99, respectively.

Table 6.16 VATM results

Test	Stirrups crossed	$V_{u\text{-}exp.}$ (kips)	$V_{n\text{-}pred.}$ (kips)	$V_{u\text{-}exp} / V_{n\text{-}pred}$
Test E1*	13	653	593	1.10
			832†	0.78
Test W1*	5	569	254	2.24
			577†	0.99
Test W2	4	580	169	3.43

* Tests did not reach ultimate failure

† Values were calculated using pick-up loops

6.4.7.5 Summary

All four methods observed in this research provided conservative predictions of the concrete cracking and ultimate shear capacity. Tests E1 and W1 were used to compare concrete cracking strengths, and Test W2 was used to compare the ultimate capacity predictions.

For the concrete cracking shear strength, the AASHTO Standard Specifications and ACI Alternate methods were the most accurate. The AASHTO Standard Specifications were more conservative than the ACI Alternate method, and they remained conservative for the three tests. The ACI Alternate was more accurate for Test E1, but became unconservative for Tests W1 and W2. The AASHTO LRFD Specifications were extremely conservative when the calculated concrete shear contributions were compared to the experimental cracking shear strengths.

For ultimate concrete strength, both the AASHTO Standard and AASHTO LRFD methods produced conservative values. For Test W2, the AASHTO Standard Specifications gave a ratio of test-to-predicted ultimate strength of 1.48 while the LRFD Specifications gave a ratio of 1.38. The VATM grossly under-predicted the ultimate shear capacity of Test W2 with a ratio of 3.43 due to the larger stirrup spacing. For Tests E1 and W1, it was unknown how conservative any of the prediction methods would have been.

The AASHTO LRFD method and VATM experienced large contributions from the pick-up loops because both incorporated compression crack angles that crossed all four pick-up loop regions. Because neither test was tested to failure, it was impossible to determine the real effect of the pick-up loops.

Table 6.17 and Figure 6.59 show the overall cracking shear results for the three tests. The LRFD predictions for cracking shear were not shown in Figure 6.59 because the concrete shear strength, V_c, was not meant to predict the cracking shears of concrete girders. From Figure 6.59, it can be seen that the ACI Alternate method became unconservative for Tests W1 and W2 while the AASHTO Standard Specifications remained accurate and conservative. Table 6.18 shows the overall ultimate shear results for all three tests. The values shown for the AASHTO LRFD Specifications were the values obtained using the interpolated compression angle, θ. This was done so that comparisons could be made with other research that did not use the physically measured angles to predict shear capacities. It is important to remember that Tests E1 and W1 were not tested to failure and their results cannot be compared with Test W2.

Table 6.17 Total cracking shear results

Test	$V_{c\text{-}Exp.}$	V_{cw} AASHTO Standard (kips)	V_c AASHTO LRFD (kips)	V_{cw} ACI Alternate (kips)	Test / Standard	Test / LRFD	Test / ACI Alt.
E1	350	308	89	344	1.14	3.93	1.02
W1	311	306	91	344	1.02	3.42	0.90
W2	311	299	141	330	1.04	2.21	0.94

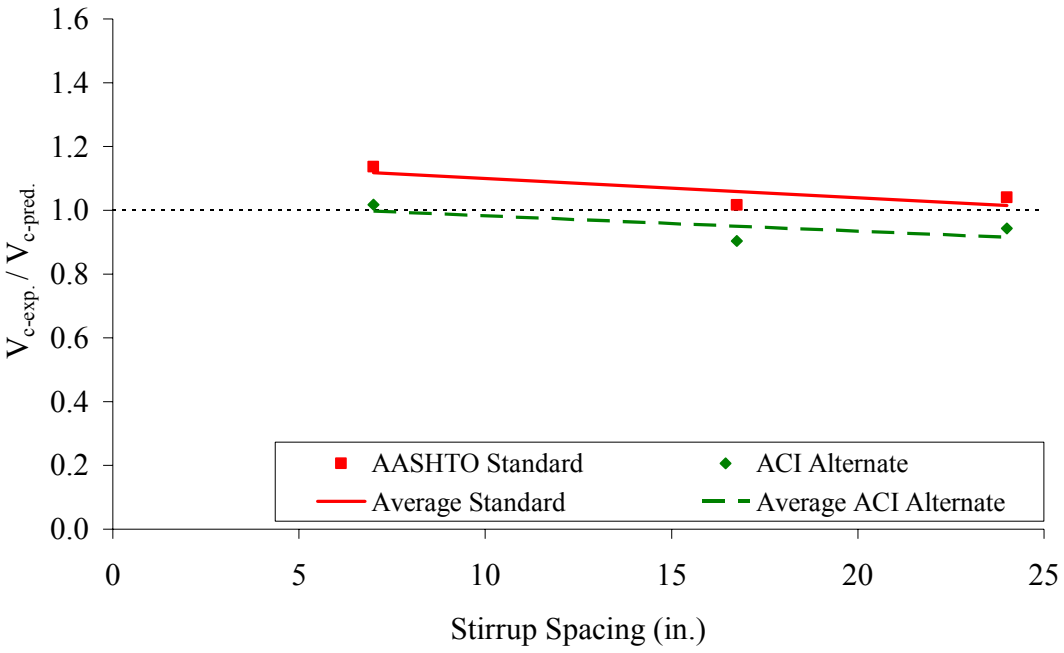

Figure 6.59 Cracking shear comparison

Table 6.18 Total ultimate shear results

Test	$V_{u\text{-}Exp.}$	V_n AASHTO Standard (kips)	V_n AASHTO LRFD (kips)	VATM (kips)	Test / Standard	Test / LRFD	Test / VATM
E1*†	653	623	696	593	1.05	0.94	1.10
E1*‡		698	902	832	0.94	0.72	0.78
W1*†	569	539	601	254	1.06	0.95	2.24
W1*‡		614	866	577	0.93	0.66	0.99
W2†	580	390	425	169	1.49	1.36	3.43
W2††		392	421	169	1.48	1.38	3.43

* Tests did not reach ultimate failure

† Test values were calculated without added pick-up strap capacity.

‡ Test values were calculated with added pick-up strap capacity.

† Values were calculated at code defined critical sections.

†† Values were calculated at the center of the shear span (71.5 in.)

6.4.8 Comparison with Other Research

The experimental and the AASHTO Standard (2002), AASHTO LRFD (1998), and AASHTO LRFD (2004) predicted results from this research were compared with the research results that are discussed in Chapter 2. The normalized experimental cracking and ultimate shear strengths from all pertinent research were compared versus their shear reinforcement ratios, effective depths, prestressing ratios, and concrete strengths. The $\rho_v f_y$ was studied to determine if the code equations adequately considered the effect of transverse reinforcement. The concrete compressive strength comparison would show if high strength/ high performance concretes were correctly considered. The ω_p comparisons showed the influence of prestressing force on the accuracy of the predictions – whether lightly reinforced girders gave similar shear strength results as heavily reinforced girders. The effect of "d_p" distances was also compared to determine if the doce equations accurately incorporate the size of various girders.

Test-to-predicted values were compared for both cracking and ultimate shear strengths. The test-to-predicted values were plotted against $\rho_v f_y$, concrete strength, and ω_p to determine how the three different properties affected the accuracy of both the AASHTO Standard and AASHTO LRFD Specifications. Equations 6.38 and 6.39 show the equations used to obtain $\rho_v f_y$ and ω_p.

$$\rho_v f_y = \frac{A_v f_y}{b_w s} \tag{6.38}$$

$$\omega_p = \frac{A_{ps} f_{ps}}{b d_p f_c'} \tag{6.39}$$

Where,

A_{ps} = Area of prestressing steel
A_v = Area of shear steel
b = Width of compression face of member
b_w = Width of concrete web
d_p = distance from extreme compression fiber to centroid of prestressed reinforcement
f_c` = Concrete strength of compression zone in concrete member
f_{ps} = Stress in the prestressing strands at nominal moment, psi
f_y = Actual yield stress of shear steel, psi
s = stirrup spacing

6.4.8.1 AASHTO Standard (2002)

The test-to-predicted values for the AASHTO Standard Specifications were compared to different research results that used the same Specifications. The values obtained from the different research were not re-calculated because there were no changes made to the Standard Specifications during the time of any of the research.

Figures 6.60 and 6.61 plot the test-to-predicted values versus $\rho_v f_y$ for cracking and ultimate shear.

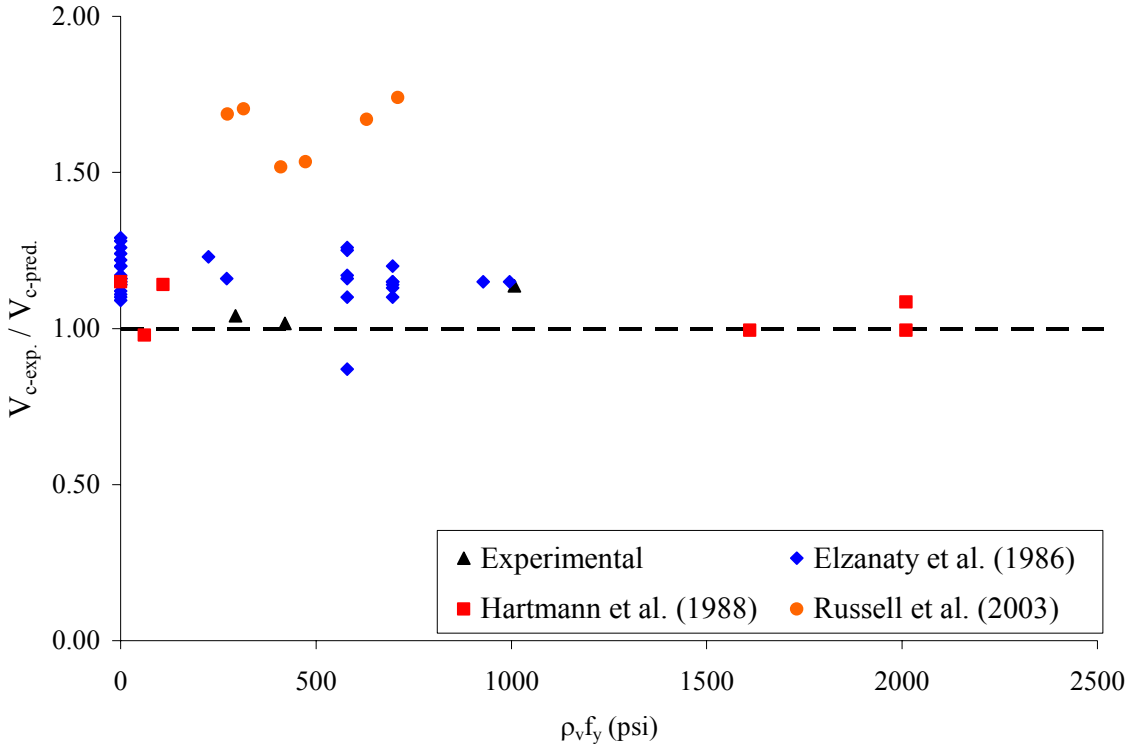

Figure 6.60 AASHTO Standard cracking shear vs. $\rho_v f_y$

The cracking shear strength of the HPC prestressed girders was accurately predicted by the AASHTO Standard Specifications. The trend in the data showed that the Standard Specifications remained conservative with any amount of shear steel. The plot also showed that the results obtained from Tests E1 and W1 closely matched the results from Elzanaty et al. (1986). The test-to-predicted values given by Russell et al. (2003) were more conservative than the other examined research.

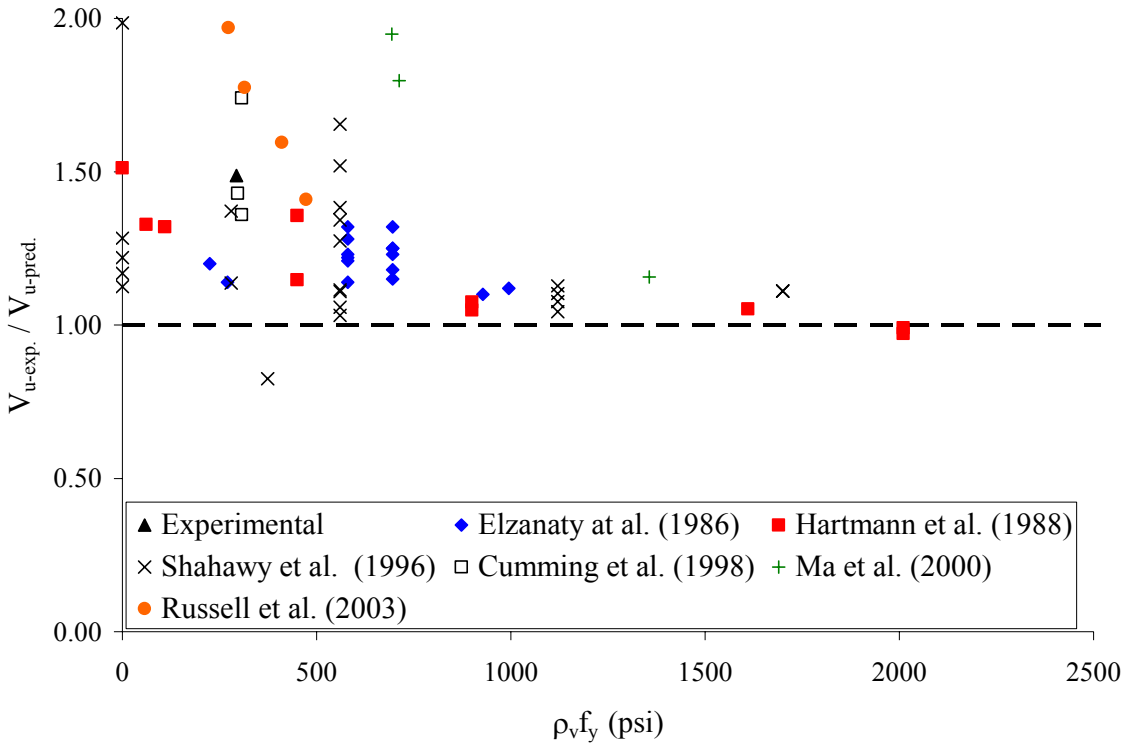

Figure 6.61 AASHTO Standard ultimate shear versus $\rho_v f_y$

As the amount of shear steel increased, the AASHTO Standard Specifications became less conservative in predicting V_u. Test W2 provided an ultimate test-to-predicted value of 1.48 at $a_s/2$, which matched what was found by Cumming et al. (1998). Both research programs tested large HPC prestressed girders and found the same amount of accuracy. The research performed by Hartmann et al. (1988) tested the ultimate capacity of small Type I sections that contained up to 3 times the amount of recommended shear steel. Even with the high amount of shear reinforcment, the Specifications were only slightly un-conservative.

Figures 6.62 and 6.63 plot the test-to-predicted values versus concrete strength for cracking and ultimate shear.

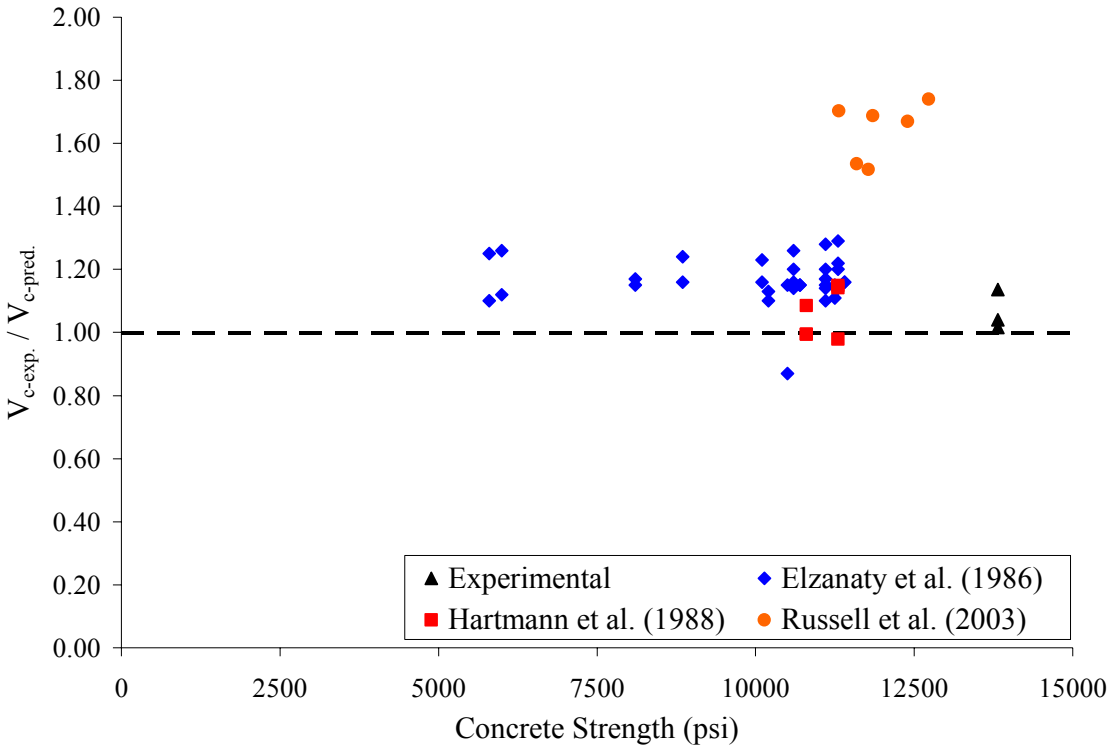

Figure 6.62 AASHTO Standard cracking shear versus concrete compressive strength

Cracking shear strength was predicted uniformly for concrete strengths between 6,000 and 13,000 psi. The test-to-predicted values for Tests E1 and W1 were very similar to the test-to-predicted values obtained from Elzanaty et al. (1986). Tests E1 and W1 had concrete strengths over 13,000 psi and Elzanaty et al. (1986) had concrete strengths as low as 6,000 psi. This demonstrated that concrete strength was accurately considered in the AASHTO Standard Specifications.

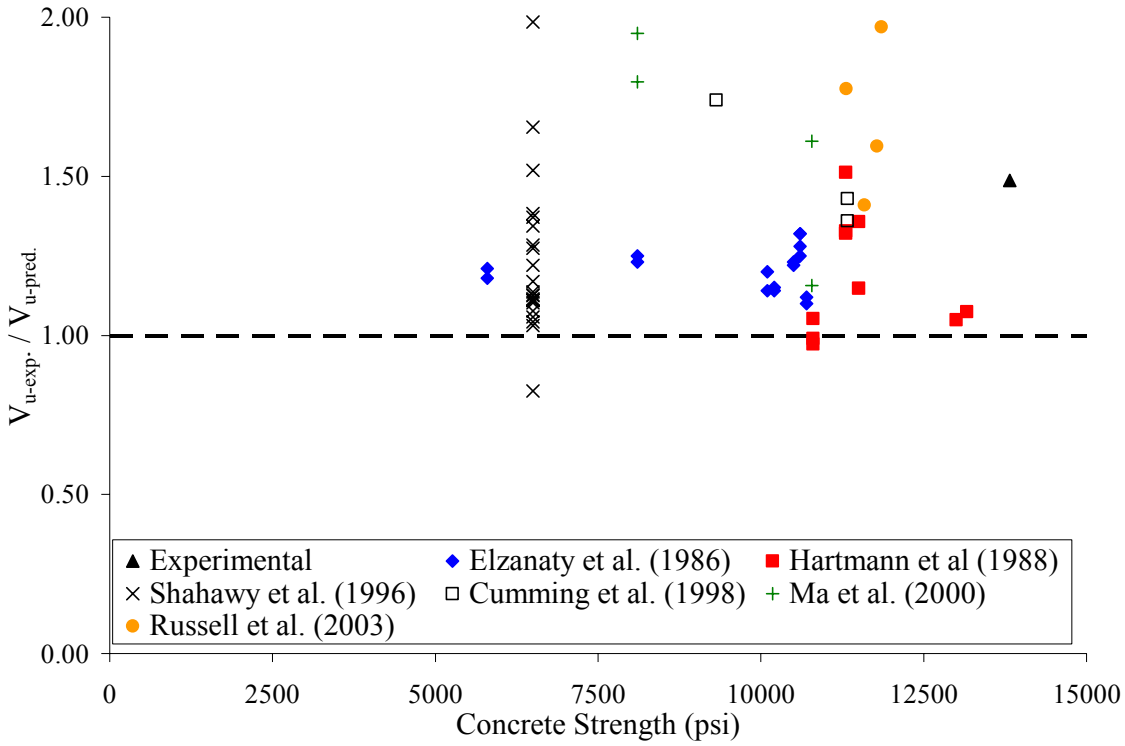

Figure 6.63 AASHTO Standard ultimate shear versus concrete strength

As with the cracking shear results, the change in concrete compressive strength did not display a specific trend for ultimate shear strength. The Specifications remained conservative through the range of concrete strengths. Therefore, the code was applicable for concrete strengths as high as 13,000 psi.

Figures 6.64 and 6.65 plot the test-to-predicted values versus ω_p for cracking and ultimate shear. Plotting the test-to-predicted values versus ω_p determined the effect that the amount of prestressing had on the shear capacities of the specimens.

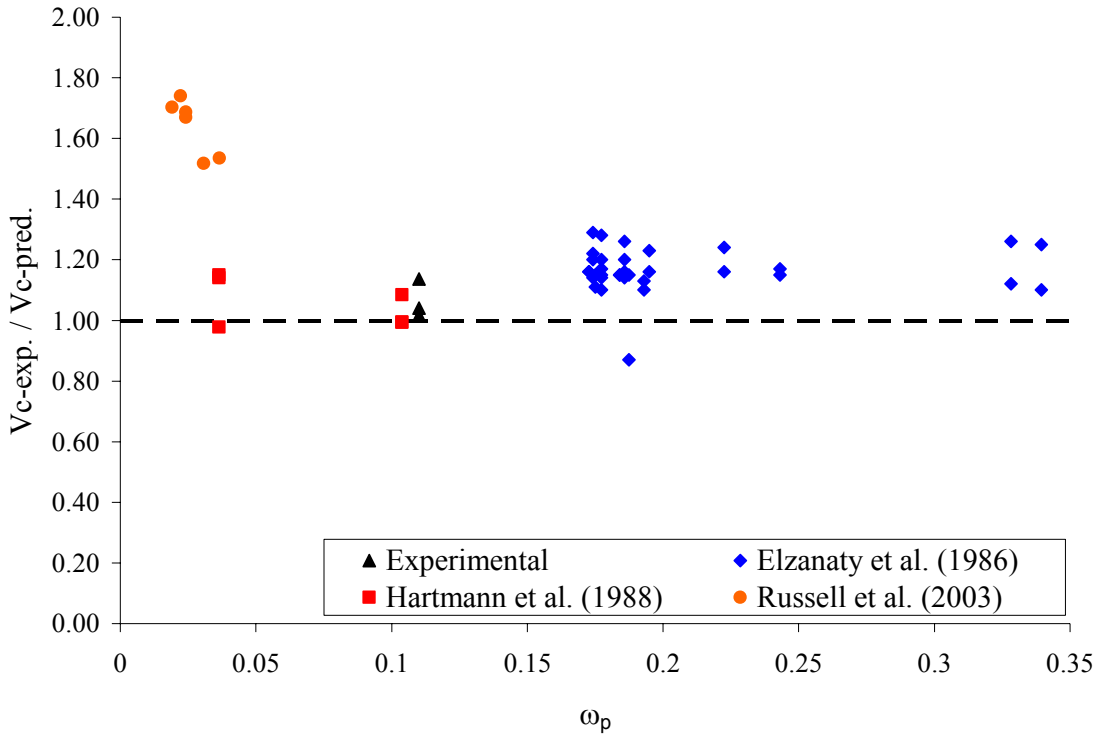

Figure 6.64 AASHTO Standard cracking shear versus ω_p

The amount of prestressing present in the specimen was examined to attempt to explain the high cracking test-to-predicted ratios obtained by Russell et al. (2003). It was seen that the specimens used in Russell's research had a relatively small amount of prestressing. However, the research performed by Hartmann also had small amounts of prestressing, and the code equations demonstrated much more accurate predictions. Therefore, the high values obtained by Russell et al. (2003) could not be explained. From the cracking plot, it was seen that the amount of prestressing did not cause the AASHTO Standard Specifications to have any change in accuracy. The data from Tests E1 and W1 closely matched the data from Hartmann et al. (1988), which tested Type I girders.

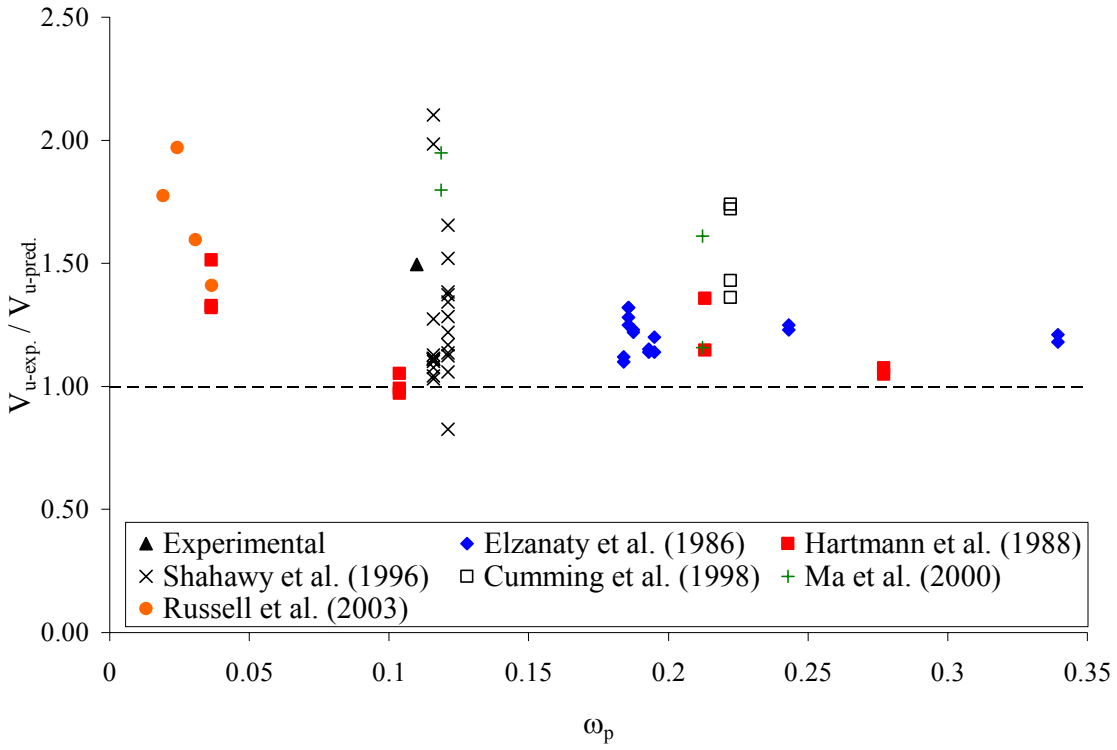

Figure 6.65 AASHTO Standard ultimate shear versus ω_p

The amount of prestressing did not seem to have an affect on the accuracy of the AASHTO Standard Specifications for ultimate shear strength. The Specifications remained conservative for both lightly and heavily prestressed girders. Once again, the size of the specimens did not seem to play a part in the accuracy of the Specifications at ultimate. The results from Test W2 most closely matched the results from Hartmann et al. (1988) and Shahawy et al. (1996).

6.4.8.2 AASHTO LRFD (1998)

The data obtained from previous research were calculated based on the AASHTO LRFD Specifications (1998). To compare the data from this study to previous listed results, the shear capacities for Tests E1, W1, and W2 were calculated using the 1998 LRFD Specifications. The 1998 LRFD Specifications were slightly more difficult to use than the 2004 LRFD Specifications because the calculated critical section depended on the interpolated compression angle. Therefore, every time the compression angle changed, the critical section changed and caused the need for recalculation of all shears and moments. The LRFD cracking comparisons demonstrated that the LRFD Specifications did not intend the concrete shear contribution to be used as an indicator of concrete cracking shears. The experimental cracking shears and LRFD calculated concrete shear contributions were also compared for comparison with other research. From this research, the test-to-predicted ratios based on the LRFD interpolated compression angles were compared to all other research.

Figures 6.66 and 6.67 show the cracking and ultimate shear capacities versus the reinforcement ratios.

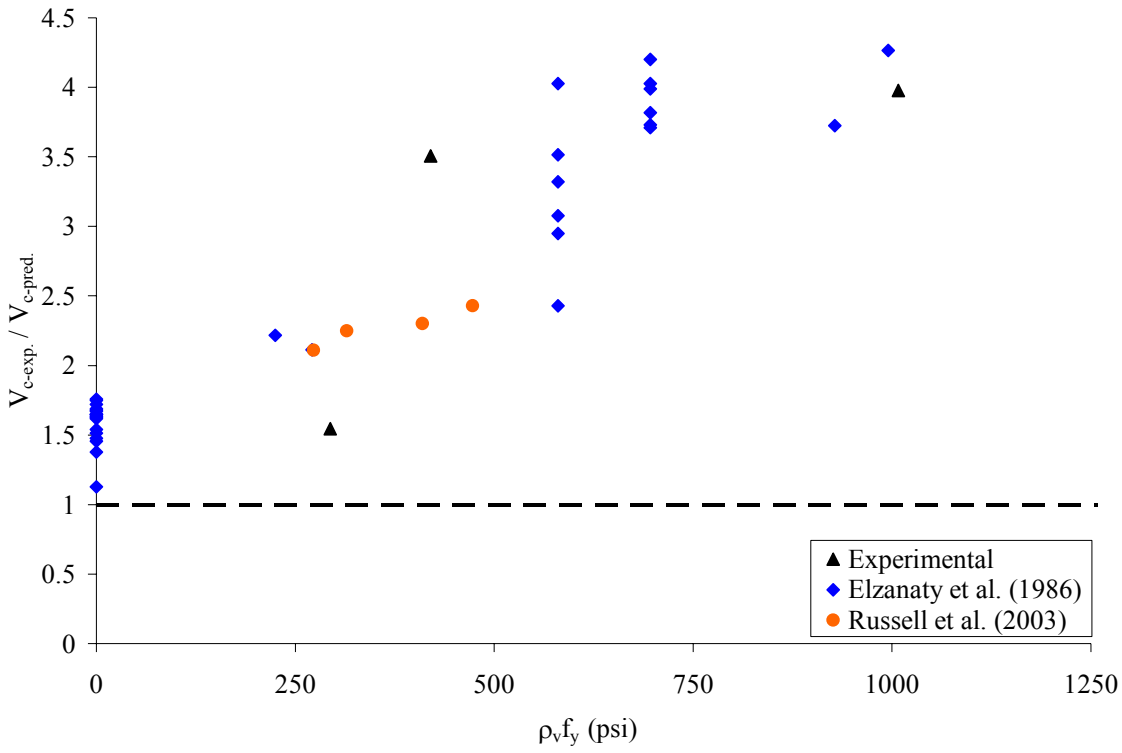

Figure 6.66 1998 AASHTO LRFD cracking shear vs. $\rho_v f_y$

The 1998 LRFD cracking shear was not accurate for any ratio of shear reinforcement. It under-predicted the concrete shear strength at an increasing rate as the shear reinforcement ratio increased. This showed that the LRFD Specifications were not a good indicator of the concrete cracking shear strength, which was expected.

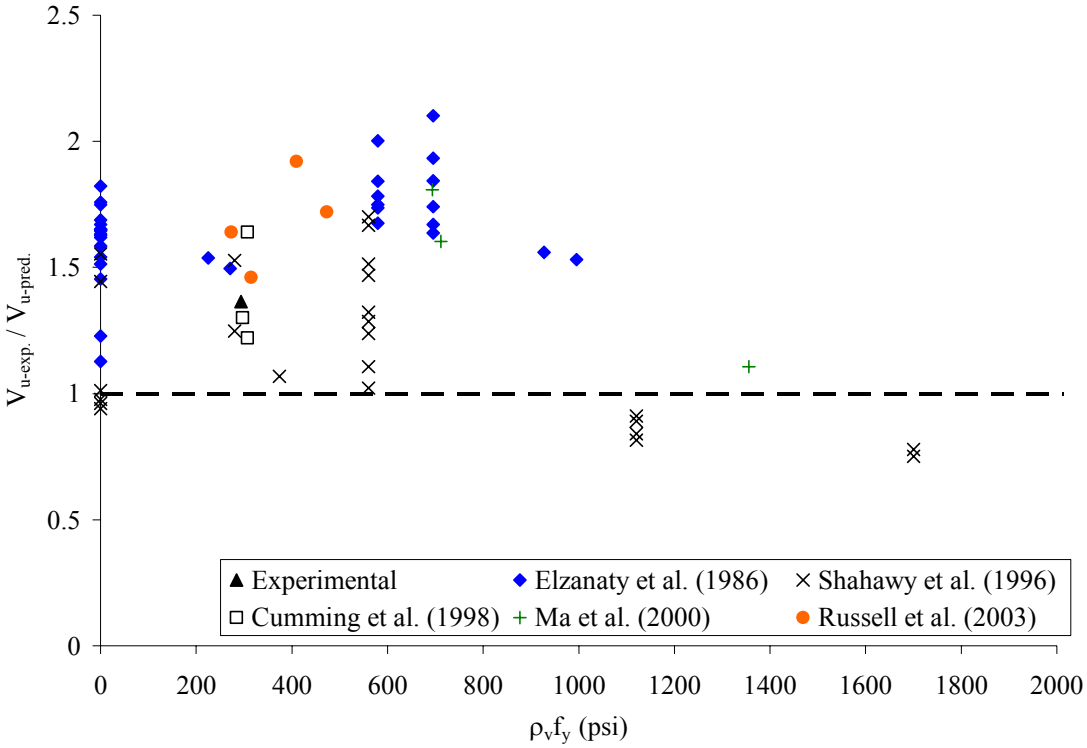

Figure 6.67 1998 AASHTO LRFD ultimate shear vs. $\rho_v f_y$

The LRFD Specifications were conservative for all tests that contained normal design amounts of shear reinforcement. When the shear reinforcement was extremely high, and surpassed 1000 psi, some values were unconservative. The general trend for the 1998 LRFD Specifications showed that as the reinforcement ratio increased, the conservative nature of the Specifications decreased. The maximum reinforcement given by the LRFD Specifications would equal about 1000 psi.

Figures 6.68 and 6.69 show the 1998 LRFD shear capacities versus concrete strength. No general trend was observed that linked the concrete strength to the accuracy of the LRFD Specifications. The experimental values from this research had the highest concrete strengths, but matched the values obtained from Elzanaty et al. (1986) with the lowest concrete strengths.

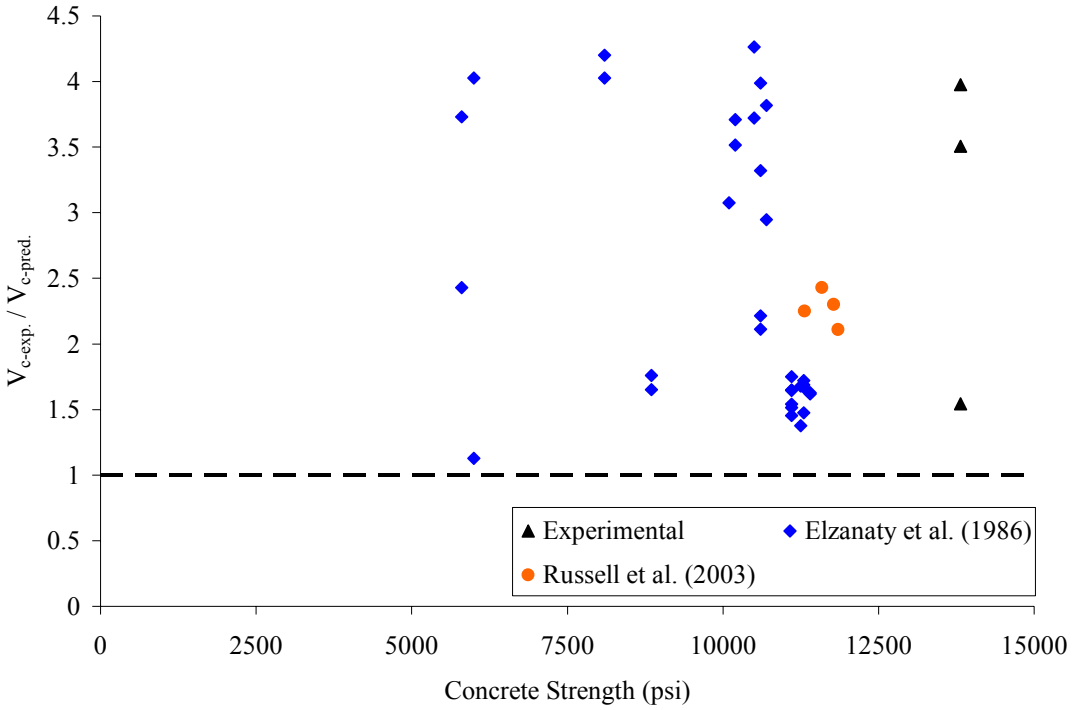

Figure 6.68 1998 AASHTO LRFD cracking shear vs. concrete strength

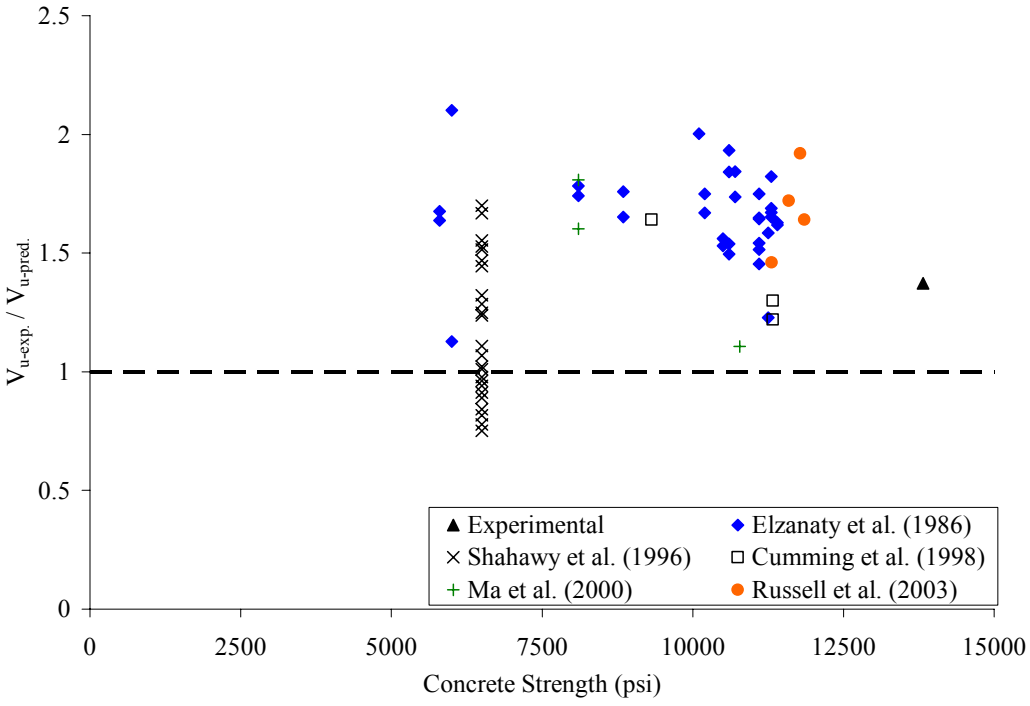

Figure 6.69 1998 AASHTO LRFD ultimate shear vs. concrete strength

Figures 6.70 and 6.71 show the 1998 LRFD Specifications versus the prestressing ratio, ω_p. As with the concrete strength, the amount of prestressing in the tested specimens did not have an effect on the accuracy of the Specifications.

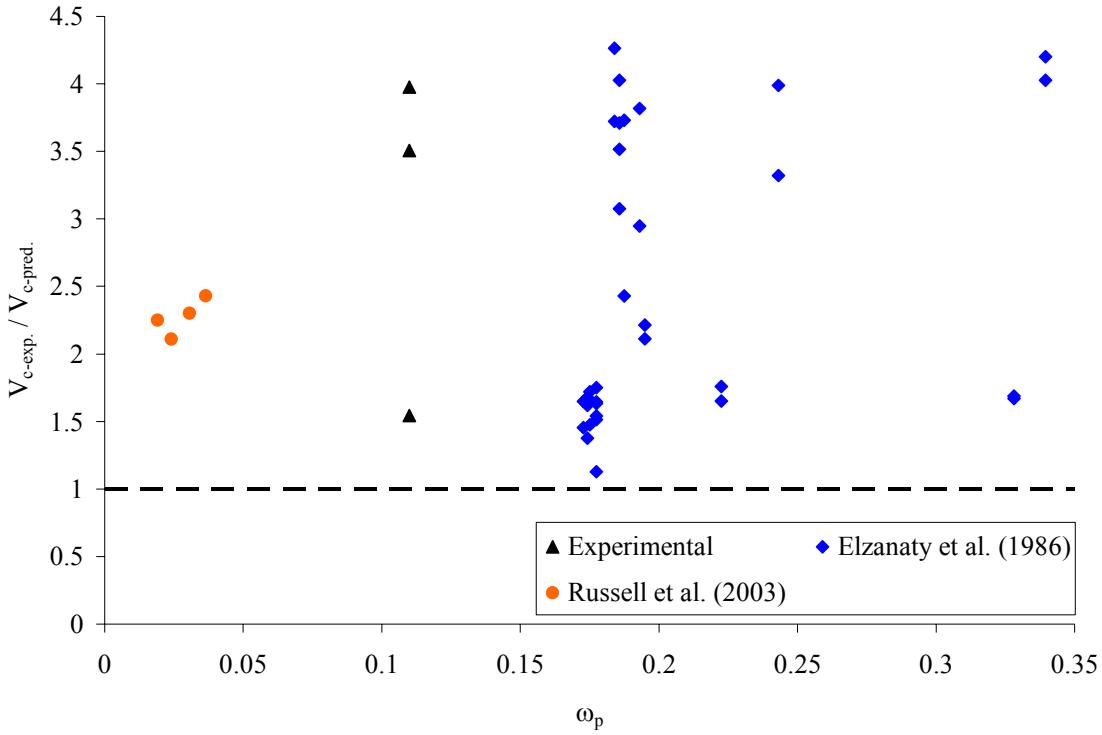

Figure 6.70 1998 AASHTO LRFD cracking shear vs. ω_p

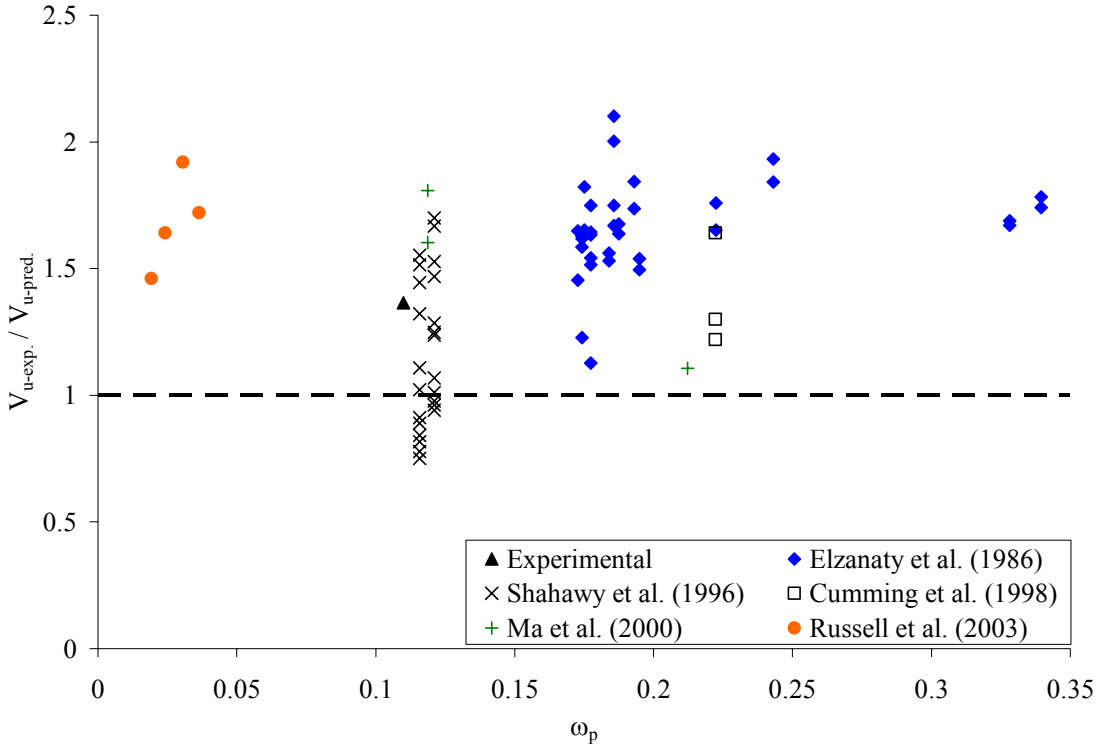

Figure 6.71 1998 AASHTO LRFD ultimate shear vs. ω_p

6.4.8.3 AASHTO LRFD (2004)

The data obtained from Chapter 2 was based on the 1998 AASHTO LRFD Specifications. Significant changes were made with the LRFD Specifications between 1998 and 2004. Therefore, all shear values obtained from previous research were recalculated using the 2004 LRFD Specifications in order to examine the accuracy of the new, revised Specifications. The method used to calculate the shear capacities based on the 2004 LRFD Specifications are presented in section 6.2.3. Measured properties were used to calculate the new shear capacities for each research specimen. When the section of failure was reported, the shear capacity was taken at that location to compare experimental values with predicted values. When the section of failure was not given, the

critical section was taken close to the point of maximum moment to obtain a more conservative value. From this research, the predicted shear capacities using the compression crack angles interpolated from LRFD figure 5.8.3.4.2-1 were used to compare shear capacities with other research. This was done because it was understood that all other research used the interpolated compression angles, not the physically measured angles from testing. The cracking comparisons only demonstrated that the LRFD Specifications did not intend the concrete shear contribution to be used as an indicator of concrete cracking shears.

Figures 6.72 and 6.73 show the shear capacities versus the reinforcement ratios for the 2004 LRFD Specifications.

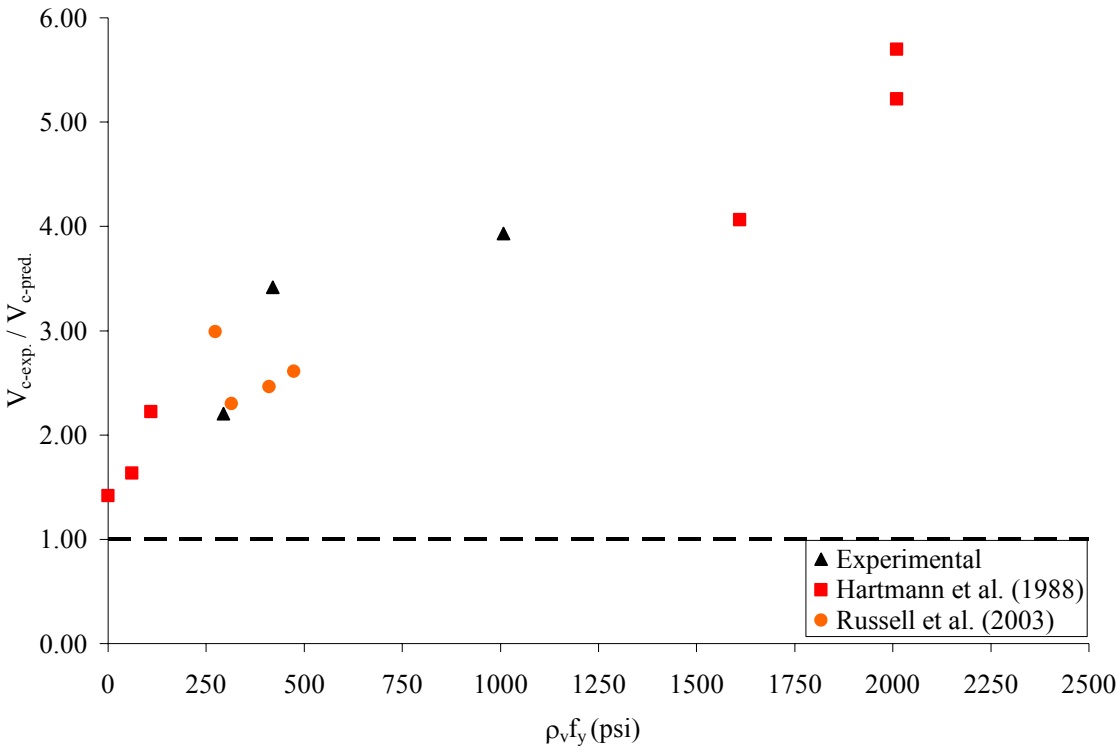

Figure 6.72 2004 AASHTO LRFD cracking shear vs. $\rho_v f_y$

As with the 1998 LRFD Specifications, the calculated concrete shear contributions were much lower than the experimental cracking shears. For normal design amounts of reinforcement ($\rho_v f_y \leq 1{,}000$ psi), the LRFD Specifications provided test-to-predicted values up to 4.0. It is important to note that the data obtained from Hartmann et al. (1988) had reinforcement ratios up to 3 times the maximum permitted design amount ($8\sqrt{f_c'}b_w d$), which was why values up to 6.0 were observed.

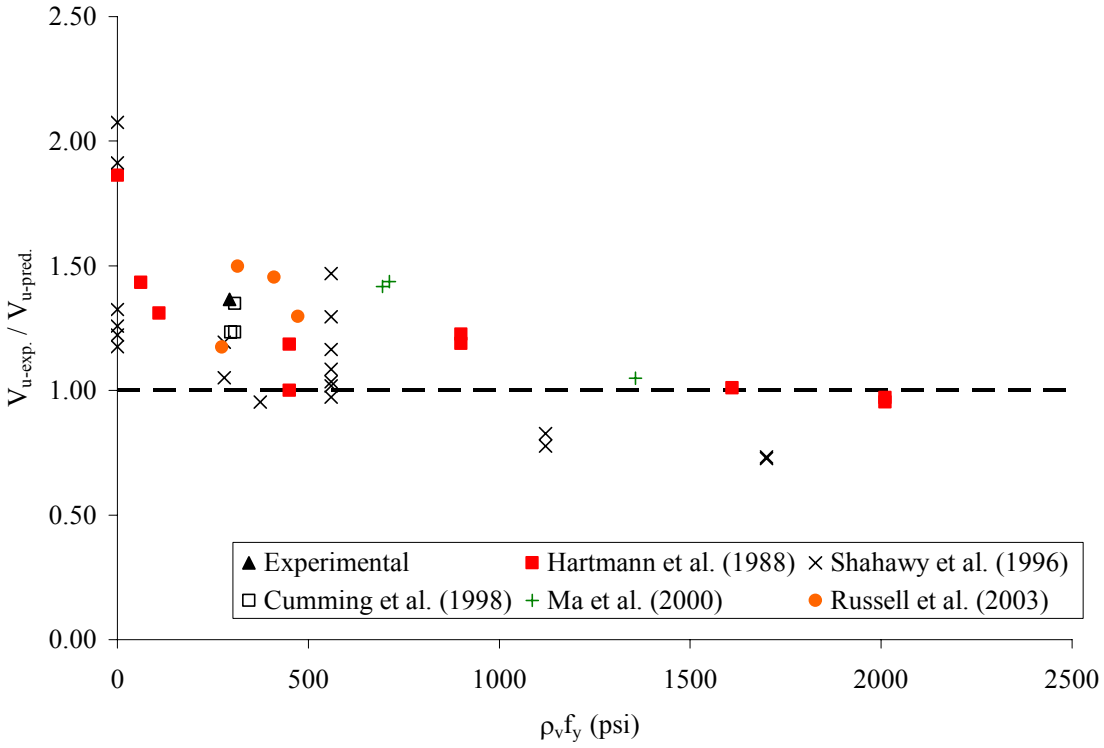

Figure 6.73 2004 AASHTO LRFD ultimate shear vs. $\rho_v f_y$

The 2004 LRFD Specifications predicted ultimate shear capacities that were mostly conservative. As the amount of transverse steel increased, the conservative nature of the Specifications decreased. The Specifications were conservative and accurate when

shear reinforcement ratios remained below 1,000 psi. However, when the ratios surpassed 1,000 psi, the LRFD Specifications became slightly un-conservative.

Figures 6.74 and 6.75 show the 2004 LRFD test-to-predicted values versus concrete strength. As with the 1998 Specifications, there was no apparent trend when comparing the effects that the concrete strength had on the test-to-predicted values given by the Specifications. The LRFD seemed as accurate for high strength as for normal strength concretes.

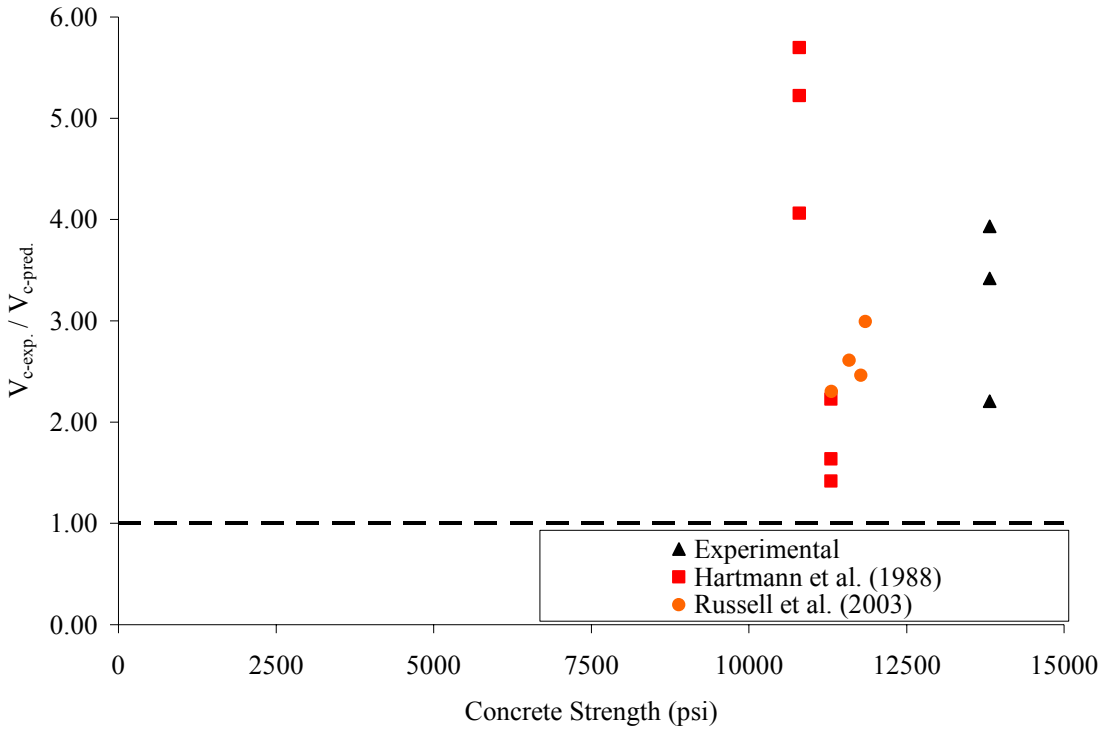

Figure 6.74 2004 AASHTO LRFD cracking shear vs. concrete strength

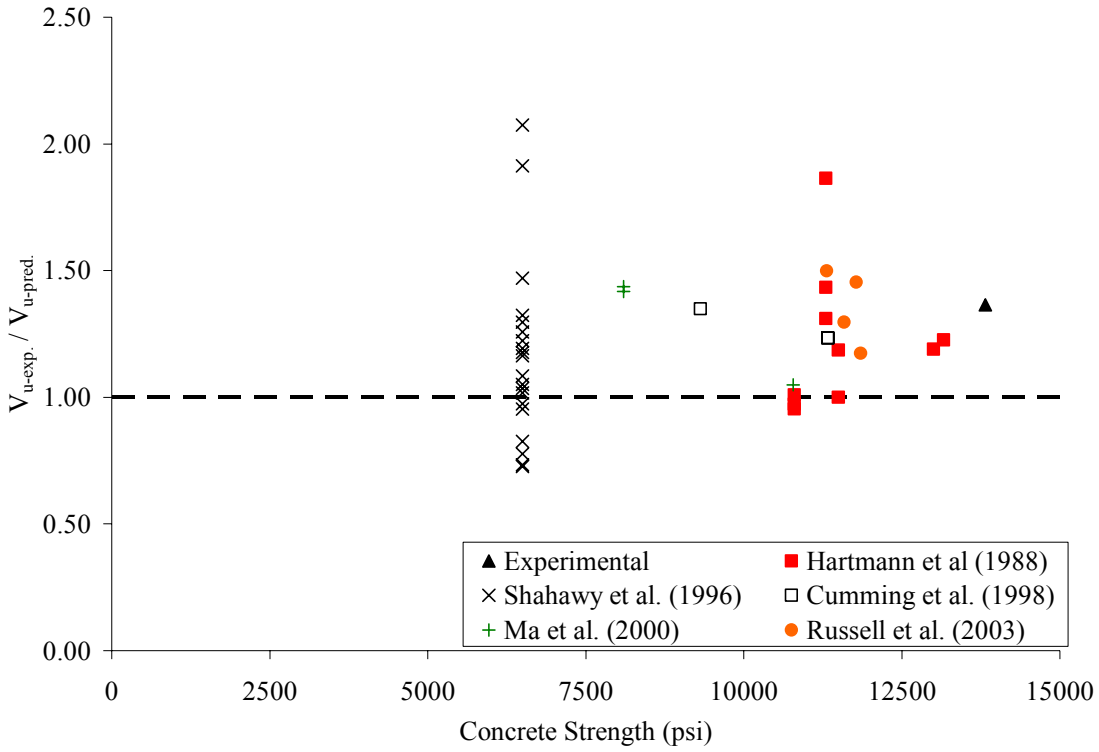

Figure 6.75 2004 AASHTO LRFD ultimate shear vs. concrete strength

Figures 6.76 and 6.77 show the 2004 test-to-predicted values versus the prestressing ratio, ω_p. The accuracy of the 2004 LRFD Specifications were independent of the amount of prestressing contained in the tested specimens for cracking and ultimate.

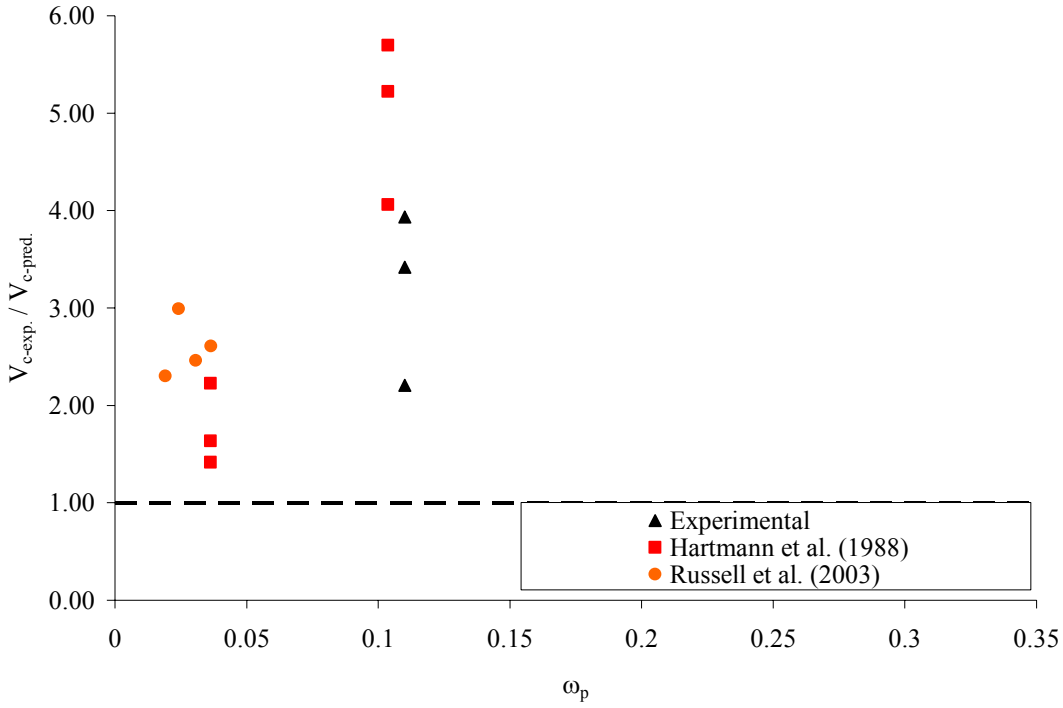

Figure 6.76 2004 AASHTO LRFD cracking shear vs. ω_p

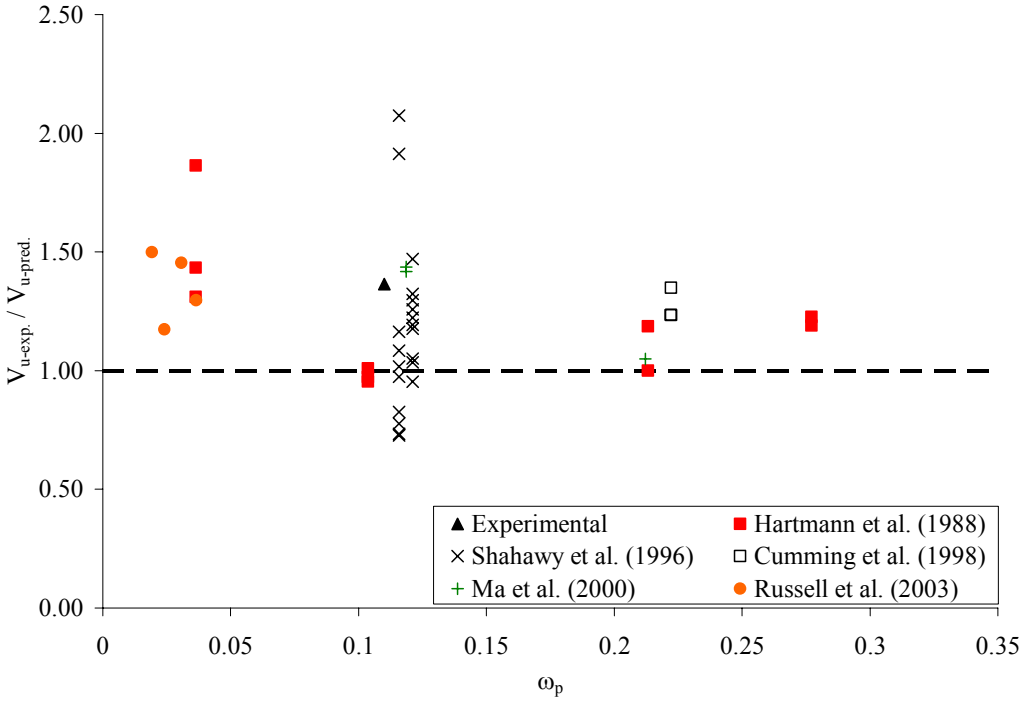

Figure 6.77 2004 AASHTO LRFD ultimate shear vs. ω_p

6.4.8.4 Specification Comparisons

This section examines the overall accuracy of the AASHTO Standard (2002), AASHTO LRFD (1998) and AASHTO LRFD (2004) Specifications for both concrete shear strength, V_c, and ultimate shear strength, V_n. The available data were used for each Specification and trend lines were produced for each set of data. The Specifications were compared using the shear steel reinforcement ratio, the concrete strength, and the amount of prestressing, ω_p.

Figures 6.78 and 6.79 show the comparison of the three Specifications versus the shear reinforcement ratio. The AASHTO Standard recommended maximum and minimum shear reinforcement ratios were placed on the chart to better represent the normal range of shear steel spacing. The maximum reinforcement ratio was calculated with the recommended $8\sqrt{f_c'}$ and a concrete compressive strength of 10,000 psi. Also, correlation values were given for each Specification to represent their relative data spread.

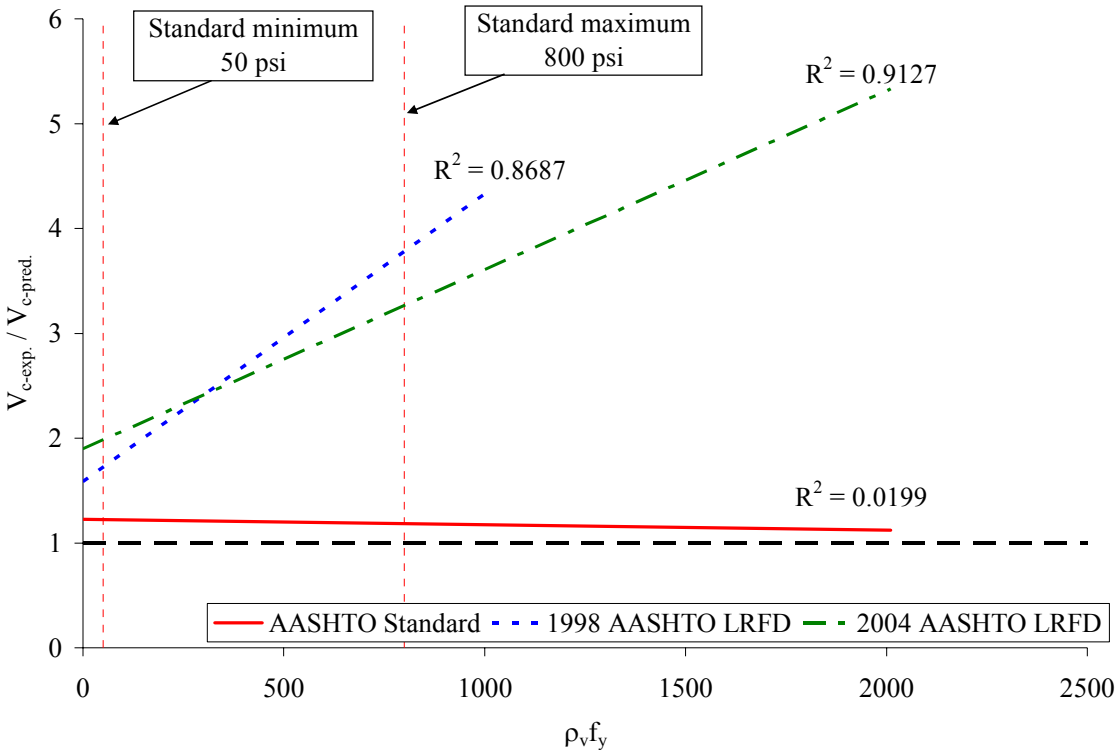

Figure 6.78 Cracking strength comparisons vs. $\rho_v f_y$

For cracking strengths, the AASHTO Standard Specifications were far superior to either edition of the LRFD Specifications. This was expected because AASHTO Standard was intended to predict the cracking strength of prestressed girders, while the AASHTO LRFD concrete shear contribution was not. Even when reinforcement ratios were 2 and 3 times the required design amount, the Standard Specifications were still accurate and conservative. The 2004 LRFD Specifications predicted the concrete shear capacity better than the 1998 Specifications, but was still extremely conservative. Because of the under-prediction of the concrete shear strength by both editions of the LRFD Specifications, it was determined that it would not be accurate to use the concrete shear contribution of either LRFD Specifications to predict cracking shear of prestressed girders.

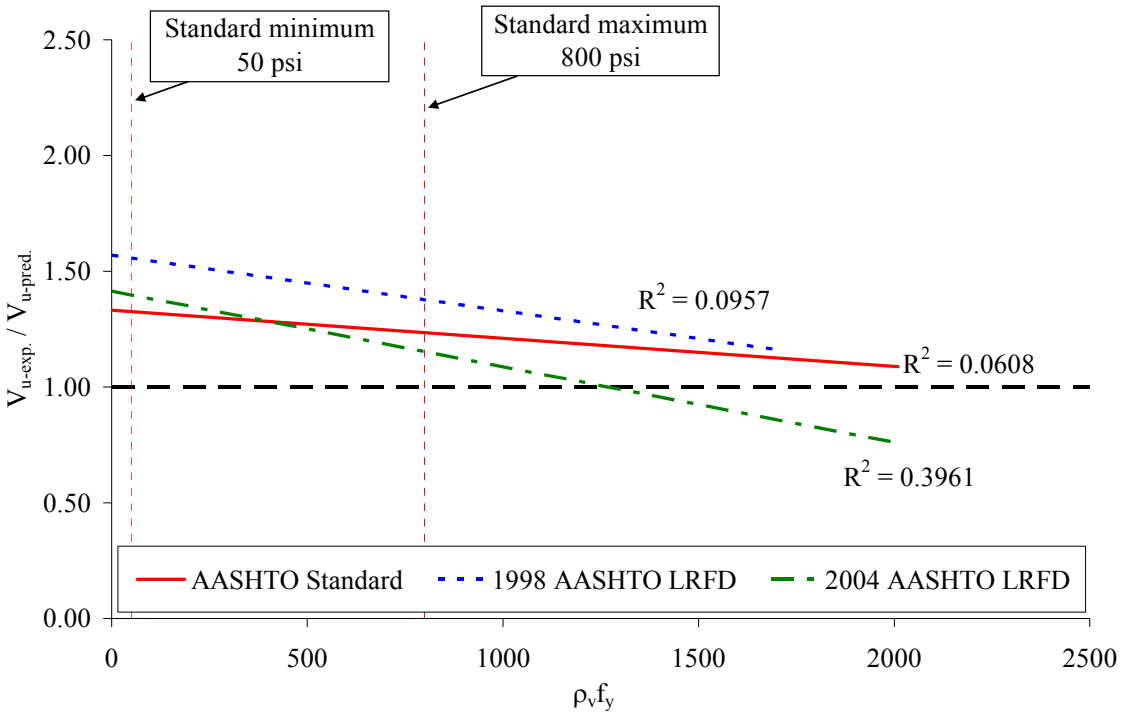

Figure 6.79 Ultimate strength comparisons vs. $\rho_v f_y$

For ultimate shear capacities, the AASHTO Standard Specifications were conservative and accurate at every level of shear reinforcement. The 1998 LRFD Specifications were conservative at every level of shear reinforcement; but it was less accurate than the Standard Specifications. There was some improvement seen in the 2004 LRFD Specifications over the 1998 LRFD Specifications. Within normal design parameters, it was seen that the 2004 LRFD Specifications became slightly more accurate than the AASHTO Standard Specifications. It only became un-conservative after a shear reinforcement ratio of 1,200 psi. The small correlation value for the AASHTO Standard Specifications were attributed to the large amount of research that used that method.

Figures 6.80 and 6.81 plot the cracking and ultimate test-to-predicted values versus concrete strength. There was no specific trend with any Specification, and they all remained conservative

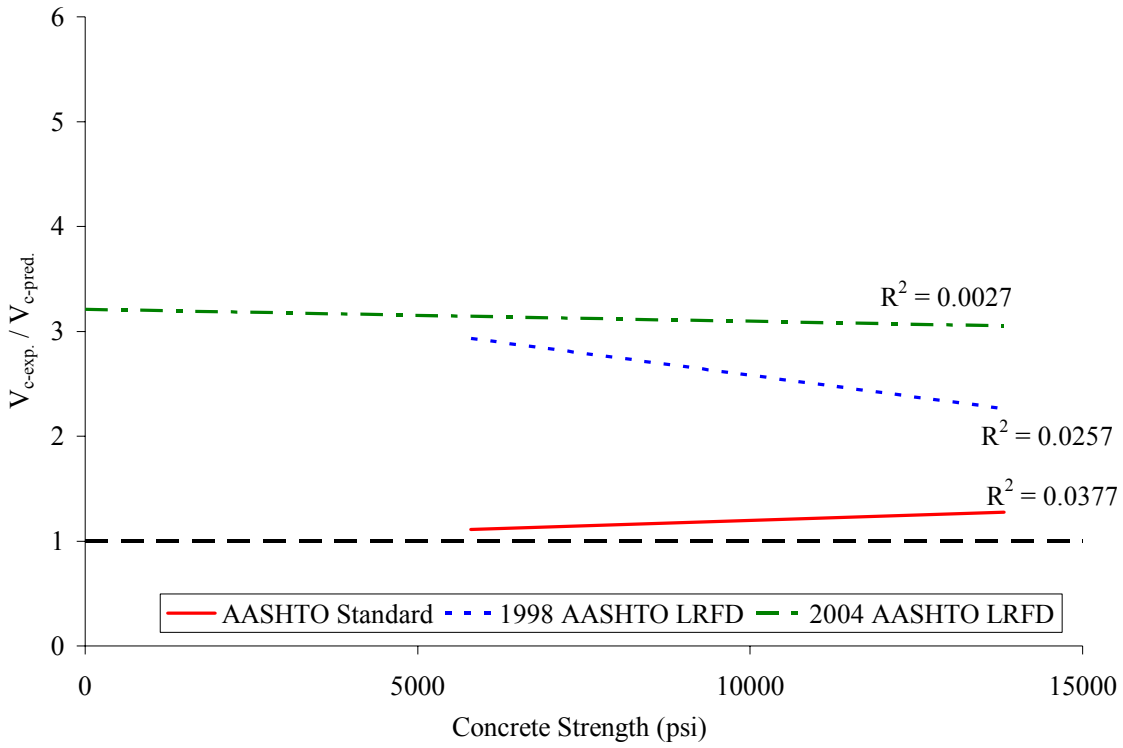

Figure 6.80 Cracking strength comparisons vs. concrete strength

The AASHTO Standard cracking predictions were accurate for all concrete strengths. The 2004 LRFD Specifications were less accurate than the 1998 LRFD Specifications when compared to concrete strength.

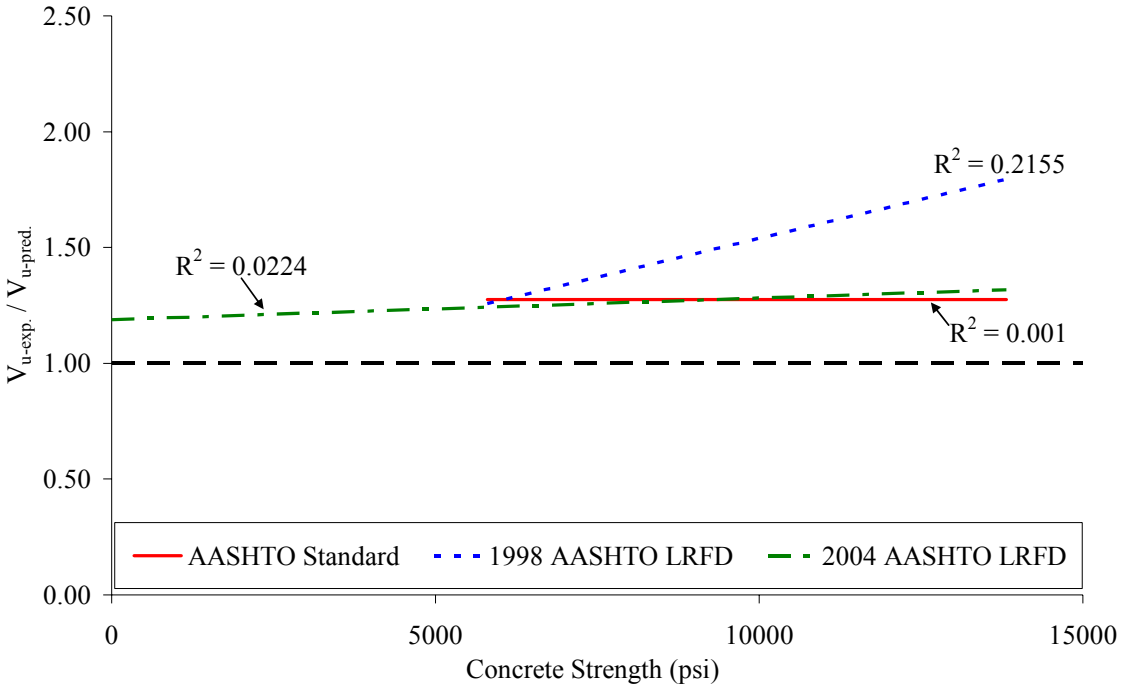

Figure 6.81 Ultimate strength comparisons vs. concrete strength

For ultimate, Figure 6.81 shows that the AASHTO Standard and 2004 LRFD Specifications uniformly considered concrete strength in their respective ultimate shear equations and that each gave a consistent and similar test-to-predicted ratio for concrete strengths from 6,000 psi to 13,000 psi.

Figures 6.82 and 6.83 present the cracking and ultimate test-to-predicted values versus the various prestressing ratios. For cracking, AASHTO Standard was accurate and conservative for all levels of prestressing. Both LRFD Specifications were overly conservative and similar. For ultimate shear capacity, all three methods were conservative. The AASHTO Standard and 2004 LRFD Specifications showed that as ω_p increased, the test-to-predicted ratios became closer to unity. The test-to-predicted ratio of the 1998 LRFD Specifications increased with increasing ω_p.

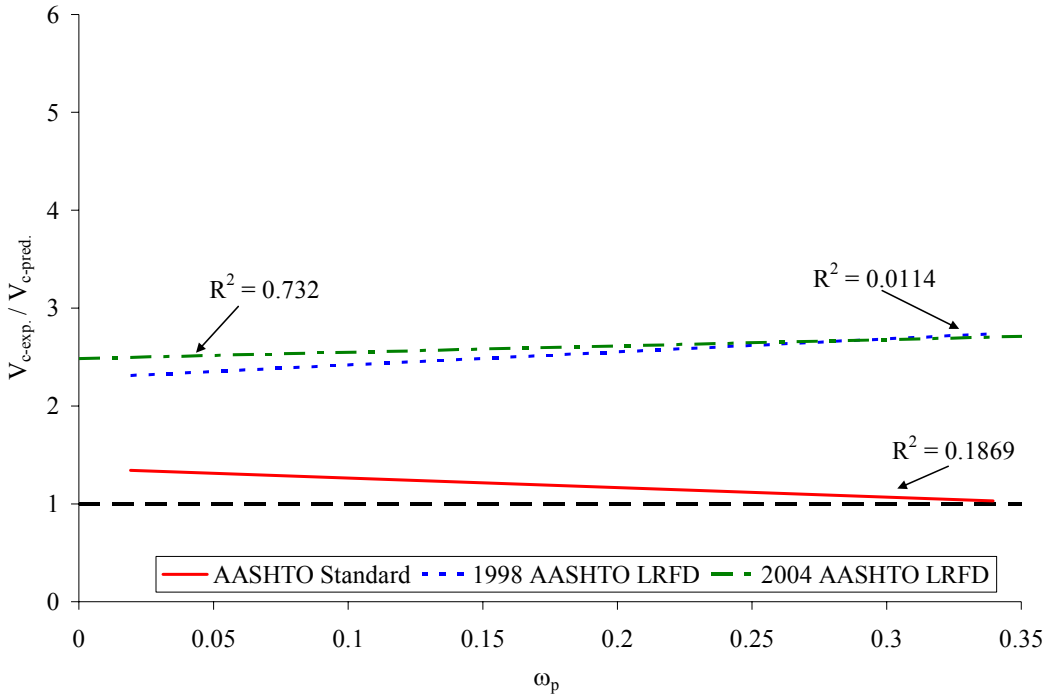

Figure 6.82 Cracking shear strength comparisons vs. ω_p

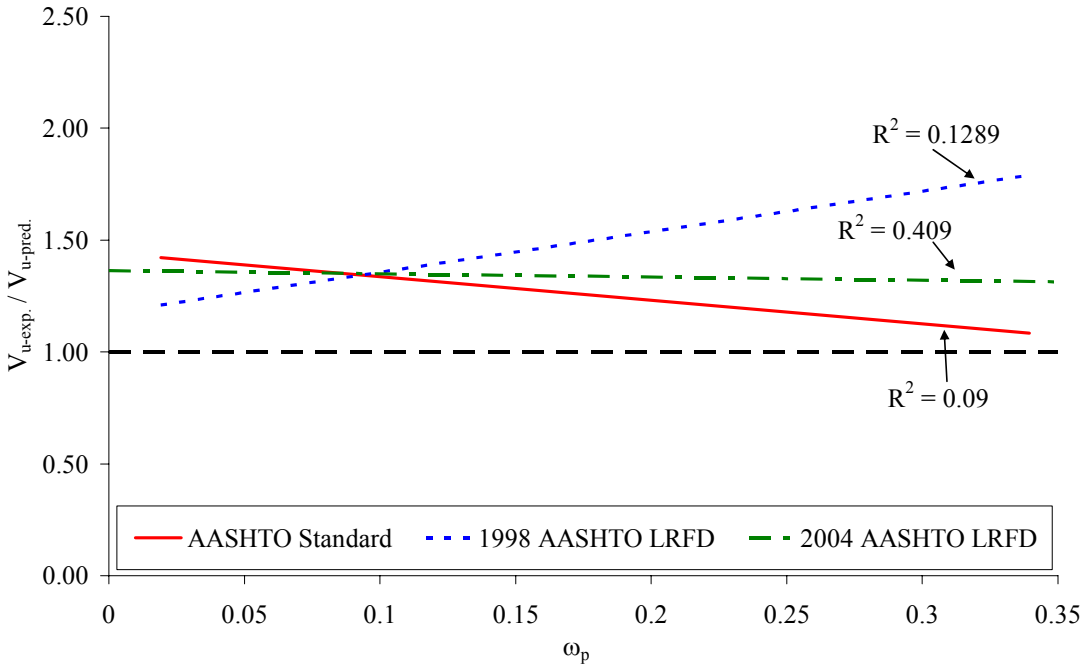

Figure 6.83 Ultimate shear strength vs. ω_p

6.4.8.5 Normalized Experimental Data Comparisons

This section presents normalized cracking and ultimate shear strength values plotted versus the shear reinforcement ratios, effective depths, prestressing ratios, and concrete strengths. These data were meant to show the shear behavior of various test specimens with many different properties. Figures 6.84 and 6.85 present the cracking and ultimate normalized values versus the shear reinforcement ratio, $\rho_v f_y$.

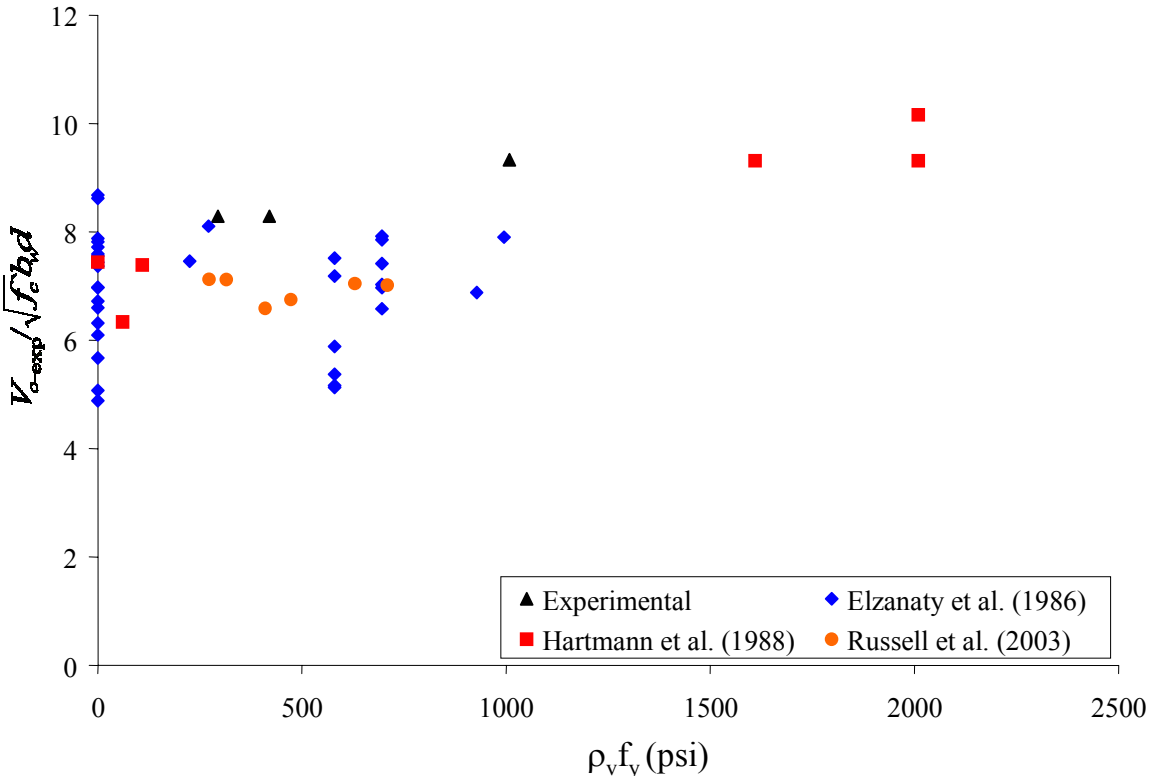

Figure 6.84 Experimental cracking shear versus $\rho_v f_y$

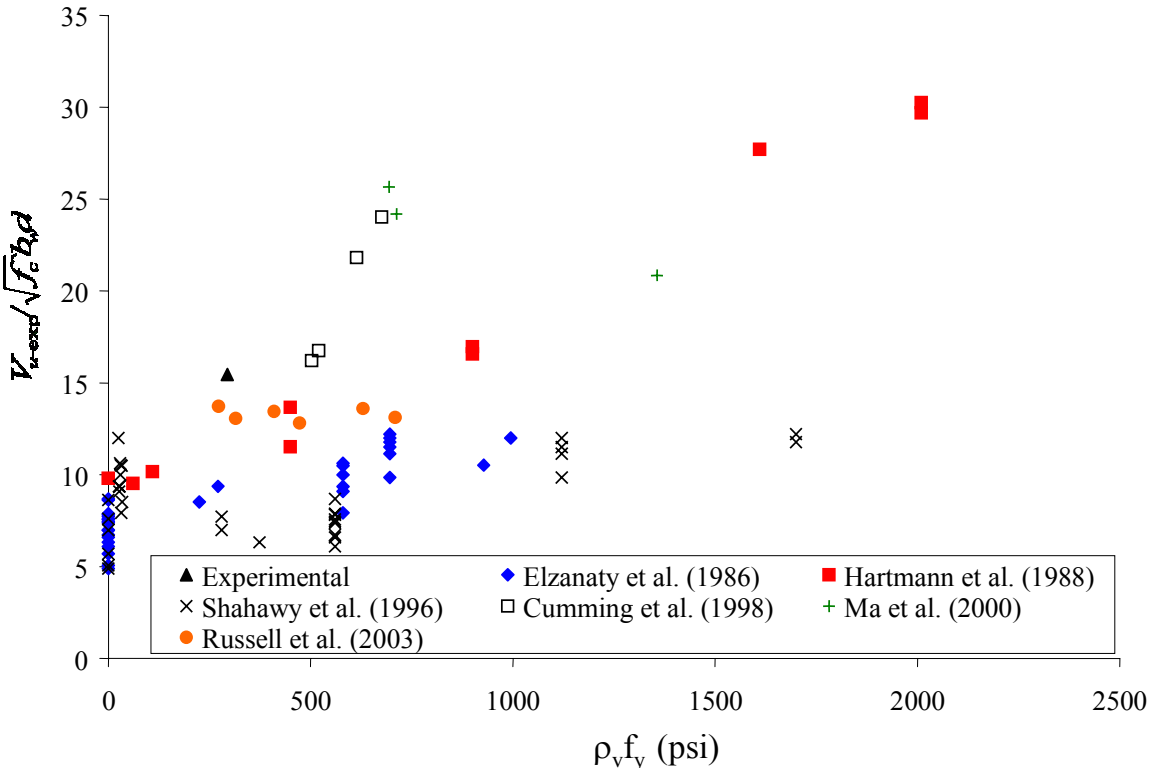

Figure 6.85 Experimental ultimate shears versus $\rho_v f_y$

Both the cracking and ultimate shear capacities slowly increased as the amount of shear reinforcement increased. This was significant for experimental cracking shears because currently, no methods to account for transverse shear reinforcement are provided when calculating concrete cracking shear capacities for prestressed girders.

Figures 6.86 and 6.87 plot the experimental cracking and ultimate shear strengths versus effective depth, d. The data were plotted versus effective depth to examine the effects of different sizes of prestressed concrete girders. The results show that the normalized cracking and ultimate shear strengths were consistent across a wide range of girder sizes. Therefore, it was determined that the size of the tested specimens had no effect on the normalized shear values.

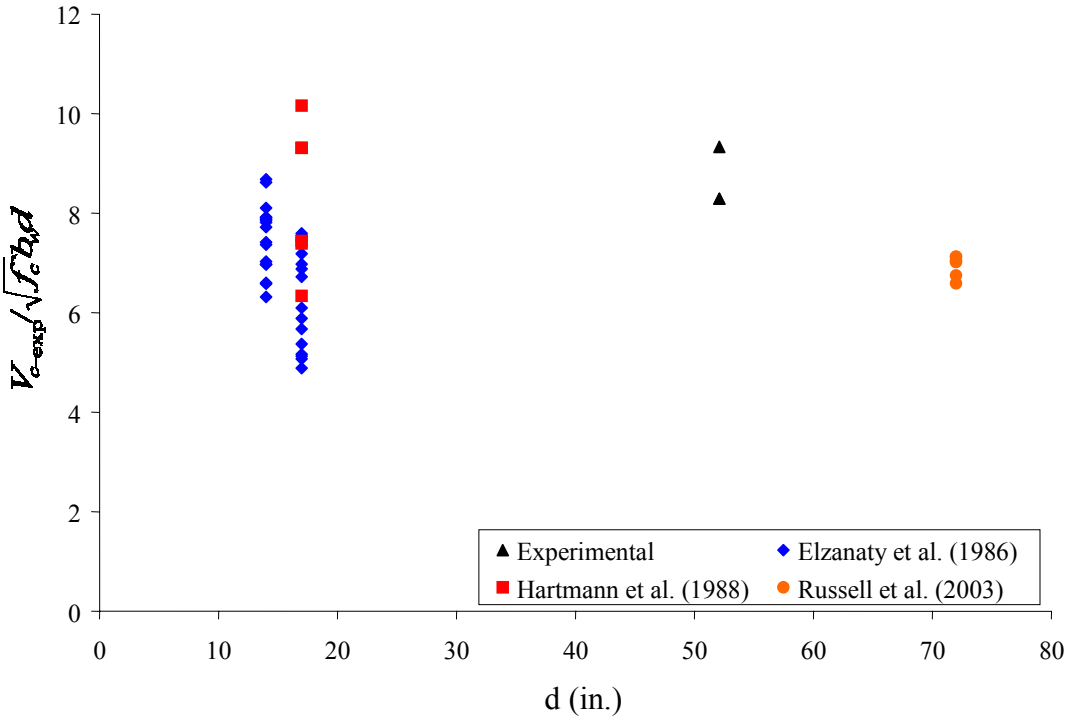

Figure 6.86 Experimental cracking shear versus effective depth, d

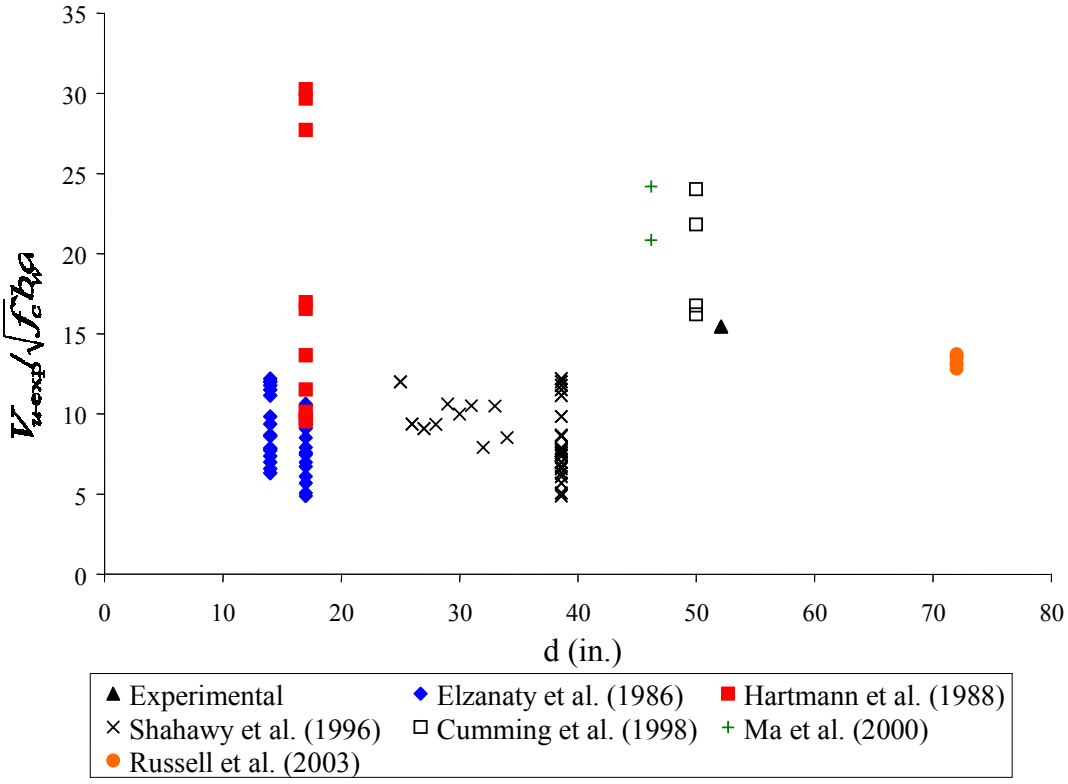

Figure 6.87 Experimental ultimate shear versus effective depth, d

Figures 6.88 and 6.89 plot the experimental cracking and ultimate shear strengths versus the prestressing ratio, ω_p. For cracking, the amount of prestressing did not have a noticeable effect. The prestressing ratio had no apparent effect on the ultimate shear capacities. This indicated that ultimate shear capacity of prestressed girders may be independent of the amount of prestressing strands in a section.

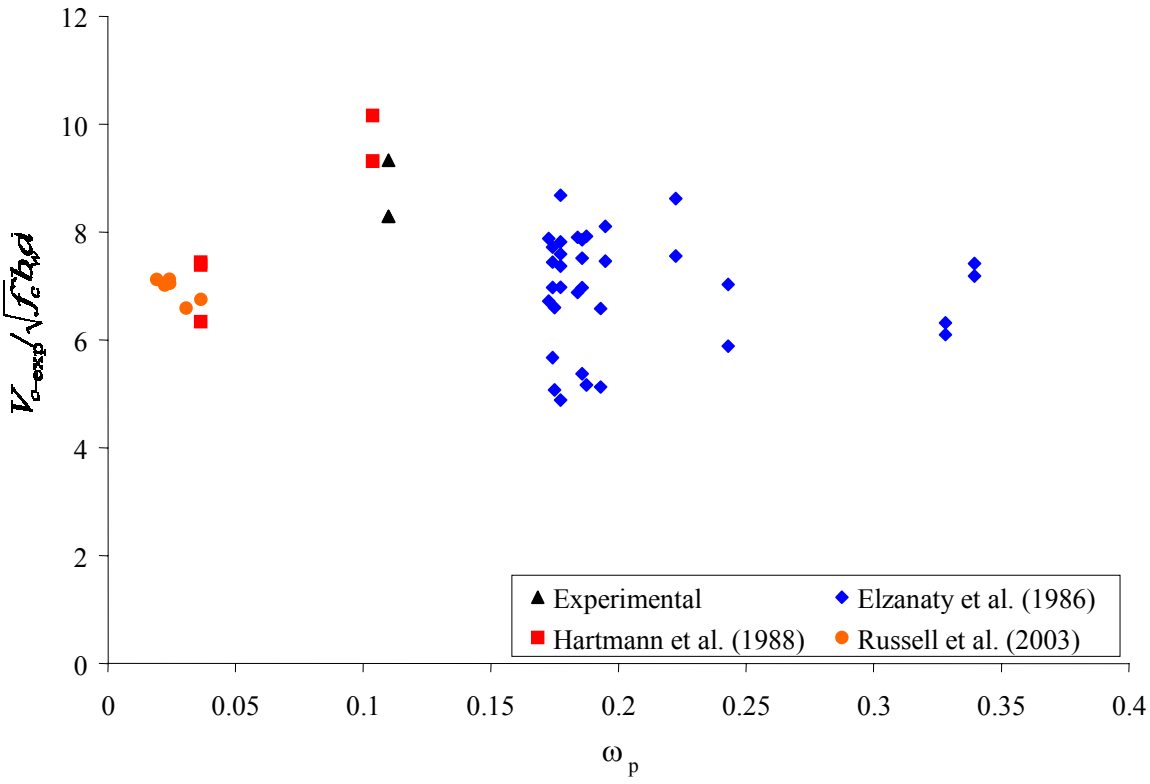

Figure 6.88 Experimental cracking shear versus the prestressing ratio, ω_p

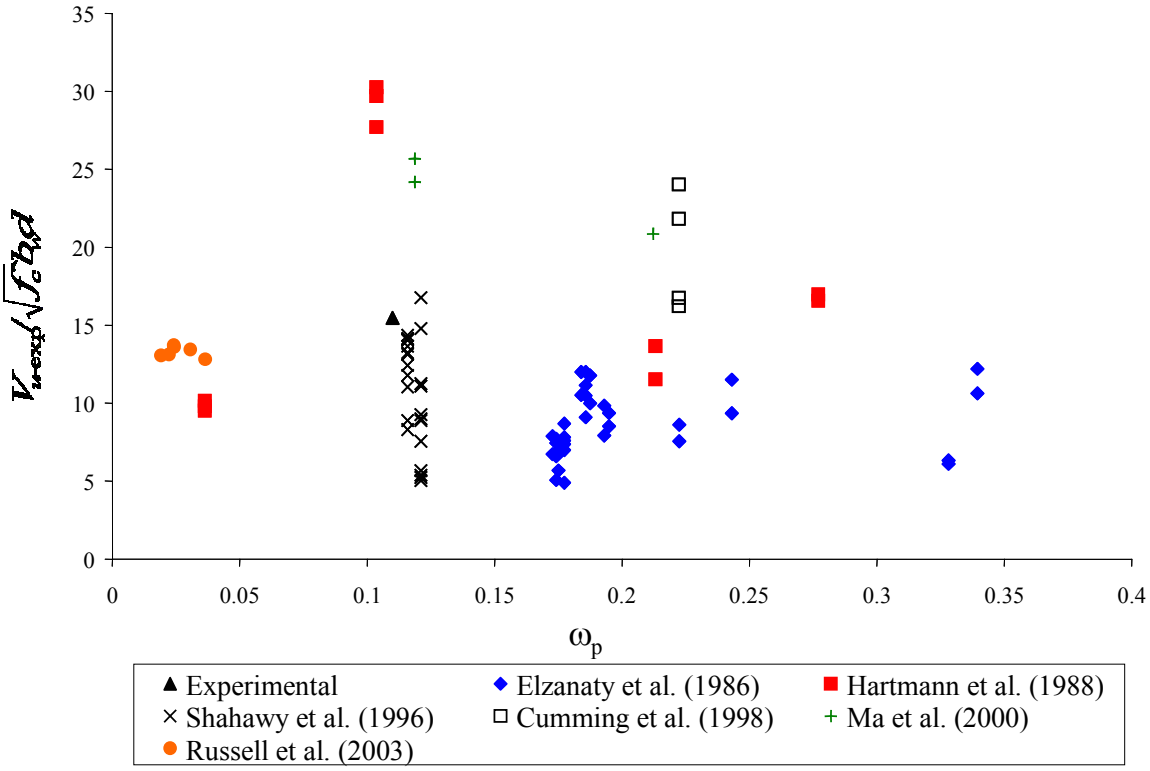

Figure 6.89 Experimental ultimate shear versus the prestressing ratio, ω_p

Figures 6.90 and 6.91 plot the experimental cracking and ultimate shear strengths versus concrete strength. The concrete strength did not have an effect on the cracking shear strength of the various test specimens. For ultimate shear capacities, no apparent trend was discerned and the concrete strength was shown to have little effect on the capacity of the tested specimens.

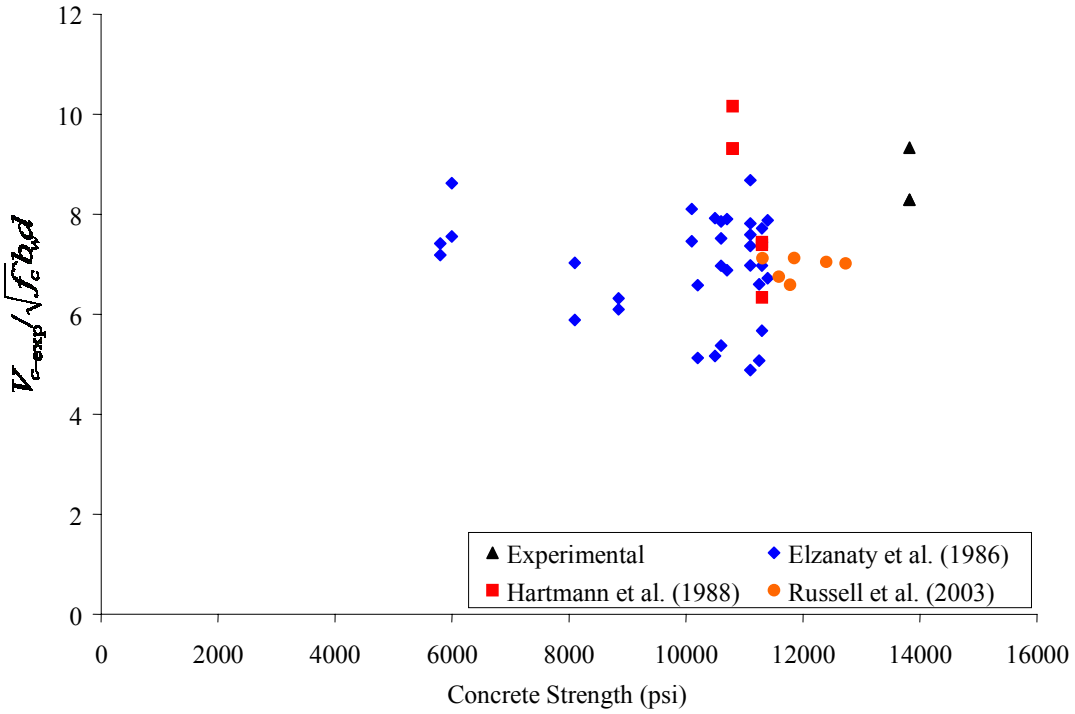

Figure 6.90 Experimental cracking shear versus concrete strength

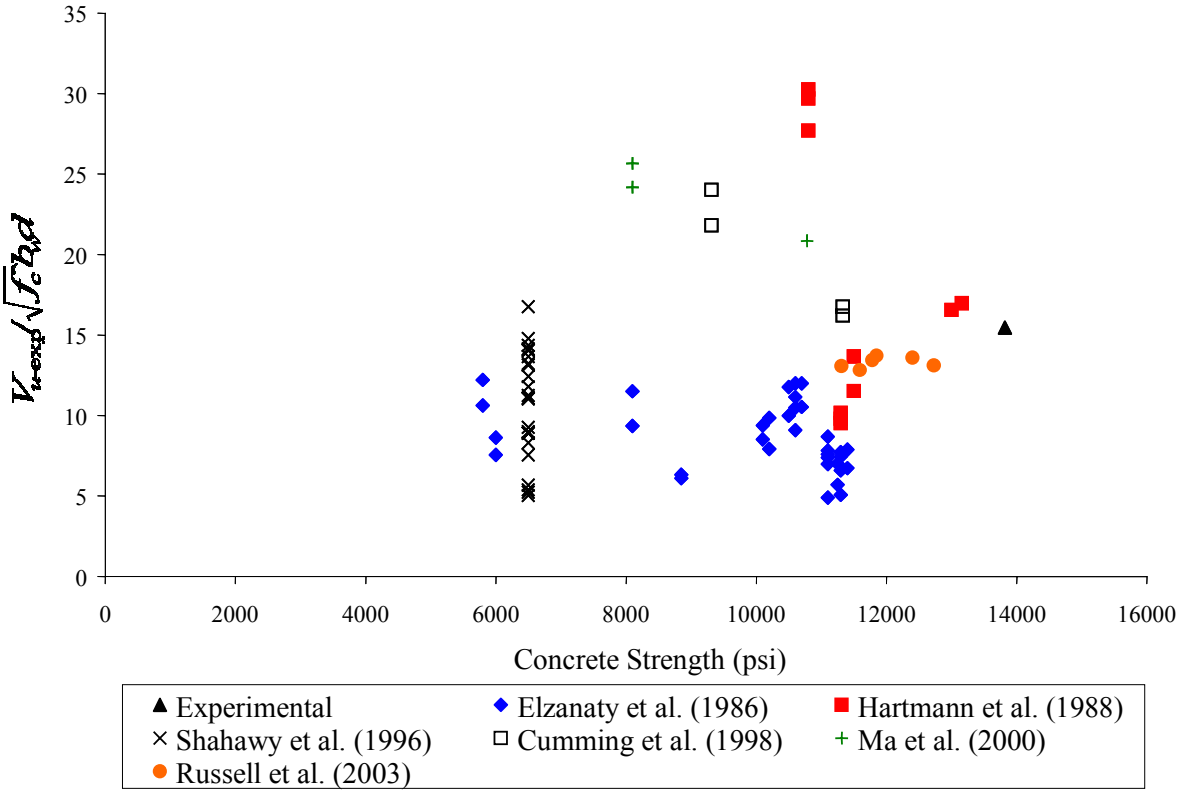

Figure 6.91 Experimental ultimate shear versus concrete strength

CHAPTER 7

SUMMARY, CONCLUSIONS AND RECOMMENDATIONS

7.1 Summary

An AASHTO Type IV and a PCI Modified Bulb Tee 56 were constructed for flexure and shear testing at the Georgia Institute of Technology, Structural Engineering and Materials Research Laboratory. These girders contained the same HPC that was used in the Jonesboro Rd. demonstration bridge located in Henry County, GA. The AASHTO Type IV girder was tested and ruptured in flexure and was not tested in shear. The BT-56 was tested in shear at three locations after the flexure tests were performed by Canfield and Kahn (2005). The BT-56 girder was prestressed with 44 0.6-in. diameter prestressing strands on 2 in. centers, with 10 of them draped. The draped strands were harped using two hold down points located at 45 percent of the span length from each end. The girder was designed with a 56-day compressive strength of 10,150 psi (68.9 MPa) and obtained an actual testing day strength of 13,820 psi (95.3 MPa). An 8-in. thick, 60-in wide unshored composite deck was poured on the BT-56 girder using a grade 1 HPC concrete mixture. The deck strength at testing was 6,600 psi (45.5 MPa).

The three shear tests were performed at different locations along the length of the BT-56 girder. A concentrated load was located approximately 143 in. from the center of bearing. Each test had an approximate shear span to total depth ratio of 2.2. The principal difference in the three tests was in the amount of transverse shear reinforcement located in the shear spans. Test E1 had a stirrup spacing of 7 in. and contained 2 pick-up

loops; Test W1 had an average stirrup spacing of 16.75 in. and contained two pick-up loops; Test W2 had a stirrup spacing of 24 in. and did not contain any pick-up loops.

Tests E1 and W1 were not tested to failure due to equipment limitations. Each section was loaded until the capacity of the testing equipment was reached. Despite the inability to rupture the girder during the two tests, information was obtained about the concrete shear strength and the serviceability behavior of the BT-56 girder. Test W2 was tested to failure and provided results on the ultimate behavior of the fully prestressed BT-56 girder.

7.2 BT-56 Girder Shear Performance

The shear capacity of the BT-56 girder was higher than expected for all three tests. The experimental results for each test were compared with the predicted capacities obtained from the AASHTO Standard (2002) Method, the ACI Alternate (2002) Method, the AASHTO LRFD (2004) Method, and the Variable Angle Truss Model (VATM). The ACI Alternate was only used to calculate cracking shear strengths and the VATM was only used to calculate ultimate shear capacities. The measured shear capacities were calculated with and without the added capacity of the pick-up loops for Tests E1 and W1 because the experiments demonstrated the significant strengthening effect of the loops. The following sections detail the conclusions drawn for each test and the performance of each prediction method pertaining to each test.

7.2.1 Test E1

Test E1 was performed on the eastern end of the BT-56; the maximum point load was 700 kips, giving a maximum shear force including dead load of 653 kips in the shear span. Although it did not reach failure at that load, large web-shear cracks were observed at approximate 4 in. spacing with crack widths up to 0.02 in. Large flexure shear cracks were located near the midspan of the girder with crack widths up to 0.04 in. All of the instrumented stirrups were beyond yield strain.

The concrete cracking shear strength of Test E1 (350 kips) was accurately and conservatively predicted by both the AASHTO Standard (2002) and ACI Alternate methods (308 kips and 344 kips, respectively). The AASHTO LRFD Specifications (2004) were conservative and inaccurate when the predicted concrete shear contribution (V_c) was compared to the experimental cracking strength (V_{cw}) of the girder. The latter was expected because the V_c component of the LRFD (2004) shear strength considers post cracking tensile strength resistance.

The experimental ultimate shear strength of Test E1 was not found. When the test was stopped, the maximum experimental shear (653 kips) was greater than the ultimate shear predictions of the AASHTO Standard Specifications and the VATM. (623 and 593 kips, respectively). It was unknown how conservative the AASHTO Standard Specifications and the VATM would have been. The AASHTO LRFD Specifications (2004) predicted an ultimate shear capacity of 696 kips when the compression angle was interpolated and an ultimate shear capacity of 612 kips when the physically measured compression angle was used. It was not known whether the LRFD Specifications using the interpolated compression angle would have been conservative. When the capacity of

the pick-up loops was added to the shear strength, the maximum experimental shear force did not reach the calculated capacities of any of the prediction methods. The total effect of the pick-up loops was unknown, but the width of diagonal cracks crossing the loops was much smaller than those found in the section without loops (Test W2) at the same loads. Therefore, the pick-up loops were determined to be effective in increasing the shear capacity of Test E1.

7.2.2 Test W1

Test W1 was performed at the western end of the BT-56 girder; the maximum load was 590 kips, giving a maximum shear of 569 kips. Neither the capacity of the girder nor the capacity of the testing equipment was reached in this test. It was determined at the 590 kip load that the testing equipment would not have the capacity to cause failure in the section. All of the instrumented stirrups were beyond yield strain, and the width of cracks within the shear span was about 0.025 in.

The calculated concrete shear strength of Test W1 was found to be similar to Test E1 by all methods. However, web-shear cracking was observed at a load of 300 kips (shear force of 311 kips), a load lower than seen in Test E1. The lower cracking strength observed during Test W1 was attributed to the larger stirrup spacing. None of the prediction methods accounted for the transverse shear reinforcement and its effect on cracking strengths. It has been traditionally assumed that the amount of transverse shear reinforcement has no effect on the cracking shear strength, V_{cw} of prestressed concrete girders. However, a ten percent decrease in cracking shear strength (V_{cw}) was observed when the larger stirrup spacing was present. The AASHTO Standard (2002) was

accurate and remained conservative despite the drop in observed cracking shear strength. The ACI Alternate method became slightly unconservative for predicting V_{cw} with a test-to-predicted ratio of 0.84. The AASHTO LRFD Specifications (2004) predicted a similar concrete shear contribution (V_c) to the one predicted for Test E1, which was overly conservative when compared to the experimental cracking shear strength.

The experimental ultimate shear strength of Test W1 was not found. When the test was stopped, the maximum experimental shear (569 kips) was greater than the ultimate shear predictions of the AASHTO Standard Specifications (2002) and the VATM (539 and 254 kips, respectively). It was unknown how conservative the two methods would have been. The AASHTO LRFD Specifications predicted an ultimate shear capacity of 601 kips when the compression angle was interpolated and an ultimate shear capacity of 565 kips when the physically measured compression angle was used. It was not known whether the LRFD Specifications using the interpolated compression angle would have been conservative. At the maximum loading, all web-shear cracks extended through the pick-up loop region. This indicated that the pick-up loops were contributing a significant amount of shear strength to the girder. When the pick-up loops were included in the calculations using a yield stress of just 69 ksi, (69 ksi was the measured yield stress of the mild reinforcement) each code predicted a shear capacity that was not attainable with the available laboratory equipment. Finally, it was seen that the pick-up loops played a major factor in the shear strength of the section. It was unknown how much strength they were contributing and more research is needed to determine the exact contribution that they may have.

7.2.3 Test W2

Test W2 was performed near the western end of the BT-56; the point load was placed about 20 ft. from the girder end, and the west end was cantilevered over the bearing support 8 ft. The shear span did not include the pick-up loops. Test W2 failed in shear at a point load of 628.5 kips, which corresponded to an ultimate shear of 580 kips. The web crushing failure extended approximately 30 in. from the center of the shear span in both directions. The instrumented stirrups were strained significantly more than the stirrups in either of the two previous tests.

The section tested for Test W2 was previously cracked by the flexure test. Nevertheless, new shear cracks were developed at the level of the centroid at a point load of 365 kips, which corresponded to a cracking shear of 311 kips. The cracking shear value was the same as observed for Test W1. Pick-up loops were not a factor for Test W2 because they were outside the shear span.

The three prediction methods were conservative when predicting the ultimate shear capacity for Test W2. The yield stress used for the stirrups was 69 ksi. It was concluded that all codes remained conservative when actual yield stresses were used to compute the shear capacity of Test W2, and that no yield stress limit was necessary for the BT-56 girder.

The most accurate prediction method was the AASHTO Standard Specifications (2002) which gave an ultimate shear capacity, V_n, of 390 kips, and a test-to-predicted value of 1.49. The AASHTO LRFD Specifications (2004) were also conservative with a test-to-predicted value of 1.36 when the compression angle was interpolated, and a test-to-predicted value of 1.55 when the physically measured angle was used. Therefore, the

AASHTO LRFD Specifications were more accurate than the AASHTO Standard Specifications (2002). When the physically measured angle was used, the LRFD was less accurate than the Standard Specifications. The difference in the two values is further discussed in the next section. Because the Variable Angle Truss Model (VATM) did not account for concrete shear strength, it provided a test-to-predicted ratio of 3.43, which was overly conservative, as expected.

7.3 Prediction Methods

This research examined the accuracy of the AASHTO Standard (2002), the 1998 AASHTO LRFD, and the 2004 AASHTO LRFD Specifications using previous experimental research and the results from the BT-56 girder. The VATM was not examined due to its limited discussion and calculation by all previous research. The ACI Alternate method is discussed based on the findings from this research. Comparisons were made to determine how the data from the BT-56 girder would fit with data from other shear research (Elzanaty et al. (1986), Hartmann et al. (1988), Shahawy et al. (1996), Cumming et al. (1998), Ma et al. (2000), and Russell at el. (2003)) for the AASHTO Standard (2002), the 1998 AASHTO LRFD, and the 2004 AASHTO LRFD Specifications.

7.3.1 AASHTO Standard (2002)

The AASHTO Standard (2002) code was the same for all research examined in this report. It was straight-forward, easy to use, and consistent despite the variability in the different shear testing programs. The results from the BT-56 girder were consistent

with the results from previous shear research for both cracking and ultimate shear capacities. When results from the current and previous shear tests were compared, it was concluded that the girder size (from 16 in. to 72 in. depths), concrete strength (f_c'from 6,000 psi to 13,800 psi), and amount of prestressing (ω_p from 0.019 to 0.34) had little effect on the accuracy of the code predictions. For concrete cracking shear capacity, the AASHTO Standard Specifications (2002) remained accurate and conservative for all shear research examined in this report. For ultimate shear capacity, that code also remained accurate and conservative. The only trend found when examining ultimate capacities was that as the shear reinforcement ratio increased, the conservative nature of the code decreased. This report examined the shear results from Type I, Type II, Type IV, BT-56, and BT-72 prestressed HPC girders and found no size effect present in the AASHTO Standard code. The code remained accurate and conservative with all sizes of specimens examined in this report. Therefore, future research on high performance concrete prestressed girders up to 80 in. deep can be done accurately using the smaller sized specimens.

7.3.2 AASHTO LRFD (1998)

Because most of the evaluation of previous shear testing was performed using the 1998 AASHTO LRFD Specifications, the shear capacities of the BT-56 girder were calculated using the 1998 Specifications. The 1998 LRFD Specifications was difficult to use and subject to interpretation. Therefore, some of the data compared in this research could have been calculated in different ways. There was a large amount of scatter when comparing the 1998 LRFD Specifications results which showed that the application of

the code was somewhat inconsistent. When results from previous shear tests were compared to the BT-56 results, it was seen that the size, concrete strength, and amount of prestressing had little effect on the accuracy of the code. The 1998 LRFD Specifications were conservative for both cracking and ultimate shear capacities.

The 1998 LRFD concrete shear strength V_c was not intended to represent a cracking shear strength. Nevertheless, the experimental results showed that as the transverse shear reinforcement ratio increased, the concrete shear contribution became smaller. At high shear reinforcement ratios, the concrete shear contribution was only 15% of the experimental cracking shear strength. The results confirmed that the predicted concrete shear contribution of the LRFD Specifications could not be successfully used to indicate when shear cracking would occur in prestressed concrete girders.

For ultimate shear strength, the 1998 LRFD Specifications were conservative and matched the ultimate shear capacities much better than it matched the cracking shear capacities. As the shear reinforcement ratio increased, the conservative nature of the code decreased. At shear reinforcement ratios greater than the maximum permitted by the Specifications, the code was unconservative. As with the AASHTO Standard Specifications, the different size of specimens had no effect on the accuracy of the code.

7.3.3 AASHTO LRFD (2004)

There were significant changes to the LRFD Specifications between 1998 and 2004. Therefore, all of the previous shear research data were recalculated using the 2004 AASHTO LRFD Specifications. The newer Specifications were still subject to some

interpretation, but all quantities were recalculated by the author of this report. The AASHTO LRFD Specifications (2004) was conservative for both cracking and ultimate shear capacities.

In this research, the AASHTO LRFD Specifications (2004) were implemented using two different methods. One method interpolated a compression strut angle from AASHTO LRFD Figure 5.8.3.4.2-1 to determine the predicted shear capacities; the other method used the physically measured compression angles from each test to determine the predicted shear capacities. Using an interpolated angle was considered to be more representative of the calculated LRFD shear capacity because no measured angle can be used for design. It was found that slight changes in compression angles caused large changes in the predicted shear capacities given by the LRFD Specifications. For example, the AASHTO LRFD Specifications predicted a compression angle of 19.85° and gave an ultimate shear strength of 425 kips; the cracks during testing were physically measured to be 23.4° , which caused the predicted shear capacity to be 373 kips. The 3.55° difference in compression angles caused a 52 kip difference in predicted shear capacity. The shear capacity using the interpolated compression angle was shown to be more accurate, but the angle was under-predicted. When the stirrup spacings were smaller (Tests E1 and W1), the small differences in angles caused larger changes in the predicted shear capacities. The reason for the larger changes was because the shallower compression angles crossed more stirrups and increased the V_s component.

As with the 1998 LRFD Specifications, the 2004 Specifications were conservative but inaccurate for predicting cracking shear. As the shear reinforcement ratio increased, the concrete shear contribution became smaller. The effects of the concrete strength and

the amount of prestressing did not have a noticeable effect on the accuracy of the concrete shear contribution. The results confirmed that the predicted concrete shear contribution of the LRFD Specifications could not be successfully used to indicate when shear cracking would occur in prestressed concrete girders, as expected.

For ultimate shear strength, the 2004 LRFD Specifications were conservative and more accurate than the 1998 LRFD Specifications. As the shear reinforcement ratio increased, the conservative nature of the code decreased. At high shear reinforcement ratios, the code was unconservative. As with the AASHTO Standard Specifications, the different sizes of specimens had no effect on the accuracy of the code.

For this research, it was seen that the AASHTO LRFD Specifications (2004) were more accurate than the AASHTO Standard Specifications (2002) when the predicted compression angle was used (test-to-predicted values of 1.36 versus 1.48, respectively). When the physically measured angle was used, the LRFD Specifications were less accurate than the AASHTO Standard Specifications (2002) (test-to-predicted values of 1.55 versus 1.48, respectively).

7.3.4 ACI Alternate Method

The ACI Alternate method considers cracking V_{cw} when the principal tensile stress equals $4\sqrt{f_c'}$. It was examined to determine its accuracy when using high strength concrete. The ACI Alternate method became unconservative when concrete strengths of 13,800 psi were used. It was noted that as the stirrup spacing became larger, the ACI Alternate method became more unconservative. These findings were also noted in Meyer et al. (2002) for lightweight high strength concrete.

7.3.5 Code Comparisons

All three codes were conservative for most of the research discussed in this report. For analysis purposes, the AASHTO Standard Specifications (2002) were the most consistent, most accurate, and easiest to use. The AASHTO Standard accurately predicted concrete shear cracking strength, while both versions of the LRFD Specifications were highly conservative but inaccurate. Again, the term V_c in the LRFD Specifications was not meant to predict the experimental cracking shear, V_{cw} in prestressed girders. The AASHTO Standard Specifications accurately predicted ultimate shear capacities for all shear specimens and never became unconservative. The range of test-to-predicted values for the great majority of the research was 0.99 to 1.98, with very few outliers.

The 2004 LRFD Specifications were clearly an improvement to the 1998 LRFD Specifications. For cracking, the two methods were comparable and neither seemed to perform better than the other. The cracking test-to-predicted ratios for the 1998 LRFD Specifications ranged from 1.12 to 4.2 while the cracking test-to-predicted ratios for the 2004 LRFD Specifications ranged from 1.42 to 5.7. It is important to note that the LRFD Specifications were not intended to predict the cracking concrete shear strength, V_{cw} of prestressed girders.

For ultimate shear capacities, the 1998 LRFD Specifications were more difficult to use and less accurate than the 2004 LRFD Specifications. The 2004 LRFD became as accurate as the AASHTO Standard at many levels of shear reinforcement. At some levels of shear reinforcement, the 2004 LRFD Specifications were more accurate than the AASHTO Standard Specifications. For the 1998 LRFD Specifications, the range of test-

to-predicted ratios was 0.75 to 2.1. For the 2004 LRFD Specifications, the range of test-to-predicted ratios was 0.72 to 2.07.

It was concluded that the 2002 Standard Specifications were easier to use and produced equivalent accuracy compared to the 2004 LRFD Specifications. It was also clear that the 2002 Standard Specifications were superior to the 2004 LRFD Specifications when predicting the cracking shear strength. For ultimate shear predictions, the 2004 LRFD Specifications were less consistent and became unconservative at high shear reinforcement ratios, while the 2002 Standard Specifications were consistent and never became un-conservative. It was also concluded that for ultimate shear capacities, the AASHTO LRFD Specifications were most accurate when the interpolated compression angles were used and the physically measured angles were ignored.

From these observations, the 2002 Standard Specifications were the best option for calculating both the cracking and ultimate shear capacities. The cracking shear predictions were considered important for accounting for the durability of bridge girders. Under service conditions, any cracking is undesirable; therefore, the ability to accurately predict shear cracking should be considered an important element in shear design.

7.4 Recommendations

It is recommended that the AASHTO Standard Specifications (2002) be used to calculate the cracking and ultimate shear strength (V_{cw} and V_n), for precast prestressed bridge girders with concrete compressive strengths up to 14,000 psi (96.5 MPa). The AASHTO LRFD Specifications (2004) may be used to calculate the ultimate shear

capacity (V_n) of prestressed girders with concrete compressive strengths up to 14,000 psi (96.5 MPa).

The ACI-Alternate method for calculating V_{cw} should not be used for girders with concrete compressive strengths greater than 10,000 (69 MPa) until further research more accurately defines the tensile capacities of high performance concrete.

7.5 Future Research

As a result of this research project, one area requiring additional research became apparent. It was the added shear strength provided by girder pick-up loops. Pick-up loops are present in every precast, prestressed girder and are never accounted for when calculating ultimate shear strengths. Ignoring them is conservative, but it was seen in this research that they can add a significant amount of shear strength to prestressed girders at their code-defined critical sections. Neither section of the BT-56 girder that contained the pick-up loops was tested to failure. Therefore, a research program should be devised so that the pick-up loop capacities can be calculated accurately and can be utilized when designing shear reinforcement.

APPENDIX A

LOAD CELL STRESSING READINGS

This appendix presents specific load cell data that supplements the results of the strand material properties given in Chapter 4. Strand tensioning data obtained from Georgia Tech load cells, and Standard Concrete Products (Atlanta Division) equipment is presented, along with the actual stress-strain curve for the strand.

Table A.1 SCP strand stress for every strand

Strand	Load	Stress		Strand	Load	Stress
1	45,600	209		27	45,000	206
2	45,200	207		28	45,000	206
3	45,100	207		29	45,000	206
4	45,000	206		30	45,000	206
5	45,200	207		31	45,000	206
6	44,900	206		32	45,200	207
7	45,600	209		33	44,900	206
8	45,000	206		34	45,100	207
9	45,000	206		35	45,000	206
10	44,700	205		36	45,100	207
11	45,000	206		37	43,500	199
12	45,100	207		38	43,500	199
13	45,100	207		39	43,700	200
14	45,100	207		40	43,800	201
15	45,100	207		41	43,700	200
16	45,000	206		42	43,600	200
17	45,000	206		43	43,700	200
18	44,800	205		44	43,400	199
19	45,000	206		45	43,500	199
20	45,000	206		46	43,800	201
21	45,100	207		47	43,500	199
22	45,100	207		48	43,500	199
23	45,100	207		49	43,400	199
24	45,100	207		50	45,200	207
25	45,000	206		51	45,500	209
26	44,900	206		52	43,500	199

Table A.2 Strand stress from all Georgia Tech load cells

	Rd 1	Rd 2	Rd 3
Date	4/22/2004	4/23/2004	4/24/2004
Time	11:45 AM	9:00 AM	9:00 AM
Load Cell	Rd 1	Rd 2	Rd 3
1s			
2s	44,294	44,471	45,185
3s		40,518	41,624
4s		41,468	42,550
5s		42,677	43,809
6s		44,176	47,470
7s		41,520	42,750
8s		41,580	42,792
9s	41,579	41,857	43,083
5	46,349	46,646	48,019
6	41,232	41,500	42,512
7	46,614	46,917	48,309
8	46,089	46,386	47,760
Avg. Load	44,360	43,310	44,655
Avg. Stress	204.6	200.2	206.3

Table A.3 Strand stress comparison: Load cells vs. SCP

Load Cell	Avg. Load Cell Stress	Strand Number	SCP Stress
1s	N/A	1	209.08
2s	208.23	3	206.79
3s	191.82	39	200.37
4s	196.08	40	200.83
5s	201.88	8	206.33
6s	218.76	10	204.95
7s	197.00	11	206.33
8s	197.20	15	206.79
9s	198.54	16	206.33
5	221.29	20	206.33
6	195.91	47	199.45
7	222.62	48	199.45
8	220.09	51	208.62
Avg. Stress	205.78		204.74

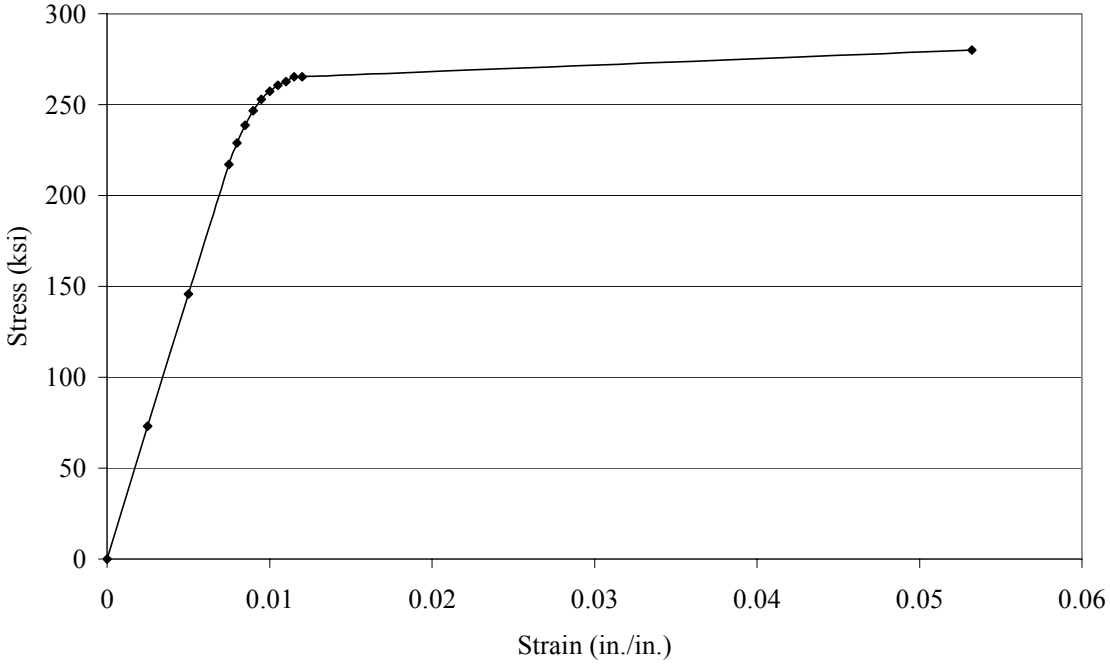

Figure A.1 Actual stress-strain curve for 0.6-in. diameter 270 ksi Lo-lax strands

APPENDIX B

CONTROL SPECIMEN TEST RESULTS

This appendix presents specific specimen testing data that supplements the results of the specimen material properties given in Chapter 4. Data are presented in the same order as in Chapter 4.

Table B.1 Compressive strengths for all Type IV tests by Georgia Tech

4 in. x 8 in. Compressive strengths of individual cylinders, psi							
Type IV							
Date Cast : 4/22/2005		BEW		BM		BEE	
Testing Day	Curing Type	Stress	Avg.	Stress	Avg.	Stress	Avg.
1 Day	ASTM			9,007	10,416		
				10,784			
				11,458			
2 Day	Insulated	10254.4	10,297	11,189	12,156	13,181	12,727
		10576.6		12,918		12,717	
		10058.6		12,362		12,284	
	ASTM			10,189	10,660		
				10,998			
				10,794			
7 Day	Insulated			12,002	12,535		
				13,216			
				12,387			
	ASTM			12,669	12,617		
				13,124			
				12,059			
28 Day	Insulated			14,170	14,056		
				14,304			
				13,694			
	ASTM			14,759	14,644		
				14,439			
				14,735			
56 Day	Insulated			13,679	13,660		
				13,915			
				13,387			
	ASTM	14,404	14,275	16,199	15,752	16,436	15,833
		13,714		16,027		15,375	
		14,709		15,030		15,688	
Test Day	Insulated	12,842	12,948	15,153	14,969	14,905	15,140
		13,054		14,785		15,376	

Table B.2 Compressive strengths for all BT-56 tests by Georgia Tech

4 in. x 8 in. Compressive strengths of individual cylinders, psi							
BT-56							
Date Cast : 4/23/2005		BEW		BM		BEE	
Testing Day	Curing Type	Stress	Avg.	Stress	Avg.	Stress	Avg.
1 Day	Insulated	11063.7	11,042	11,871	12,105	11,924	12,119
		10749.3		11,828		12,810	
		11312.7		12,615		11,623	
	ASTM			9,068	8,986		
				8,897			
				8,992			
7 Day	Insulated			12,546	11,982		
				11,517			
				11,883			
	ASTM			12,218	12,443		
				12,755			
				12,356			
28 Day	Insulated			14,922	13,969		
				13,216			
				13,769			
	ASTM			13,986	14,284		
				13,936			
				14,929			
56 Day	Insulated			13,697	13,819		
				13,334			
				14,427			
	ASTM	14,560	14,559	15,965	15,176	14,233	14,846
		14,034		14,205		15,325	
		14,635		14,892		14,692	
		15,008		15,643		15,132	
Test Day	Insulated	14,626	14,626	14,968	14,968	15,840	15,840

Table B.3 Compressive Strengths for BT-56 Statistical Samples

BT-56 Compressive statistical samples (psi)					
56-Day ASTM Cured					
Batch 1		Batch 2		Batch 3	
14,011	14,691	14,941	15,129	14,758	15,223
15,806		15,538		15,343	
14,255		14,909		15,569	
Batch 4		Batch 5		Batch 6	
14,988	14,649	14,090	13,578	15,210	14,848
14,322		12,171		14,376	
14,637		14,472		14,959	

Table B.4 Elastic modulus results for both girders

TYPE IV					
Specimen	Testing Day	Curing Type	Ultimate Compressive Stress (6 x 12) (psi)	Modulus of Elasticity (ksi)	Poisson's Ratio
BEW	2	Insulated	12,036	4,689	0.16
BM	2	Insulated	12,923	4,668	0.16
BEE	2	Insulated	10,731	4,658	0.16
BEW	56	Insulated	13,267	4,633	0.16
BM	56	Insulated	12,792	4,818	0.16
BEE	56	Insulated	13,184	4,699	0.16
BEW	56	ASTM	15,118	4,891	0.12
BM	56	ASTM	13,825	5,118	0.18
BEE	56	ASTM	13,962	5,314	0.19
BT-56					
Specimen	Testing Day	Curing Type	Ultimate Compressive Stress (6 x 12) (psi)	Modulus of Elasticity (ksi)	Poisson's Ratio
BEW	1	Insulated	12,190	4,861	0.20
BM	1	Insulated	12,943	4,877	0.20
BEE	1	Insulated	11,700	4,575	0.19
BEW	56	Insulated	13,141	4,601	0.18
BM	56	Insulated	11,915	4,691	0.19
BEE	56	Insulated	13,083	4,977	0.19
BEW	56	ASTM	15,118	4,386	0.18
BM	56	ASTM	13,825	5,091	0.17
BEE	56	ASTM	13,962	5,151	0.18
BEW	Test Day	Insulated	15,840	4,245	0.14
BM	Test Day	Insulated	14,626	4,225	0.14
BEE	Test Day	Insulated	14,968	4,388	0.17

Table B.5 Modulus of rupture values for both girders

Type IV				
Testing Day	Location	Ultimate Compressive Strength (psi)	Load (lb)	Experimental Modulus (psi)
56 Day	BEW	14,275	5,000	1,009
	BM	15,752	4,900	963
	BEE	15,833	4,550	950
BT-56				
Testing Day		Ultimate Compressive Strength (psi)	Load (lb)	Experimental Modulus (psi)
56 Day	BEW	14,410	4,640	1,001
	BM	15,021	4,860	1,025
	BEE	14,750	4,720	1,009

Table B.6 Deck compressive strengths for all specimens

4 in. x 8 in. Compressive strengths of individual cylinders, psi					
Type IV Deck					
Date Cast :	6/30/2004	Batch 1		Batch 2	
Testing Day	Curing Type	Stress	Avg.	Stress	Avg.
1 Day	ASTM	3,926	3,540	2,204	2,414
		3,446		2,430	
		3,247		2,609	
7 Day	ASTM	4,716	4,526	4,428	3,778
		4,593		3,981	
		4,269		2,925	
28 Day	ASTM	6,576	6,755	6,312	6,001
		7,056		5,653	
		6,635		6,039	
56 Day	ASTM	7,067	7,411	6,693	6,920
		7,322		7,126	
		7,844		6,943	
Test Day	ASTM	7,457	7,829	8,046	7,929
		8,179		8,282	
		7,851		7,458	
BT-56 Deck					
Date Cast :	9/1/2004	Batch 1		Batch 2	
Testing Day	Curing Type	Stress	Avg.	Stress	Avg.
1 Day	ASTM	2,547	2,669	1,966	2,036
		2,770		2,109	
		2,690		2,032	
7 Day	ASTM	3,725	3,987	3,754	4,188
		4,089		4,660	
		4,148		4,148	
28 Day	ASTM	5,670	5,732	6,646	6,682
		5,937		6,465	
		5,590		6,934	
56 Day	ASTM	6,094	6,107	7,042	7,240
		6,072		7,440	
		6,154		7,238	
Test Day	ASTM	6,762	6,554	6,775	6,933
		6,346		7,090	

Table B.7 Elastic modulus results for both decks

Type IV Deck					
Specimen	Testing Day	Curing Type	Ultimate Compressive Stress (6 x 12) (psi)	Modulus of Elasticity (ksi)	Poisson's Ratio
Batch 1	1	ASTM	3,801	3,094	0.13
Batch 1	1	ASTM	3,234	2,679	0.14
Batch 2	1	ASTM	2,650	2,053	0.15
Batch 2	1	ASTM	2,523	2,448	0.13
Batch 1	56	ASTM	7,794	3,743	0.20
Batch 1	56	ASTM	7,463	3,641	0.17
Batch 2	56	ASTM	6,440	3,550	0.20
Batch 2	56	ASTM	7,072	3,310	0.17
Batch 1	Test Day	ASTM	7,571	3,628	0.16
Batch 1	Test Day	ASTM	7,909	3,624	0.17
Batch 2	Test Day	ASTM	7,600	3,571	0.17
Batch 2	Test Day	ASTM	7,674	3,359	0.16
BT-56 Deck					
Specimen	Testing Day	Curing Type	Ultimate Compressive Stress (6 x12) (psi)	Modulus of Elasticity (ksi)	Poisson's Ratio
Batch 1	1	Insulated	2,621	2,389	0.13
Batch 1	1	Insulated	2,397	2,703	0.11
Batch 2	1	Insulated	2,199	2,475	0.16
Batch 2	1	Insulated	2,254	2,308	0.09
Batch 1	56	Insulated	6,304	3,454	0.17
Batch 1	56	Insulated	6,063	3,385	0.17
Batch 2	56	ASTM	7,479	3,732	0.17
Batch 2	56	ASTM	7,104	3,539	0.16
Batch 1	Test Day	ASTM	6,278	3,367	0.17
Batch 1	Test Day	Insulated	6,623	3,339	0.16
Batch 2	Test Day	Insulated	7,349	3,729	0.17
Batch 2	Test Day	Insulated	7,311	3,667	0.17

Table B.8 Average CTE values for both girders

Girder CTE Summary (με/°F)		
Time (days)	Type IV	BT-56
3.55		5.84
63.61	6.07	
62.68		7.87
222.71		8.49
223.65	7.28	
224.65	7.20	
223.71		8.09

Table B.9 Average CTE values for both decks

Deck CTE Summary (με/°F)				
	Type IV		Bulb Tee	
Time (days)	Batch 1	Batch 2	Batch 1	Batch 2
2.13			5.15	5.36
3.86	4.63	4.55		
55.98			4.74	5.09
62.61	5.36	5.58		
91.98			5.12	5.71
92.98			5.62	6.58
154.71	5.97	5.80		
155.71	6.11	6.24		

APPENDIX C

Statistical Analysis of BT-56 Girder Concrete

This appendix presents the specific method used to determine the characteristic strength for the BT-56 girder at 56 days. The compression data presented here supplement the results of the specimen compression data given in Chapter 4 and Appendix B. The method determined the 5^{th} percentile of the two-parameter Weibull distribution for the 30 56-day 4 in. x 8 in. concrete specimens.

Table C.1 Statistical analysis data

Statistical Analysis

Step 1: Consider MNR, and CV, and eliminate outliers, one by one.
if CV is less than MNR, must eliminate the outlier and run process again

Number	Specimen	Iteration 1	Iteration 2
	Strength (psi)	$(x_i-x)/s$	$2.(x_i-x)/s$
*1	12171	3.549	ELIMINATED
2	14011	1.022	1.516
3	14034	0.991	1.474
4	14090	0.914	1.373
5	14205	0.757	1.164
6	14233	0.718	1.112
7	14255	0.688	1.073
8	14322	0.595	0.950
9	14376	0.522	0.853
10	14472	0.390	0.678
11	14560	0.269	0.518
12	14635	0.166	0.382
13	14637	0.164	0.379
14	14692	0.087	0.277
15	14758	0.002	0.159
16	14892	0.187	0.086
17	14909	0.210	0.116
18	14941	0.254	0.174
19	14959	0.279	0.207
20	14988	0.318	0.259
21	15008	0.347	0.297
22	15132	0.516	0.521
23	15210	0.623	0.663
24	15325	0.781	0.873
25	15343	0.805	0.904
26	15538	1.074	1.260
27	15569	1.116	1.315
28	15643	1.217	1.450
29	15806	1.441	1.746
30	15965	1.660	2.036
Average	$\bar{x} = \frac{\sum_{i=1}^{n} x_i}{n}$	14755.891	14845.01267
Standard Deviation	$s_{n-1} = \sqrt{\left(\sum_{i=1}^{n}(x_i - \bar{x})^2\right)/(n-1)}$	728.3231	550.1012065
Coefficient of Variation	$\text{C.O.V} = \frac{s_{n-1}}{\bar{x}}$	4.9358123	3.705629753
MNR	$MNR = \max\left(\frac{x_i - \bar{x}}{s}\right)$	3.5485859	2.035661174
CV =	$CV \approx \left(2 - \frac{8}{5\sqrt{n}}\right)^2$	2.9168585	2.916858544

* Because the MNR in iteration 1 is greater than the CV value, it must be eliminated for iteration

Table C.2 Beta calculation

Calculation of Beta through trial and error

$$\frac{\sum_{i=1}^{n} x_i^{\beta} \ln(x_i)}{\sum_{i=1}^{n} x_i^{\beta}} - \frac{1}{\beta} - \frac{1}{n} * \sum_{i=1}^{n} \ln(x_i) = 0$$

β Calculation	
β =	**28.3217**

Specimen	Strength (psi)	$x_i^{\beta}\ln(x_i)$	x_i^{β}	1/β	$\ln(x_i)$
1	14011	2.60E+118	2.7235E+117	0.03531	9.547613
2	14034	2.72E+118	2.8534E+117	0.03531	9.549258
3	14090	3.05E+118	3.1922E+117	0.03531	9.55322
4	14205	3.84E+118	4.0153E+117	0.03531	9.56132
5	14233	4.07E+118	4.2511E+117	0.03531	9.563334
6	14255	4.24E+118	4.4366E+117	0.03531	9.564843
7	14322	4.85E+118	5.0732E+117	0.03531	9.569577
8	14376	5.40E+118	5.6362E+117	0.03531	9.573292
9	14472	6.52E+118	6.8092E+117	0.03531	9.579968
10	14560	7.75E+118	8.0899E+117	0.03531	9.586053
11	14635	8.97E+118	9.3534E+117	0.03531	9.591178
12	14637	9.00E+118	9.3823E+117	0.03531	9.591286
13	14692	1.00E+119	1.0448E+118	0.03531	9.595085
14	14758	1.14E+119	1.1845E+118	0.03531	9.599516
15	14892	1.47E+119	1.5315E+118	0.03531	9.608588
16	14909	1.52E+119	1.5809E+118	0.03531	9.60971
17	14941	1.61E+119	1.6794E+118	0.03531	9.611842
18	14959	1.67E+119	1.7386E+118	0.03531	9.613067
19	14988	1.76E+119	1.8354E+118	0.03531	9.61498
20	15008	1.84E+119	1.9086E+118	0.03531	9.616359
21	15132	2.32E+119	2.4065E+118	0.03531	9.624544
22	15210	2.68E+119	2.7836E+118	0.03531	9.629685
23	15325	3.32E+119	3.448E+118	0.03531	9.637243
24	15343	3.43E+119	3.5613E+118	0.03531	9.638384
25	15538	4.92E+119	5.0999E+118	0.03531	9.651063
26	15569	5.20E+119	5.3886E+118	0.03531	9.653007
27	15643	5.95E+119	6.1632E+118	0.03531	9.65775
28	15806	7.99E+119	8.2682E+118	0.03531	9.668124
29	15965	1.06E+120	1.0981E+119	0.03531	9.678144
		6.48E+120	**6.7186E+119**		**278.538**

β Calculation = 0.000000

Finish Statistical Calculation

1. Find α

$$\alpha = \left(\frac{\sum x_i^{\beta}}{n} \right)^{\frac{1}{\beta}}$$

α = 15,093.3

2. Find α_u and β_u

$$\alpha = \alpha_u$$

α_u = 15,093.30

$$\beta_u = \left(1 - \frac{1.48}{n} \right)$$

$\beta_u < 5$, Material is unacceptab le

$\beta_u > 25$, a value of 25 shall be used

β_u = 26.88 so, β_u = 25

3. Obtain the nominal value of the sample data as the 5th percentile of the two-parameter Weibull distribution.

$$x_{0.05} = \alpha_u * [0.0513]^{\frac{1}{\beta_u}}$$

$x_{0.05}$ = 13514.2

4. Calculation of the reduction coefficient

$$R = \left(1 - \frac{2.8 \beta_u^{-0.092}}{\sqrt{n}} \right)$$

R = 0.97483

5. Calculation of the characteristic value

$$x_{char} = R * x_{0.05}$$

x_{char} = 13,040 psi -- -- Becomes design strength

6. Determine if characteristic value meets the minimum required compressive strength, f'_{cr}, specified by the ACI 318-02 code for 10,000 psi concrete

ACI 5.3.2.1

$$f'_{cr} = f'_c + 1.34\, s$$

$$f'_{cr} = 0.90\, f'_c + 2.33\, s$$

So, 14,845 - 1.34*(550) = **14,108 psi ----- -- Becomes ACI final design strength**

and (14,845 - 2.33 *550)/0.90 = 15,071 psi

Appendix D

Sample Calculations

This appendix presents the specific methods, assumptions, and calculations required to estimate the cracking and ultimate shear capacities of the three tests performed on the BT-56 girder. The calculations for the AASHTO Standard (2002), ACI Alternate (2002), and AASHTO LRFD (2004) methods are presented along with their design assumptions. A sample calculation is provided for each method. The variable angle truss model was not provided in this appendix due to the detail provided in Chapter 6.

D.1 AASHTO Standard (2002)

AASHTO Standard Code, 17th Edition 2002

Measured Calculations at defined critical location of 32.56 inches

Test E-1

Gross Section Properties

$A_g := 717.5\ in^2$ $y_{tnc} := 28.71\ in$

$I_g := 312529\ in^4$ $y_{bnc} := -27.54\ in^2$

Composite Section Properties

$A_c := 1198.5\ in^2$ $y_{tc} := 25.285\ in$

$I_c := 578420\ in^4$ $y_{bc} := -39.09\ in$

General Properties

$k := 1000$ lb

$ksi := 1000$ psi

$f'_c := 13819$ psi

$f_{se} := 168$ psi

$F_{se} := f_{se} \cdot A_{ps}$ *

$A_{st} := .2181$

$A_{ps} := 9.5964\ in^2$

$e := -11.81\ in$

$E := 57\sqrt{f'_c}$

$d_p := 52.1\ in$

$b' := 6.125$ in

$n := 10$ angled strands

$Crit_1 := 32.56$ in

$R_1 := 57.487$ kips

$R_2 := 57.487$ kips

$D_1 := 1019.44$ in

D1 =distance from west end

$A_{psang} := n \cdot A_{st}$ *

Loads and Moments at critical section

$w_d := 1.3115\ \frac{k}{ft}$

$V_d := R_1 - \left(\frac{w_d}{12} \cdot D_1\right)$ *

$V_d = -53.929$ kips

$M_d := R_1 \cdot D_1 - \left[\frac{\left[\frac{w_d}{12} \cdot (D_1)^2\right]}{2}\right]$ *

$M_d = 1813.433$

*For x < 909 inches, $\left(\frac{V_i}{M_{max}}\right) := \left(\frac{1}{x}\right)$

*For x > 909 inches, $\left(\frac{V_i}{M_{max}}\right) := \left(\frac{1}{1052 - x}\right)$

*Live load shears and moments are unknown, but the ratio can be determined as shov

General Equations

Stress at bottom of section due to prestressing force

$$f_{pe} := \frac{F_{se}}{A_g} + \frac{F_{se} \cdot e \cdot y_{bnc}}{I_g}$$

$f_{pe} = 3.925$ ksi compression

$$f_d := -\left(\frac{M_d \cdot y_{bnc}}{I_g}\right) \quad *$$

$f_d = 0.1598$ ksi tension

Flexure Shear, V_{ci}

$$M_{cr} := -\left(\frac{I_c}{y_{bc}}\right) \cdot \left[\left(6 \cdot \frac{\sqrt{f'_c}}{1000}\right) + f_{pe} - f_d\right] \quad *$$

$M_{cr} = 66147.509$ kip – in

$M_{max} := 32.56$

$\alpha := .061328$

$V_i := 1$

$V_p := A_{psang} \cdot f_{se} \cdot \sin(\alpha)$ * $V_p = 22.457$ kips

$$V_{ci} := 0.6\left[\frac{\left(\sqrt{f'_c}\right)}{1000}\right] \cdot b' \cdot d_p + V_p + \frac{V_i \cdot M_{cr}}{M_{max}} \quad *$$

$V_{ci} = 2076.522$ kips

Web Shear, V_{cw}

$$f_{pc} := -\left(\frac{F_{se}}{A_g}\right) - \left[\frac{F_{se}\cdot e\cdot\left(-y_{bc} + y_{bnc}\right)}{I_g}\right] - \left[\frac{M_d\cdot\left(-y_{bc} + y_{bnc}\right)}{I_g}\right] \quad *$$

$f_{pc} = -1.61$ ksi compression

$$V_{cw} := \left(3.5\frac{\sqrt{f'_c}}{1000} - 0.3\cdot f_{pc}\right)\cdot b'\cdot d_p + V_p \quad *$$

$V_{cw} = 307.915$

Web Reinforcement Shear Strength

$A_v := .61359 \text{ in}^2$

$s := 7$ in

$f_y := 69$ ksi

$$V_{sc} := \left(\frac{A_v\cdot f_y\cdot d_p}{s}\right) + A_{pickup}\cdot f_y \quad *$$

$V_{sc} = 390.358$ kips

$$V_{smax} := \frac{\left(8\cdot\sqrt{f'_c}\cdot b'\cdot d_p\right)}{1000} \quad *$$

$V_{smax} = 300.104$

Total Shear, V_n

$V_n := V_{cw} + V_{sc}$ *

$V_n = 698$ kips

Pickup straps - 5 strands at h/2 location
Assume f_y=68 ksi.

$A_{pickup} := 1.0905 \text{ in}^2$

Total Shear, V_n, without pickup strap

$$V_s := \left(\frac{A_v\cdot f_y\cdot d_p}{s}\right) \quad *$$

$V_s = 315.114$

$V_n := V_{cw} + V_s$ *

$V_n = 623.029$

D.2 ACI Alternate

ACI Alternate Approach: Measured Properties

Test E-1

Gross Section Properties

$A_g := 717.5\ in^2$ $y_{tnc} := 28.71\ in$

$I_g := 312529\ in^4$ $y_{bnc} := -27.54\ in^2$

Composite Section Properties

$A_c := 1198.5\ in^2$ $y_{tc} := 25.285\ in$

$I_c := 578420\ in^4$ $y_{bc} := -39.09\ in$

General Properties

$k := 1000$ lb

$ksi := 1000$ psi

$f'_c := 13819$ psi

$f_{se} := 168$ psi

$F_{se} := f_{se} \cdot A_{ps}$

$A_{st} := .2181$

$b_v := 6.125$ in

$A_{ps} := 9.5964\ in^2$

$e := -11.81\ in$

$E := 57\sqrt{f'_c}$

$d_p := 52.1\ in$

$b' := 6.125$ in

n := 10 angled strands

$Crit_1 := 32.56$ in

$R_1 := 57.487$ kips

$R_2 := 57.487$ kips

$D_1 := 980$ in

D1 =distance from west end

$A_{psang} := n \cdot A_{st}$

Loads and Moments at critical section

$w_d := 1.3115\ \frac{k}{ft}$

$V_d := R_1 - \left(\frac{w_d}{12} \cdot D_1\right)$

$V_d = -49.619$ kips

$M_d := R_1 \cdot D_1 - \left[\frac{\left[\frac{w_d}{12} \cdot (D_1)^2\right]}{2}\right]$

$M_d = 3855.402$

*For x < 909 inches, $\left(\frac{V_i}{M_{max}}\right) := \left(\frac{1}{x}\right)$

*For x > 909 inches, $\left(\frac{V_i}{M_{max}}\right) := \left(\frac{1}{1052 - x}\right)$

Loads and Moments at critical section, (h/2) = 32 inches

$$f_{pc} := -\left[-\frac{F_{se}}{A_g} - \left[\frac{F_{se} \cdot e \cdot \left(-y_{bc} + y_{bnc} \right)}{I_g} \right] - \left[\frac{M_d \cdot \left(-y_{bc} + y_{bnc} \right)}{I_g} \right] \right]$$

$f_{pc} = 1.686$ ksi compression

$\alpha := .061328 \quad V_p := A_{psang} \cdot f_{se} \cdot \sin(\alpha) \qquad V_p = 22.457$ kips

Cracking Shear

$f'_{tpred} := \left(4 \cdot \sqrt{f'_c} \right) \quad f'_{tpred} = 470.217$ psi

$$V_{cwPred} := \left[\frac{f'_{tpred}}{1000} \cdot \sqrt{1 + \frac{f_{pc}}{\left(\frac{f'_{tpred}}{1000} \right)}} \cdot b_v \cdot d_p \right] + V_p$$

$V_{cwPred} = 344$ kips

The experimental cracking shears were obtained from each test to determine f'_{texp}
The two components of the shear are the principal tension force and the vertical prestress
force, Vp. The vertical prestressing force must be taken out of the exp. cracking shear in
to determine f_{texp}.

$V_{exp} := 350$

$V_{cwexp} := V_{exp} - V_p$

$V_{cwexp} = 327.543$

$$f'_{texp} := \left[\sqrt{\left(\frac{V_{cwexp}}{b_v \cdot d_p} \right)^2 + \left(\frac{f_{pc}}{2} \right)^2} - \left(\frac{f_{pc}}{2} \right) \right]$$

$f'_{texp} = 0.485$ ksi

Normalized tension value ξ_t

$$\xi_t := \frac{f'_{texp}}{\frac{\sqrt{f'_c}}{1000}} \qquad \xi_t = 4.128$$

D.3 AASHTO LRFD (2004)

AASHTO LRFD Code, 3rd Edition 2004

Design Calculations at defined critical location

Compression angle interpolated from Figure 5.8.3.4.2-1

Test E-1

Gross Section Properties

$A_g := 717.5\ in^2$ $y_{tnc} := 28.71\ in$

$I_g := 312529\ in^4$ $y_{bnc} := -27.54\ in^2$

Composite Section Properties

$A_c := 1205\ in^2$ $y_{tc} := 26.035$

$I_c := 578420\ in^4$ $y_{bc} := -39.09$

$h := 65.125$

General Properties

$f'_c := 13819\ psi$

$f_{se} := 168\ psi$

$F_{se} := f_{se} \cdot A_{ps}$

$A_{st} := .2181$

$A_{psang} := n \cdot A_{st}$

$d_p := h - \left(-y_{bc} + e_{plc}\right)$

$d_p = 51.125$

$D_1 := 908.5\ in$

$D_2 := 143.5\ in$

$L_s := D_1 + D_2$

$L_s = 1052$

$A_{ps} := 9.5964\ in^2$

$f_{pu} := 280\ ksi$

$f_{py} := 257\ ksi$

$f_{pe} := 166.9\ ksi$

$n := 10$ angled strands

$b_v := 6\ in$

$e_{plc} := -25.09$

$\beta_1 := .65$

$cgs_{end} := 16.2965$

$cgs_{middle} := 9.59$

$A_{ps'} := A_{ps} - \left(4 \cdot d_b{}^2 \frac{\pi}{4}\right)$

$E_c := 57\sqrt{f'_c}$

$R_1 := 57.487\ kips$

$R_2 := 57.487\ kips$

$e_e := -11.43\ in$

$e_{ec} := -23.08\ in$

$e_c := -17.94\ in$

$e_{cc} := -29.66\ in$

$b := 60\ in$

$d_b := .6$

$E_{ps} := 29682\ ksi$

$A_{c'} := 333\ in^2$

$f_y := 69\ ksi$

$A_v := .643592\ in^2$

$s := 7\ in$

Ac' is the area of the BT-56 on the flexural tension side as defined by LRFD

A_{ps}' is the amount of steel located in the flexural tension side of the member

d_p is the distance from top fiber to centroid of steel at point load (maximum moment).

e_{plc} is the eccentricity at the point load from composite section for flexural capacity

e_e is the eccentricity at the girder ends, taken from the girder centroid

e_{ec} is the eccentricity at the girder ends, taken from the composite centroid

e_c is the eccentricity at the girder center, taken from the girder centroid

e_{cc} is the eccentricity at the girder center, taken from the composite centroid

Estimated flexural data needed for determining shear capacity

Maximum moment occurs at 143 in. from east end.

$$C := \frac{A_{ps}\cdot f_{pu} - 0.85\beta_1\cdot\left[\frac{f'_c}{1000}\cdot(b-42)\cdot 8\right]}{.85\cdot\frac{f'_c}{1000}\cdot\beta_1\cdot b + k\cdot A_{ps}\cdot\frac{f_{pu}}{d_p}} \qquad \text{where, } k := 2\cdot\left(1.04 - \frac{f_{py}}{f_{pu}}\right)$$

$C = 3.371$ $\qquad a := \beta_1\cdot C \quad a = 2.191$

$$f_{ps} := f_{pu}\cdot\left[1 - k\cdot\left(\frac{C}{d_p}\right)\right] \quad \text{where, } k := 2\cdot\left(1.04 - \frac{f_{py}}{f_{pu}}\right)$$

$f_{ps} = 275.49$ ksi

Critical Section

The critical section shall be taken as [illegible]

d_v is taken as the largest of the distance between the centroid of the compressive and ter forces, $0.9d_e$, or $0.72h$. d_e = the distance from the top of the section to centroid of strand

$d_e := h - \left(-y_{bc} + e_{plc}\right)$

$d_e = 51.125$ $\qquad 0.9\cdot d_e = 46.013$

$.72\cdot h = 46.89$

$d_v := d_e - \left(\frac{a}{2}\right)$

$d_v = 50.029$

$d_v := \max\left(.9\cdot d_e, .72\cdot h, d_v\right)$

$d_v = 50.029$

Iteration 2:

$\theta_d := 28.5$ so, $\theta := \theta_d \cdot \left(\frac{\pi}{180}\right)$ $C_{s1} := .5 \cdot d_v \cdot \frac{1}{\tan(\theta)}$ $C_{s1} = 46.071$

$C_s := \max(d_v)$ $C_s = 50.029$ in

Transfer and Development length

$l_t := 60 \cdot d_b$ $l_t = 36$ in

$l_d := \left[f_{ps} - \left(\frac{2}{3}\right) \cdot f_{pe} \right] \cdot d_b$ $l_d = 98.534$ in

From end of girder, the critical section is $C_s + 9 = 59.029$ in

f_{ps} can be assumed to vary linearly from f_{pe} to f_{ps} between the transfer and development length and is referred to as f_{psv}

$f_{psv} := f_{pe} + \left(\frac{f_{ps} - f_{pe}}{l_d - l_t}\right) \cdot (C_s + 9 - l_t)$ $f_{psv} = 206.89$ ksi

Percent of strands fully developed $= 100 \cdot \left(\frac{f_{psv}}{f_{ps}}\right) = 75.099$ percent

Multiply A_{ps} in the ε_x equation by this percentage $R_d := \left(\frac{f_{psv}}{f_{ps}}\right)$

Loads, Shears and Moments

Assume test load = 600 kips $P_u := 746$ kips

$w_d := 1.3115$ k / ft

$$V_{LL} := P_u \cdot \left(\frac{D_1}{L_s} \right) \qquad M_{LL} := V_{LL} \cdot C_s$$

$V_{LL} = 644.24$ kips $M_{LL} = 32230.974$ k – in

$$V_D := \left[\frac{\left[\left(\frac{w_d}{12} \right) \cdot L_s \right]}{2} - \frac{(R_1 + R_2)}{L_s} \cdot C_s \right] \qquad M_D := \left[\frac{C_s \cdot \left[\left(\frac{w_d}{12} \right) \cdot L_s \right]}{2} \right] - \left(\frac{w_d}{12} \right) \cdot \frac{C_s^{\,2}}{2}$$

$M_D = 2739.286$

$V_u := V_{LL} + V_D \qquad V_u = 696.26$ kips

$M_u := M_{LL} + M_D \qquad M_u = 34970.26$ kip – in

Shear Calculations

V_p

$\alpha := .0623675$

$V_p := A_{psang} \cdot f_{se} \cdot \sin(\alpha) \qquad V_p = 22.837$ kips

Shear stress in concrete

$$v := \frac{V_u - V_p}{b_v \cdot d_v} \qquad v = 2.243 \text{ ksi}$$

$$v' := \frac{v}{\frac{f'_c}{1000}}$$

$v' = 0.162$

Cgs at critical section:

$$Cgs_{cr} := cgs_{end} - \left[\frac{cgs_{end} - cgs_{middle}}{481}\cdot\left(C_s + 9\right)\right] \quad Cgs_{cr} = 15.473$$

$$e_{Cs} := y_{bnc} + Cgs_{cr}$$

$$f_{po} := .7\cdot f_{pu}$$

$$f_{po} = 196 \quad ksi$$

$$\varepsilon_x := \left[\frac{\left(\frac{M_u}{d_v}\right) + .5\cdot\left(V_u - V_p\right)\cdot\left(\frac{1}{\tan(\theta)}\right) - \left(R_d\cdot A_{ps'}\cdot f_{po}\right)}{2E_{ps}\cdot R_d\cdot A_{ps'}}\right]$$

$$\varepsilon_x = 1.936\times 10^{-4}$$

Linear interpolation of β and θ

$$I_1 := 29.7 - \left[\frac{(29.7 - 28.8)}{.175 - .150}\right]\cdot(.175 - v') \quad I_2 := 28 - \left(\frac{28 - 26.9}{.175 - .150}\right)\cdot(.175 - v')$$

$$I_3 := \left|\left|\left[\left(\frac{I_2 - I_1}{.125 - .25}\right)\cdot\left(.125 - \varepsilon_x\cdot 1000\right)\right] - I_2\right|\right|$$

$$I_1 = 29.24436297$$

$$I_2 = 27.4431103$$

$$I_3 = 28.4320873$$

So , 28.4 degrees is an acceptable predicted angle of compression.

$$I_1 := 2.44 - \left[\frac{(2.44 - 2.52)}{.175 - .150}\right]\cdot(.175 - v') \quad I_2 := 2.52 - \left(\frac{2.52 - 2.60}{.175 - .150}\right)\cdot(.175 - v')$$

$$I_3 := \left|\left[\left(\frac{I_2 - I_1}{.125 - .25}\right)\cdot\left(.125 - \varepsilon_x\cdot 1000\right)\right] - I_2\right|$$

$I_3 = 2.517$

$\beta := I_3$

$I_1 = 2.481$

$I_2 = 2.561$

$$V_c := .0316\cdot\beta\cdot\sqrt{\left(\frac{f'_c}{1000}\right)}\,b_v\cdot d_v$$

$V_c = 88.739$ kips

$$V_s := \frac{A_v\cdot f_y\cdot d_v\cdot\left(\frac{1}{\tan(\theta)}\right)}{s} \qquad V_s = 584.551 \quad \text{kips}$$

$V_n := V_c + V_s + V_p \qquad V_n = 696.127$

Max $V_{nm} := .25\cdot d_v\cdot\left(\frac{f'_c}{1000}\cdot b_v\right)$

$V_{nm} = 1.037\times 10^3$

$V_n = V_u$; therefore, the shear capacity at this location is 696 kips

Longitudinal Reinforcement Check

$$A_{ps'}\cdot f_{ps} \geq \frac{M_u}{d_v} + \left(V_u - .5V_s\right)\cdot\left(\frac{1}{\tan(\theta)}\right)$$

$A_{ps'}\cdot f_{ps} = 2.207\times 10^3$

$$\frac{M_u}{d_v} + \left(V_u - .5V_s\right)\cdot\left(\frac{1}{\tan(\theta)}\right) = 1.302\times 10^3$$

Aps'fps is greater than the right hand of the equation. **Section checks.**

AASHTO LRFD Code, 3rd Edition 2004

Design Calculations at defined critical location

Compression angle obtained from physical measurement

Test E-1

Gross Section Properties

$A_g := 711\ in^2$ $y_{tnc} := 28.47\ in$

$I_g := 304701\ in^4$ $y_{bnc} := -27.53\ in^2$

Composite Section Properties

$A_c := 1198.5\ in^2$ $y_{tc} := 28.47\ in$

$I_c := 577426\ in^4$ $y_{bc} := -39.25\ in$

$h := 64\ in$

General Properties

$f'_c := 10000\ psi$

$f_{se} := 168\ psi$

$F_{se} := f_{se} \cdot A_{ps}$

$A_{st} := .217$

$A_{psang} := n \cdot A_{st}$

$d_p := h - \left(-y_{bc} + e_{plc}\right)$

$d_p = 49.82$

$D_1 := 909\ in$

$D_2 := 143\ in$

$L_s := D_1 + D_2$

$L_s = 1052$

$A_{ps} := 9.548\ in^2$

$f_{pu} := 270\ ksi$

$f_{py} := 243\ ksi$

$f_{pe} := 171.5\ ksi$

$n := 10$ angled strands

$b_v := 6\ in$

$e_{plc} := -25.07$

$\beta_1 := .65$

$cgs_{end} := 16.2965$

$cgs_{middle} := 9.59$

$A_{ps'} := A_{ps} - \left(4 \cdot d_b{}^2 \frac{\pi}{4}\right)$

$E_c := 57\sqrt{f'_c}$

$R_1 := 54.35\ kips$

$R_2 := 54.35\ kips$

$e_e := -11.43\ in$

$e_{ec} := -23.08\ in$

$e_c := -17.94\ in$

$e_{cc} := -29.66\ in$

$b := 60\ in$

$d_b := .6$

$E_{ps} := 28500\ ksi$

$A_{c'} := 333\ in^2$

$f_y := 60\ ksi$

$A_v := .643592\ in^2$

$s := 7\ in$

Ac' is the area of the BT-56 on the flexural tension side as defined by LRFD

A_{ps}' is the amount of steel located in the flexural tension side of the member

d_p is the distance from top fiber to centroid of steel at point load (maximum moment).

e_{plc} is the eccentricity at the point load from composite section for flexural capacity

e_e is the eccentricity at the girder ends, taken from the girder centroid

e_{ec} is the eccentricity at the girder ends, taken from the composite centroid

e_c is the eccentricity at the girder center, taken from the girder centroid

e_{cc} is the eccentricity at the girder center, taken from the composite centroid

Estimated flexural data needed for determining shear capacity

Maximum moment occurs at 143 in. from east end.

Calculated $f_{psc} := 209.6$

Measured $f_{psm} := 192$ ksi

Ultimate $f_{psult} := 272.5$

Experimental c distance $c := 36.17$ in

$a := .65 \cdot c$

This is based on a calculated initial strain profile plus the added experimental loading strain.

Critical Section

d_v is taken as the largest of the distance between the centroid of the compressive and ter forces, $0.9d_e$, or $0.72h$. d_e = the distance from the top of the section to centroid of strand

$d_e := h - \left(-y_{bc} + e_{plc}\right)$

$d_e = 51.125$ $0.9 \cdot d_e = 46.013$

$.72 \cdot h = 46.89$

$d_v := d_e - \left(\frac{a}{2}\right)$

$d_v = 39.37$ $d_v := \max\left(.9 \cdot d_e, .72 \cdot h, d_v\right)$

$d_v = 46.89$

Experimental $\theta = 31.5$ degrees

$\theta_d := 31.5$ so, $\theta := \theta_d \cdot \left(\frac{\pi}{180}\right)$ $C_{s1} := .5 \cdot d_v \cdot \frac{1}{\tan(\theta)}$ $C_{s1} = 38.259$

$C_s := \max\left(d_v\right)$ $C_s = 46.89$ in

Transfer and Development length

$l_t := 60 \cdot d_b \quad l_t = 36 \quad in$

$l_d := \left[f_{psc} - \left(\frac{2}{3}\right) \cdot f_{pe} \right] \cdot d_b \quad l_d = 59 \quad in$

From end of girder, the critical section is $C_s + 9 = 55.89 \quad in$

f_{ps} can be assumed to vary linearly from f_{pe} to f_{ps} between the transfer and development length and is referred to as f_{psv}

$$f_{psv} := f_{pe} + \left(\frac{f_{psm} - f_{pe}}{l_d - l_t} \right) \cdot \left(C_s + 9 - l_t \right) \qquad f_{psv} = 188.606 \quad ksi$$

Percent of strands fully developed $= 100 \cdot \left(\frac{f_{psv}}{f_{psm}} \right) = 98.232 \quad percent$

Multiply A_{ps} in the ε_x equation by this percentage $\qquad R_d := \left(\frac{f_{psv}}{f_{psm}} \right)$

Loads, Shears and Moments

Test load = 635 kips Try a $P_u := 635 \quad kips$

$w_d := 1.3115 \quad k / ft$

$$V_{LL} := P_u \cdot \left(\frac{D_1}{L_s} \right) \qquad M_{LL} := V_{LL} \cdot C_s$$

$V_{LL} = 548.382 \quad kips \qquad M_{LL} = 25713.616 \quad k - in$

$$V_D := \left[\frac{\left[\left(\frac{w_d}{12} \right) \cdot L_s \right]}{2} - \frac{\left(R_1 + R_2 \right)}{L_s} \cdot C_s \right] \qquad M_D := \left[\frac{C_s \cdot \left[\left(\frac{w_d}{12} \right) \cdot L_s \right]}{2} \right] - \left(\frac{w_d}{12} \right) \cdot \frac{C_s^{\,2}}{2}$$

$M_D = 2575.437$

$V_u := V_{LL} + V_D \quad V_u = 601 \quad kips$

$M_u := M_{LL} + M_D \quad M_u = 28289.052 \quad kip - in$

Shear Calculations

V_p

$\alpha := .061328$

$V_p := A_{psang} \cdot f_{se} \cdot \sin(\alpha)$ $\quad V_p = 22.457$ kips

Shear stress in concrete

$$v := \frac{V_u - V_p}{b_v \cdot d_v} \qquad v = 2.055 \text{ ksi}$$

$$v' := \frac{v}{\frac{f'_c}{1000}}$$

$v' = 0.149$

Cgs at critical section:

$$Cgs_{cr} := cgs_{end} - \left[\frac{cgs_{end} - cgs_{middle}}{481} \cdot (C_s + 9) \right] \qquad Cgs_{cr} = 15.517$$

$e_{Cs} := y_{bnc} + Cgs_{cr}$

$f_{po} := .7 \cdot f_{pu}$

$f_{po} = 196$ ksi

$$\varepsilon_x := \left[\frac{\left(\frac{M_u}{d_v} \right) + .5 \cdot (V_u - V_p) \cdot \left(\frac{1}{\tan(\theta)} \right) - (R_d \cdot A_{ps'} \cdot f_{po})}{2 E_{ps} \cdot R_d \cdot A_{ps'}} \right]$$

$\varepsilon_x = -1.124 \times 10^{-3}$

Obtain θ and β values from LRFD chart 5.8.3.4.2-1

Because ε_x is negative, a correction factor must be applied.

$$\varepsilon_{x.adj} := \frac{\left(\frac{M_u}{d_v}\right) + .5\cdot\left(V_u - V_p\right)\cdot\left(\frac{1}{\tan(\theta)}\right) - \left(R_d\cdot A_{ps'}\cdot f_{po}\right)}{2\left(E_{ps}\cdot R_d\cdot A_{ps'} + E_c\cdot A_{c'}\right)}$$

$$\varepsilon_{x.adj} = -1.119\times 10^{-4}$$

Linear interpolation of β and θ

θ was determined by observing actual crack angles in the structure

$\theta = 0.55$ radians (31.5 degrees)

β must be determined through linear interpolation

$$I_1 := 2.79 - \left[\frac{(2.79 - 2.99)}{.150 - .125}\right]\cdot(.150 - v') \qquad I_2 := 2.88 - \left(\frac{2.88 - 3.18}{.150 - .125}\right)\cdot(.150 - v')$$

$I_1 = 2.8$ $\qquad$ $I_2 = 2.895$

$$I_3 := \left|\left[\left(\frac{I_2 - I_1}{-.20 - -.10}\right)\cdot\left(-.20 - \varepsilon_{x.adj}\cdot 1000\right)\right] - I_2\right|$$

$I_3 = 2.811$

$\beta := I_3$

$$V_c := .0316 \cdot \beta \cdot \sqrt{\left(\frac{f'_c}{1000}\right)} b_v \cdot d_v$$

$V_c = 92.913$ kips

$$V_s := \frac{A_v \cdot f_y \cdot d_v \cdot \left(\frac{1}{\tan(\theta)}\right)}{s}$$

$V_s = 485.426$ kips

$V_n := V_c + V_s + V_p$

$V_n = 601$ kips

$V_n = V_u$; The shear capacity at this location is 601 kips.
The pickup straps must be taken into account according to the LRFD method.

The shear cracks, according to θ, will cross all four sections of pickup points. Thier distanc
and spacing must be determined to account for thier effectiveness. The yield stress of the
ksi bars were used for the strands.

$A_{vp} := 1.0905\,in^2$ $d_{pickup} := 22$ in where, d_{pickup} is the horizontal distance that tl
pickups cover.

$s_{vp} := 5.5$ in

$V_{spickups} := A_{vp} \cdot f_y$ $V_{spickups} = 75.245$ kips

$$V_{sp} := \frac{\left(V_{spickups} \cdot d_{pickup}\right)}{s_{vp}} \qquad V_{sp} = 300.978$$

Total shear capacity, after pickup strengths are added:

$V_{st} := V_s + V_{sp}$ $V_n := V_c + V_{st} + V_p$ $V_n = 902$ kips

Maximum shear capacity:

Max $V_{nm} := .25 \cdot d_v \cdot \left(\frac{f'_c}{1000} \cdot b_v\right)$ Max $V_{nm} = 971.959$

APPENDIX E

Concrete Surface Strain Data

This appendix provides the raw data obtained from the DEMEC readings taken for shear Tests E1 and W1. The raw data and running averages are presented for the north and south sides of both tests.

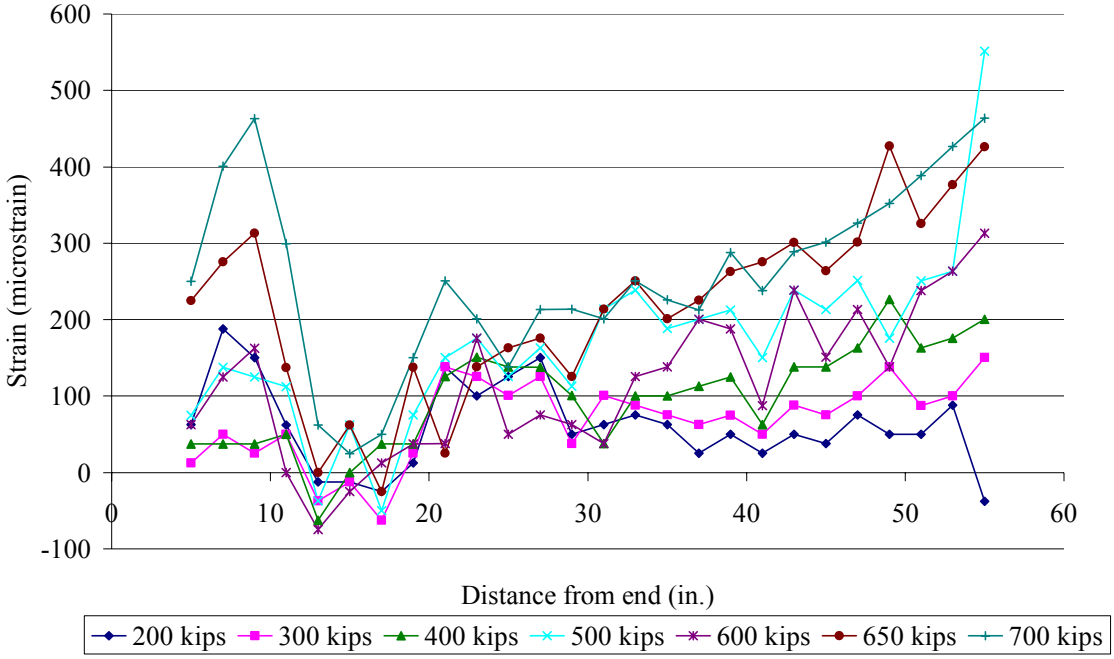

Figure E.1 Test E1 north side raw data

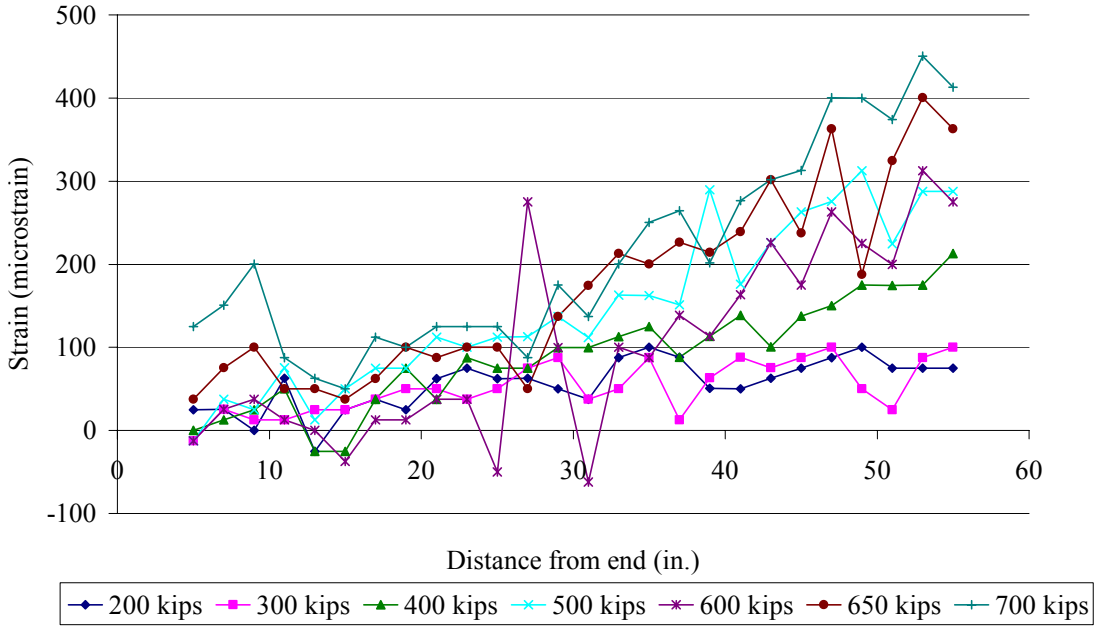

Figure E.2 Test E1 south side raw data

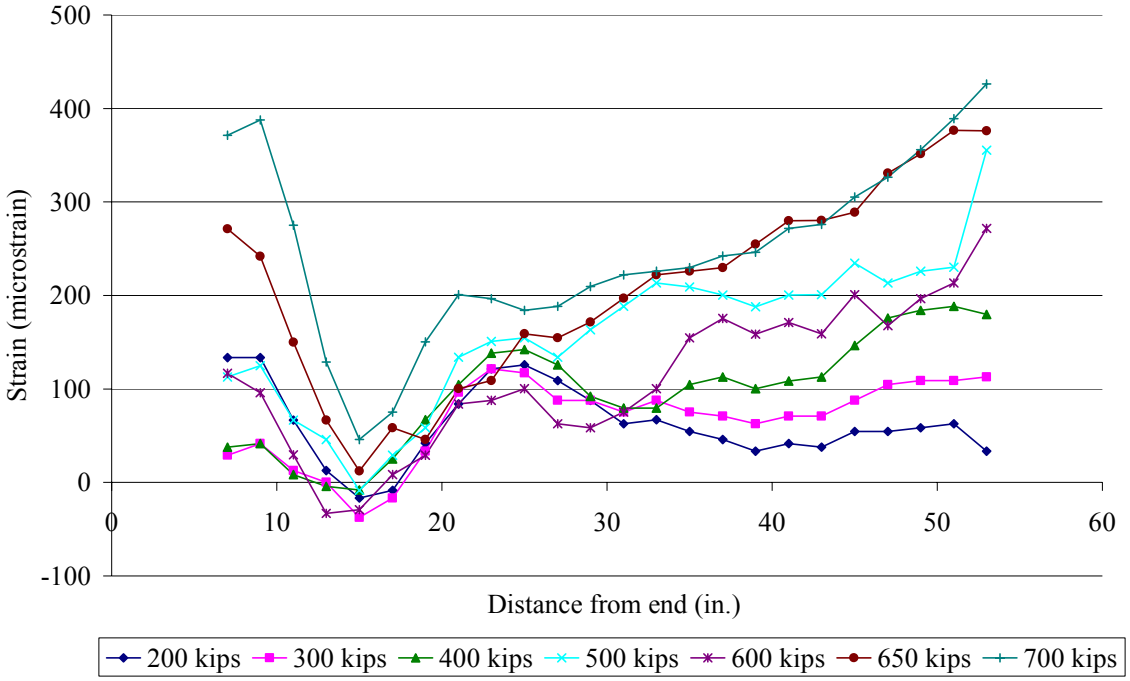

Figure E.3 Test E1 north side running average

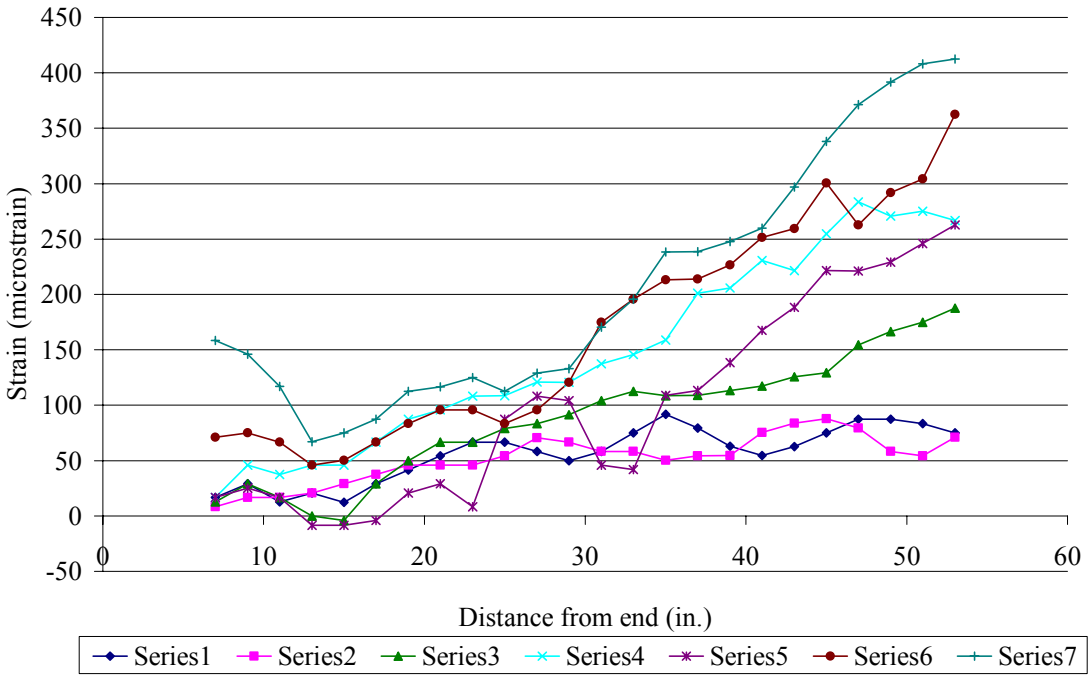

Figure E.4 Test E1 south side running average

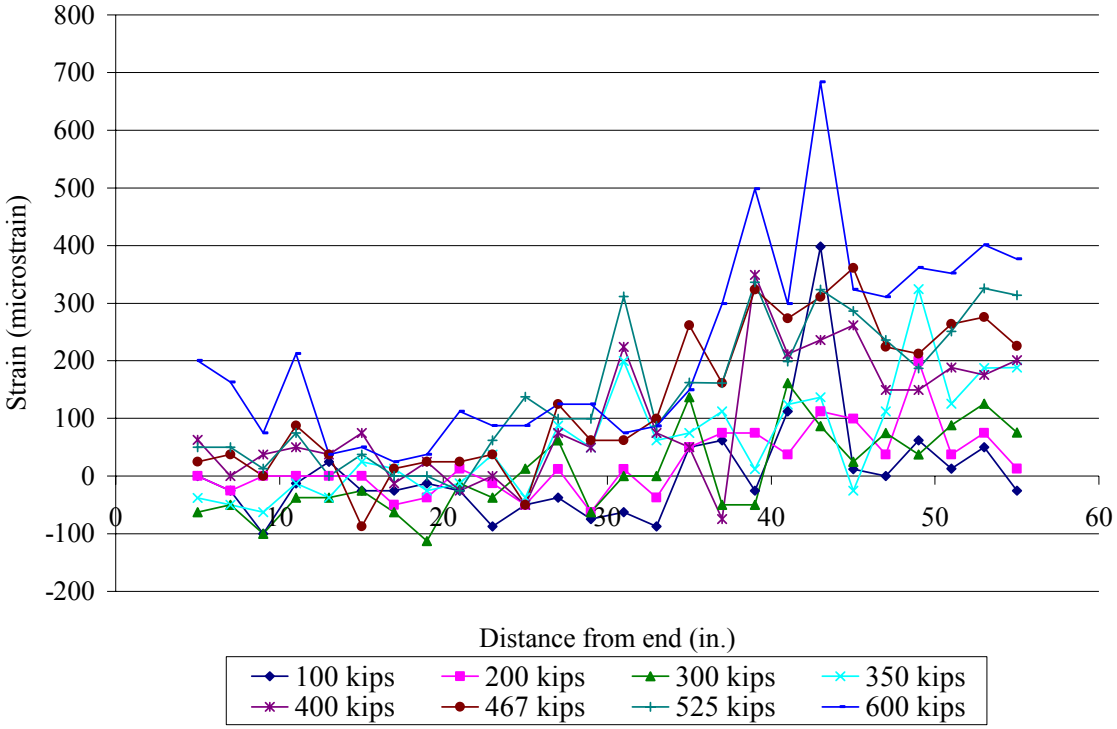

Figure E.5 Test W1 north side raw data

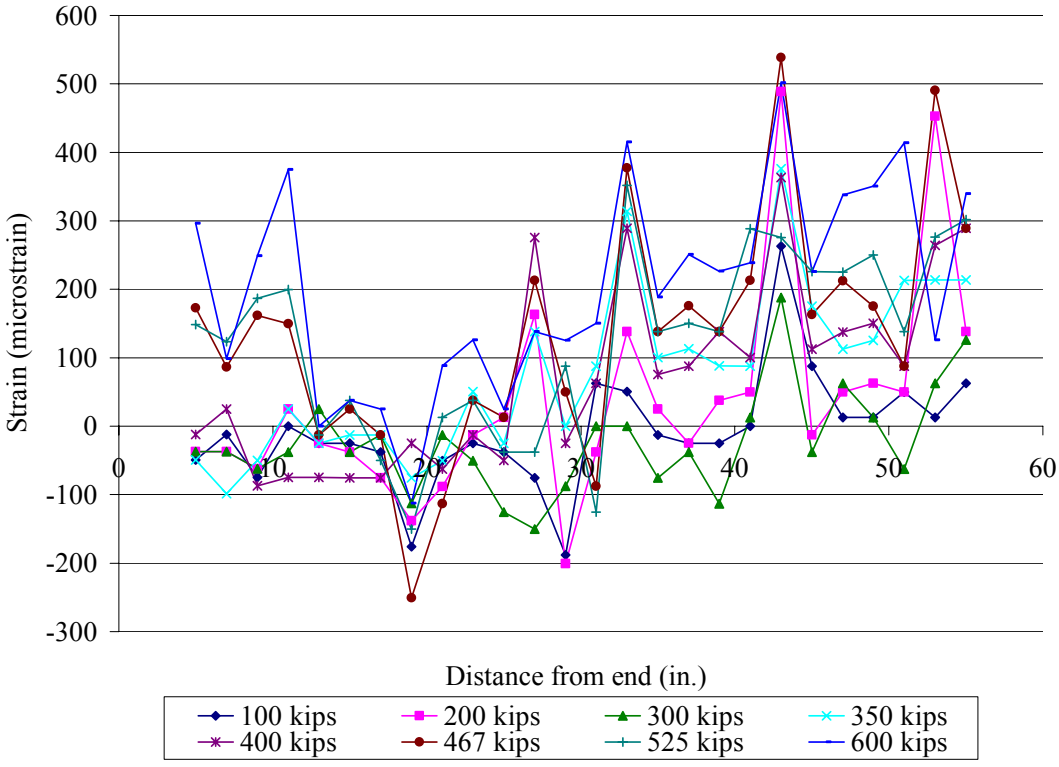

Figure E.6 Test W1 south side raw data

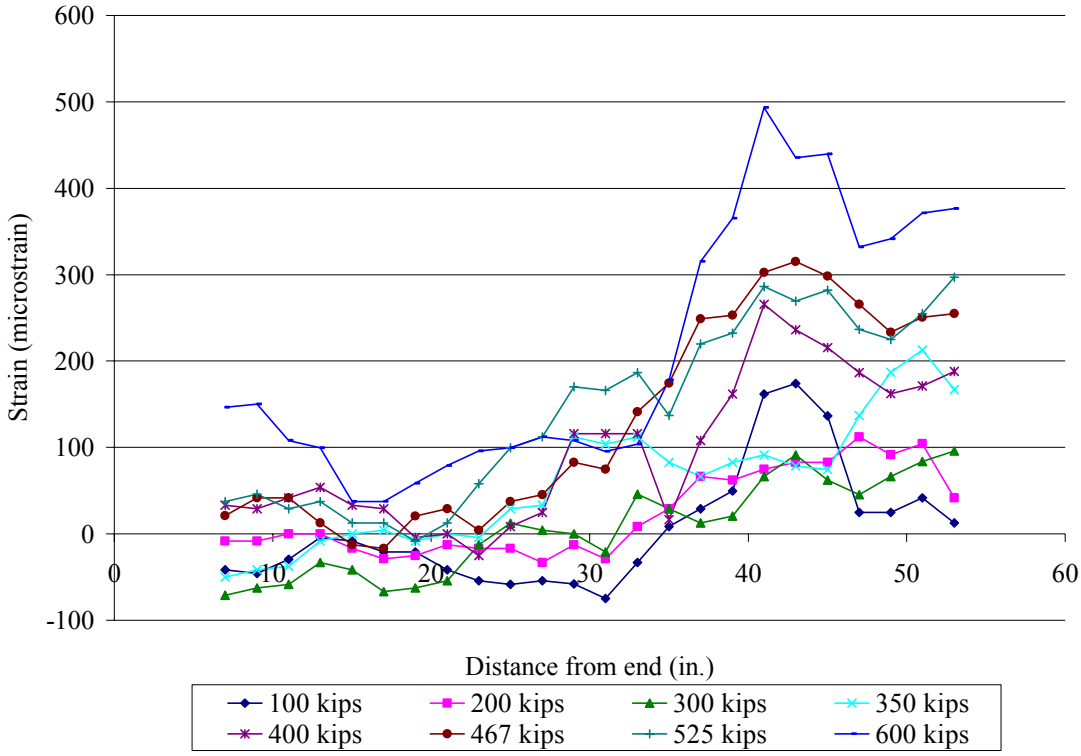

Figure E.7 Test W1 north side running average

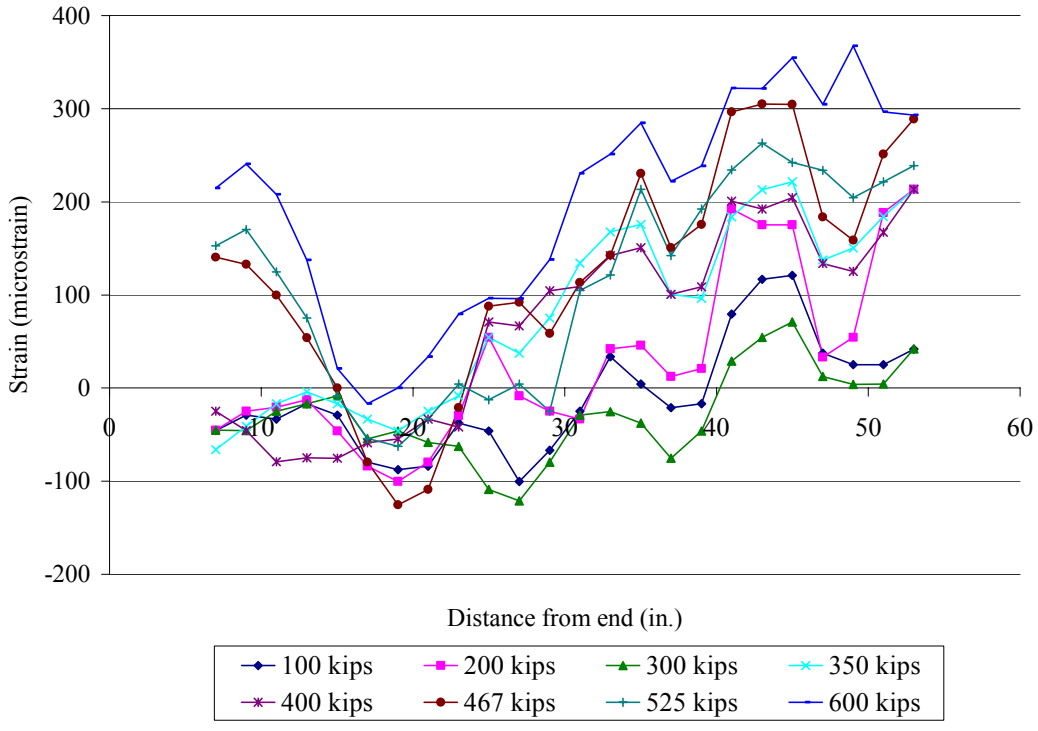

Figure E.8 Test W1 south side running average

REFERENCES

1. ACI Committee 209 (1997), "Prediction of Creep, Shrinkage, and Temperature effects in Concrete Structures" (ACI 209R-92, Reapproved 1997) American Concrete Institute, Farmington Hills, Michigan 1997.

2. ACI Committee 318 (2002), "Building Code Requirements for Structural Concrete" (ACI 318-02), and Commentary (ACI 318R-02),"American Concrete Institute, Farmington Hills, Michigan 2002.

3. ACI Committee 363 (1992), "State-of-the-art Report on High-Strength Concrete" (ACI 363R-92) American Concrete Institute, Farmington Hills, Michigan 1992.

4. AASHTO (1998), "Standard Specifications for Highway Bridges, Load and Resistance Factor Design," 2nd Edition, American Association of State Highway Transportation Officials, Washington D.C., 1998.

5. AASHTO (2002), "Standard Specifications for Highway Bridges," 17th Edition, American Association of State Highway Transportation Officials, Washington, D.C., 2002.

6. AASHTO (2004), "Standard Specifications for Highway Bridges, Load and Resistance Factor Design," 3rd Edition, American Association of State Highway Transportation Officials, Washington D.C., 2004.

7. ASTM C 31/C 31 M, (2000), "Standard Practice for Making and Curing Concrete Test Specimens in the Field," Annual Book of ASTM Standards, Vol. 04.02, American Society for testing Materials, 2000, West Conshohocken, PA.

8. ASTM C 39, (1996), "Standard Method for Compressive Strength of Cylindrical Concrete Specimens, Annual Book of ASTM Standards, Vol. 04.02, American Society for testing Materials, 2000, West Conshohocken, PA.

9. ASTM C 78, (1994), "Standard Test Method for Flexural Strength of Concrete (Using Simple Beam with Third-Point loading), Annual Book of ASTM Standards, Vol. 04.02, American Society for testing Materials, 2000, West Conshohocken, PA.

10. ASTM C 138, (2001), "Standard Test Method for Unit Weight, Yield, and Air Content (Gravimetric) of Concrete," Annual Book of ASTM Standards, Vol. 04.02, American Society for testing Materials, 2000, West Conshohocken, PA.

11. ASTM C 157/C 157M, (1999), "Standard Test Method for Length Change of Hardened Hydraulic-Cement Mortar and Concrete,"Annual Book of ASTM Standards, Vol. 04.02, American Society for testing Materials, 2000, West Conshohocken, PA.

12. ASTM C 192, (1995), "Standard Practice for Making and Curing Concrete Test Specimens in the Laboratory," Annual Book of ASTM Standards, Vol. 04.02, American Society for testing Materials, 2000, West Conshohocken, PA.

13. ASTM C 469, (1994), "Standard test Method for Static Modulus of Elasticity and Poisson's Ratio of Concrete in Compression," Annual Book of ASTM Standards, Vol. 04.02, American Society for testing Materials, 2000, West Conshohocken, PA.

14. ASTM C 512 (1987), "Standard Test Method for Creep in Concrete in Compression,"

15. Annual Book of ASTM Standards, Vol. 04.02, American Society for testing Materials, 2000, West Conshohocken, PA

16. ASTM C1202, (1997), "Standard Test Method for Electrical Indication of Concrete's Ability to Resist Chloride Ion Penetration," Annual Book of ASTM Standards, Vol. 04.02, American Society for testing Materials, 2000, West Conshohocken, PA

17. Budynas, R.G., *Advanced Strength and Applied Stress Analysis*, 2nd Edition, McGraw-Hill, Boston, 1999, 935 pp.

18. Castrodale, R.W., Personal telephone conversation on April 27th, 2005 concerning the differences between the 1998 and 2004 LRFD codes.

19. Collins, M.P., Mitchell, D., *Prestressed Concrete Structures*, Prentice Hall, Englewood Cliffs, New Jersey, 1991.

20. Cumming, D.A., French, C.E., Shield, C., "Shear Capacity of High-Strength Concrete Prestressed Girders," Master's Thesis, Department of Civil Engineering, University of Minnesota, St Paul, MN, 1998, 291 pp.

21. Deatherage, J.H., Burdette, E.G., and Chew, C.K., "Development Length and Lateral Spacing Requirements of Prestressing Strand for Prestressed Concrete Bridge Girders, " *PCI Journal*, V. 39, No. 1, January-February 1994, pp. 70-83.

22. Dill, J. (2000), "Development Length of 0.6-inch Diametere Prestressing Strands in High-Performance Concrete," Master's Thesis., School of Civil and Environmental Engineering, Georgia Institute of Technology, Atlanta, GA, 2000, 417 pp.

23. Elzanaty, A.H., Nilson, A.H., and Slate, F.O., "Shear Capacity of Prestressed Concrete Beams Using High-Strength Concrete," *ACI Structural Journal*, V. 83, No. 3, May-June 1986, pp. 359-368.

24. Hartmann, D.L., Breen, J.E., Kreger, M.E., "Shear Capacity of High Strength Prestressed Concrete Girders," Research Report 381-2, Center for Transportation Research, The University of Texas at Austin, Jan. 1988.

25. Hibbeler, R.C., "*Structural Analysis*," 4th Edition, Prentice Hall, New Jersey, 1999, 600 pp.

26. Kahn, L.F., Lai, J.S., Reutlinger, C., Dill, J., and Shams, M. (2000), "Direct Pull-Out Capacity, Transfer and Development Length of 0.6-inch Diameter Prestressing Strands in High Performance Concrete," task 3, Use of High-Strength/High-Performance Concrete for Precast, Prestressed Concrete Bridges in Georgia, Structural Engineering Research Report No. 00-3, prepared for Georgia department of Transportation Project No. 9510, School of Civil and Environmental Engineering, Georgia Institute of Technology, Atlanta, GA, April 2000 pp. 419.

27. Lai, J.S., Kahn, L.F., Travis, D., Champney, M., Prada, J., Shams, M, Saber, A. (1999), "Mix Design and Properties of High Performance Concrete," Task 3, Use

of High-Strength/High-Performance Concrete for Precast, Prestressed Concrete Bridges in Georgia, Structural Engineering, Mechanics and Materials research Report No. 99-1 prepared for the Office of Materials and Research: Georgia Department of Transportation, March, 1999, 320 pp.

28. Lane, S.N., *A New Development Length Equation for Pretensioned Strands in Bridge Beams and Piles, Final Report*, No. FHWA-RD-98-116, Federal Highway Administration, December, 1998 131 pp.
29. Lin, T.Y., Burns, N.H., *Design of Prestressed Concrete Structures* (1981), Third Edition, John Wiley and Sons, New York, New York, 1981, 646 pp.

30. Logan, D.R., (1997), Acceptance Criteria for Bond Quality of Strand for Pretensioned, Prestressed Cocnrete Applications," PCI Journal, V. 42, No. 2, March / April, 1997, pp 52-90

31. Ma, J., Tadros, M.H., Baishya, M, "Shear Behavior of Pretensioned High-Strength Concrete Bridge I-Girders," *ACI Structural Journal*, Vol. 97, No. 1, January-February 2000, pp. 185-192.

32. MacGregor, James G., (1997), "*Reinforced Concrete: Mechanics and Design*", Third Edition, Prentice-Hall, Inc., New Jersey, 1997, 939 pp.

33. *Manual of Steel Construction Load and Resistance Factor Design,* 3rd Edition, American Institute of Steel Construction, Inc., United States of America, 2003.

34. Nawy, E.G., *Prestressed Concrete: A Fundamental Approach*, Third Edition, Prentice Hall, Upper Saddle River, New Jersey, 2000.

35. Nawy, E.G., *Prestressed Concrete: A Fundamental Approach*, Fourth Edition, Prentice Hall, Upper Saddle River, New Jersey, 2006.

36. Neville, A.M. (1981), "*Properties of Concrete*," Fourth edition, Addison Wesley Longman Limited Publishing, Harlow, England, 1981, 844 pp.

37. PCI (1999), "PCI Design Handbook, Precast and Prestressed Concrete," 5th Edition, Precast / Prestressed Concrete Institute, Chicago, 1999.

38. Russell, H.G., Bruce, R.N., Roller, J.J., "Shear Tests of High Performance Concrete Bulb-Tee Girders," Interim Report – Department of Civil and Environmental Engineering, Tulane University, Louisiana Transportation Research Center, Research Report No. 00-6SS, Baton Rouge, LA, 2003, 21 pp.

39. Reutlinger, C. (1999), "Direct Pull-out Capacity and Transfer Length of 0.6-inch Diameter Prestressing Strand in High-Performance Concrete," Master's Thesis, Georgia Institute of Technology, Atlanta, GA, May 1999, 352 pp.

40. Shahawy, M., and Batchelor, B. DeV, "Shear Behavior of Full-Scale Prestressed Concrete Girders: Comparison Between AASHTO Specifications and LRFD Code," *PCI Journal*, V. 41, No. 3, May-June 1996, pp. 48-62.

41. Shahawy, M., and Batchelor, B. DeV, Discussion of "Shear Behavior of Full-Scale Prestressed Concrete girders: Comparison Between AASHTO Specifications and LRFD Code," *PCI Journal*, V. 42, No. 3, May-June 1997, pp. 72-93.

42. Shahawy, M., and Cai, C.S., "A New Approach to Shear Design of Prestressed Concrete Members," *PCI Journal*, V. 44, No. 4, July-August 1999, pp. 92-109.

43. Shams, M, Kahn, L.F. (2000), "Time-Dependant Behavior of High-Performance Concrete," Georgia Tech Structural Engineering, Mechanics and Materials Research Report No. 00-5, Georgia Department of Transportation Research Project No. 9510, April 2000, 395 pp.

44. Shams, M. (2000-2), "Time Dependent Losses of High-Performance Concrete", Doctoral thesis, Georgia Institute of Technology, May, 2000, 572 pp.

45. Slapkus, A., Kahn, L.F. (2002), "Evaluation of Georgia's High Performance Concrete Bridge," Master's Thesis, Georgia Institute of Technology, Atlanta, GA, August 2002.

46. Tawfig, Kamal S., "Cracking and Shear Capacity of High Strength Concrete Girders," Final Report WPI 0510612, FAMU/FSU College of Engineering, January 1995.